Department of Mechanical Engineering
University of Canterbury

Thermodynamic Modelling and Simulation for High Efficiency Design and Operation of Geothermal Power Plants

Submitted in partial fulfilment of the requirements for the Degree of
Ph.D. in Mechanical Engineering
in the University of Canterbury by Mohammed Imroz Sohel

University of Canterbury

2011

Abstract

This thesis analyses long term and short term environmental effects on geothermal power plant performance and discusses adaptive ways to improve performance. Mokai 1 geothermal power plant has been used as a case study for this investigation. Mokai 1 is a combined cycle plant where the binary cycles are air-cooled. The plant performance of an air-cooled binary cycle geothermal power plant is dependent on the environment (resource characteristics as well as weather conditions). For modelling such a power plant, two time scales are of interest: the yearly basis for aggregate plant performance for design and operations; and the daily basis for hourly plant performances for an accurate dispatch prediction.

Adaptive methodology for long term performance improvement has been introduced in this work which would save money and effort in the future by keeping the provisions to adapt to changes in resource characteristics based on geothermal reservoir modelling. The investigation was carried out using a steady state computer simulator of Mokai 1 geothermal power plant. The steady sate simulator was built specifically for this work. The deviation in performance of various components is less than 5% compared to the original plant design. The model is very generic and it can be used for other plants with simple adaptation or can be used for future plant design.

One of the main contributions of this work is an iterative method for modelling the environmental effect on short term performance on the air-cooled organic Rankine cycle. The ambient temperature is identified as the most influencing parameter on short term performance which influences the performance of the whole cycle in two ways. Firstly, by changing the equilibrium pressure inside the condenser, the turbine outlet pressure changes and hence, the turbine pressure ratio also changes. The turbine pressure ratio is a major parameter determining power generated by a turbine; therefore, the plant output is affected. Secondly, by changing the condenser outlet temperature with the ambient temperature, the pump inlet and outlet condition and consequently vaporizer equilibrium temperature and pressure are influenced. The developed method sought the equilibrium conditions of both condenser and vaporizer iteratively. In short, ORC cycle shifts on the *T-s* plane depending on the ambient temperature. This method iteratively seeks the shifted ORC on the *T,s* plane.

Two case studies have been carried out to demonstrate the method. The developed method shows robustness and converges exponentially. The model is effective for cycles that use saturated vapour as well as superheated vapour. The model essentially assumes steady state operation of the power cycle. The possible unit time where this model can be applied is bounded by the time required by a system to come into steady state. The saturated vapour cycle yielded average error 4.20% with maximum error 9.25% and the superheated vapour cycle yielded average error 2.12% with maximum error 5.60%. The main advantage of the developed method is that it requires a minimum number of inputs: condenser (p,T), vaporizer (p,T), condenser heat load, turbine efficiency (overall), pump work and the extremum conditions of all the components. These inputs should represent typical operating conditions of a plant. The model can predict the appropriate plant performance depending on the system heat input (geothermal fluid flow in this case) and the heat sink temperature. As the method is based on basic thermodynamics rather than empirical or semi-empirical approaches, this method is widely applicable. The main focus of this work is on the

ORC but the developed method is applicable to any closed Rankine cycle. In addition, application of the developed iterative method to predict plant performance based on mean yearly weather data is also discussed in the thesis.

Water-augmented cooling system and optimization of plant operating point parameters have been proposed as adaptive measures to improve short term performance. Developed iterative method has been used for the short term performance analysis. The water-augmented cooling system is specifically suitable to mitigate the reduced power output during the summer. The simulated average gain in power during the summer (Jan, Feb, Nov and Dec) of an ORC of Mokai 1 geothermal power plant by incorporating a water-augmented cooling system was 2.3% and the average gain for the whole year was 1.6% based on the weather data of Taupo for the year 2005. A cost benefit analysis showed that water-augmented cooling system is more economical compared to other alternative renewable energies considered to meet summer peak demand. From the green house gas emissions perspective, water-augmented cooling is a better option than the gas fired peaking plants.

Adaptive approach for short term performance improvement by optimizing operating point parameters of an air-cooled binary cycle has huge potential with possible maximum improvement in power output by about 50%. The optimization takes in to account the effects of the geothermal resource characteristics and the weather conditions. The optimization is achieved by manipulating cycle mass flow rate and vaporizer equilibrium condition. Further study on the optimizing operating points to achieve improved short term performance has been recommended for future work.

Acknowledgements

I would like to express my acknowledgment foremost to my senior supervisor, Associate Professor Susan Krumdieck. Her guidance has always been there when I needed it; however, I have enjoyed autonomy in my work. She is an outstanding academic with exemplary human qualities and it has been my honour to be her graduate student. My deepest thanks go to my co-supervisor, Dr Mathieu Sellier of Mechanical Engineering and assistant supervisor, Dr Larry J. Brackney of Electrical and Computer Engineering (currently working overseas). Simply, I would not have been able to reach this stage without their help. My sincere thanks and gratitude go to all the staff of the department including Paul, who kept me going. Thanks to my colleagues and friends who have been a great source of inspiration and a dependable source of knowledge, including Samuel, Montira, Mauvi, Vi, Stacy, Shannon to name a few. My thanks also go to Rob Munn of Mighty River Power for his advice and data used in this work. I am indebted to my father, mother and aunt who have always been sources of inspiration, support and blessing. It is my wife Nazneen, and children: Nafis and Nazif, who have been constant sources of support and have endured the inconveniences associated with my work.

I am thankful to the Mechanical Engineering Department and the University of Canterbury for the Premier International PhD scholarship. Mighty River Power has supported and partially funded this research, which I thankfully acknowledge.

Table of Contents

Table of Figures

Chapter 1

Introduction

1.1 Introduction

We are at a point of time when on one hand, the negative effects of anthropogenic atmospheric alteration are more evident than ever, and on the other, the demand for energy is ever increasing. Moreover, we are very close to peak oil if not experiencing it [1]. Peak oil does not mean we will run out of oil, rather it refers to the end of the first half cycle of the oil era. Growth has remained the prime mover of the economy for the first half cycle of the oil era [2], but after the peak oil, it may not be possible to achieve economic growth [3]. However, societies have yet to prepare for the post peak oil situation.

Some 20 years have passed since the publication of "Our Common Future" by the World Commission on Environment and Development in 1987, where the concept of sustainable development was formally stated [4]. However, an accepted practice of sustainable development and a definition of the acceptable limits to development are still far from being reached. With universal membership, (189 countries) *The United Nations Framework Convention on Climate Change* came into being [5].

The Convention sets an overall framework for intergovernmental efforts to tackle the challenge posed by climate change. It recognizes that the climate system is a shared resource whose stability can be affected by industrial and other emissions of carbon dioxide and other greenhouse gases. The convention entered into force on 21 March 1994 and member nations have approved a more stringent treaty, *The Kyoto Protocol* to combat climate change [6] which is also legally binding. The treaty came into force on 16 February 2005 and a total cut in emission of at least 5% from 1990 levels in the commitment period 2008-2012 was targeted.

1.2 Motivation

The huge challenge of emission reduction, growing energy demand and peak oil can be approached in two ways. Firstly, by improving energy conversion efficiency of traditional energy sources and secondly, switching to more and more renewable energy sources. Unfortunately, most renewable energy sources are dependent on climatic variation and are not suitable for base load operations. Geothermal energy, on the contrary, provides a clean, reliable source of renewable energy and is available in many parts of the world including New Zealand. Energy concentration in geothermal sources is much higher than in many other renewable sources.

Moreover, geothermal energy does not produce significant emissions[7, 8]. Geothermal power plants are considered to have significant lower CO_2 emissions than a standard combined cycle power plant or a pulverized coal fired power plant. Figure 1-1 shows a comparison of CO_2 emission from various geothermal power plants around the world and some conventional power plants.

Geothermal power production is not as dependent on variable precipitation levels as hydro electricity and it is uniquely reliable, achieving typical load factors of over 90%. The Wairakei power station in New Zealand has operated at a load factor of more than 90% for over 50 years with low operating costs [9]. This reliability makes geothermal power plants a very important part of New Zealand's diverse electricity supply system and currently, 7.6% of electricity is generated from geothermal power plants, from an installed capacity of 434.3 MW [10]. Geothermal power plants provide the base load generation for New Zealand, therefore these plants are of the

utmost importance to New Zealand's power supply system. Sustainable development in this sector relies on cautious and optimum utilization of resources. Installing plants with proper analysis including modelling and simulation can ensure this optimal utilization of resources.

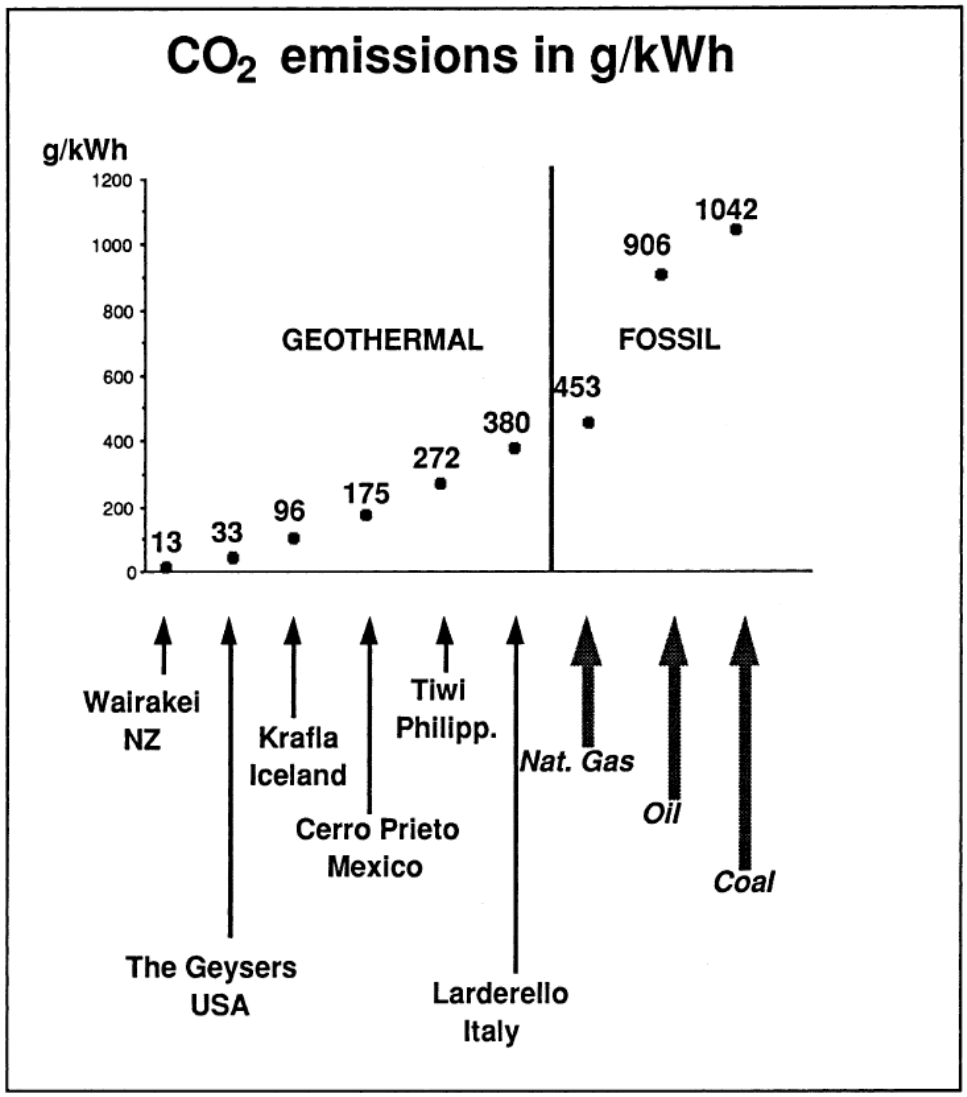

Figure 1-1: Comparison of carbon dioxide emissions from geothermal and fossil fuel-fired power plants (from [7])

1.3 Geothermal energy resources

Geothermal energy is defined as the heat that originates within the earth. This heat results from a combination of two sources: the original heat produced from the formation of the earth by gravitational collapse and the heat produced by the radioactive decay of various isotopes [11]. Direct use of geothermal energy was

noticed even in prehistoric time and the Etruscans, Romans, Greeks, Indians, Chinese, Mexicans and Japanese have all left evidence that they used hot water from geothermal sources [7]. Direct use of geothermal energy includes bathing, washing, cooking, space heating etc. To understand the source of geothermal energy it is very important to have a basic idea of the geological background and the next few sections discuss the geological background of geothermal energy.

1.3.1 The structure of the earth

The Earth is mainly made up of three concentric zones, namely, the crust, the mantle and the core. Figure 1-2 shows a schematic diagram of these zones. The Earth is sometimes compared to a chicken's egg, with the crust as the shell of the egg [12]. However, the Earth's crust is very insignificant compared to its diameter (about 35 km compared to 12700 km) and has very low thermal conductivity; therefore it is taking the Earth a billion years to cool down. The temperature of the crust's base is about 1100°C and the typical heat flow from the continental crust is 57 mW/m^2, whereas it is 99 mW/ m^2 for the oceanic crust. The Earth's average heat flow is 82 mW/ m^2 and the total global output is over $4x10^{13}$ W, four times more than the current world energy consumption of about 10^{13} W [7]. The crust is composed of some radioactive isotopes, in particular, uranium (U-235, U-238), thorium (Th-232) and potassium (K-40). Radioactive decay of these isotopes is responsible for geothermal energy in addition to the heat of the Earth's inner zones.

The mantle lies under the Earth's crust and extends from the base of the crust for about 2900 km. The mantle is closer to the Earth's surface beneath the ocean (about 7 km) compared to the continents (20-65 km). The Earth's crust and the uppermost mantle are together called the lithosphere which is very rigid and brittle and splits into a number of large blocks called lithospheric plates. More discussion regarding these plates is presented in the plate tectonic theory section.

The core of the Earth is divided into two zones. The outer core is about 2900 km to 5100 km from the Earth's surface. This zone is made up of liquid iron with a

temperature of 3700-4500 °C. The inner core is about 5100 km to the centre of the Earth and is made of solid iron with a temperature of 4500-6600 °C.

Our knowledge of the Earth, however, beyond a few kilometres from the surface, is based on indirect evidence and Figure 1-2 only depicts an ultra-simplified version. The interfaces of various zones are likely to be so irregular and the boundaries are so fuzzy that Figure 1-2 merely gives an idea.

1.3.2 The plate tectonic theory

The revolutionary "plate tectonic" theory was proposed by the German scientist Alfred Wegener (1880-1930) in 1915 [13]. According to this theory the rigid outer shell of the Earth, or the lithosphere is divided into several blocks or plates (continental and oceanic). All the landmasses were once connected in a gigantic supercontinent known as "Pangaea". The plates move slowly across the Earth's surface, at a speed of a few centimetres per year. These plates either pull away from each other, slide past each other, or move towards each other on top of the underlying plastic asthenosphere. The boundaries between plates are of three types: diverging plate boundaries, converging plate boundaries and conservative plate boundaries. Diverging plate boundaries occur when two plates are moving apart and this permits the upwelling of magma from the asthenosphere to form a new lithosphere.

Converging plate boundaries correspond to oceanic trenches, where two plates converge and collide. One plate slips or sinks below the other in the asthenosphere. Conservative plate boundaries are formed when two plates slide past each other and no lithosphere is created or destroyed in this process. Figure 1-3 explains the basic concept of plate tectonics.

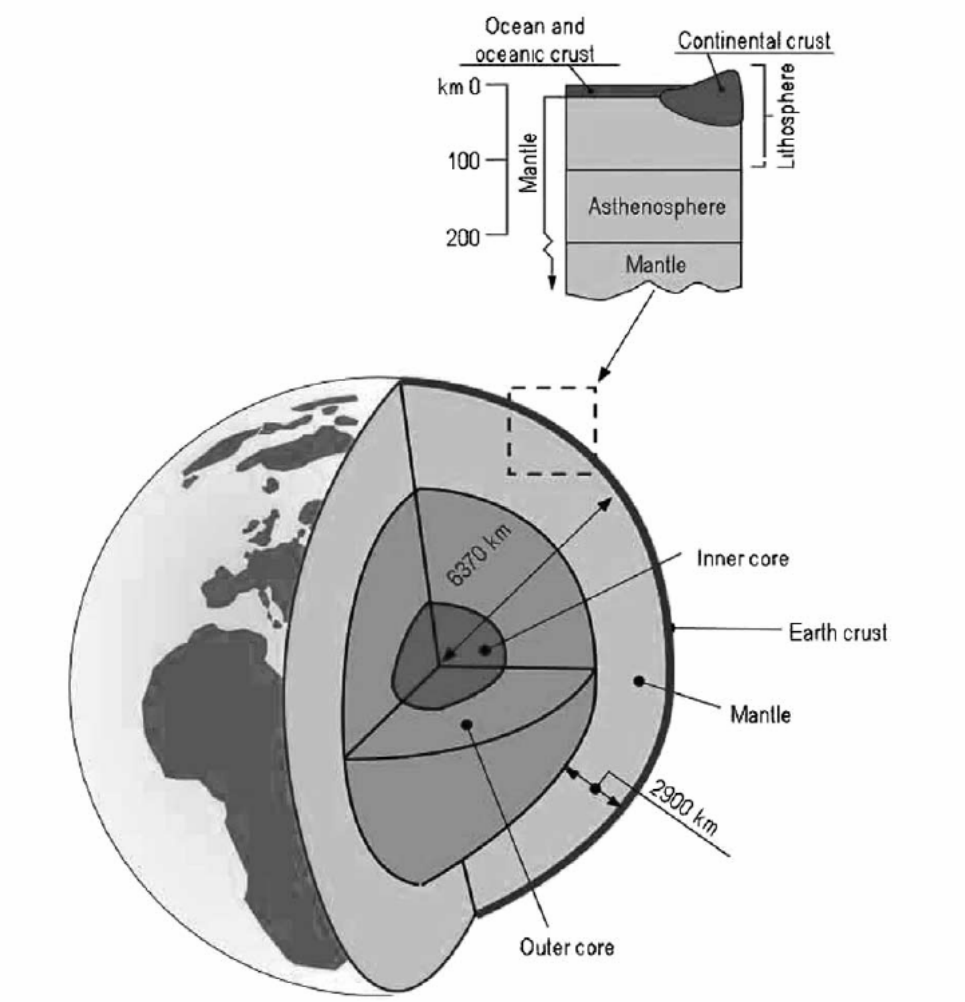

Figure 1-2: A schematic diagram showing the Earth's structure (from [7])

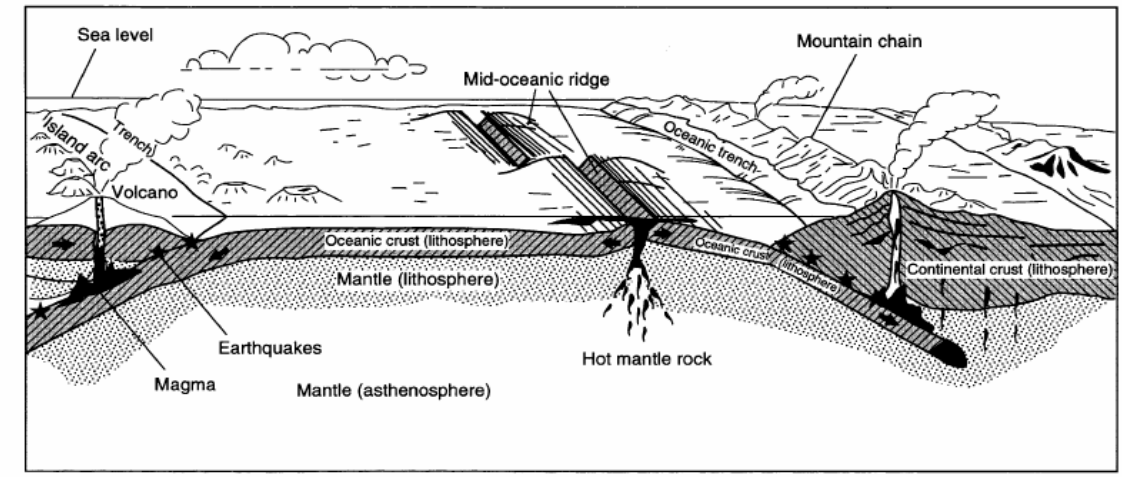

Figure 1-3: The basic concept of plate tectonics. Plates of rigid lithosphere overlie the asthenosphere of low strength. Mantle material rises below diverging plate boundaries (oceanic ridges) and plate material descends into the mantle at converging plate boundaries (oceanic trenches) (from [7])

1.3.3 Geothermal systems

As discussed earlier, the Earth's heat originates from two sources: original heat from the formation of the Earth by gravitational collapse and radioactive decay of various isotopes. In normal areas of the world, the temperature increases as a function of depth at a fairly constant rate of 3 °C per 100 m. However, in anomalous regions associated with volcanic or tectonic activity, the temperature gradient is about 10-30 times higher than normal. Temperatures of 300 °C are common in such regions at a depth of 1 km.

The extraction and utilisation of this large quantity of heat require a carrier to transfer the heat to accessible depths beneath the Earth's surface. Generally the heat is transferred from depth to sub-surface regions firstly by conduction and then by convection, with geothermal fluids acting as the carrier in this case. These fluids are essentially rainwater that has penetrated into the Earth's crust from the recharge areas, has been heated on contact with the hot rocks, and has accumulated in aquifers, occasionally at high pressures and temperatures (around 300°C). These aquifers (reservoirs) are the essential parts of most geothermal fields. In most cases, the reservoir is covered with impermeable rocks that prevent the hot fluids from easily reaching the surface and keep them under pressure.

We can obtain industrial production of superheated steam or steam mixed with water, or hot water only, depending on the hydro-geological situation and the temperature of the rocks present. Wells are drilled into the reservoir to extract the hot fluids, and their use depends on the temperature and pressure of the fluids and includes generation of electricity (the most important of the so-called high-temperature uses), or space heating and industrial processes (low-temperature uses). Geothermal fields, as opposed to hydrocarbon fields, are generally systems with a continuous circulation of heat and fluid, where fluid enters the reservoir from the recharge zones and leaves through discharge areas (hot springs, wells). During industrial exploitation fluids are recharged to the reservoir by reinjecting through wells the waste fluids from the utilisation plants. Figure 1-4 shows a geothermal steam field with its elements: recharge area, impermeable cover, reservoir and heat source. This reinjection process

may compensate for at least part of the fluid extracted by production, and to a certain limit will prolong the commercial lifetime of the field.

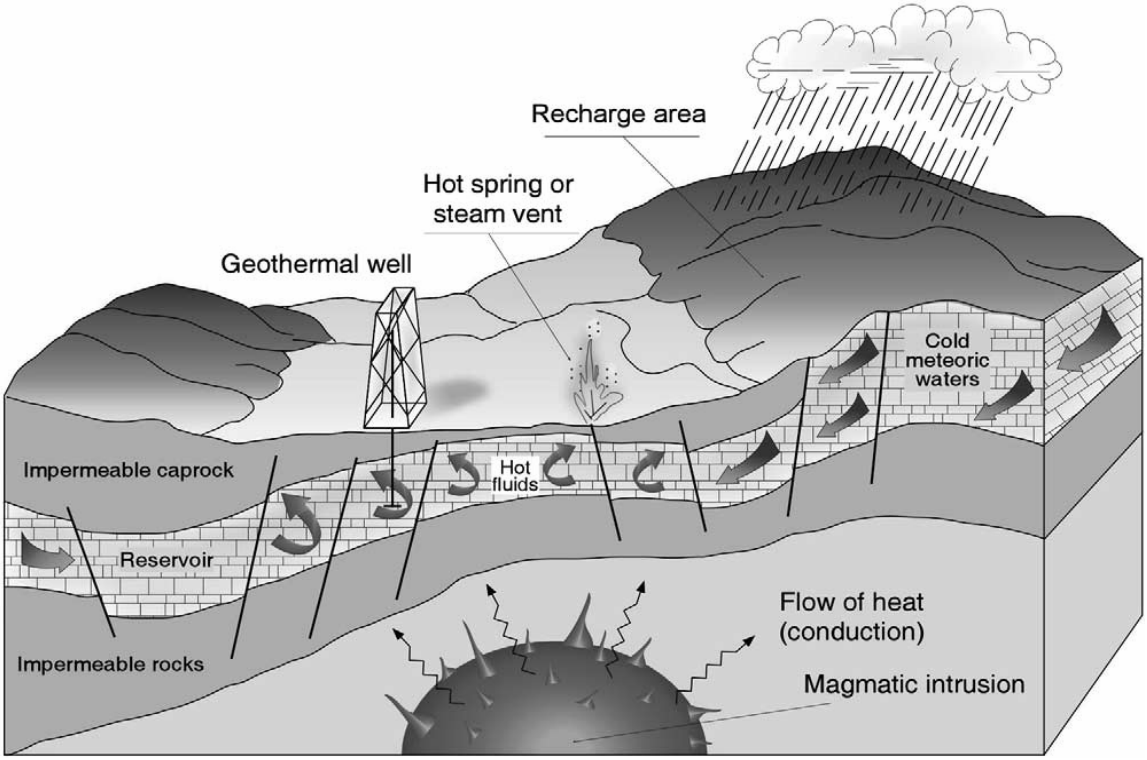

Figure 1-4: A schematic diagram explaining a geothermal steam field with its elements (from [7])

A geothermal field passes through four different phases or periods: (1) development, (2) sustainment, (3) decline and (4) renewable. During the last phase, a geothermal resource approach the ideal of a sustainable and renewable resource, and to attain it requires prudent management of the resource. In phase (1), the field is developed incremental, building up its power capacity in a number of plants. In phase (2), a reasonably steady state is achieved as the wells operated at some fraction of their full capacity. In phase (3), make-up wells are drilled to compensate for decline in well outputs but the thermodynamic properties of the resource begin to decline under continued exploitation. In phase (4), by scaling back the output of the power system, a sustainable level can be achieved.

With reservoir modelling and simulation, it is now possible to predict future characteristics of a reservoir with reasonable accuracy. A reservoir simulator is a computer code that embodies all of the essential properties of the formation, the geo-

fluid, and the environment together with the physical and chemical laws controlling their interactions to allow the extrapolation of the performance of the reservoir from the present time to a future time, usually, several decade away.

For geothermal resources with low permeability and/or porosity, Enhanced (or Engineered) Geothermal Systems (EGS) have been proposed [14]. It is supposed that if we can dig a well as far at the hot rock i.e. granite layer, introduce cracks to it, circulate water from surface via one hole and take out compressed water from another, we can unleash virtually unlimited amount of energy trapped in various granite layers through out the world. However, this technology is still in the stage of research and development, therefore, no further discussion is presented here.

Depending upon the reservoir temperatures, geothermal resources are divided into several categories. Table 1.1 summarizes the classification of various authors as presented by Etemoglu and Can [15].

Table 1.1 : Classification of geothermal resources by temperature (from [15])

Source	**Muffer and Cataldi (°C)**	**Hochstein (°C)**	**Benderitter and Cormy (°C)**	**Haenal et al. (°C)**
Low	<90	<125	<100	<150
Medium	90-150	125-225	100-200	-
High	>150	>225	>200	>150

1.3.4 Electricity Generation from Geothermal Energy

Electricity generation from geothermal sources is a much more recent industry, dating back to the beginning of the last century. The first experiments to produce electricity from natural steam from a geothermal source were conducted in Italy by Prince Piero Ginori Conti in 1904 and it was in 1913 that the first commercial generation of electricity began in Larderello, Tuscany, Italy. The global electricity production from geothermal energy reached 60 TWh in 2006 [16]. Although, at the global level, geothermal power production has a very small share of the mix, it meets a significant share of the total electricity demand in many countries e.g. Iceland (26%), El Salvador (20%), Philippines (18%), Costa Rica (14%), Nicaragua (11%) and New Zealand

(7%). Power generation is projected to triple to almost 180 TWh by 2030, doubling geothermal's share of 0.3% of global electricity-generation mix in 2006 [16]. Table 1.2 summarises some of the geothermal power plants installed and technology used in various parts the world.

Table 1.2 : Some geothermal power plants and technology used (from [17])

Plant name	Location (Country)	Technology used
Brady bottoming	USA	Binary
Rotokawa	New Zealand	Binary: recuperated
Nigorikawa (Mori) pilot	Japan	Binary
Kalina KCS-34, Husavik	Iceland	Binary
Rotokawa	New Zealand	Binary: simple
Blundell	USA	Single-flash
Rotokawa	New Zealand	Hybrid flash-binary
Heber SIGC	USA	Binary: dual-level
Beowawe	USA	Double-flash
Otake pilot	Japan	Binary: flash evaporator

1.4 Geothermal power plants

Geothermal energy can be utilized to generate electricity economically if the resource temperature is above 90°C [11]. There are two main reasons behind this. Firstly, below this temperature level, geothermal power plants are unlikely to be economically feasible and secondly, minerals dissolved in the geothermal fluid lose solubility significantly below a temperature of 80-90°C. Consequently, huge problems of corrosion and scale formation can occur in geothermal equipment. Nevertheless, the geothermal resources are very site specific and the characteristics of one reservoir can differ largely from another even when situated close to each other.

The current power plants for generating electricity from geothermal resources can be divided into two general types: steam and binary [11]. For steam rich geothermal field, steam can be directly used for power generation. Steam plants are the most cost-effective technology when the resource temperature is above 175 °C. Because such sites are rare, it is much more common for hot water from a geothermal resource to be flashed to steam by spraying it into a tank where its pressure is decreased. This can occur in either a single- or dual-stage process. A schematic of a typical flash plant is shown in Figure 1-5. The steam based (high quality resource) geothermal plants have

a simple design. Due to limited number of high quality resource around the world, the number of the steam plants is limited.

For the lower quality resource temperatures below about 175 °C, flash plants lose their efficiency. It is more efficient to transfer heat from the geothermal fluid to a volatile working fluid. Such plants are called binary plants because a secondary fluid is used in the actual power cycle. If the geothermal fluid is composed of steam and brine then a separator is used to separate them. The steam is normally first passed through a steam turbine and then used to heat the binary fluid and the brine is normally used directly to heat the binary fluid. Because all of the geothermal fluid is returned to the reservoir, the binary-cycle plants do not require mitigation of gaseous releases and the reservoir fluid volume is maintained. A schematic of a typical binary plant is shown in Figure 1-6.

Various kinds of working fluids have been proposed and used for binary cycle power plants including propane, pentane, hexane, R22, R113, R114, ammonia, ammonia-water solution etc. Environmental impact including greenhouse gas emission potential, toxicity, hazardous, and life time are important in working fluid selection. Some working fluids might ensure high cycle efficiency but may have high environmental impact to warrant their application in plant design.

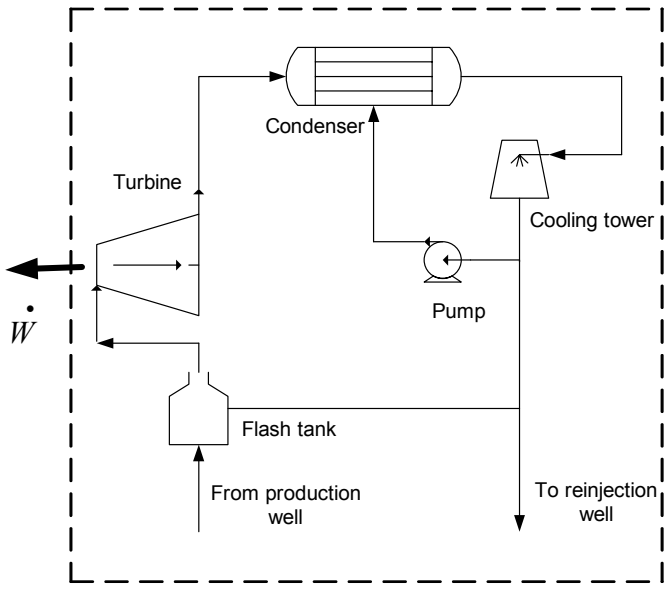

Figure 1-5: Schematic of a flash-steam geothermal power plant

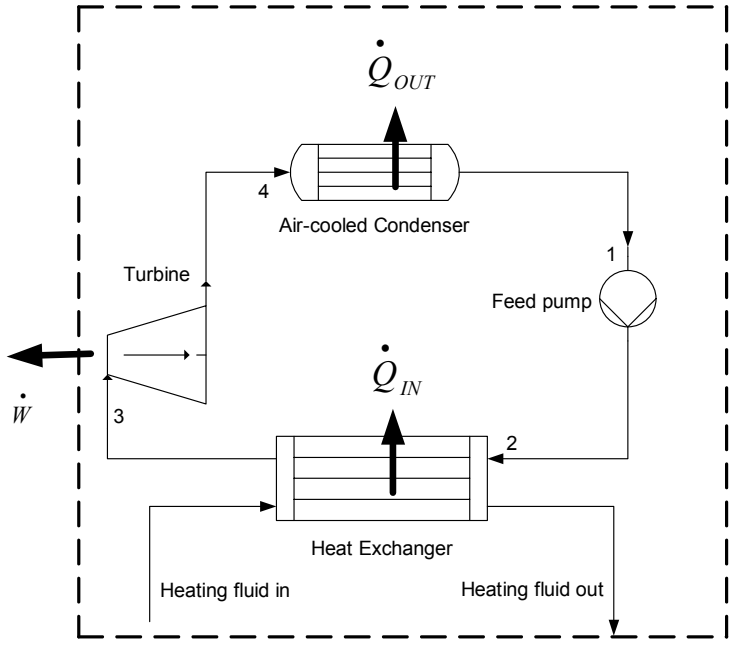

Figure 1-6: Schematic of a binary-cycle geothermal power plant

1.5 Plant performance

Geothermal power plants are generally designed based on constant resource characteristics. However, it has been observed in many geothermal power plants that the resource characteristics change significantly (yearly) throughout the lifetime of the plant. Consequently, deterioration of plant performance and unplanned design changes occur.

Local weather conditions affect the geothermal power plant performance in the short term (hourly) and cumulatively in the long term (yearly). Being a low temperature heat source, geothermal power plant often use binary cycles. Generally, binary cycles use air-cooled condensers, making the binary cycles more susceptible to weather conditions. As the ambient temperature increases, especially during the summer, the performance of an air-cooled binary cycle significantly reduced.

This dissertation discusses the environmental (geothermal resource characteristics and local weather) effects on geothermal power plant; and adaptive approaches to address the effect of change in environmental conditions to ensure optimal plant performance.

A new method for modelling the environmental effect on organic Rankine cycle has also been presented in this dissertation.

1.6 The aim of the present work

The aim of this work includes development of models for geothermal power plant applications that can be used for both long term and short term performance analysis. Developed models should be generic in nature which ensures wide range of application in geothermal power plants including performance prediction, design and optimization problems. Typically, when the model gets very complicated, a large number of parameters are required. However, the physical understanding as well as generality of the model becomes limited. Therefore models of this study should require few parameters but the models should be able to provide clear physical understanding, moreover the models should be reasonably accurate.

The scope of this work is to understand both long term and short term environmental effect on geothermal power plant performance and develop adaptive strategies to overcome them. Here "environment" is referred to as the weather conditions and location of the plant vicinity as well as the geothermal resource characteristics.

1.7 Outline of the Dissertation

This chapter has presented an introduction, the motivation and the aim of this work. Chapter 2 presents the literature review. Chapter 3 discusses the basics of the binary cycles. Chapter 4 presents an introduction to the Mokai 1 geothermal power plant which will be used as a case study in this work. Chapter 5 presents component models. The system model of Mokai 1 geothermal power plant based on the steady state operation and design conditions can be found in chapter 6. Adaptive approaches for long term performance improvements are discussed in chapter 7. Chapter 8 presents a new method to model a closed type organic Rankine cycle and two case studies. Adaptive approaches for short term performance improvements are discussed in Chapter 9. Concluding remarks are available in chapter 10.

Chapter 2

Literature review

2.1 Introduction

With unprecedented development in hardware and software, and the availability of a highly accurate physical properties database, it is now possible to model power plants to a high degree of accuracy in the quest for the best-case scenarios for cost, technical feasibility and optimum utilization of natural resources. This kind of study is very useful for "what if analysis" even before building a new plant. This chapter presents first: literature review on general methodology for modelling the power plants; second: previous work on geothermal power plant; and third: significance of this work to the literature. The main contributions of this work are also discussed towards the end of this chapter.

2.2 Literature review on general methodology for power plant modelling

This section discusses general methodology for modelling the power plants. Mathematical models are abstract representation of the physical world; there will always be modelling errors due to un-modeled dynamics and parametric uncertainties. Therefore, the aim of modelling is to achieve an objective with acceptable accuracy rather than accuracy of the model itself [18]. Objectives of modelling of power plant can be categorized in four major groups; however these groups may encompass more than one objective: a) controller design; b) power plant safety; c) power plant performance prediction and optimization; and d) power plant performance analysis and improvements. Following subsections discuss previous works encompassing the above four categories.

a) Controller design

Controller design mostly use semi-empirical modelling techniques. Semi-empirical models use a limited number of physically meaningful parameters that can be easily identified from performance measurements, while deterministic models require an exact knowledge of the geometry of all components. Usually, semi-empirical models are more robust than deterministic models and allow sharp decrease of the computational time [19].

Weng et al. [20] have proposed a robust feedforward-feedback controller for a wide range of operations of nuclear power plant. The feedforward element provides optimized performance over a wide operating range and the feedback element provides robust stability and performance. The feedforward control law is sythesized via nonlinear programming, which generates an optimal control sequence over a finite-time horizon under specified constraints.

Weng et al. [18] have discussed modelling of plant dynamics and uncertainties as needed for controller design of a 525 MW conventional power plant. The model was based on fundamental laws of physics and lumped-parameter approximation. The model was found to simulate power ramp up and ramp down in the range 40-100% under specified performance requirements.

b) Power plant safety

Power plant safety is a major area of application of modelling techniques to power plants. Models used for dynamic operation of nuclear power plants are the example of most rigorous modelling technique used in power plants. These models can be deterministic or combination of deterministic and semi-empirical with very high degree of accuracy. It helps to design robust safety system by “what if” analysis.

Pampin et al. [21] have presented a three-dimensional computational tool which has been developed and extensively used to assist in the safety and environmental assessment of the European Power Plant Conceptual Study (PPCS). The model was used for evaluation of activation inventories and temperature excursions in structures following hypothetical worst-case accident scenarios.

The United States Nuclear Regulatory Commission (USNRC) has been developing an advanced thermal hydraulic code named TRACE for nuclear power plant safety analysis. Wang et al. [22] have used TRACE for transient analyses of scenarios such as load reduction and turbine trip. The results were compared with the corresponding plant data from Maanshan nuclear power plant startup tests. The Maanhan TRACE model was found to predict the behaviour of important plant parameters with acceptable accuracy.

Kaliatka et al. [23] have presented modelling of a twin-unit, graphite moderated, boiling water, multichannel reactors nuclear power plant. Kaiatka et al. [23] have analysed large loss of coolant accident (LOCA) with emergency core cooling system failure and station blackout cases without any operator intervention; and when the cooling of reactor control rods are restored.

c) Power plant performance prediction and optimization

The plant performance can be expressed as an empirically derived function of various operating parameters including ambient temperature and condenser working pressure and temperature, result in a set of charts or curves. Empirical modelling approaches are common practice in industry and are well described in the literature [24, 25]. Such fitted curves are often plant specific and only apply for a narrow range of operations, rendering them limited for addressing the broader class of plant design and optimization problems.

In recent years application of artificial neural network and genetic algorithm in modelling thermal power plant are receiving attention [26, 27]. Models based on artificial neural network and genetic algorithm provide high degree of accuracy without complicated physics based model and are therefore interesting in plant performance prediction. However, models based on artificial neural network and genetic algorithm, are plant specific and often physical understanding of the process gets lost.

Ghaffari et al. [26] have presented a soft computing approach for modelling power plants in order to characterize the essential dynamic behaviour of the plant subsystems. The soft computing method consists of fuzzy logic, neural networks and

genetic algorithms. The measured data from a complete set of field experiments is the basis for training the models. The genetic algorithm is applied to the modelling approach in order to optimize the procedure of the training. The model was validated with the experimental data.

Smrekar et al. [27] have reported application of artificial neural network (ANN) for modelling real power plants. Input parameters for this prediction were selected from a large number of available parameters. Initial selection was made on a basis of expert knowledge and previous experience. However, the final set of input parameters was optimized with a compromise between smaller number of parameters and higher level of accuracy through sensitivity analysis. ANN was found to be particularly suitable for plant performance prediction for real life operation as uncertainty of a physical model increases with time as the equations representing the plant processes may become inappropriate due to the degradation of the plant [27].

Modelling helps optimizing plant performance. Korakianitis et al. [28] have reported that performance of a combined cycle cogeneration power plant is dominated by the gas-turbine performance. The performance of combined cycle cogeneration power plants can be improved by: i) maximizing turbine rotor inlet temperature in the gas turbine; ii) optimizing the gas turbine pressure ratio for gas-turbine performance; iii) optimizing steam turbine boiler pressure; and iv) maximizing steam injection in the gas turbine.

Exergy analysis became a standard tool for the thermal systems design, analysis and optimization. Szargut et al. [29] and Bejan et al. [30, 31] have provided the major tools needed for the application of exergy analysis to thermal systems and processes. El-Masri has used [32] exergy analysis to optimize operation of an air-cooled Brayton cycle gas turbine of a combined cycle plant. Chin and El-Masri [33] have used exergy analysis to identify optimum operating parameters of a dual-pressure bottoming cycle as a function of gas turbine exhaust temperature.

d) Power plant performance analysis and improvements

One of the major areas of application of modelling is power plant performance analysis for addressing the broader class of plant performance improvements. The

performance of gas turbines is highly affected by the ambient conditions. Erdem and Sevilgen [34] have analysed the effect of ambient temperature on the electricity production and fuel consumption of gas turbine plant. The design condition of the gas turbine was: sea level, 15ºC and 60% relative humidity. The model was used to simulate plant performance based on monthly average data of seven climate regions of Turkey. In the region where the ambient temperature was higher than the designed value, electricity generation reduces between 1.67% and 7.22%. Electricity generation increases about 0.27–10.28% when inlet air is cooled to 10ºC.

Dowoud et al. [35] have studied the gas-turbine inlet air cooling for boosting the power output during hot seasons. Reducing the inlet air temperature increases air density, consequently, decreases the compressor specific work. In a typical gas turbine plant, about one third of the power generated is consumed in the compressor. Therefore reduction in compressor work input lead to increased net power output in a plant. Dawoud et al. [35] have considered five possible inlet air cooling techniques: evaporative cooling, fogging cooling, absorption cooling using LiBr–H_2O solution, absorption cooling using NH_3-H_20 solution and vapour-compression cooling systems. Weather data in the form of ambient air temperature and relative humidity of two locations of Oman: Marmul and Fahud have been used as the case study. Net power out increased in all techniques considered. The vapour-compression cooling system increased the net power the most followed by absorption cooling using NH_3-H_20 solution, absorption cooling using LiBr–H_2O solution, fogging cooling and evaporative cooling.

Chuang and Sue [36] experimentally analysed the effect of condenser pressure and plant load on performance of a combined cycle power plant of Taiwan. The plant uses gas turbine (Brayton cycle) as the topping cycle and steam turbine plant (Rankine cycle) as bottoming cycle. This plant uses air cooled condenser (vacuum pressure) to cool the steam from low pressure steam turbine. With increase in ambient temperature the condenser pressure increased and consequently the plant power output and efficiency reduced. However, according to the power purchase agreements (PPA) in Taiwan, the capacity payment is based on the guaranteed power output during the operating period. To meet the obligation of PPA, Chuang and Sue [36] suggested lowering the air cooled condenser operating pressure as an option. The air-cooled

condenser is fitted with fans for forced convection. Increasing the number of fans in full load operation can lower the condenser operating pressure required to ensure power output of the plant as per the PPA.

Durmayaz and Sogut [37] presented an iterative method to calculate the condenser equilibrium condition of a pressurized water reactor nuclear power plant with cooling water temperature affected by weather conditions, increasing the cooling water temperature result in decrease in plant performance. The iterative approach allows the performance of the whole plant to be calculated using fundamental (deterministic) rather than empirical relationships.

Liu et al. [38] have reported the effect of wind flow on the plant performance of air-cooled conventional power plant. Liu et al. [38] have suggested change in physical orientation of the condenser and manipulations of the condenser fan speed as the measure to minimize the effect of wind direction and speed.

2.3 Previous works related to geothermal power plant modelling

This section discusses some previous works related to geothermal power plant. Modelling of conventional thermal power plants (e.g. coal fired steam turbine power plant and gas fired combined cycle power plant) is well known and mature. However, modelling of geothermal power plant is a developing area. One of the major differences between the conventional thermal power plant and geothermal power plant is the heat transfer in the boiler. In conventional power plant heat input is controlled by the operators depending on the power demand. In case of geothermal power plant, heat input is dependent on geothermal brine inlet flow and it varies depending on the reservoir characteristics. Therefore, the aim is to maximize the power output depending on available brine inlet flow. It makes modelling of geothermal power plant very complex and different from conventional thermal power plants. Moreover, geothermal resources are site specific and the resource characteristics may vary significantly from site to site or even in the same site among different wells.

Casella [39] has presented a model for controller design and optimization of a flush type geothermal power plant "Latera" of Italy. This plant uses low enthalpy heat source (low steam content) and also the geothermal fluid has high CO_2 content of about 3%. The geothermal fluid is flushed two times to produce steam used in the steam turbine. The high CO_2 content in the geothermal fluid is not suitable for the steam turbine so CO_2 is separated and discharged to the atmosphere. The model is used as an aid to design and test standard level and pressure control loops, whose actual performance would otherwise be difficult to predict due to the high degree of interconnection of the plant components. The model has also helped operating point optimizations for better plant performance.

When the geothermal resource temperature is low, it is more efficient to transfer heat to a low boiling temperature fluid, such plants are called binary cycle. A current trend towards the application of binary cycle to use the low temperature heat sources for electricity generation is noticeable [19, 40-47]. The advantages of Kalina cycle have been theoretically demonstrated [48], but organic Rankine cycle power plants have been found to be the most economic and proven technology [17]. Being a low temperature heat source, geothermal energy is an area of major application of the ORC [49-52].

Bai et al. [53] have presented a dynamic model for the transient performance of hot Spring Thermal Energy Conversion (STEC) plant, which uses a novel power cycle with binary mixtures as the working fluid. The dynamic model was based on thermodynamics and structural features of the power cycle. Bai et al. [53] have used models based on lumped parameter forms of the heat exchanging devices in order to avoid complicated model structures. Bai et al. [53] have concluded that STEC dynamic model offers a far less expensive method to understand the transients of STEC power plant than only experimental based approach.

Wei et al. [44] have presented a dynamic model to be used for the design of control and diagnostics systems of an ORC for waste heat recovery. This model has potential geothermal application. Wei et al. [44] have used two modelling approaches, based on moving boundary and discretization techniques for modelling heat exchanging devices and compared in terms of accuracy, complexity and simulation speed.

Simulations showed that both the models predicted the data within an accuracy of 4%. Moving boundary model was found less complex than the discretized version and moving boundary method is characterized by smaller order and higher computational speed. Therefore Wei et al. [44] have concluded that moving boundary method is more useful for controller design applications for modelling heat exchanging devices to be used in the ORCs.

Wei et al. [54] have presented optimization of a binary cycle power plant using exergy analysis. The results show: maximizing the usage of exhaust heat (in case of geothermal power plant it is geothermal fluid) as much as possible is a good way to improve system net power and efficiency; when the ambient temperature is too high, the system net power and efficiency will deteriorate with the departure from nominal state possibly exceeding 30%. Wei et al. [54] have concluded that choosing a proper nominal state is a good idea for improving the system net power and efficiency.

DiPippo [17] has reported system level exergetic efficiencies of several real geothermal power plant operating throughout the world. Exergetic efficiencies of these plants varied within 16% to 54%, depending on technology used.

2.4 Significance and main contributions of this work to the literature

This section discusses the significance of this dissertation in the context of the existing literature. This dissertation tries to analyse the environmental effect on geothermal power plant, specifically the binary cycle plant, and ways to improve plant performance under different environmental conditions. Here environment stands for both geothermal resources and ambient weather conditions.

Typically, geothermal power plants are designed based on constant environment conditions (resource characteristics and stable ambient temperature). However, it has been observed in many plants that the resource characteristics change significantly throughout the lifetime of the plant [55]. Binary cycle plants, specifically, air cooled condenser plants, are highly dependent on ambient air temperature [17, 56], which changes daily and seasonally. Consequently, deterioration of plant performance and unplanned design changes occur.

The environmental effect on geothermal power plant can be categorized as: long term and short term.

a) Long term environmental effect on geothermal power plant

A geothermal field passes through four different phases or periods [55]: (1) development, (2) sustainment, (3) decline and (4) renewable. During the last phase, a geothermal resource approach the ideal of a sustainable and renewable resource, and to attain it requires prudent management of the resource.

Geothermal power plants are very capital intensive and it is not very easy to change a plant to adapt to resource characteristics different from the original design. However, by appropriate reservoir modelling, it is now possible to predict future resource characteristics depending on various parameters including the rate of resource utilization, the percentage of brine reinjection etc. [57]. As an example, results of reservoir modelling of Rotokawa geothermal power plant of New Zealand are briefly discussed here. Figure 2-1 shows simulated pre-production natural state temperatures at Rotokawa field. There is an existing plant called Rotokawa I and another is in under development. Figure 2-2 shows the simulated enthalpy response for Rotokawa I plus Rotokawa II with 67% reinjection. Reduction in resource enthalpy is noticeable in Figure 2-2 for Rotokawa I and II with 67% reinjection.

Although the resource characteristics change over the life time (in the order of 30- 40 years) of a geothermal plant has been accepted as an established fact, a methodological approach to address the problem has not been discussed in the literature. This research tries to reduce the gap in the literature by introducing the concept of adaptive design approach for long term performance improvements for geothermal power plant.

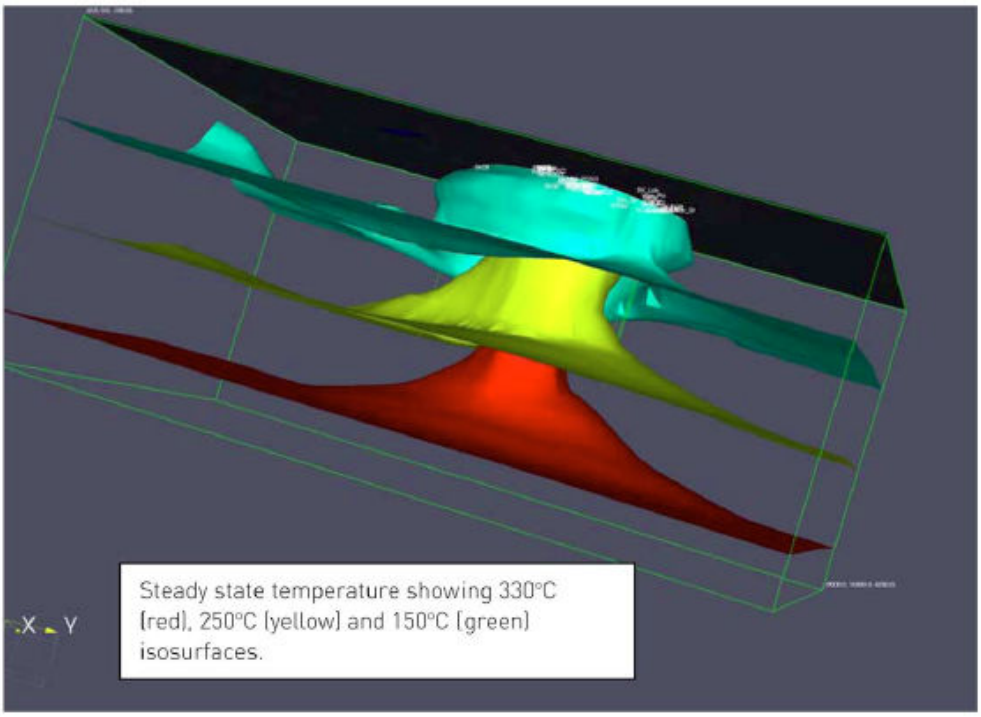

Figure 2-1: Simulated pre-production natural state temperatures at Rotokawa (from [57])

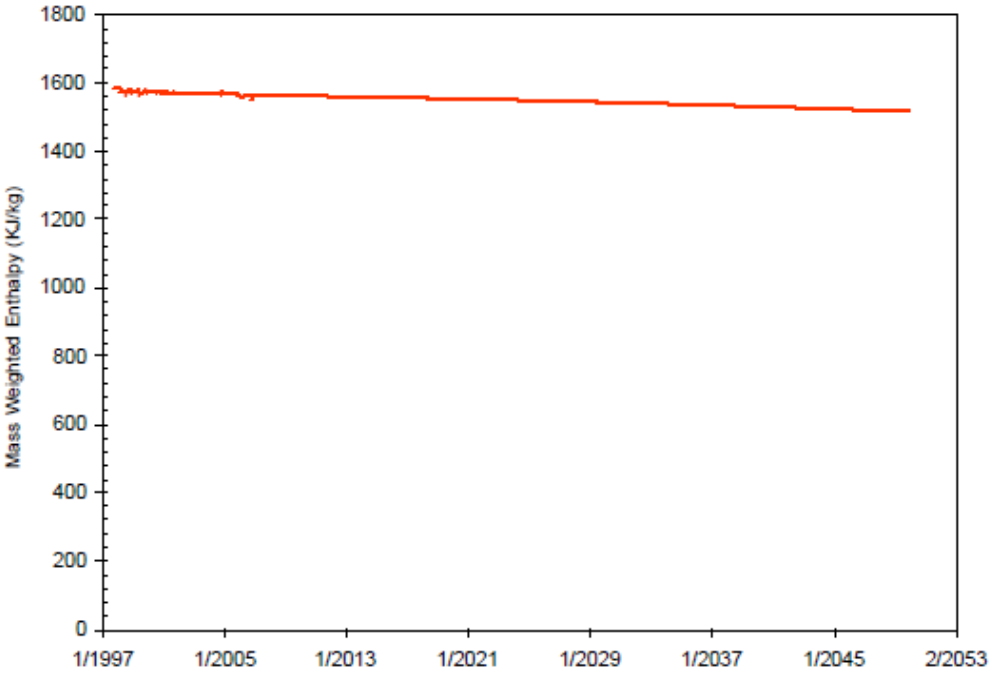

Figure 2-2: Simulated enthalpy response for Rotokawa I plus Rotokawa II with 67% reinjection (from [57])

b) Short term environmental effect on geothermal power plant

Binary cycle geothermal power plants often use air-cooled condensers that make these power plants more susceptible to weather conditions [17]. The second law of thermodynamics puts limit to the maximum efficiency of a system known as the Carnot efficiency. The efficiency of a Carnot cycle is given by

$$\eta = 1 - \frac{T_L}{T_H} \tag{2.1}$$

where, T_H is the heat source temperature and T_L is the heat sink temperature in absolute scale. If we assume the resource temperature to be constant in case of a geothermal power plant, the maximum possible efficiency for a thermodynamic system is achieved when T_L reaches ambient temperature. However, in reality, T_L never reaches ambient temperature, but is always a function of ambient temperature. When T_L increases, the Carnot efficiency deteriorates and if T_L decreases, the Carnot efficiency improves.

The short term modelling efforts of this work involved in plant performance prediction as well as plant performance improvements.

Plant performance prediction

New Zealand, Australia and some parts of the UK and the USA use a centrally coordinated nodal type of spot market for electric power. In this type of market, in a given time period, each node of the transmission network may receive offers from generating companies to inject power in the form of a price-quantity pair. At each node, there may also be a demand for electricity. A central dispatcher must then solve a network flow optimization problem to decide which generator supply offer to accept in order to meet all the demands [58].

Sometimes producers offer their output to the market at negative prices. Such negative offers are common in many electricity markets. Producers try to address by negative pricing, the problem of large, inflexible thermal power plants, which would be costly to shut down during periods of temporarily low demand. In New Zealand, to avoid the difficult problem of negative pricing, the producers are offered the right to produce (must run right) and can offer electricity at zero price; all other producers can

offer at very low prices (0.001 cent/kWh). The quantity of rights created is limited so that it will not be possible to meet all demands from zero-price generation alone [58].

When the demand is high, the electricity price is high [59]. It is therefore, very important for the power producers to generate power at a high rate to get the benefit of high demand. However, the producers need to inform their output in advance and it is very difficult to predict within 5% in variable weather conditions in advance.

The sensitivity of binary cycle power plants (such as the organic Rankine cycle) to ambient conditions creates challenges for producers to predict power output accurately. A model that can predict hourly plant performance on a daily basis would be very useful for optimizing capacity. Plant performance can be modelled in many ways including: empirical, semi-empirical and deterministic approaches discussed in section 2.2. Empirical and semi-empirical approaches are very plant specific and only apply for a narrow range of operations, rendering them limited for addressing the broader class of plant design and operation.

Condenser equilibrium pressure of an air-cooled condenser is directly related to the plant power output [36]. The ambient temperature influences the condenser equilibrium condition (pressure-temperature) and hence, power output. Durmayaz and Sogut [37] presented an iterative method to calculate the condenser equilibrium condition of a pressurized water reactor nuclear power plant with cooling water temperature (heat sink) affected by weather conditions. The effect of ambient temperature on an air-cooled organic Rankine cycle (ORC) is different than effect of ambient temperature on a pressurized water reactor nuclear power plant. First: the ORC has closed cycle operation and second: due to air-cooled condenser, the effect of ambient temperature is more prominent on the ORC. As ambient temperature acts as the heat sink temperature and the ORC has closed cycle operation, changing ambient temperature shifts the ORC on the *T-s* plane.

Modelling based on such level of physical understanding for plant performance prediction as well as broad range of conceptual design and optimization was not found in the recent literature. Therefore in the literature a need exists for a deterministic model of the ORC which can predict plant performance with reasonable

accuracy as well as provide better understanding of the physical process to be used in plant performance improvements. This dissertation presents an iterative method for modelling the air-cooled organic Rankine cycle which would provide plant performance with reasonable accuracy as well as better physical understanding of the process.

Plant performance improvement

The air-cooled organic Rankine cycle geothermal power plant produces less power when the ambient temperature is high. Kutcher and Costenaro [59] have done an assessment of evaporative cooling enhancement methods for air-cooled geothermal power plants. The analysis is based on a 1 MW binary cycle plant at Empire, Nevada USA. Kutcher and Costenaro [59] have concluded that the air-cooled binary cycle geothermal power plants can benefit significantly from the use of evaporative cooling enhancement in the summer. However, an analysis of evaporative cooling enhancement for air-cooled binary cycle based on a commercial ORC geothermal power plant using local weather data is not available in the literature. This dissertation tries to fill the gap in the literature by providing performance improvements analysis using evaporative cooling as an option of a commercial air-cooled ORC geothermal power plant using local weather conditions.

Several studies have been reported in the literature that deals with the optimization of binary cycles in pursuit of improved efficiency, cost reduction and maximization of outputs. Desideri and Bidini [60] have showed that, there exists a potential for optimisation of the binary cycle geothermal power plant performance by modifying parameters such as the turbine inlet pressure and the type of working fluid used.

Lu and Goswami [61] have presented optimization study of a novel combined power and refrigeration cycle. A procedure for optimizing the operating conditions of the cycle based on maximizing the second law efficiency, power output, and refrigeration output of the cycle with variable temperature heat sources is discussed in Lu and Goswami's work [61].

Madhawa Hettiarachchi et al. [50] have presented a optimum design criterion for ORC power cycles utilizing low-temperature geothermal heat sources. The objective

function was to minimize the ratio of the total heat exchanger area to net power output which ensured a cost-effective design.

Dai et al. [62] have presented optimization of thermodynamic parameters of ORC for different working fluid. Exergetic efficiency was used as the objective function. The optimization was performed using genetic algorithm.

The optimization studies discussed above, represent the design phase. In real life operation of a plant, the operating parameters of a binary plant may change resulting in suboptimal operation.

Applications of real time optimization and control techniques are often noticeable in building utility services industry to minimize energy consumption. For example, Santamouris and Lefas [63] have discussed design and control of hybrid solar houses using microcomputers. Bakos [64] has discussed the optimal control operation of an auxiliary heating system used as backup in a passive-solar-heated system. Ekren and Kucuka [65] have analysed energy saving potential of chiller system with fuzzy logic control. However, application of real time (or hourly) optimization techniques in power plant operation is rare.

Conventional power plants are associated with large load and are mostly water-cooled. Water cooling makes conventional power plants less susceptible to weather conditions. Thus a real time plant performance optimization may not be very suitable in water-cooled conventional power plant. On the contrary, binary cycle geothermal power plants are often built as modular basis [46] and very sensitive to ambient temperature change making them good candidate for real time (or hourly) optimization. This dissertation introduces optimization of ORC plant performance by optimizing operating points parameters based on hourly weather data and geothermal fluid flow rate in the quest of performance improvements.

The main contributions of this work

The main contributions of this dissertation to the subject are summarized as follows:

- Adaptive design concept for long term plant performance improvements

- A physics based iterative method for modelling environmental effect on short term performance
- Adaptive approach for short term performance improvements by using water-augmented cooling system
- Adaptive approach for short term performance improvements by optimizing cycle operating point parameters of the plant

In an adaptive design, if provisions are allowed for a plant to adapt to resource characteristics change at the time of building, a great deal of effort and money can be saved in the long run. However, the initial investment cost might go up as a consequence of adaptive design but over the life span of the plant the total benefit may be greater.

This work presents an approach for modelling an organic Rankine cycle (closed cycle) that uses fundamental thermodynamic (deterministic) models of components. The novel approach in this work is to use the design conditions as an initial guess and then to fit the fundamental model to real plant data. Of course, a real geothermal power plant does not have sufficient data to fit all parameters. The condenser operating conditions are considered as the most influencing parameter on a 24 hours time scale. The method is implemented by an iterative method that searches for both condenser and vaporizer exit state that satisfies the ORC cycle energy balances on all components. The termination of search can be achieved by either attainment of a desired equilibrium condition or by reaching constrains (either physical or supplied by an operator to run a plant at optimum condition). This work also explains how the ambient temperature affects an ORCs and how it is shifted in the *T,s* plane from its original operating point due to change in the ambient temperature. Although, the main interest of this work was mainly in ORCs, the developed method can be applied to any closed cycle operation of a Rankine cycle.

Plant performance improvements by adopting water augmented cooling and optimizing plant operating parameters are also presented here and considered as important contributions of this work. The short term improvement in plant

performance ultimately leads to better performance cumulatively over long period of time.

2.5 Summary

Modelling of conventional power plant is a mature field. However, modelling geothermal power plant is a developing area. One of the major differences between the conventional thermal power plant and geothermal power plant is the heat transfer in the boiler. In conventional power plant heat input is controlled by the operators depending on the power demand. In case of geothermal power plant, heat input is dependent on geothermal brine inlet flow and it varies depending on the reservoir characteristics.

Geothermal power plants performance is dependent on the environment. There are long term variations as well as short term variation in the environment leading to deterioration of plant performance. In the literature, there exists scope for both long term and short term performance improvements. A need for a deterministic model of the ORC is also felt. This dissertation fills some of these gaps.

Chapter 3

Basics of Binary Cycle

3.1 Introduction

This chapter discusses basics of binary cycles. At first the classification of the binary cycle is presented. Then organic Rankine cycle and Kalina cycle are discussed. The advantage of the Kalina cycle over the organic Rankine cycle is then discussed. The discussion is mainly limited to the thermodynamic aspect of these cycles.

3.1 The binary cycle

Owing to technological development, as well as the increased price of fossil fuel, many technologies are now becoming more realistic and feasible than before. As a result, much interest in binary cycle geothermal power plants is noticeable. Many binary cycle geothermal plants have been built during the last decades and many are under way throughout the world. A schematic of a typical binary plant is shown in Figure 3-1. When the geothermal resource temperature is low (below 175 ºC), it is more efficient to transfer heat from the geothermal fluid to a relatively volatile working fluid.

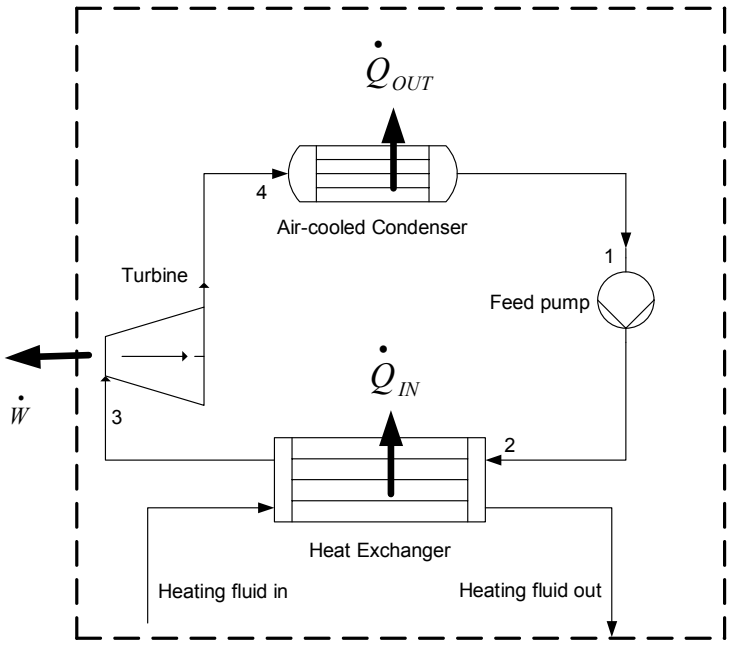

Figure 3-1: Schematic of a binary-cycle geothermal power plant

The ability to use low temperature resources (low enthalpy) and the possibility of reinjecting the used geothermal thermal brine (low emission) are the two most attractive features of binary cycle geothermal power plants. Binary cycles are divided into two major groups depending on the working fluids: pure substance and a mixture of two or more pure substances. Examples of pure substances include propane, pentane, R22, R13, ammonia etc. The binary cycle that uses organic fluids is also known as the Organic Rankine Cycle (ORC). Examples of mixtures include ammonia-water, also known as the Kalina Cycle. A third type of working fluid, non-flammable azeotropic fluid has been proposed by some authors [49]. The following sub-sections explain some of these binary cycles.

3.2 The organic Rankine cycle

An Organic Rankine Cycle (ORC) plant uses the same principle as the Rankine cycle except the working fluid is an organic fluid instead of water. The following four basic processes [66, 67] are involved as depicted in Figure 3-1:

1-2: Reversible adiabatic pumping process in the pump

2-3: Constant-pressure heat transfer in the vaporizer/preheater

3-4: Reversible adiabatic expansion in the turbine

4-1: Constant-pressure heat transfer in the condenser

Rankine cycles are classified in two groups depending on the shape of the temperature dependence vapour-liquid equilibrium line and the operating pressure at which the working fluid takes heat from the heat source.

The shape of the vapour-liquid equilibrium line is an important parameter in designing a power plant. Designers always try to make sure that the turbine operates at the superheated zone to avoid expensive repair or replacement of turbine blades damaged by erosion that may be caused by droplets of wet vapour. Figure 3-2 presents a typical bell shaped vapour-liquid coexistence curve and Figure 3-3 presents a typical vapour-liquid coexistence curve inclined to the right hand side in *T,s* diagrams. The advantage of the latter over the former is that even without superheating, the chance of condensation of the working fluid is minimal inside a turbine where the working fluid undergoes isentropic expansion.

The operating pressure of the working fluid in the vaporizer determines whether there will be liquid-vapour phase change or not at constant temperature-pressure. If the working pressure is more than the critical pressure then the working fluid vaporizes without constant temperature-pressure phase change. Both Figures 3-2 and 3-3 present subcritical working pressures. Figure 3-4 presents a supercritical cycle as suggested by Gu and Sato [68, 69]. A supercritical cycle may be able to extract more heat from the heating medium as there is no constant temperature-pressure phase change process as it is present in the subcritical pressure zone. The constant temperature-pressure phase change puts constrain to the maximum possible heat transfer between the heat transferring fluids. The maximum possible heat transfer is limited by the minimum temperature difference between the heat transferring fluids, known as the pinch point.

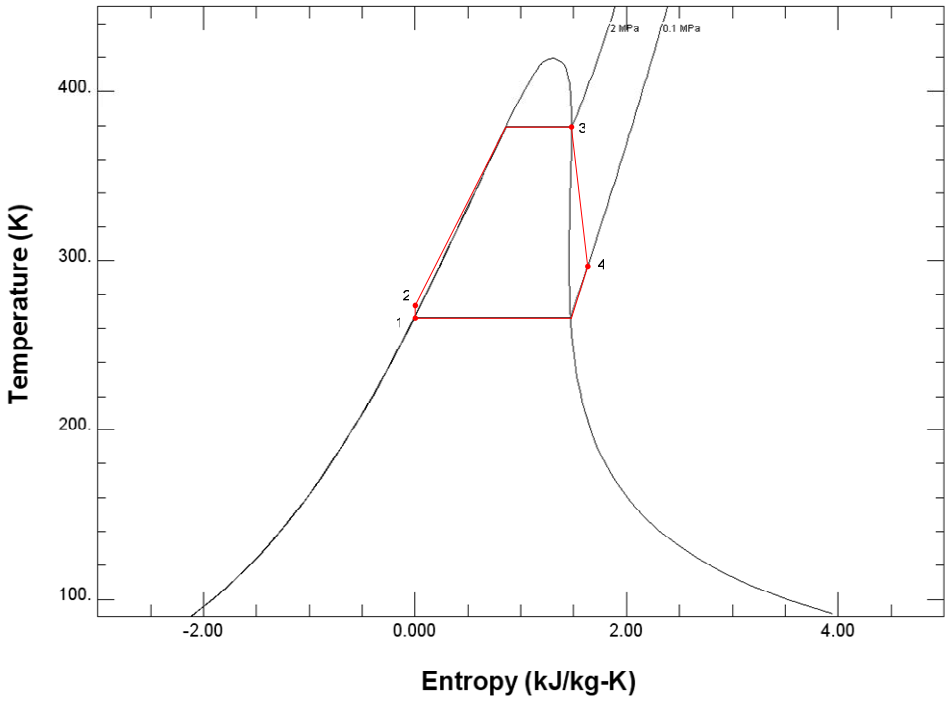

Figure 3-2: ORC in the *T,s*- plane for a typical bell-shaped coexistence curve fluid (butane) and saturated vapour at the turbine inlet (generated by Refprop [70] physical properties database)

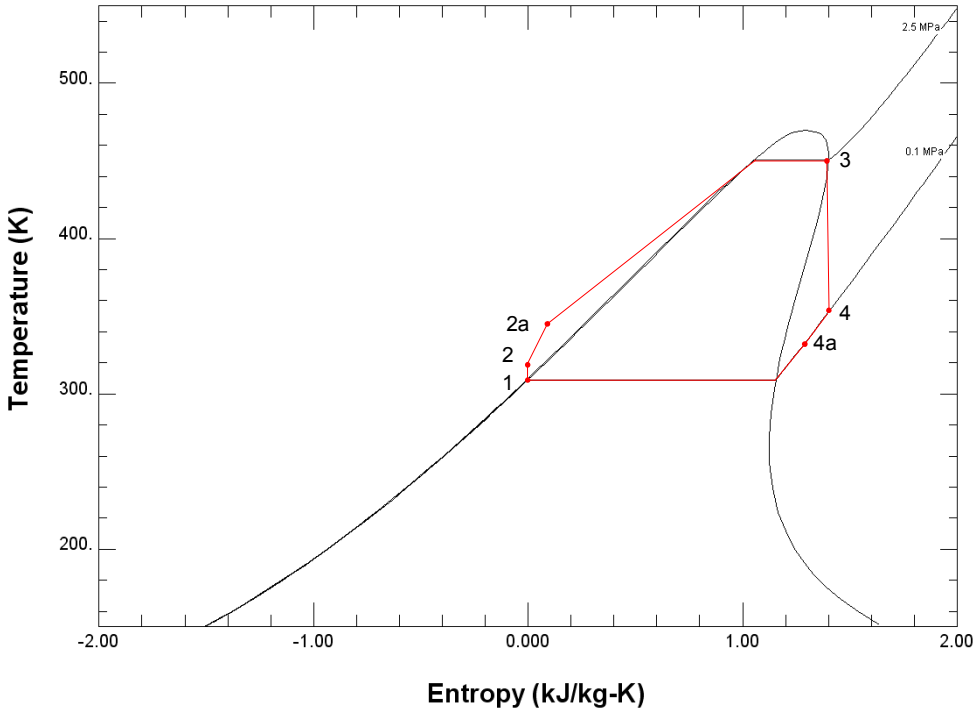

Figure 3-3: ORC in the *T,s*-plane for a typical inclined vapour-liquid coexistence curve fluid (pentane) and saturated vapour at the turbine inlet (generated by Refprop [70] physical properties database)

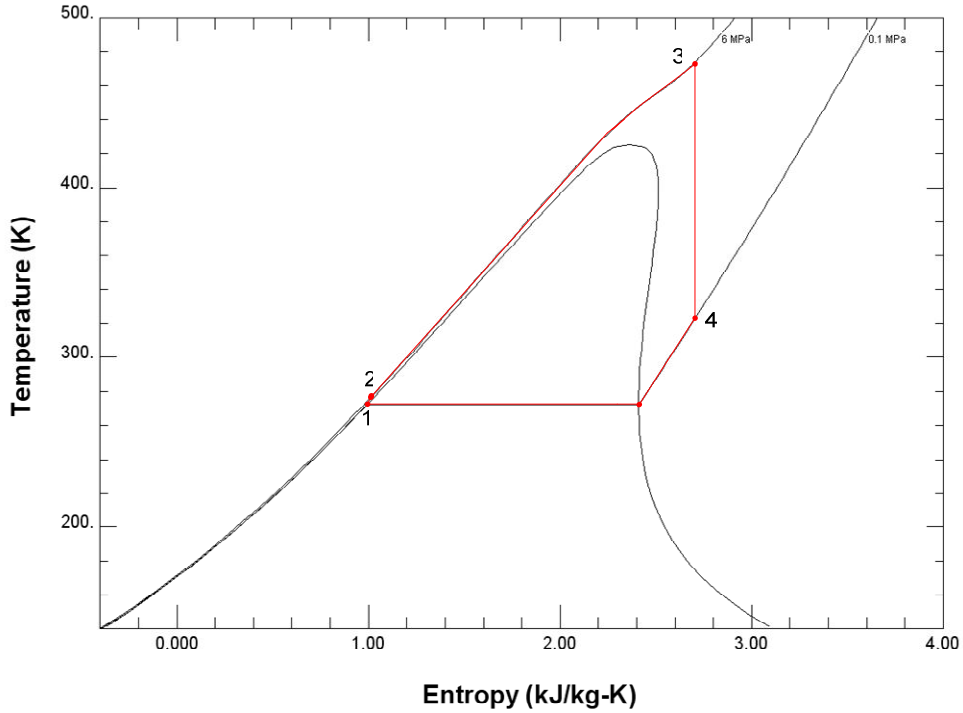

Figure 3-4: ORC in the *T,s*- plane for a supercritical pressure cycle with butane as the working fluid (generated by Refprop [70] physical properties database)

3.3 The Kalina cycle

The Kalina cycle is a modified Rankine cycle receiving a great deal of interest recently. In a Kalina cycle instead of pure working fluid, an ammonia-water mixture is used as the working fluid. An ammonia-water mixture has a range of variable boiling points depending on the percentage of the two components. This allows more heat to be extracted from a high temperature heat source or brine in a boiler or vaporizer. This is in distinct contrast to the constant boiling/condensing temperature of pure components such as water or organic fluids [48].

A basic parameter in sizing heat exchangers is called pinch point and is simply the minimum temperature difference between two fluids. If there is a large temperature difference between fluids, the hotter fluid can easily transfer energy to the cooler fluid with a smaller surface area in a heat exchanger. However, if the temperature difference is small, the surface of the heat exchanger must be increased. A pure substance has a fixed temperature for a given pressure when the substance changes its phase. In a Kalina cycle, evaporation and condensation both happen at constant pressure but variable temperature. The temperature range depends on the composition

of the fluid. The use of a mixture as the working fluid adds one degree of freedom, which allows manipulating the pressure in the system by changing the composition of the mixture.

Figure 3-5 depicts a schematic diagram of simplified arrangements of a Kalina cycle with the process explained in Figure 3-6. A 70/30 ammonia-water solution has been taken as an example. The work is produced by isentropic expansion of working fluid in the turbine (process 3 to 4). Then it passes through a recuperator where some of the heat is recovered from the exhaust of the turbine. As the heat transfer process is more efficient in the Kalina cycle, internal heat recovery is a very common practice.

The fluid after recovering heat in the recuperator is dumped into a condenser where a lean mixture of 34 percent ammonia is sprayed. This changes the concentration of the turbine exhaust stream from 70 to 45 percent ammonia. The mixture is then cooled to a final temperature of 20°C (state point 1). By changing the concentration to 45 percent, the condenser can at the same heat sink temperature, condense the turbine exhaust at a lower pressure of 200 kPa (state point 1). This is an added advantage of the Kalina cycle over the conventional Rankine cycle.

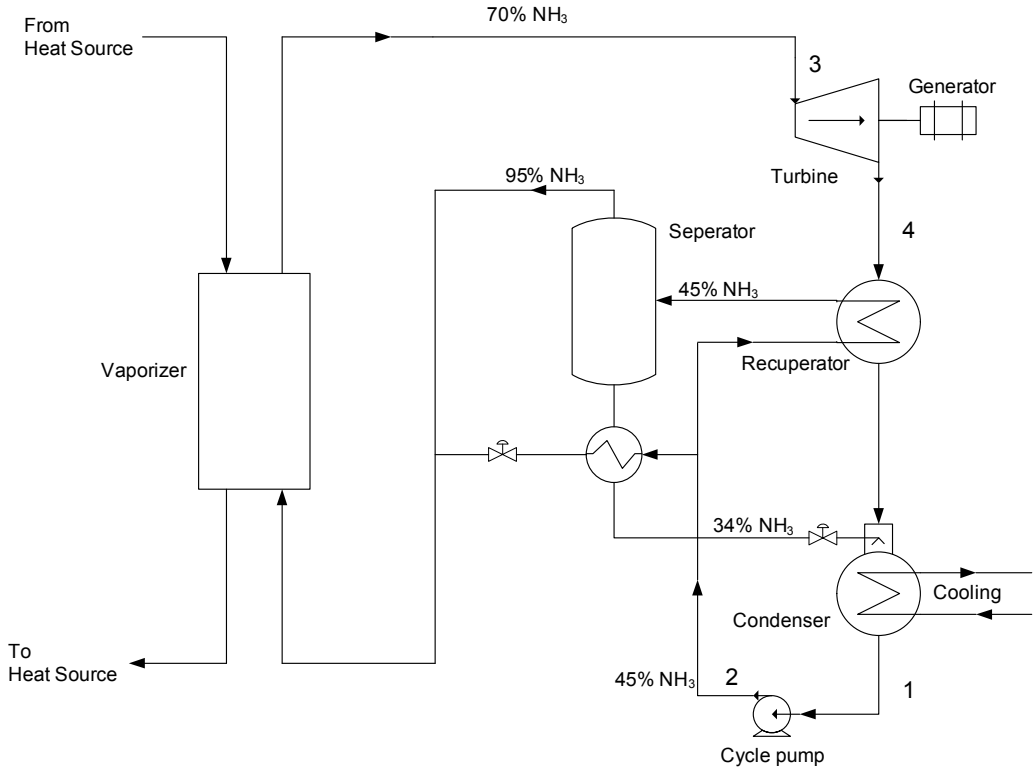

Figure 3-5: Schematic of a simple Kalina cycle (adjusted from [48])

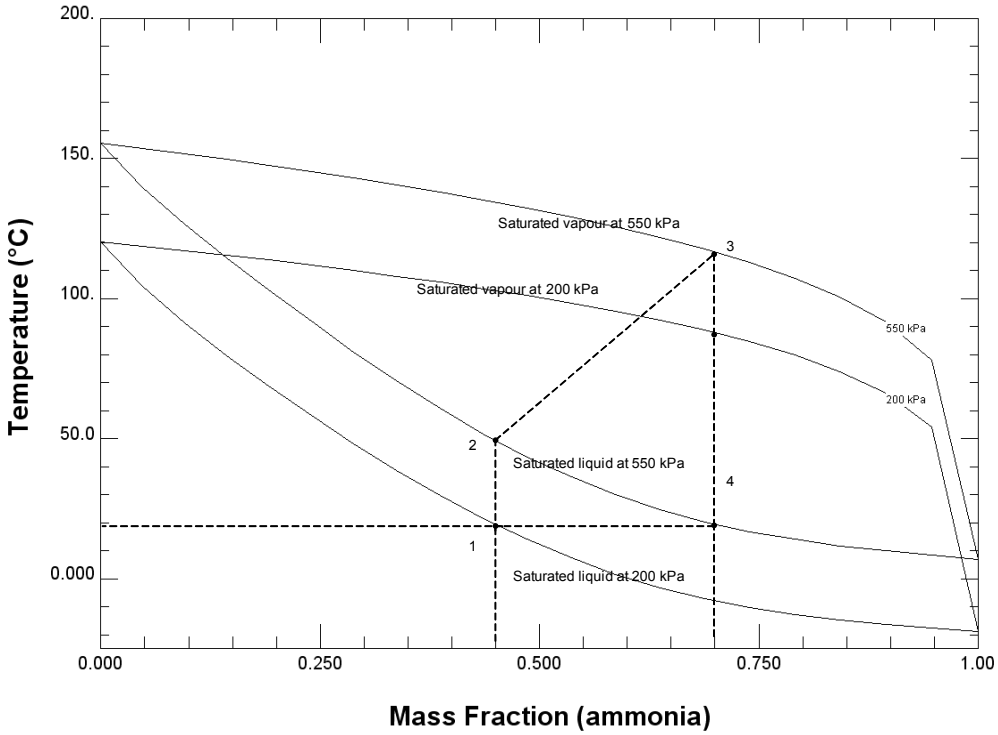

Figure 3-6: The ammonia-water phase diagram explaining the absorption process of the Kalina cycle presented in Figure 3-5 (generated by Refprop [70] physical properties database)

3.4 Summary

This chapter has discussed the basics of binary cycle. Then the classification of binary cycles is presented. Two types of binary cycles which are receiving recent interest are discussed in detailed: the organic Rankine cycle and the Kalina cycle. In contrast to organic Rankine cycle, which uses pure substances as the working fluid, Kalina cycle uses ammonia-water mixture as the working fluid. . An ammonia-water mixture has a range of variable boiling points depending on the percentage of the two components. This allows more heat to be extracted from a high temperature heat source or brine in a boiler or vaporizer.

Chapter 4

The Mokai 1 Geothermal Power Plant

4.1 Introduction

This chapter introduces the Mokai 1 geothermal power plant which has been chosen for the case study of this work. Tuaropaki Power Company and Mighty River Power Company (MRP) jointly own this plant and MRP also operates this plant. The Mokai 1 plant was built by a company named Ormat in 1998, and although, this plant is run by MRP, much information as well as the reasoning behind many designs is not readily available from MRP.

4.2 Location and weather in the plant vicinity

The plant is situated about 30 km north-west of the township of Taupo, in the North Island of New Zealand (Figure 4-1). Figure 4-2 represents the ambient temperature in the form of dry bulb and wet bulb for the year 2005 of the Taupo volcanic region. During the summer (November – February), the temperature averages about 15-20°C and in the winter (March – October) the temperature averages about 10-15°C.

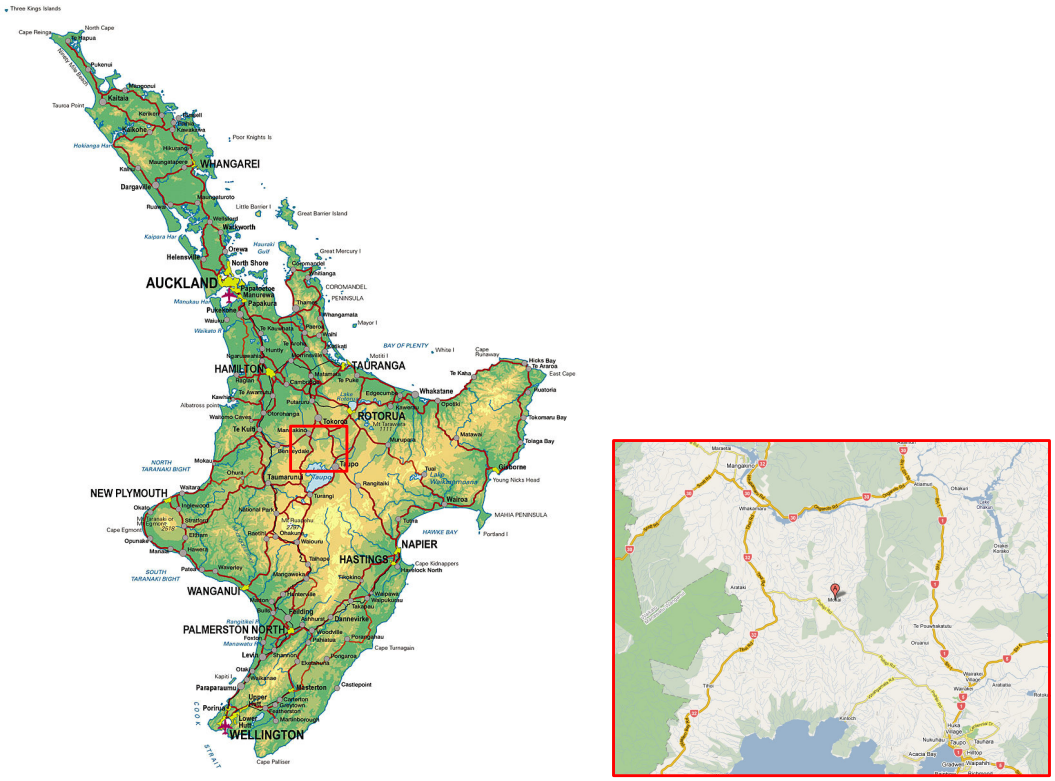

Figure 4-1: Location of Mokai in the North Island of New Zealand (source [71])

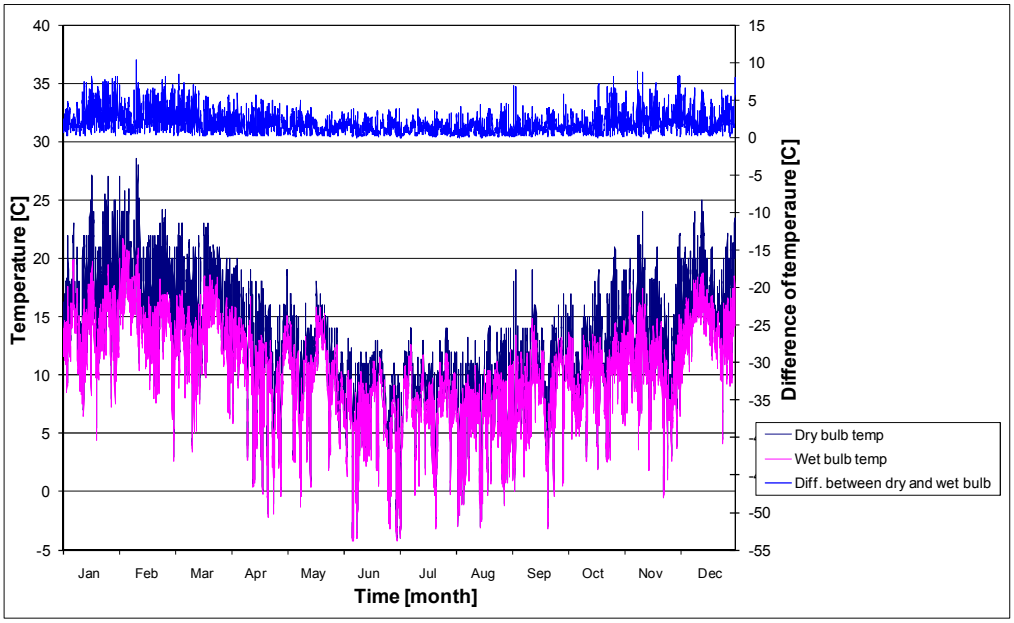

Figure 4-2: Dry bulb and wet bulb temperatures of Taupo (Latitude -38.744, Longitude 176.081 and Height 400 m) in the year 2005 (source [72])

4.3 Brief description of Mokai 1 geothermal power plant's process flow

In this section brief description of Mokai 1 geothermal power plant's process flow is presented. Mokai 1 has a design output of 59 MW. Figure 4-3 schematically presents the heat and mass balance of the plant. The geothermal fluid is a mixture of brine and steam. The steam is first separated in a separator from the brine and is fed into the steam turbine. The waste heat of the steam turbine is recovered from the exhaust steam in a vaporizer by heating pentane to be used in the bottoming ORC units, named after the manufacturer, Ormat Energy Converter (OEC).

The steam is equally divided among four identical OECs namely: 11, 12, 21 and 22. The steam from the vaporizer is collected as condensate in a condenser and it is used in the preheater to raise the temperature of the incoming pentane liquid before it enters the vaporizer. Each of the OECs comprises two turbines coupled to a single generator. Figure 4-4 shows the heat and mass balance of a bottoming OEC.

The separated brine is used to run two identical units, OEC 1 and OEC 2. Figure 4-5 shows the heat and mass balance of one of these plants. Both plants have two turbines, high pressure and low pressure. High-pressure pentane vapour from the vaporizer first passes through the high-pressure turbine then to the low-pressure turbine and is then dumped into the air-cooled condenser via a recuperator.

Pictures of the Mokai 1 geothermal power plant along with major components are presented in appendix 1.

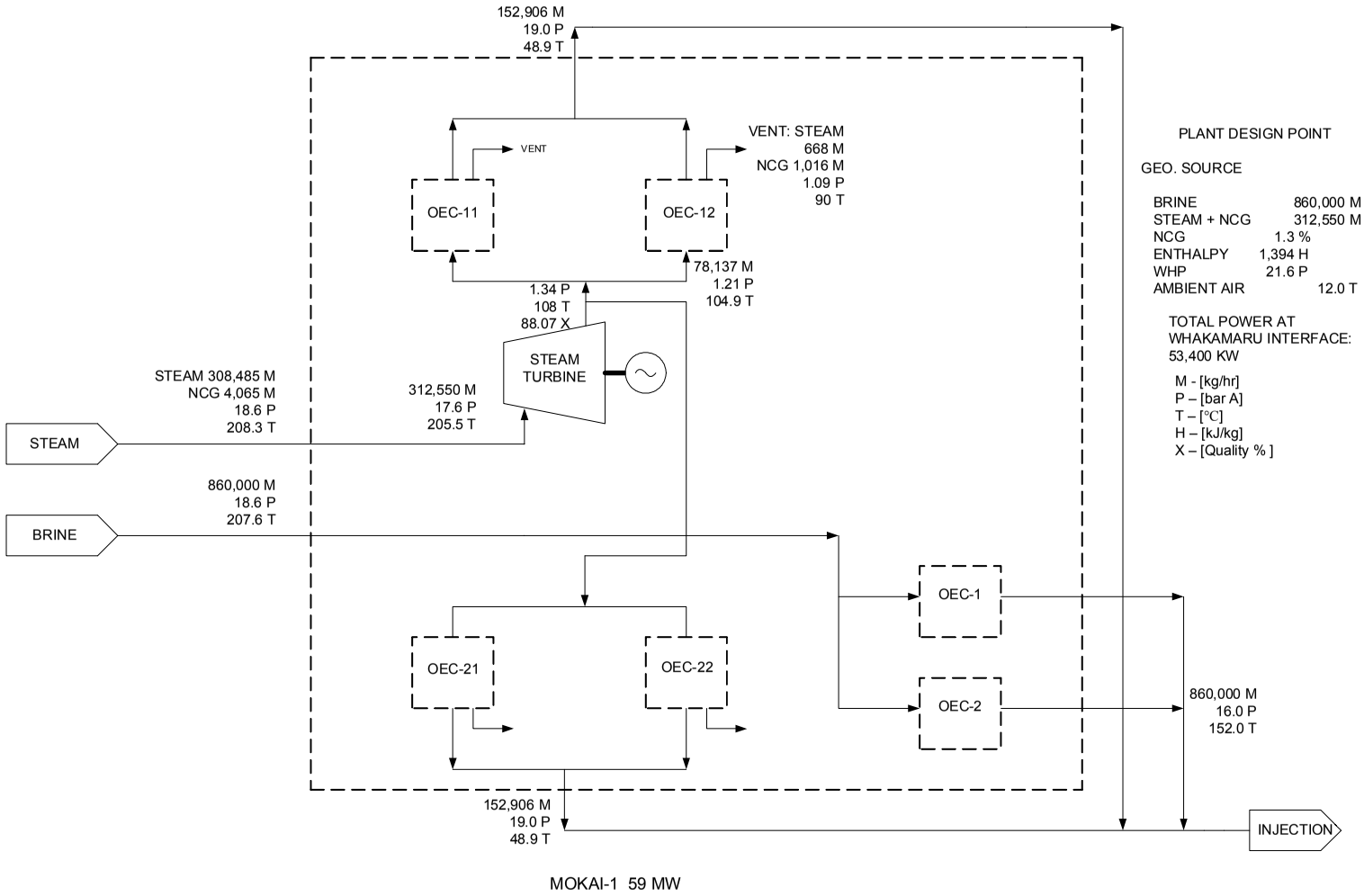

Figure 4-3: Heat and mass balance diagram of the Mokai- 1 Power Plant supplied by MRP

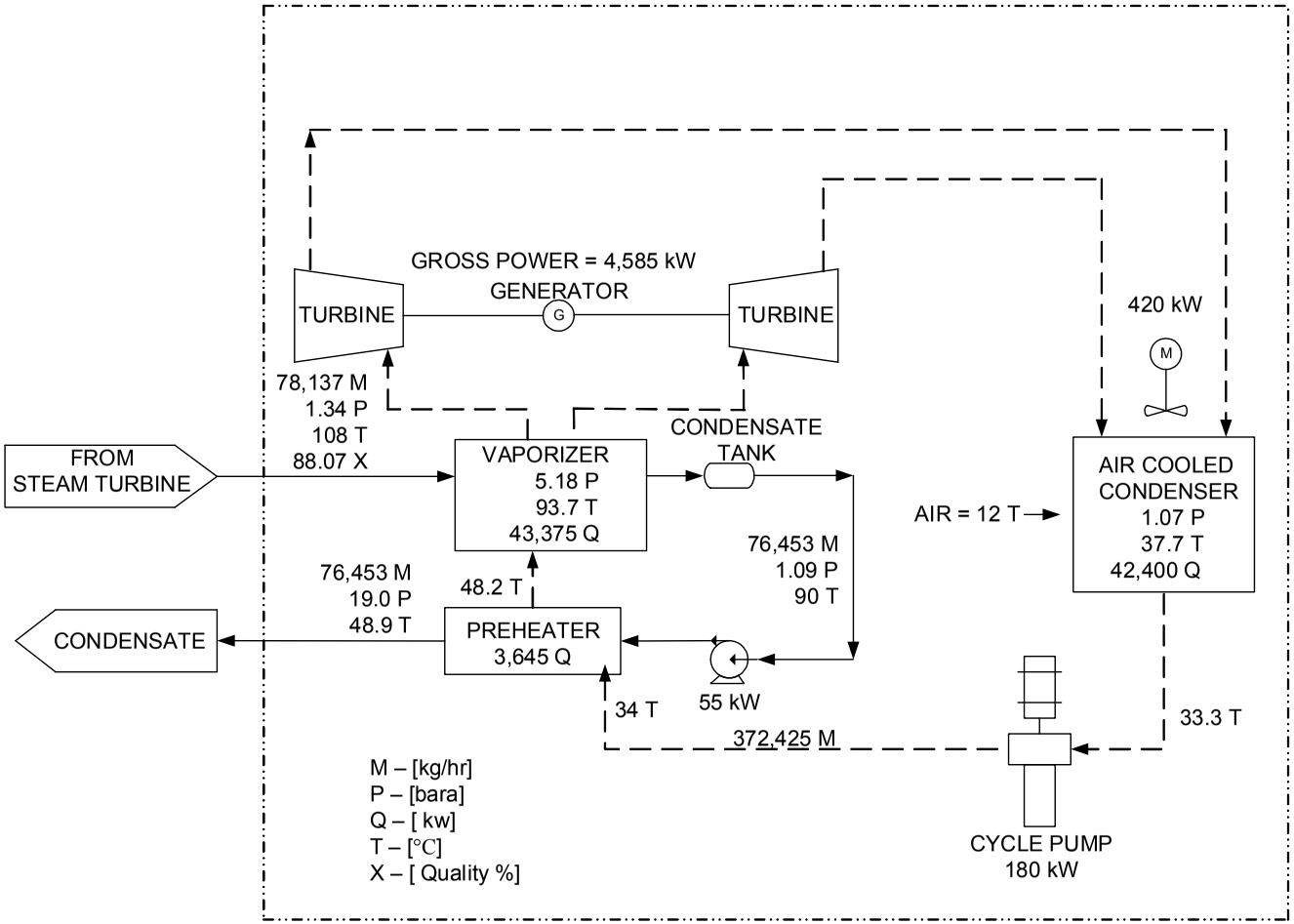

Figure 4-4: Heat and mass balance diagram of a Bottoming OEC unit of the Mokai- 1 Power Plant supplied by MRP

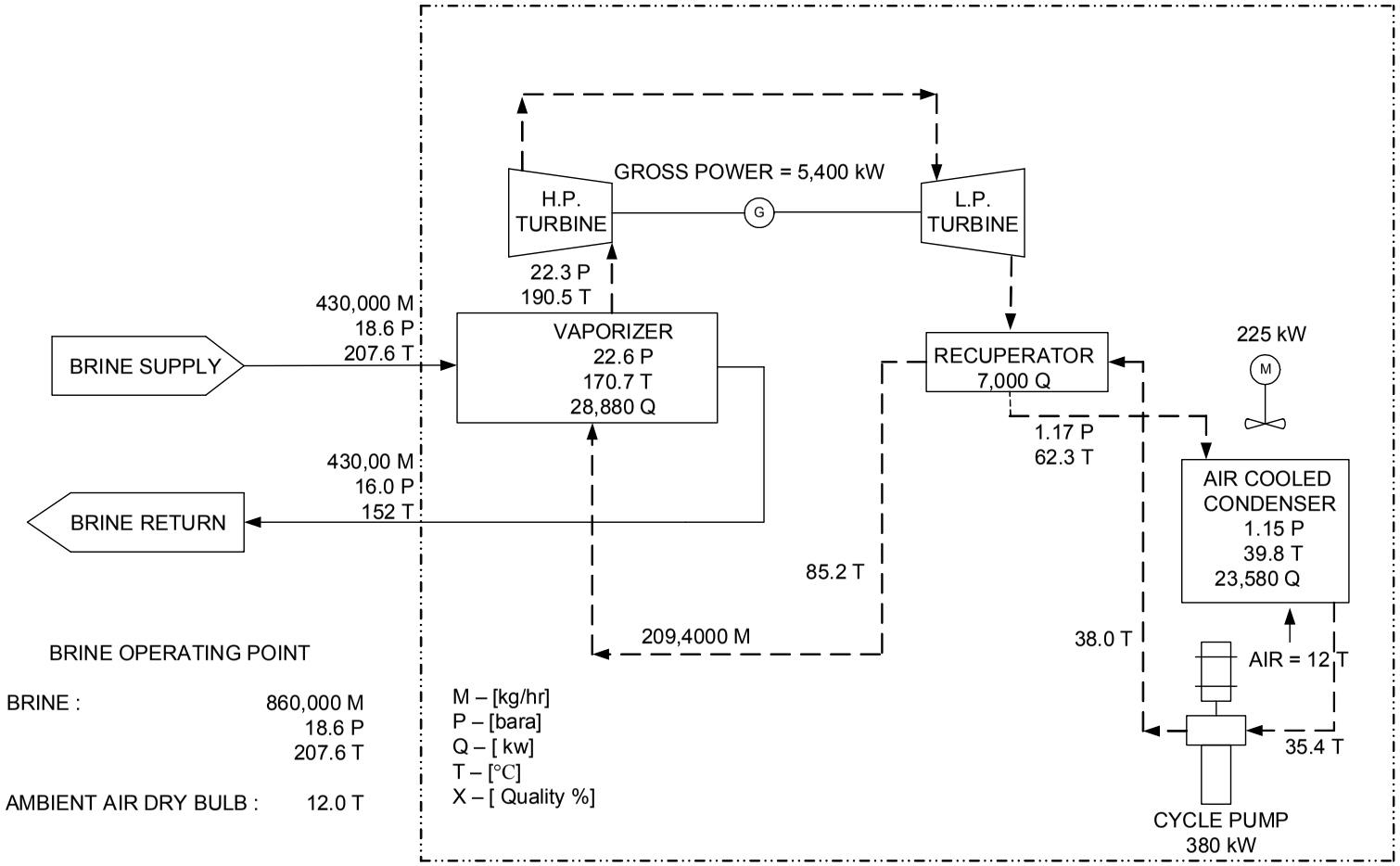

Figure 4-5: Heat and mass balance diagram of a Brine OEC unit of the Mokai- 1 Power Plant supplied by MRP

4.4 Thermodynamic cycles of the Mokai 1 geothermal power plant

There are three different power cycles used in the Mokai 1 geothermal power plant. Figure 4-6 presents the *T,s*-diagram of the power cycle used for the steam turbine. The power cycle used in the steam turbine is essentially bell-shaped, which prevents the cycle from being very effective for low temperature heat sources. Figure 4-7 shows the *T,s*-plane representation of the of the brine OEC and Figure 4-8 shows the *T,s*-plane representation the bottoming OEC. Figures 4-6 to 4-8 are generated using Refprop [70] physical properties data base with the state point data available from the design and from the steady state model of the plant discussed in chapter 6.

The OECs use pentane as the working fluid which has an inclined bell shape of the *T,s*-diagram. The inclined bell shaped of the *T,s* diagram allows the working fluid to reduce its pressure to a much lower value without the problem of phase change. It makes turbine design less complicated as the formation of pentane liquid particles that erode the turbine blades is avoided.

In Figure 4-6, process 1-2 represents the work done in the steam turbine in the Mokai 1 geothermal power plant. The Mokai 1 plant uses wet-steam turbine to use available steam from the geothermal source; consequently, a large problem of erosion was observed in the Mokai 1 geothermal power plant. The process 2-3 presents the heat transfer to the bottoming cycles.

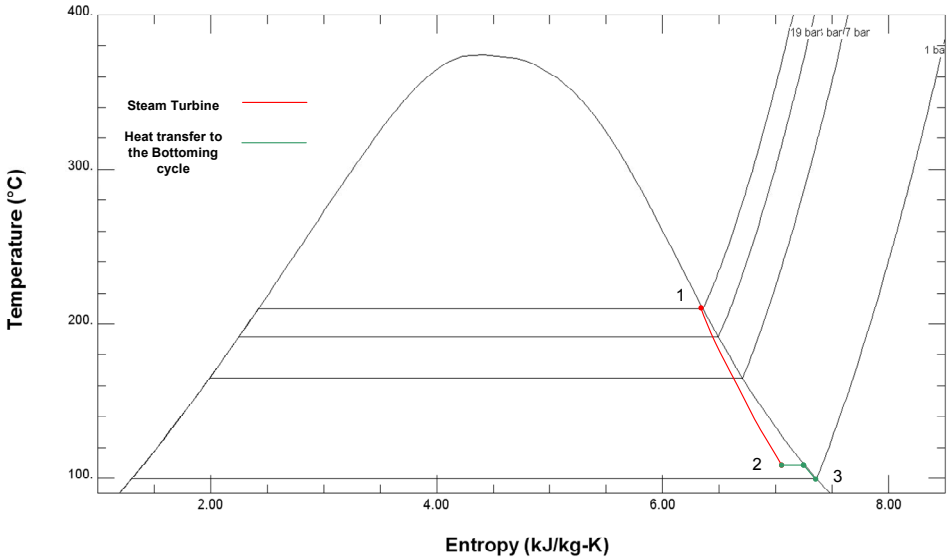

Figure 4-6: *T,s*-diagram explaining the steam turbine work carried out and heat transfer to the bottoming cycle of Mokai 1

In Figure 4-7, process 1-2 represents the work required by the cycle pump; process 2-2a represents the heat recovery in the recuperator; process 2a-3a represents heat transfer in the vaporizer; process 3a-3 represents heat transfer in the superheater; process 3-4 represents the work done by the pentane turbines; process 4-4a represents heat rejection by the working fluid in the recuperator, which is equal to heat input in the process 2-2a; and process 4a-1 represents the heat rejection by the working fluid in the condenser.

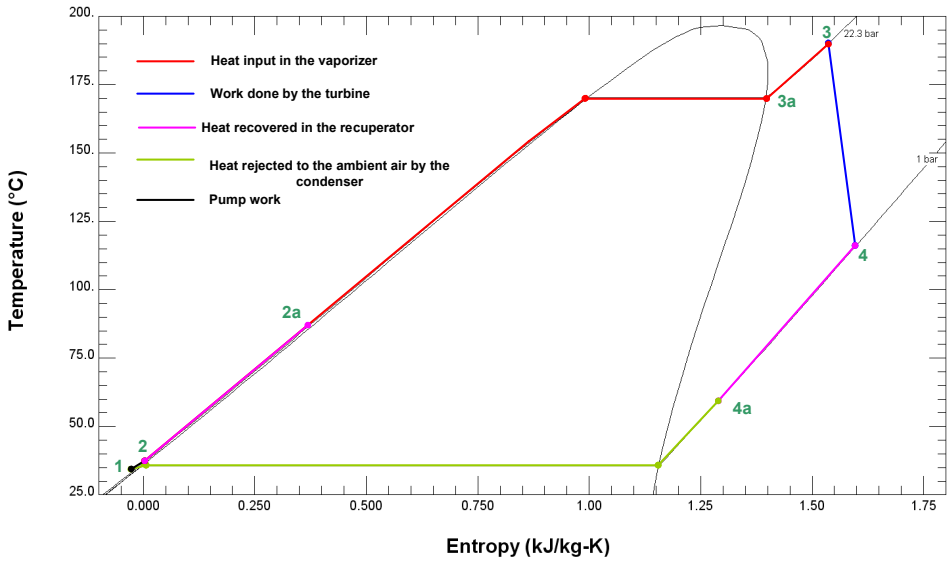

Figure 4-7: *T-s* diagram of OEC 1

In Figure 4-8, process 1-2 represents the work required by the cycle pump; process 2-2a represents the heat recovery in the preheater; process 2a-3 represents heat transfer in the vaporizer; process 3-4 represents the work done by the pentane turbines; and process 4-1 represents the heat rejection in the condenser by the working fluid.

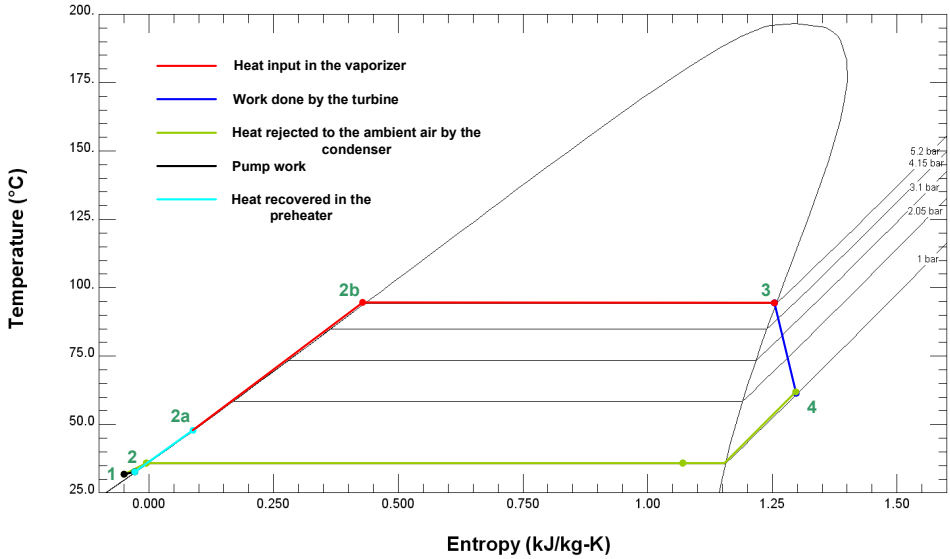

Figure 4-8: *T-s* diagram of OEC 11

4.5 Summary

This chapter has presented an introduction to the Mokai 1 geothermal power plant which is used as a case study in this dissertation. At first brief discussion on plant location and local weather condition is presented. Then the heat and mass balance of the Mokai 1 geothermal power plant is discussed. A brief discussion of the thermodynamic power cycles used in the Mokai 1 geothermal power plant is also presented in this chapter.

Chapter 5

Component Models

5.1 Introduction

Modelling of a theoretical Rankine cycle or even a combination of individual cycles is not a challenging problem if enough information is specified, known, or measured to fix the states at the inlet and outlet of each component and if the performance characteristics of the components are known. One of the aims for this research was to develop a modelling approach that is simple for plant engineers to use, accurate enough to make design decisions about plant modifications, and that can reflect off-design conditions and previous plant modifications. The challenge in meeting this objective is data. The manufacturer of the organic Rankine cycle (ORC) conversion plants does not provide all of the design specifications in order to protect their commercial position. The operating power plant has measurements sufficient to operate and control the plant, but not sufficient to develop even a basic thermodynamic model, let alone a model that includes heat losses and viscous losses.

The approach developed during this research project is progressive. We start first by using the simplest component and thermal system model of an ORC assuming adiabatic and reversible processes. The available design point data is specified, and an iterative solution process is used to fit the unknown parameters to design plant output. The next step is to use the ideal design model state points as initial guess values for the ORC model using actual plant measurements.

In this chapter models of the individual components for an ideal ORC are presented then the modelling approach for the real ORCs used in the Mokai 1 geothermal plant is described. The models presented in this chapter are generic and based on the fundamental laws of mass and energy conservation. These models will be used for long and short term performance analysis of geothermal power plant discussed in chapter 7 and 9, respectively.

5.2 Component Models

The components used in a Rankine cycle (Figure 5-1) can be divided into two major categories: energy conversion (i.e. turbines and pumps) and heat exchanger (i.e. boilers and condensers). The basic component models are developed subject to the following assumptions:

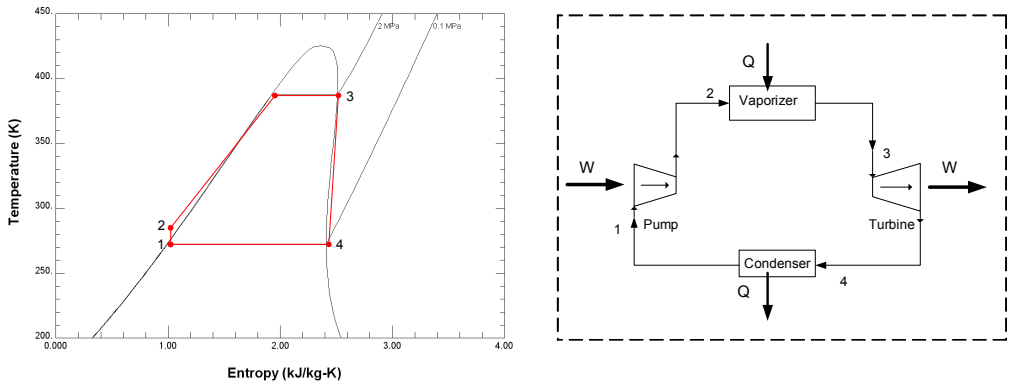

Figure 5-1: *T-s* diagram of the ORC represented in the right hand side

General assumptions for all the components:

- Kinetic and potential energies are negligible
- Steady state process
- Ambient temperature is constant
- Heat loss to the ambient is negligible

Liquid pump

Inputs: $\dot{m}$, p_1, t_2

Parameters: p_2, η_s

Conservation of mass:

$$\dot{m}_i = \dot{m}_o = \dot{m} \tag{5.1}$$

Conservation of Energy:

$$W_{12} = \dot{m}(h_1 - h_2) \tag{5.2}$$

Irreversibility:

$$\eta_s = \frac{h_1 - h_{2s}}{h_1 - h_2} \tag{5.3}$$

Outputs: t_2, h_2

Where $\dot{m}$ is the mass flow rate of the working fluid, p_1 is the pressure at state point 1, p_2 is the pressure at state point 2, h_1 is the enthalpy at state point 1, h_2 is the enthalpy at state point 2, h_{2s} is the ideal enthalpy at state point 2, t_2 is the temperature at state point 2, η_s is isentropic efficiency of the pump and W_{12} is the work input to the pump.

Vaporizer

Assumptions:

- Isobaric process
- No work done in the process

Inputs: $\dot{m}$, p_2, t_2, $\dot{m}_{geo}$, $h_{i,geo}$

Parameter: $\dot{Q}_{23}$

Conservation of mass:

$$\dot{m}_i = \dot{m}_o = \dot{m} \tag{5.4}$$

Conservation of Energy ($W_{23} = 0$):

$$\dot{Q}_{23} = \dot{m}\,(h_3 - h_2) \tag{5.5}$$

$$\dot{Q}_{23} = \dot{m}_{geo}\,(h_{i,geo} - h_{o,geo}) \tag{5.6}$$

Isobaric process:

$$p_3 = p_2 \tag{5.7}$$

Outputs: t_3 , h_3 , $h_{o,geo}$

Where p_3 is the pressure at state point 3, h_3 is the enthalpy at state point 3, $\dot{Q}_{23}$ is heat transfer in the vaporizer, $\dot{m}_{geo}$ is the mass flow of the geothermal fluid, $h_{i,geo}$ is inlet enthalpy of the geothermal fluid, $h_{o,geo}$ is outlet enthalpy of the geothermal fluid and t_3 is the temperature at state point 3.

Turbine

Inputs: $\dot{m}$, p_3 , t_3

Parameters: η_G , η_s , r_p

Conservation of mass:

$$\dot{m}_i = \dot{m}_o = \dot{m} \tag{5.8}$$

Conservation of Energy:

$$W_{34} = \eta_G \dot{m}\,(h_3 - h_4) \tag{5.9}$$

Irreversibility:

$$\eta_s = \frac{h_3 - h_4}{h_3 - h_{4,s}} \tag{5.10}$$

$$r_p = \frac{p_3}{p_4} \tag{5.11}$$

Outputs: p_4, h_4, W_{34}

Where p_3 is the pressure at state point 3, p_4 is the pressure at state point 4, h_4 is the enthalpy at state point 4, h_{4s} is the ideal enthalpy at state point 4, η_G is generator efficiency, η_s is isentropic efficiency of the turbine, r_p is the pressure ratio, and W_{34} is the turbine work done.

Condenser

Assumptions:

- Isobaric process
- No work done in the process

Inputs: $\dot{m}$, p_4, t_4

Parameter: $\dot{Q}_{41}$

Conservation of mass:

$$\dot{m}_i = \dot{m}_o = \dot{m} \tag{5.11}$$

Conservation of Energy ($W_{41} = 0$):

$$\dot{Q}_{41} = \dot{m}\,(h_1 - h_4) \tag{5.12}$$

Isobaric process:

$$p_1 = p_4 \tag{5.13}$$

Outputs: p_1, h_1

Where $\dot{Q}_{41}$ is the heat rejection from the condenser.

Equation (5.1) to (5.13) should be solved simultaneously for a given value of $\dot{m}$ to calculate the performance of the whole system, which represents the performance of the individual components as well as the overall performance. In the thermodynamic descriptions presented above, the heat transfer in the vaporizer and the condenser are assumed as parameters. Following section discusses the heat transfer processes in the vaporizer and the condenser.

5.3 Heat transfer models

The models presented in the previous section represent an ideal case only. A real plant may vary significantly from the ideal case. Mokai 1 geothermal power plant has been taken as the case study for implementation of the models presented above. This plant was built over a decade ago. Significant design and performance change is noticeable.

The Mokai 1 geothermal power plant is designed and built by Ormat®. Limited information about the vaporizer and condenser designs are available, so the heat transfer models developed here are based on the basic configuration and idealized conditions. For example, the effect of scale deposits is not considered.

In the thermodynamic descriptions presented in section 5.2, the vaporizer heat transfer and condenser heat load are supplied to the models as parameters. In reality the heat transfer varies significantly depending on various parameters such as: geothermal fluid flow rate, ambient temperature, etc. In the following sections basics of heat exchangers are presented then the modelling of Mokai 1 ORC vaporizer and condenser is discussed. Adjustments of the turbine and pump models to Mokai 1 geothermal power plant are also discussed in the following sections.

5.3.1 Heat exchangers background

In this section, the basics heat exchanger models are presented. Two different approaches in heat exchanger design are presented: the log mean temperature difference (LMTD) approach and heat exchanger effectiveness approach. Heat exchangers are classified in four major groups depending on the fluid flow paths

through the heat exchangers. Figure 5-2 illustrates flow path configurations for these four categories of heat exchangers. In parallel-flow units, the two fluid streams enter together at one end, flow through in the same direction and leave together at the other end. In counterflow units, the two fluid streams move in opposite directions. In the single-pass crossflow units, the fluids flow at right angle to each other through the heat exchanger. In multi-pass crossflow units, one fluid stream moves back and forth across the flow path of the other fluid stream.

The most important difference between these four basic types lies in the relative amounts of heat transfer surface area required to produce a given temperature rise for a given temperature difference between the two fluid streams where they enter the heat exchanger. The counterflow heat exchanger requires the least area throughout the range.

The LMTD approach to heat exchanger analysis is useful when the inlet and outlet temperatures are known or are easily determined. The LMTD is then easily calculated and the heat flow, surface area, or overall heat transfer coefficient may be determined. The heat flow in a parallel/counter flow heat exchanger based on LMTD approach is as follows:

$$\dot{Q} = U\,A\;\Delta T_m \tag{5.14}$$

Here, $\dot{Q}$ is the heat flow from the hot fluid to the cold, U the overall heat transfer coefficient, A the surface area for heat transfer consistent with the definition of U and ΔT_m is the LMTD across heat exchanger. LMTD is defined as follows:

$$\Delta T_m = \frac{(T_{h2} - T_{c2}) - (T_{h1} - T_{c1})}{\ln[(T_{h2} - T_{c2})/(T_{h1} - T_{c1})]} \tag{5.15}$$

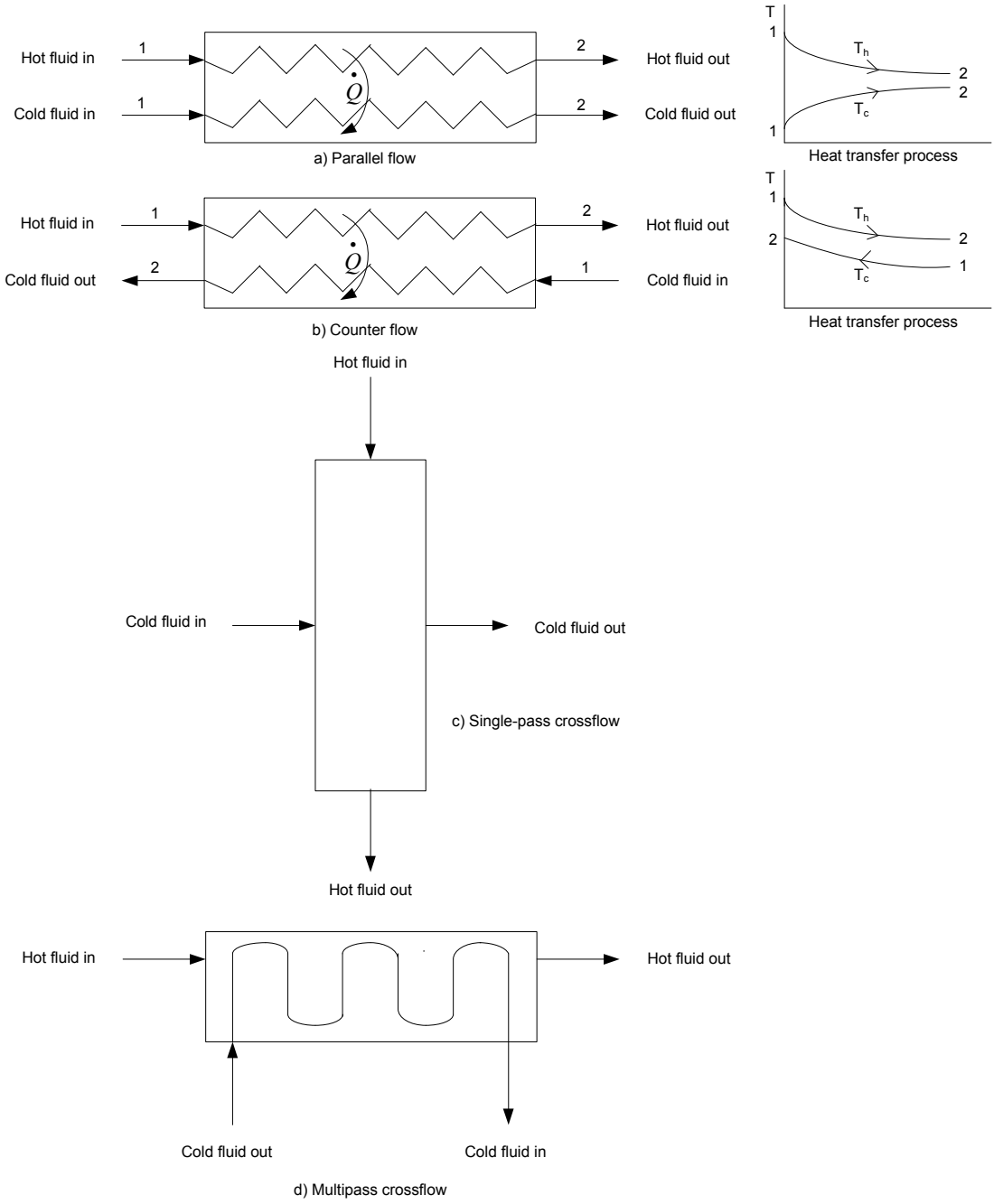

Figure 5-2: Types of flow-path configuration through heat exchangers

where, T_{h1} and T_{c1} are the inlet temperatures of the hot fluid and the cold fluid; T_{h2} and T_{c2} are the outlet temperatures of the hot fluid and the cold fluid.

The overall heat transfer coefficient of a heat exchanger, for example a heat exchange tube may be calculated as:

$$U = \frac{1}{\frac{1}{h_i} + \frac{A_i \ln(r_o / r_i)}{2\pi kL} + \frac{A_i}{A_o}\frac{1}{h_o}} \tag{5.16}$$

where, h_i and h_o are the convective heat transfer coefficients of inside and outside of the smaller tube, r_i and r_o are the inside and outside radius, A_i and A_o are the inside and outside areas, k is the thermal conductance of the material and L is the length of the heat tube.

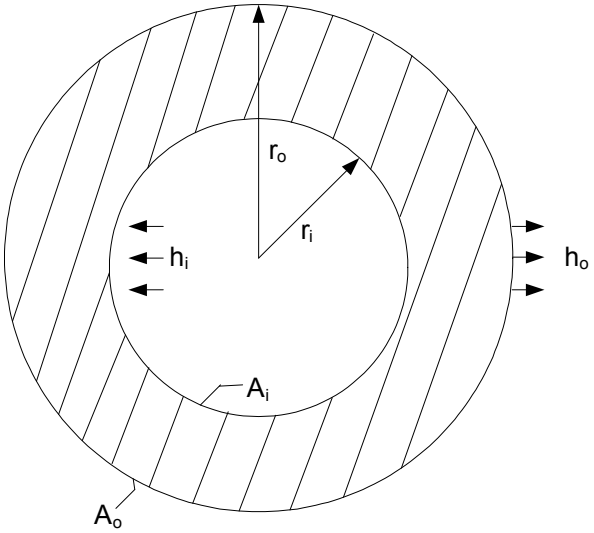

Figure 5-3: Cross-sectional view of a heat exchange tube

If a heat exchanger other than the heat exchanger tube is used, the heat transfer is calculated by using a correction factor applied to the LMTD. The heat transfer equation then takes the form:

$$\dot{Q} = U\,A F\,\Delta T_m \tag{5.17}$$

Here, F is LMTD correction factor. When a phase change is involved, i.e. condensation or evaporation, the condensing or boiling fluid normally remains at essentially constant temperature and the relation is simplified to F =1.0, [73].

When the inlet or outlet temperatures are to be evaluated for a given heat exchanger, the LMTD analysis frequently involves an iterative procedure. The analysis method based on the effectiveness of heat exchangers can be useful to solve such problems. The heat exchanger effectiveness is defined as:

$$\text{Effectiveness, } \varepsilon = \frac{\dot{Q}}{\dot{Q}_{\max}} \tag{5.18}$$

here, $\dot{Q}$ is the actual heat transfer and $\dot{Q}_{\max}$ is the maximum possible heat transfer by the heat exchanger.

The actual heat transfer can be computed by calculating either the energy lost by the hot fluid or the energy gained by the cold fluid. To determine the maximum possible heat transfer for the exchanger, we recognise that this maximum value could be attained if one of the fluids were to undergo a temperature change equal to the maximum temperature difference present in the exchanger, which is the difference in the entering temperatures for the hot and cold fluids. The fluid that might undergo this maximum temperature difference is the one with the minimum value of $\dot{m}c_p$ because the energy balance requires that the energy received by one fluid is equal to that given up by the other fluid. The maximum possible heat transfer is expressed as:

$$\dot{Q}_{\max} = (\dot{m}c_p)_{\min}(T_{h,in} - T_{c.in}) \tag{5.19}$$

here, $\dot{m}$ is the mass flow rate, c_p the specific heat at constant pressure, $T_{h,in}$ the inlet temperature of the hot fluid and $T_{c,in}$ the inlet temperature of the cold fluid.

A dimensionless property known as number of transfer units (*NTU*) is used to calculate the heat exchanger effectiveness (ε):

$$NTU = \frac{UA}{(\dot{m}c_p)_{\min}} \tag{5.20}$$

Empirical heat exchanger performance is normally given in the form of ε vs. NTU chart. In case of heat exchangers with evaporation and condensation, ε can be expressed by the following simple equation:

$$\varepsilon = 1 - e^{-NTU} \tag{2.21}$$

The heat exchanger effectiveness (ε) of a well-designed heat exchanger is usually close to its theoretical value i.e. 1 for a counterflow heat exchanger and 0.5 for parallel-flow heat exchangers when the heat capacities of the heat carrying media are the same. However, in practical operation high value of ε may not be always feasible as high ε is associated large heat transfer area which is directly linked to high capital cost and large space. A trade off between high value of ε and cost and space constrains is necessary. The heat exchanger effectiveness remains practically constant for a wide range of heat exchanger operation conditions. Figure 5-4 shows a one shell pass and 2, 4, 6 etc. tube passes. It is evident from the Figure that ε tends to flatten quickly for NTU number more than 2.

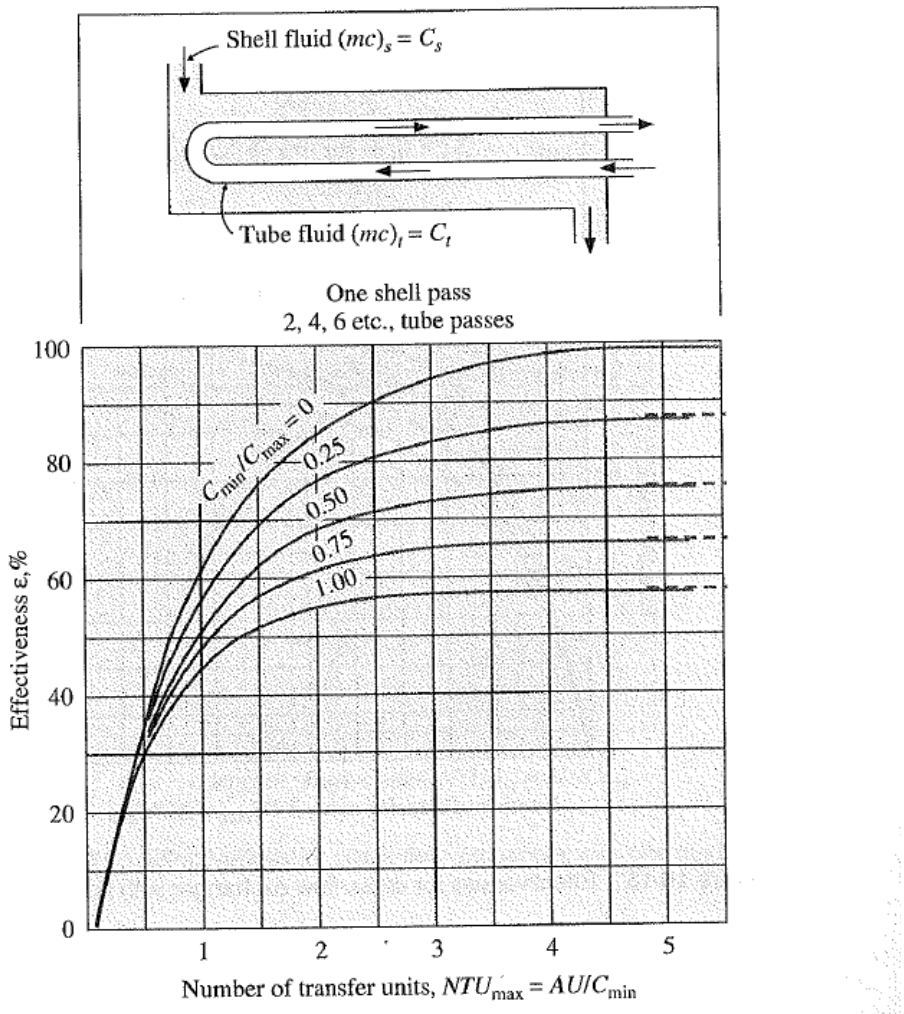

Figure 5-4: Effectiveness for 1-2 parallel couterflow heat exchanger performance (from [73])

5.3.2 The ORC vaporizer model of Mokai 1

In this section the vaporizer (evaporator) models are presented. There are two types of vaporizer-separator assemblies used in the Mokai 1 geothermal power plant: one for saturated vapour cycle (BOT-ORC) and the other for superheated vapour cycle (BRN-ORC). The actual design is presented where available.

The vaporizer design heat transfer calculation for the saturated ORC

The BOT-ORCs used in the Mokai 1 geothermal power plant are run by the exhaust steam of the steam turbine. Figure 5-5 shows the vaporizer-separator assembly of the BOT-ORC. The vaporizer is a shell and tube type heat exchanger with steam in the tube side and pentane in the shell side. Figure 5-6 shows the simplified cross-sectional view of the vaporizer. This vaporizer is a single shell double pass shell-tube heat exchanger. The tubes are arranged in staggered condition.

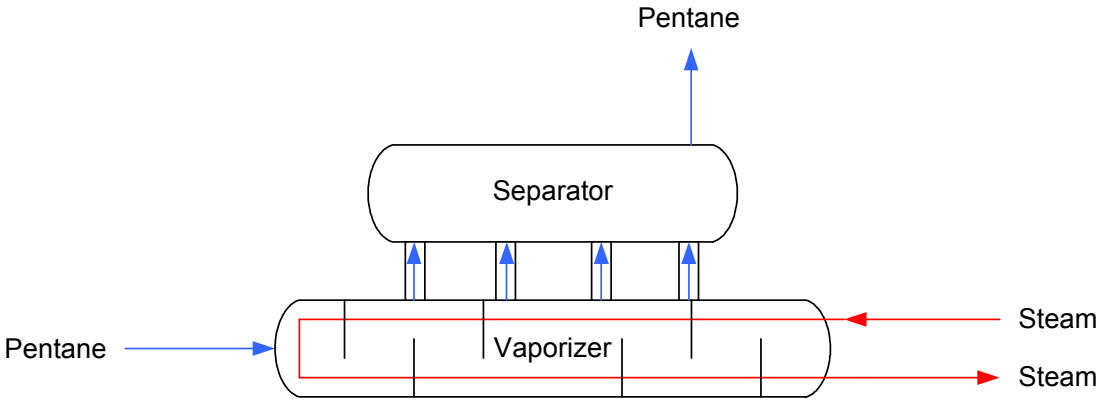

Figure 5-5: Schematic view of the vaporizer-separator assembly for the saturated vapour ORC.

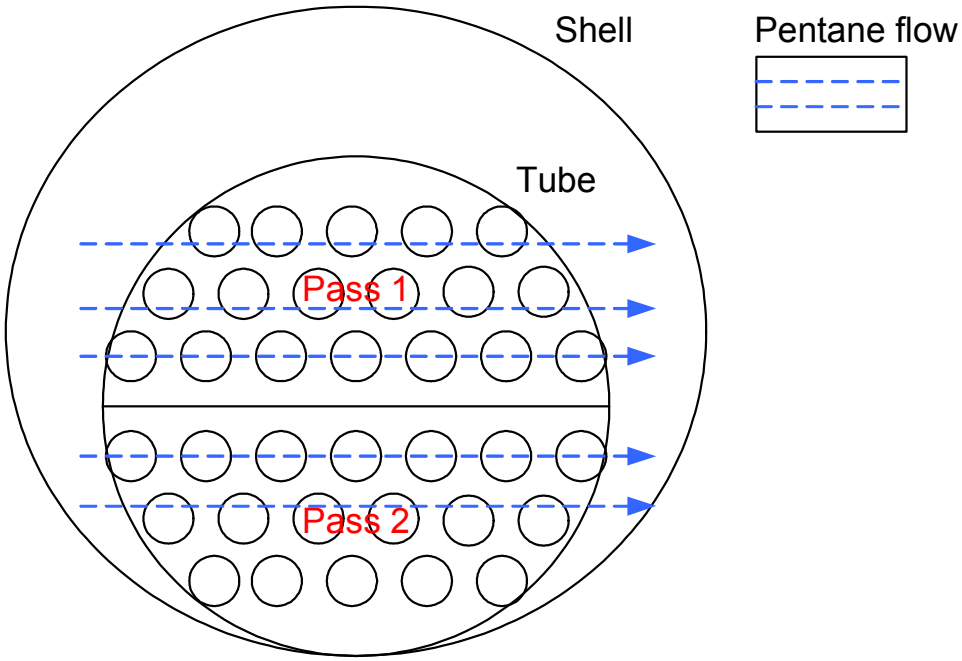

Figure 5-6: Simplified cross-sectional view of the vaporizer of the saturated vapour unit with pentane flow direction.

There are 1376 tubes in the pass 1 and 1375 tubes in pass 2. Figure 5-7 explains the dimensions needed for heat transfer calculation.

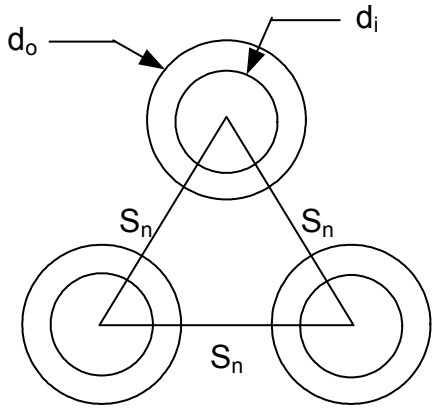

Figure 5-7: Explanations of tube orientations and dimensions needed for the tube bank.

The pentane side heat transfer coefficient is calculated assuming flow across tube banks with a staggered arrangement. The Nusselt number is calculated from the empirical relation presented by Zukauskas [74]:

$$Nu = \frac{\bar{h}_o d}{k} = C\,\mathrm{Re}_{d,\max}^{n}\,\mathrm{Pr}^{0.36}\left(\frac{\mathrm{Pr}}{\mathrm{Pr}_w}\right)^{1/4} \qquad (5.22)$$

where $\bar{h}_o$ is the average convective heat transfer coefficient of the tube, d is the diameter of the tube and k is the thermal conductance. All properties except Pr_w are evaluated at bulk temperature. Pr_w is calculated at wall temperature. The values of the constants are C = 0.022 and n = 0.84 for $\mathrm{Re}_{d,\max} > 2 \times 10^5$. The $\mathrm{Re}_{\max}$ is calculated based on maximum velocity as:

$$u_{\max} = u_\infty \left(\frac{S_n}{S_n - d}\right) \tag{5.23}$$

$$\text{and} \quad \mathrm{Re}_{d,\max} = \frac{\rho u_{\max} d}{\mu} \tag{5.24}$$

where u_∞ and $u_{\max}$ represent free stream and maximum velocity, respectively. The tube side convective heat transfer coefficient for horizontal tubes with a stratified layer can be calculated form the following empirical relation [75]:

$$h_i = \Omega \left[\frac{k_l^3 \rho_l (\rho_l - \rho_g) g \Delta h_v}{\eta_l d_i (T_{sat} - T_w)}\right]^{1/4} \tag{5.25}$$

where, h_i is the tube side convective heat transfer coefficient, ρ_l the density of fluid at liquid state, ρ_g the density of fluid at vapour state, η_l the dynamic viscosity, T_{sat} the saturation temperature, T_w the wall temperature and Δh_v the change in enthalpy. Ω is the correction factor based on void fraction and calculated as [75]:

$$\Omega = 0.728\left[1 + \left(\frac{1 - x_g}{x_g}\right)\left(\frac{\rho_g}{\rho l}\right)^{\frac{2}{3}}\right]^{-3/4} \tag{5.26}$$

here, x_g is the vapour fraction of steam. Table 5.1 summarises the dimensions necessary for the heat transfer calculation of the BOT-ORC. The overall heat transfer coefficient (U) is calculated using Equation (5.16) and values from Table 5.1. The wall conductance (titanium alloy) is $k_{\text{steel-titanium}}$ = 7.62 W/mK. The calculated value of U = 1.028 kW/m^{2}K. Pentane inlet and outlet temperatures are 33.3ºC and 93.7ºC; steam inlet temperature is 104.9ºC and condensate outlet temperature is 90ºC.

Table 5.2 shows the summary of heat transfer calculation for the saturated vapour ORC with steam mass flow rate 23.5 kg/s instead of designed 21.7 kg/s. The LMTD correction factor (F) is calculated using the chart of reference [73], the chart is attached in appendix 2. In the original design of the saturated vapour cycle, there is a

preheater to recover some heat from the condensate before it is reinjected. In the current state of operation, the preheater is not in operation due to increased enthalpy of the resource over time. The LMTD value is adjusted accordingly.

The calculated value of heat transfer in the vaporizer is 46929 kW, which lies less than 1% variation from that of the combined vaporizer and preheater (47020 kW) of original design.

Table 5.1: Dimensions necessary for heat transfer in the vaporizer for BOT-ORC (from design)

Pass and tube number	Internal diameter of the tube (d_i) [mm]	External diameter of the tube (d_o) [mm]	Centre to centre distance between the tubes (S_n) [mm]	Length of the tube (L) [m]
1; 1376	19.45	22.52	25.6	10.72
2; 1375	19.45	22.52	25.6	10.72

Table 5.2: Summary of heat transfer calculation for the vaporizer of the saturated vapour ORC

Steam mass flow rate [kg/s]	23.5	R* [-]	0.24
Pentane mass flow rate [kg/s]	103.45	F [-]	0.78
$\mathrm{Re}_{d,\max}$	$8.03\text{x}10^5$	h_i [kW/m^{2}K]	3.611
h_o [kW/m^{2}K]	2.218	U [kW/m^{2}K]	1.028
A [m^2]	2086.42	ΔT_m [ºC]	28.05
P* [-]	0.85	$\dot{Q}$ [kW]	46929

$* P = \frac{(T_{c2} - T_{c1})}{(T_{h1} - T_{c1})}$, $R = \frac{(T_{h1} - T_{h2})}{(T_{c2} - T_{c1})}$ (appendix 2)

The separator in this cycle separates the pentane droplets from the pentane vapour. The separator has nozzles and perforated plates to impinge any pentane droplets before the vapour enters the turbines. In the actual plant design, the separator is assumed have no pressure loss. At first the saturated pentane vapour from the vaporizer passes through nozzles then it passes through perforated plates then enters the turbines.

The vaporizer-separator design heat transfer calculation for the superheated ORC

Figure 5-8 shows the schematic view of the vaporizer-separator assembly of the superheated vapour unit (BRN-ORC). The vaporizer-separator is also a shell-tube type heat exchanger with pentane in the shell side and geothermal brine in the tube side. Figure 5-9 shows the cross-sectional view of the vaporizer of the BRN-ORC. There are 4 passes involved in the tube side. The vaporizer is divided into preheat and boiling zones. Pentane liquid is heated to the saturated liquid state in the preheat zone while passing over tubes of pass 4. Then the pentane liquid is heated where phase change takes place from saturated liquid to saturated vapour while passing over tube banks of passes 1-3. Saturated vapour from the vaporizer is then passed through nozzles in the separator to get rid of pentane droplets. The pentane vapour is superheated while passing over tube banks of 2 passes of the entering geothermal brine. Unfortunately, required information like the number of tubes, the dimension and orientation are not available.

The inlet and outlet temperatures for pentane: 85.2ºC and 193.5ºC; brine: 207.6ºC and 152ºC, respectively. The pentane saturation temperature is 170.6ºC. Table 5.3 summarises the information necessary for the heat transfer calculation of the vaporizer of the superheated vapour ORC. The vaporizer heat transfer is calculated for the preheat zone and the boiling zone. The intermediate temperature of brine is not available.

The required values of the intermediate temperatures of the brine are estimated from design heat transfer and an assumed pinch point temperature. Figure 5-10 shows the heat transfer in the vaporizer schematically. T_1 and T_2 represents brine inlet and outlet temperatures. T_4 represents the pinch point temperature of brine. As no information is available, the pinch point temperature difference is assumed to be at least 5ºC. Various authors in the literature [76-78] have used pinch point temperature difference around 2ºC-10ºC. So the assumption made here is reasonable. The value of T_4 (175.6ºC) can be estimated by adding the pinch point temperature difference with the saturated temperature of pentane. The brine outlet temperature from the separator (or vaporizer inlet temperature) T_3 (195.1ºC) is calculated from the energy balance:

$$T_3 = T_4 + \frac{\dot{m}_{pentane} L}{\dot{m}_{brine} c_{P,brine}} \tag{5.27}$$

where, $\dot{m}_{pentane}$ is the pentane mass flow rate, $\dot{m}_{brine}$ is the brine mass flow rate, L is the latent heat of vaporization of pentane and $c_{P,brine}$ is the specific heat of brine at constant pressure.

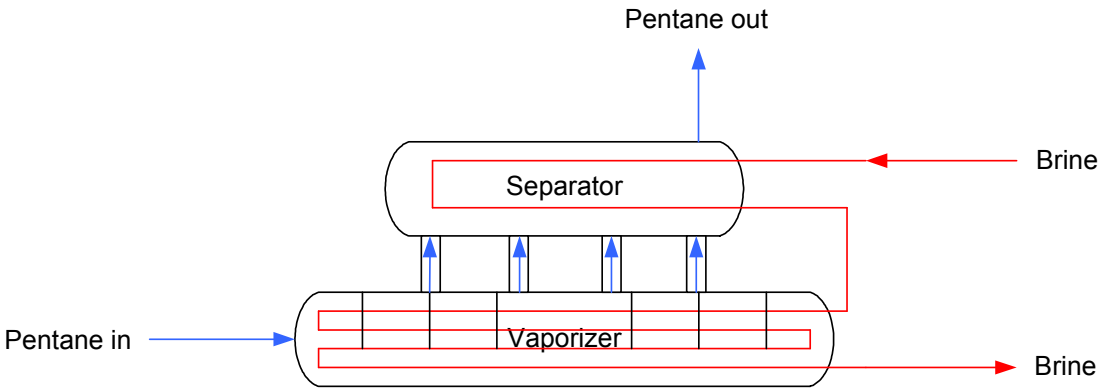

Figure 5-8: Schematic view of the vaporizer-separator assembly for the superheated vapour ORC

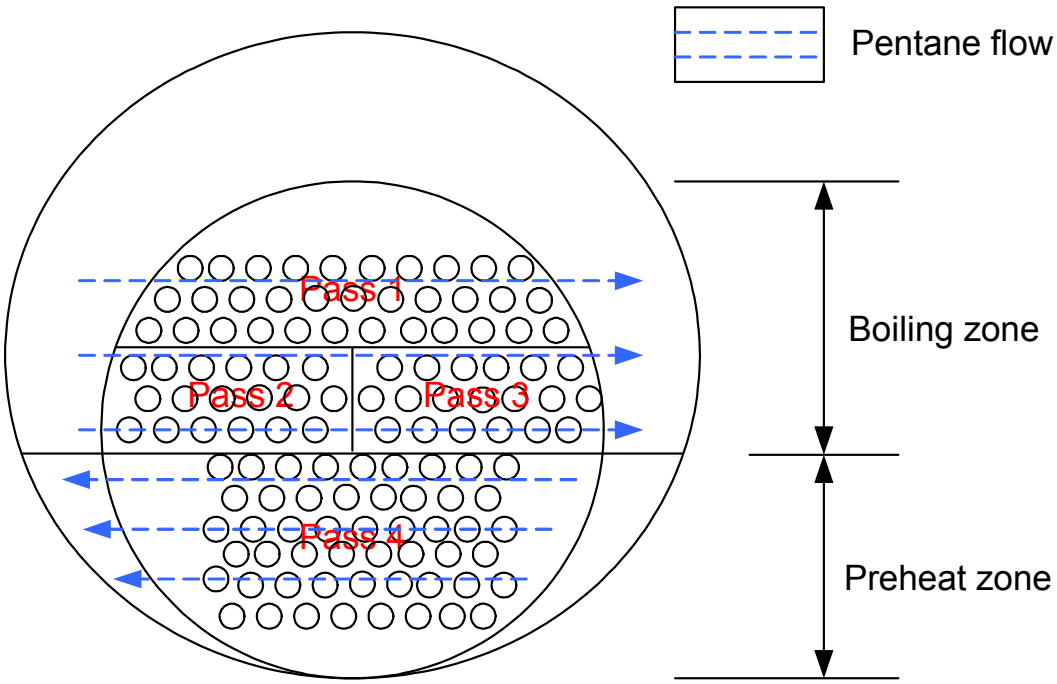

Figure 5-9: Vaporizer cross-section for the superheated vapour ORC with direction of pentane flow

Table 5.4 summarises the calculation necessary for the preheat zone heat transfer. Table 5.5 summarises the calculation necessary for the boiling zone. The tube side (brine) heat transfer coefficient is calculated from the empirical relationship presented by Gnielinski [79]:

$$Nu = \frac{h_i d}{k} = 0.0214(\mathrm{Re}^{0.8} - 100)\,\mathrm{Pr}^{0.4} \qquad (5.28)$$

where 0.5<Pr<1.5; and 10^4<Re<5 x 10^6.

The shell side heat transfer coefficient is calculated using Equation (5.22).

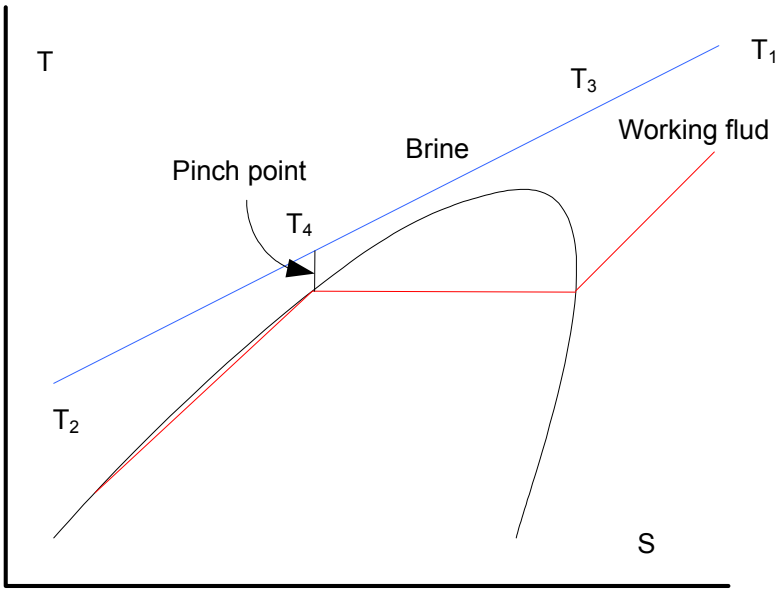

Figure 5-10: Schematic of the heating process of the superheated vapour cycle

Table 5.3: Dimensions used for heat transfer in the vaporizer for superheated vapour ORC (from design)

Pass and tube number	Internal diameter of the tube (d_i) [mm]	External diameter of the tube (d_o) [mm]	Centre to centre distance between the tubes (S_n) [mm]	Length of the tube (L) [m]
1; 356	19.45	21.53	23.63	11.58
2; 349	19.45	21.53	23.63	11.58
3; 349	19.45	21.53	23.63	11.58
4; 356	19.45	22.42	25.4	11.58

Table 5.4: Summary of heat transfer calculation for the preheat zone of the vaporizer of the superheated vapour ORC

Brine mass flow rate [kg/s]	119.44	F [-]	0.65
Pentane mass flow rate [kg/s]	58.167	Re	90760
$\mathrm{Re}_{d,\max}$	1103900	h_i [kW/m^{2}K]	6.975
h_o [kW/m^{2}K]	15.022	U [kW/m^{2}K]	1.77
A [m^2]	424.13	ΔT_m [ºC]	28.16
P* [-]	0.9	$\dot{Q}$ [kW]	11725
R* [-]	0.51		

Table 5.5: Summary of heat transfer calculation for the boiling zone of the vaporizer of the superheated vapour ORC

Brine mass flow rate [kg/s]	119.44	R* [-]	0.51
Pentane mass flow rate [kg/s]	58.167	F [-]	0.65
$\mathrm{Re}_{d,\max}$	51740	h_o [kW/m^{2}K]	15.09
h_i [kW/m^{2}K]	4.19	U [kW/m^{2}K]	1.85
A [m^2]	825.55	ΔT_m [ºC]	10
P* [-]	0.9	$\dot{Q}$ [kW]	9926

$* P = \frac{(T_{c2} - T_{c1})}{(T_{h1} - T_{c1})}$, $R = \frac{(T_{h1} - T_{h2})}{(T_{c2} - T_{c1})}$ (appendix 3)

The exact design and dimensions of the separator are not known. The heat transfer in the separator is estimated from an energy balance on the pentane side across the separator inlet and outlet (7126 kW). The separator ΔT_m is 18.82 ºC. Therefore, for separator UA = 582.52 kW/K, can be calculated from Equation (5.17) with F=0.65 (appendix 3). To verify our calculation we can add up the total heat transfer in the vaporizer-separator assembly and compare it with the design. The total heat transfer found is 28777 kW compared to the design value of 28880 kW. The heat transfer calculation presented here lies within 1% of the actual design.

5.3.3 Off-design heat transfer calculation of ORC vaporizer of Mokai 1

Modelling of the off-design heat transfer and its effect on the whole cycle operation is carried out and compared to the results with the actual data from plant operational log. There is no pentane mass flow measurement inside the ORCs. In the plant operational

log, mass flow rates of brine/steam and their corresponding inlet and outlet temperatures are available. Therefore, any effort to model the ORCs should be based on heat transfer calculation from the brine/steam side. Due to the control mechanism present in the ORC cycles, it is possible to model the ORCs with reasonable accuracy.

The vaporizer pentane level is controlled by a flow control valve, called vaporizer level control valve (VLCV), and the cycle pump (Figure 5-11) during the start up of the ORC unit or when a need to change the vaporizer liquid level arises. However, when ambient temperature changes, the vaporizer pressure-temperature equilibrium condition is also changed, consequently minor changes in vaporizer pentane level occurs, the vaporizer level control valve is not effective in such minor change in pentane level due to ambient temperature change. In typical operating conditions of the vaporizer with phase change, pressure and temperature are coupled. Detailed information regarding the PID control loops is not available but general information is supplied by the thermal system engineer of MRP.

The vaporizer is fitted with sensors, which signals the controller to adjust the VLCV and the cycle pump to achieve any new vaporizer pentane level set point. If the vaporizer pentane level is below a set point, this signals the VLCV and the cycle pump to increase the flow rate result in increase in vaporizer liquid pentane level. The VLCV comes to its initial position once desired vaporizer pentane level is achieved. If the vaporizer pentane level is more than a set point, this signals the VLCV and the cycle pump to decrease the flow rate which results in decrease in the vaporizer liquid pentane level.

If there is a significant change in geothermal resource characteristics or ambient conditions, the operator can change the vaporizer pentane level to meet these extreme conditions. Moreover, the bypass control valve ensures safety against sudden change in operating conditions. If pressure inside the vaporizer increases more than set point provided by the operators, the bypass valves opens and allow pentane vapour to dump directly to the condenser. The bypass valve is specifically responsible for addressing the ambient temperature effect. There is also a flow control valve (not shown in the figure) is attached to control the pentane flow from vaporizer to the turbines. Usually this valve is open to the full.

Figure 5-12 shows the simplified cross-sectional view of the ORC vaporizers. The line *AC* represents the level of pentane in the vaporizer. The volume of vapour above this line can be calculated by multiplying area bounded by *ABC* with the length of the vaporizer. This area is equal to the area bounded by *ABCO* minus the area of the triangle *ACO*.

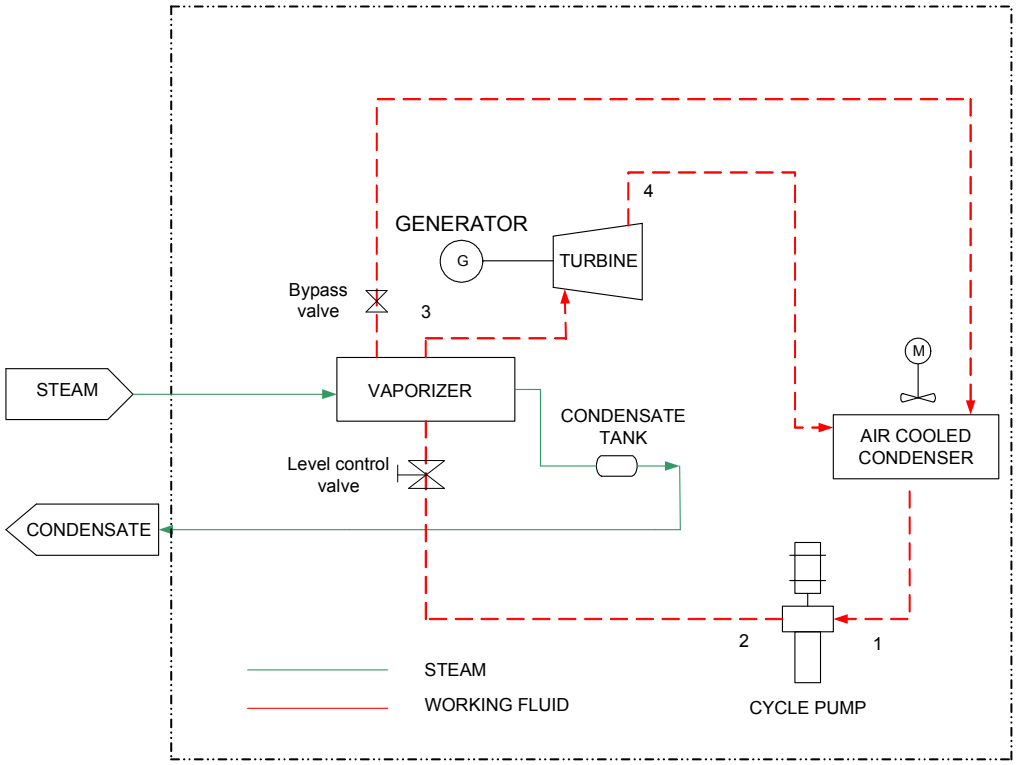

Figure 5-11: Schematic of an ORC showing the level control arrangement

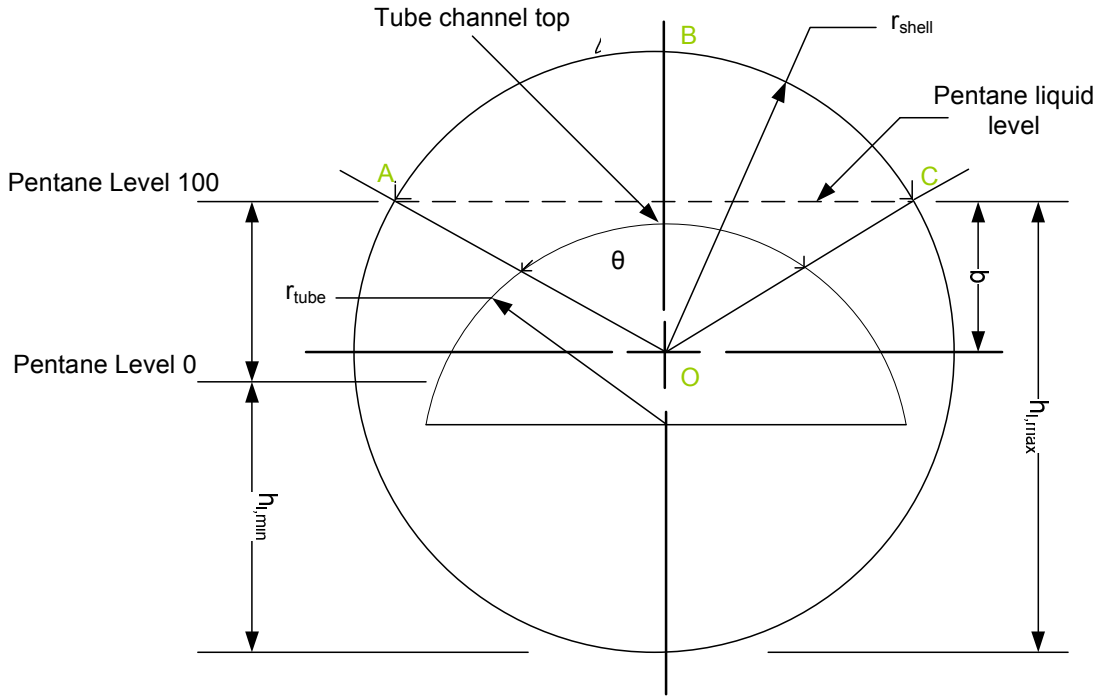

Figure 5-12: Simplified cross sectional view of the vaporizers

For a pentane level higher that or equal to the top of the tube channel, volume occupied by the pentane liquid is given by:

$$V_l = (V_{Shell} - V_{tube}) - V_{vapour} \tag{5.29}$$

where V_{tube} is the volume (external) of the tube side channel, V_{Shell} is the volume of the space inside the shell, V_l is the volume occupied by the pentane liquid and V_{vapour} is the vapour occupied by pentane vapour.

$$V_l = (V_{Shell} - V_{tube}) - (\frac{1}{2} r_{shell}^2 \theta - A_{ACO}) L_V \tag{5.30}$$

where r_{shell} is the inside radius of the shell, θ is the angle as shown in Figure 5-12, A_{ACO} is the area bounded by triangle AOC and L_V is the length of the vaporizer. Now, Equation (5.30) reduces to:

$$V_l = (V_{Shell} - V_{tube}) - (\frac{1}{2} r_{shell}^2 (2\cos^{-1}((h_l - r_{shell})/r_{shell})) - (h_l - r_{shell})\sqrt{(2h_l r_{shell} - h_l^2)})L_V \tag{5.31}$$

where, h_l is the height of the pentane liquid level from the bottom of the vaporizer, r_{shell} is the internal radius of the shell and r_{tube} is the outer radius of the tube.

If the liquid pentane level is lower than the top of the tube channel,

$$V_l = (V_{Shell} - V_{tube}) - V_{vapour} - V_{tube,APL} \tag{5.32}$$

where $V_{tube,APL}$ is the volume of the tube above pentane liquid line.

Equation (5.32) reduces to the following Equation:

$$V_l = (V_{Shell} - V_{tube}) - (\frac{1}{2} r_{shell}^2 (2\cos^{-1}((h_l - r_{shell})/r_{shell})) - (h_l - r_{shell})\sqrt{(2h_l r_{shell} - h_l^2)})L_V + (\frac{1}{2} r_{tube}^2 (2\cos^{-1}((h_l - r_{tube})/r_{tube})) - (h_l - r_{tube})\sqrt{(2h_l r_{tube} - h_l^2)})L_V \tag{5.33}$$

The liquid level, h_l is shown in Figure 5-12:

$$h_l = r_{shell} + b \tag{5.34}$$

The percentage of liquid level is calculated from the following equation:

$$l_{\%} = \frac{(h_l - h_{l,\min})}{(h_{l,\max} - h_{l,\min})} \times 100 \tag{5.35}$$

Equations (5.29) – (5.35) assume that there is no vapour below the liquid surface level. As below the liquid surface level boiling heat transfer is occurring, such assumption is an approximation only. A numerical simulation of the vaporizer pentane level of one of the BRN-ORC using the above assumption was carried out [80]. The simulated vaporizer pentane level remained largely within 5% of observed value so "there is no vapour below the liquid surface" is a reasonable assumption to serve our modelling purpose.

In the ORC cycles, brine/steam inlet and out temperatures as well as mass flow rates are known. Therefore the brine/steam side heat transfer can be easily calculated from the following equation:

$$\dot{Q}_g = \dot{m}_g (c_{P,g} \Delta T + L) \tag{5.36}$$

Where $\dot{Q}_g$ is the heat transfer from the geothermal fluid, $\dot{m}_g$ is the geothermal fluid flow rate, $c_{P,g}$ is specific heat of geothermal fluid at constant pressure, ΔT is the temperature difference of sensible heat and L is the latent heat of condensation (if there is any). If the geothermal fluid is at liquid state only, $L = 0$. There are some practical issues to be addressed prior to applying Equation (5.36) directly to Mokai 1 ORCs, especially for the BOT-ORCs where some of the steam is vented from the vaporizer along with the NCGs. The quantity of vented steam and NCGs is not known.

Nakaoka and Uehara [81] have presented experimental results showing the relationship between the overall heat transfer coefficient and the heating fluid mass flow rate for shell and plate heat exchanger. Bai et al. [53] have used this correlation for the overall heat transfer coefficient to model heat exchangers used in a binary cycle plant. The overall heat transfer coefficient as a function of geothermal fluid flow rate is calculated as:

$$U = U_r (\dot{m} / \dot{m}_r)^{0.5} \tag{5.37}$$

here, U_r and $\dot{m}_r$ are the reference (design) overall heat transfer coefficient and the reference (design) geothermal fluid mass flow rate. In case of ORC Mokai 1, these are design parameters. U and $\dot{m}$ are the actual (off design) overall heat transfer coefficient and the actual (off design) mass flow rate.

Now, from Equation (5.17) we can calculate the heat transfer in the vaporizer:

$$\dot{Q}_{23} = U_r (\dot{m} / \dot{m}_r)^{0.5} A \; F \Delta T_m \tag{5.38}$$

The above Equation can be written as

$$\dot{Q}_{23} = U_r (\dot{m} / \dot{m}_r)^{0.5} A \; \Delta T_{m,c} \tag{5.39}$$

where $\Delta T_{m,c} = F \Delta T_m$.

5.3.4 The ORC condenser model of Mokai 1

Figure 5-13 presents a schematic of the air-cooled cross-flow condenser used in the Mokai 1 power plant. There are three banks of horizontal finned tubes that cooled by forced convection. Pentane vapour enters first into the inlet header (not shown in the figure). Then pentane vapour cools while passing through horizontal tubes and changes phase from gas to liquid. When pentane reaches the outlet header of the condenser, it is 100% liquid. The flow of pentane inside the tubes can be assumed as stratified [75] layer for Mokai 1 geothermal power plant. The following paragraphs present the models used for the condenser heat load calculations.

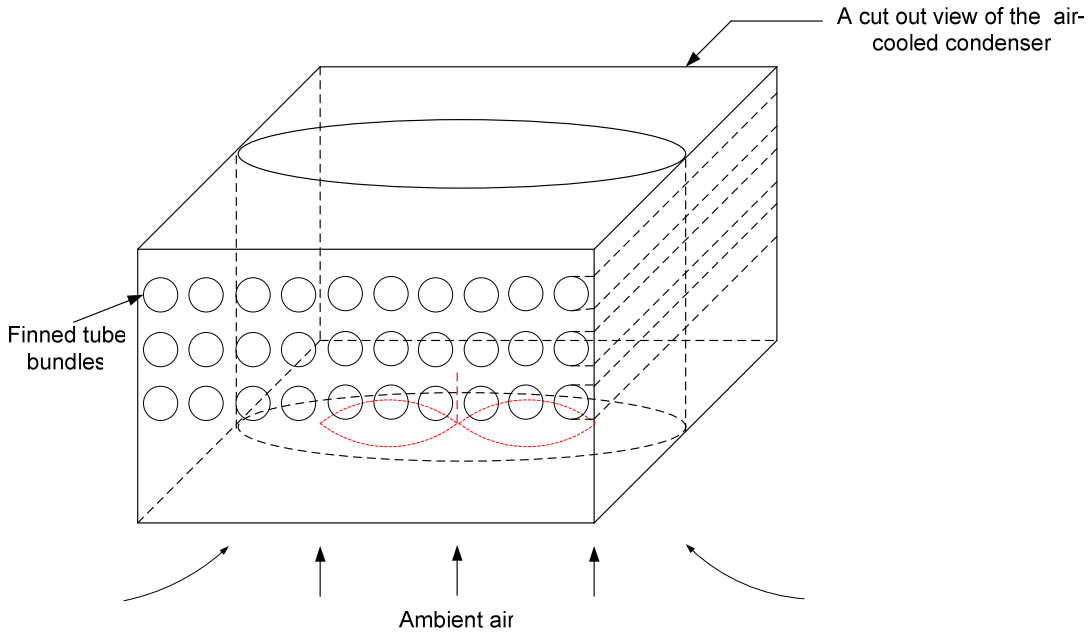

Figure 5-13: Schematic of air-cooled condenser used in the Mokai 1 power plant

The tube side convective heat transfer coefficient

The tube side convective heat transfer coefficient for horizontal tubes with a stratified layer can be calculated form the Equation (5.25) and (5.26) with pentane as the working fluid.

The airside convective heat transfer coefficient

The condenser tubes have circular fins attached to them to enhance the airside heat transfer rate. The weighted airside convective heat transfer coefficient for the finned tube is calculated as follows [75]:

$$h_o A_t = \alpha(A_f \eta_f + A_r) \tag{5.40}$$

where, A_r is the surface of the tube that is not covered by fins, A_f is the surface of the fin and A_t is the total surface area, $A_t = A_f + A_r$. The fin efficiency, η_f is calculated from following Equations [75]:

$$\eta_f = \left[1 + \frac{1}{3}(ml_c)^2 \sqrt{\frac{\frac{d}{2} + h}{\frac{d}{2}}} \right]^{-1} \tag{5.41}$$

$$m = \sqrt{\frac{\alpha}{k y_b}} \tag{5.42}$$

where, α is calculated from [75] using $l_c = h + y_b$.

The average Nusselt number for a finned tube in a bank with a staggered tube arrangement with the number of rows fewer than four can be calculated using following empirical Equation [75]:

$$Nu = 0.19(\frac{a}{b})^{0.2}(\frac{s}{d})^{0.18}(\frac{h}{d})^{-0.14}\,\mathrm{Re}^{0.65}\,\mathrm{Pr}^{0.33} \tag{5.43}$$

where, d is the tube diameter at the fin base, $a = s_1/d$, $b = s_2/d$, s_1, s_2 are transverse and longitudinal bank pitch (Figure 5-14), and s is fin spacing. This equation is valid in the range $10^2 < \mathrm{Re} < 2 \times 10^4$.

$$Nu = \frac{\alpha d}{k} \tag{5.44}$$

And

$$\mathrm{Re} = \frac{\rho w d}{\eta} \tag{5.45}$$

where, w is the maximum velocity of the fluid which occurs at the minimum free cross section of the finned-tube bank (Figure 5-14).

The overall heat transfer from a finned-tube heat surface with fouling layer can be obtained from 1D thermal resistance method for series thermal resistance:

$$\frac{1}{U} = R_{fi}(\frac{A_t}{A_i}) + \frac{1}{\alpha_i (A_i / A_t)} + \frac{b_w}{k_w (A_{nb} / A_t)} + \frac{1}{\alpha_0} + R_{fo} \tag{5.46}$$

Where, R_{fi} = fouling resistance on the inside surface; A_i = inside surface area; A_{nb} = means the bare surface area; b_w = tube wall thickness; R_{fo}= fouling resistance on the outside surface. k_w is the thermal conductivity of the wall material.

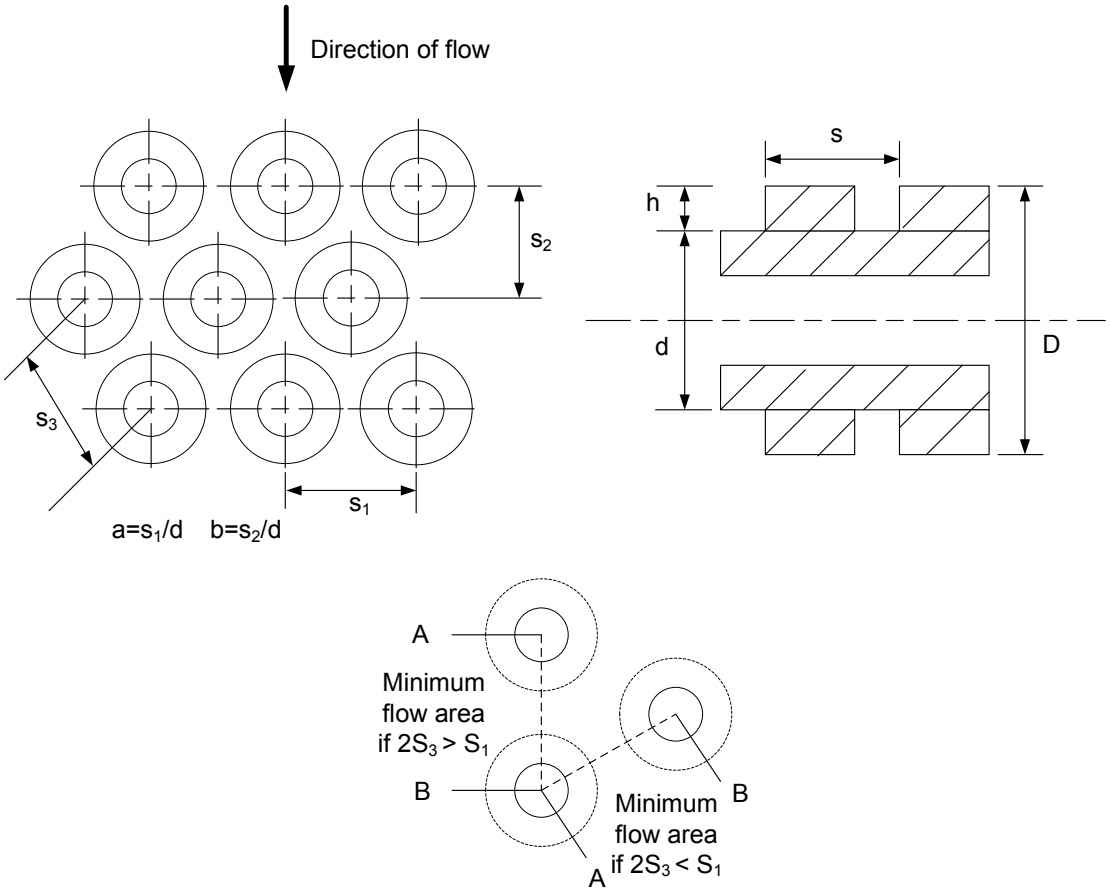

Figure 5-14: Definitions of quantities for flow in finned-tube banks.

The heat rejection rate from the condenser is:

$$\dot{Q}_{41} = UA_t \Delta T_m \tag{5.47}$$

The logarithmic mean temperature difference (LMTD) needed in the above equation is calculated as:

$$\Delta T_m = \frac{T_o - T_i}{\ln\left[(T_w - T_i)/(T_w - T_o)\right]} \tag{5.48}$$

Where, T_o and T_i are outlet and inlet temperatures of cooling air, respectively. T_w is the wall temperature which is not known and it should be calculated iteratively. The fluid properties are evaluated at the average temperature of inlet and outlet.

In Equation (5.48), the outlet temperature of air, T_o is not known and is calculated from following Equation derived from energy balance.

$$T_o = T_w - e^{-\frac{UA}{\dot{m}_{air} c_{P,air}}} (T_w - T_i) \tag{5.49}$$

The value of T_w is obtained iteratively. At first T_w is assigned a value very close to T_{sat} then the condenser heat load is calculated, this process is repeated until the condenser heat load converges to a tolerance of |e|<0.1 (difference between subsequent values of condenser heat load in iterations) and consequently T_w is determined. If |e| is assigned a bigger value less number of iteration will be required and the accuracy will decrease, whereas if |e| assigned a smaller value then more number of iteration will be required but the accuracy will increase.

Table 5.6 summarises parameter values of ORC condenser of Mokai 1 geothermal power plant.

Table 5.6: Condenser parameter values (from design)

Symbol	Value	Symbol	Value
s_1	57.00 [mm]	d	25.41 [mm]
s_2	99.75 [mm]	d_i	23.41 [mm]
s_3	63.73 [mm]	D	57.00 [mm]
s	2.54 [mm]	h	15.80 [mm]
b	4.09 [-]	a	2.24 [-]
A_f	28.44 [m2]	A_i	1.35 [m2]
A_t	29.61 [m2]	A_r	1.17 [m2]
A_{nb}	1.46 [m2]	y_b	1.0 [mm]
b_w	1 [mm]		

Condenser air velocity

Figure 5-15 shows the velocity profile of the condenser inlet air measured over the span of the fan. The volumetric flow can be calculated by

$$\dot{V} = \int_a^b A(r)dr \tag{5.50}$$

where *A(r)* is the area of flow velocity of the fan as a function of radius, *a* and *b* represent limits of integral. *A(r)* is calculated as $A(r)= 2\pi rf(r)$. Here *f(r)* represents the flow velocity as a function of the fan radius.

The integral is evaluated using piecewise method. The velocity profile is divided into three sections. The data and equations are supplied by MRP based on measurements.

For section 1:
r =0 to 1.09, f(r) = 1.92 m/s
For section 2:
r =1.09 to 1.33, f(r) = 2.26 m/s
For section 3:
r =1.33 to 2.46, $f(r) = 0.5702r^3 - 1672r^2 + 61.68r - 51.543$ m/s

Solving Equation (5.50) the flow rate 108.4 m^3/s is obtained. We can now find the flow velocity (average) over the tubes by dividing the volumetric flow rate with the cross-sectional area (30.31m^2) at the entry of tube bundle (rectangular area). The calculated value of air flow velocity is 3.58 m/s and it will be used for subsequent simulations of the air cooled condenser.

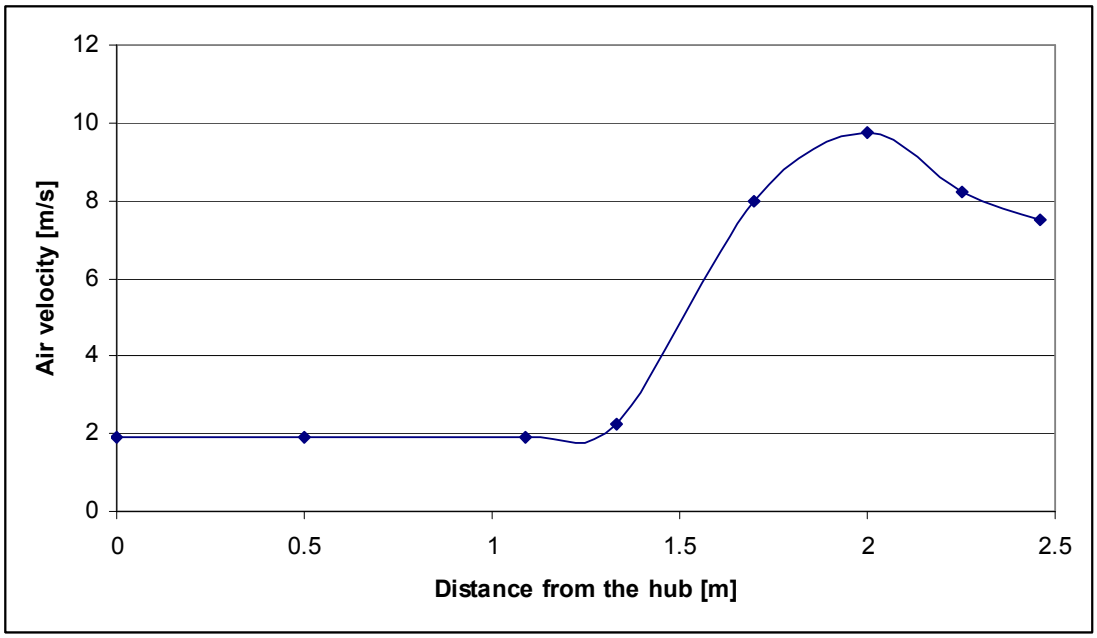

Figure 5-15: Air inlet velocity profile of the condenser

5.4 The turbine models for the mokai 1 geothermal power plant

In this section, the modelling approach to different kinds of turbines used in the Mokai 1 geothermal power plant is discussed. There are two types of turbine used in the plant, namely: steam turbine and pentane turbine. There is only one steam turbine and a total 12 pentane turbines used in the plant. Two pentane turbines are coupled to a generator for each of the binary cycles (two brine OECs and four for bottoming OECs).

The steam turbine model

The steam turbine is modelled using Equation (5.8) – (5.11). The turbine isentropic efficiency is assumed constant (however, provision is in Simulink® model to change the isentropic efficiency) and same as the original design (85.77%) subjected to the following assumptions to represent the design conditions:

- The steam is saturated when it enters the turbine. In the actual operations of the plant, the inlet property of the steam entering the steam turbine is controlled accurately to the design level (saturated at 205.5°C).
- The effect of Non-Condensable Gases (NCG) is negligible and can be treated as water vapour as the percentage of NCG is very low; less than 2%.

- The mass flow is conserved in the turbine.
- The ambient temperature is fixed at 12°C same as the design.
- The heat loss to the surrounding is negligible

The exact composition of NCGs is not available. However, MRP suggest that CO_2 is the main constituent of the NCGs. Therefore, an analysis was performed assuming NCGs to be made from 100% CO_2. In the literature such assumption has been made before [82, 83]. Here the effect of NCGs on the total enthalpy of steam at the entry of steam turbine is considered as the indicator of whether one should neglect the effect of NCGs. Figure 5-16 shows the total enthalpy at turbine inlet as a function of CO_2 content. Figure 5-17 shows the percentage error introduced by neglecting the effect of NCGs on the total enthalpy at the turbine inlet, at about 2% CO_2 content, the error is about 1.5%. This calculation is specific to REFPROP property database [70] where reference temperature and pressure are assumed to be 25˚C and 1 bar, respectively. For calculation of total enthalpy, the steam enthalpy 2795.1 kJ/kg (saturated at 205.5ºC) and CO_2 enthalpy 667.87 kJ/kg (205.5ºC and 17.6 bar) is used. Gokcen and Yildirim [82] have analysed the effect of NCGs on the steam turbine power output and their study supports that NCGs at a level 1-2% can be ignored.

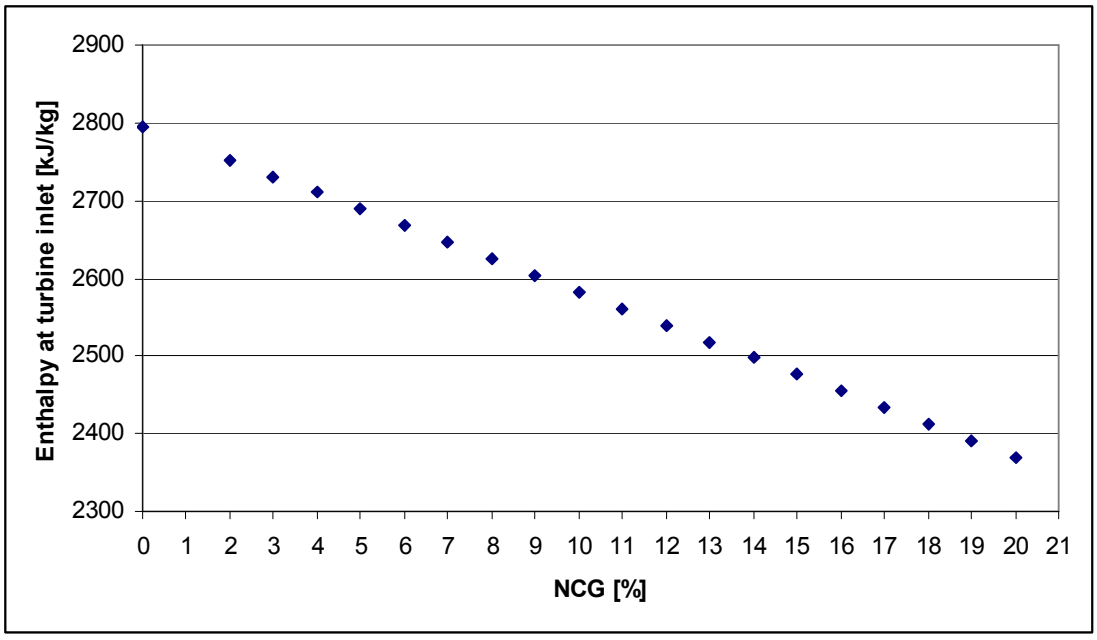

Figure 5-16: The effect of NCGs (assuming 100% CO_2) content on the enthalpy at the inlet of the steam turbine

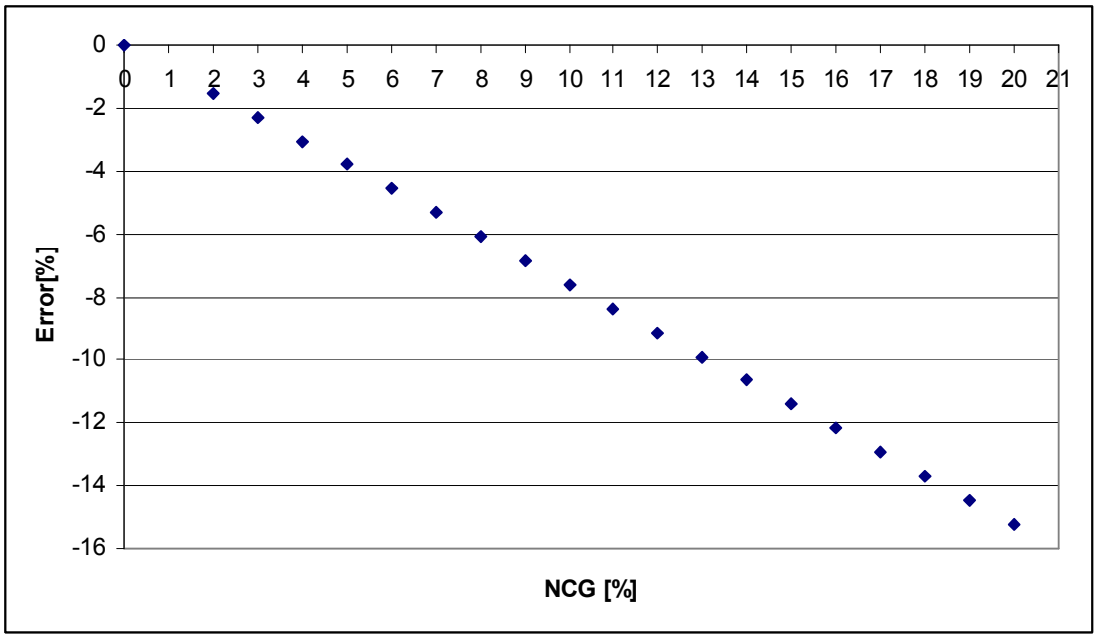

Figure 5-17: The percentage error introduced in the enthalpy at the steam turbine inlet assuming NCGs (assuming 100% CO_2) effect negligible

The pentane turbine model

There are two types of arrangements of pentane turbines in the Mokai 1 geothermal power plant. One type is for the BOT-ORC and the other is for the BRN-ORC. In the BOT-ORCs, two pentane turbines are fed from two separate vaporizer-separator arrangements and these two turbines are coupled to a single generator. In BRN-ORCs, pentane vapour first passes through the high pressure turbine then the low pressure turbine. Similarly to the BOT-ORCs, turbines in BRN-ORCs are also coupled to a single generator. BOT-ORCs operate at low pressure and temperature, whereas BRN-ORCs operate at high pressure and temperature. The pentane turbine model for steady state operation is very similar to the steam turbine model. It is subject to the following assumptions to represent the design conditions:

- Two coupled turbines are modelled as a single machine running a generator.
- The combined isentropic efficiency of the turbines is fixed and specified. However, option has been kept in the Simulink® model to change the isentropic efficiency. For short term performance analysis (Chapter 8), effect of change of isentropic efficiency has been taken into account.
- The mass flow is conserved in the turbine.
- The ambient temperature is fixed at 12°C same as the design.

- The heat loss to the surrounding is negligible

5.5 The Pump Model for the Mokai 1 Geothermal Power Plant

Very simple model is used for the pumps of Mokai 1 geothermal power plant (Equation (5.1) –(5.3)). The ratio of work input to the cycle pumps to the power output in the turbines used for the Mokai 1 geothermal power plant are in the order of 4% to 7%. Figure 5-18 shows pump characteristics curve of one of the pumps where the change in work input to the pumps changes very little under different working conditions. Thus the pumps can be assumed to have constant work input throughout the operating range of the plant.

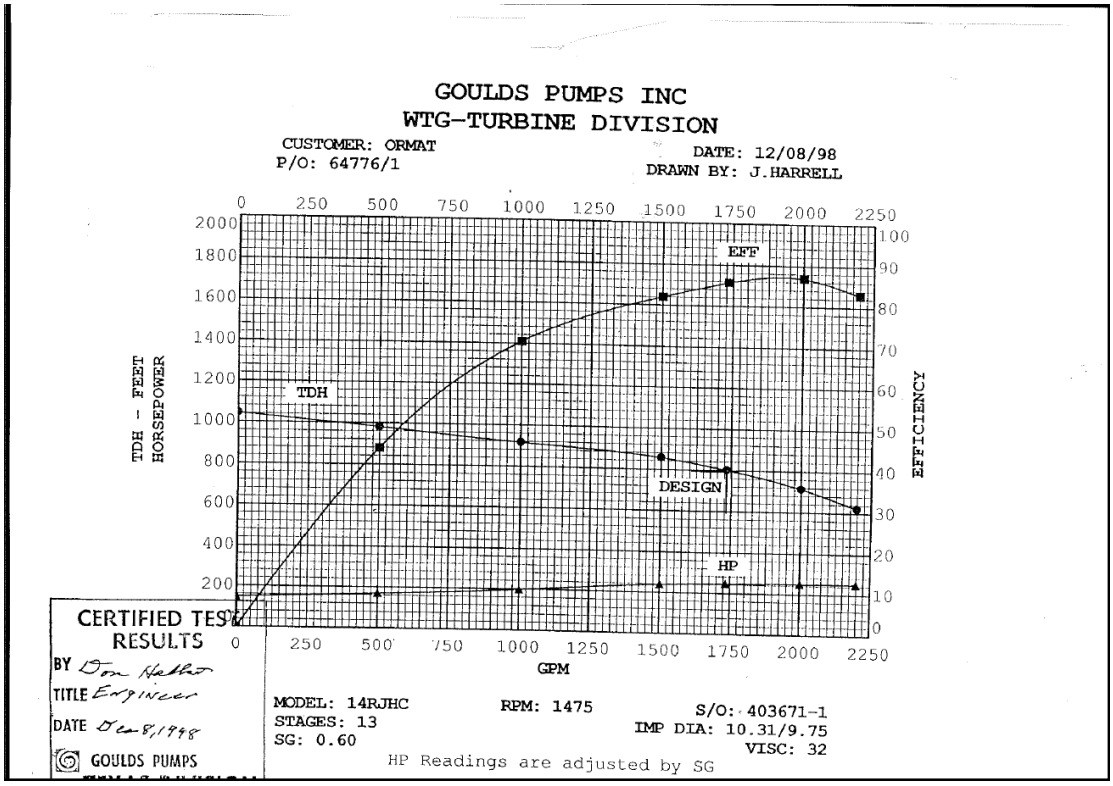

Figure 5-18: Pump performance curve of one of the cycle pumps of BRN-ORC

5.6 Simplified vaporizer heat transfer model for the short term performance

The LMTD values of the ORC vaporizers of the Mokai 1 geothermal power plant do not change much in the short term. The main reason is that most of the operating temperatures across the vaporizers are controlled. If LMTD remains unchanged the number of iteration required to come to a solution get reduced. From energy balance,

$\dot{Q}_g$ and $\dot{Q}_{23}$ must be equal (i.e., $\dot{m}_g(c_{P,g}\Delta T + L) = U_r(\dot{m}/\dot{m}_r)^{0.5} A\ \Delta T_{m,c}$) which means total heat transfer is related to both LMTD and geothermal fluid flow rate. However, if change in geothermal fluid flow remains minimal, the effect of change in geothermal fluid flow rate can be ignored; the proof is presented in appendix 4. In short term operation of Mokai 1 plant, the geothermal fluid flow rates do not change much. Figure 5-19 presents measured geothermal brine and steam mass flow rates for short term operations (two days) taken from Mokai 1 plant operational log. The steam mass flow rate remained within 2% with average change less than 1% and the brine mass flow rate remained within 10% with average change less than 3% of the initial value.

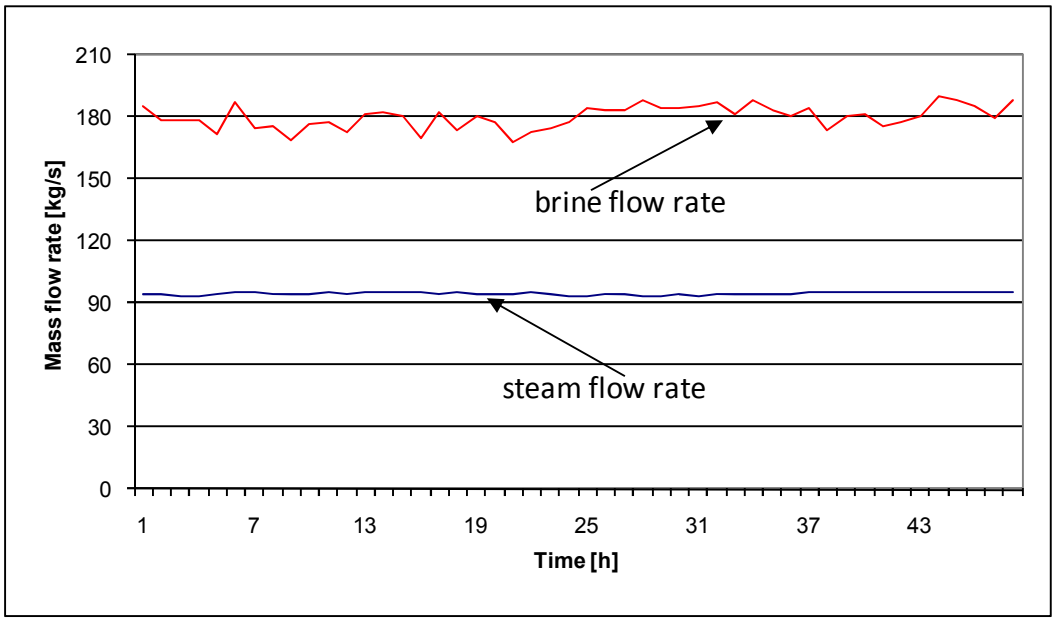

Figure 5-19: Hourly (10/01/2007-11/01/2007) total steam (BOT-ORC X 4) and brine (BRN-ORC X 2) mass flow rates

In cases where the LMTD does not change (and consequently nor does the correction factor F) and as the heat transfer area is fixed Equation (5.39) can be written as:

$$\dot{Q}_{23} = \dot{Q}_{23,r}(\dot{m}/\dot{m}_r)^{0.5} \tag{5.51}$$

here, $\dot{Q}_{23,r}$ is the reference heat transfer of the ORC vaporizer of Mokai 1. For OEC 11, $\dot{Q}_{23,r}$ is equal to the design value. For OEC 1, $\dot{Q}_{23,r}$ can be use as the design value if the brine outlet flow is 140ºC (Figure 5-26) as the error introduced will be

negligible compared to the design brine outlet temperature of 152ºC. If the unit is adjusted to run at 120ºC brine outlet temperature then the $\dot{Q}_g$ should be updated using Equation (5.36) and hence $\dot{Q}_{23,r}$ is updated. The simplification of vaporizer heat transfer (Equation (5.51)) applies only to chapter 8 and 9.

5.7 Sensitivity analysis for simplified heat transfer equation on pentane side

The bottoming organic Rankine cycle

For the BOT-ORC, steam inlet and outlet (condensate) temperature and the vaporizer pentane outlet temperature are controlled in the plant. Figure 5-20 and Figure 5-21 show steam inlet temperature and condensate outlet temperature of a BOT-ORC (OEC 11) vaporizer. Figure 5-22 shows the vaporizer pentane outlet temperature of OEC 11. In these three figures the parameters remain nearly unchanged. The steam inlet temperature to OEC 11 increased about 0.5ºC over a period of one year. This is due to the fact the resource enthalpy of the Mokai 1 field is increasing. For Figure 5-21 and 5-22 values below 80ºC and 90ºC, respectively should be disregarded as they represent either sensor error or the unit is not in operation.

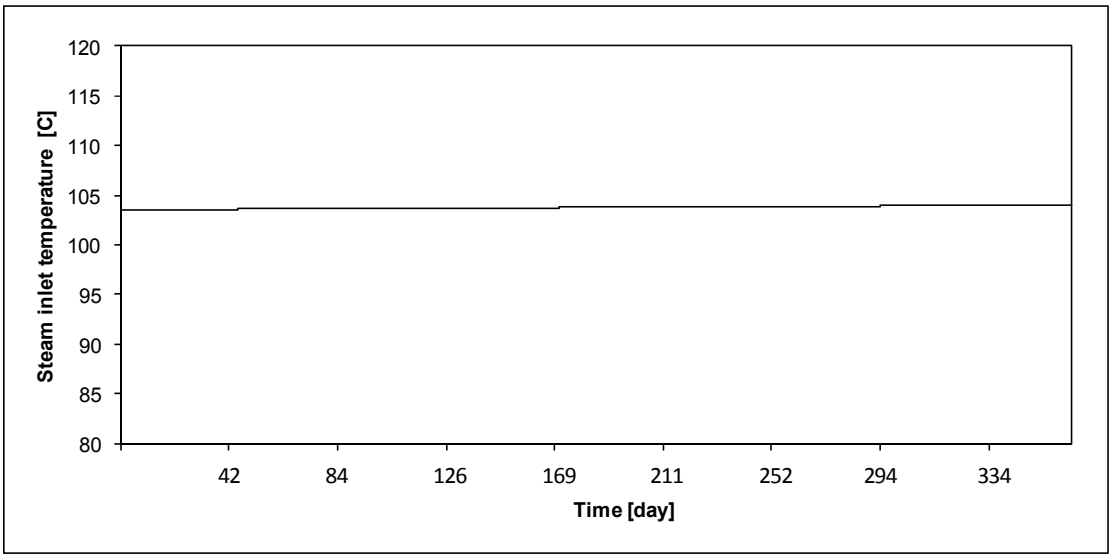

Figure 5-20: Steam inlet temperature to the vaporizer of OEC 11 for the year 2007

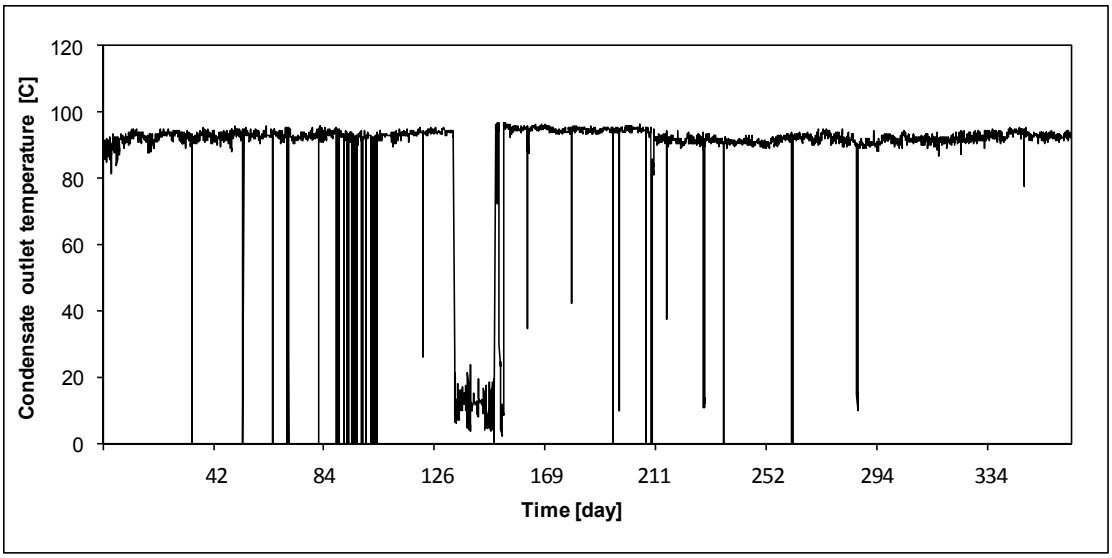

Figure 5-21: Condensate outlet temperature from vaporizer of OEC 11 for the year 2007

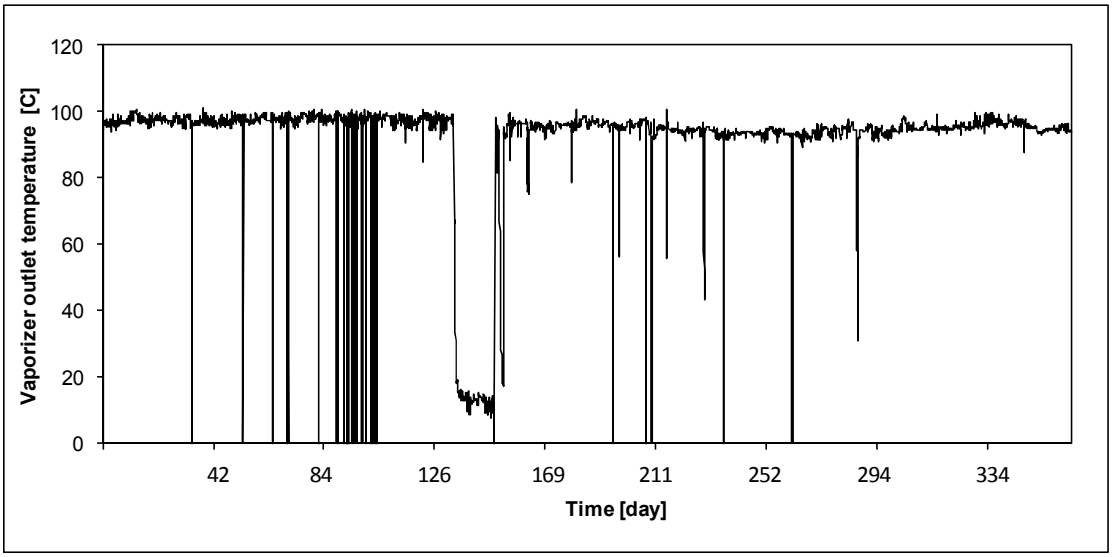

Figure 5-22: Vaporizer pentane outlet temperature of OEC 11 for the year 2007

Among the four temperatures required to calculate the LMTD and correction factor (F) for the OEC 11, three are nearly unchanged. The original OEC 11 design had a preheater which would act as a capacitor to stabilise the vaporizer inlet pentane temperature. However, it will be shown that the pentane inlet temperature to the vaporizer has less significant effect on the total heat transfer in the vaporizer. The vaporizer pentane inlet temperature is directly related to the condenser outlet temperature. Unfortunately, the condenser outlet temperature of OEC 11 is not available. However, all the OECs have identical air cooled-condensers. Both the

BRN-ORC unit and the BOT-ORC units have similar level of design working conditions for the condenser. Therefore, the condenser outlet temperatures of OEC 1 (a BRN-ORC) can be used for the analysis of OEC 11.

Figure 5-23 shows the condenser outlet temperatures of OEC 1. The temperatures are most likely to be within 5ºC-35ºC. We can change the vaporizer inlet pentane temperature (5ºC-40ºC) of OEC 11 model and analyse the effect. Let us divide the vaporizer into two zones: preheat and boiling. The calculated heat transfer in the preheat zone is 8754 kW (calculated form pentane side energy balance) and total heat transfer is 46929 kW i.e., about 18.65 % heat is used in the preheat zone at design condition without preheater. Figure 5-24 shows the effect of vaporizer inlet temperature on LMTD value of preheat zone (not the whole vaporizer) of OEC 11. A change in the vaporizer inlet temperature of 35ºC (from 5ºC to 40ºC) results in about 20ºC change in the LMTD i.e., about a half.

The LMTD value of the boiling zone will remain unchanged. The heat transfer is calculated based on the bulk (average) temperature which does not change largely for the preheat zone as a result of pentane inlet temperature change. So we can assume the overall heat transfer coefficient for the preheat zone to be constant. This means that the heat transfer in the preheat zone is directly proportional to the LMTD in that zone. However, as the heat transfer in the preheat zone is much less than the total heat transfer in the vaporizer of OEC 11, if we assume the LMTD to be constant the error introduced to the global heat transfer will be minimal. Table 5.7 shows the error introduced by assuming unchanged LMTD for OEC 11.

In Table 5.7 column 3 is obtained by multiplying the *UAF* value for the preheat zone with corresponding LMTD. The *UAF* for the preheat zone is obtained from designed preheat zone heat transfer (8754 kW) divided by designed LMTD. Column no. 4 is obtained by adding column 3 with design boiling zone heat transfer (38175 kW) with the assumption boiling zone heat transfer does not change as LMTD of boiling zone will be relatively unchanged. The error introduced assuming constant LMTD (and hence constant heat transfer as mass flow is assumed constant) is presented in column 5. For relatively large change in pentane inlet temperature in the vaporizer has less significant impact on the global heat transfer.

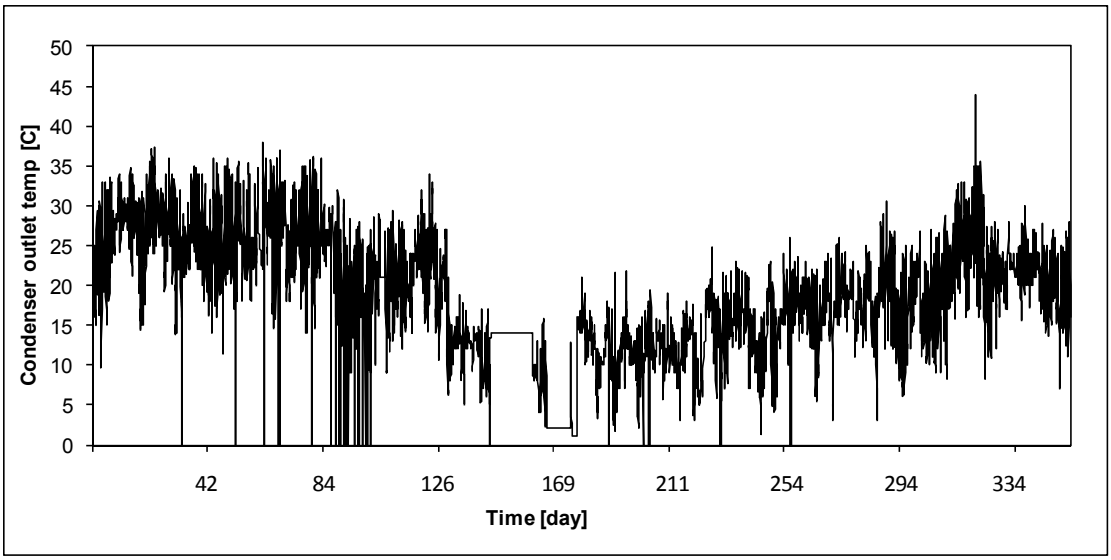

Figure 5-23: Condenser outlet temperature of OEC 1 for the year 2007.

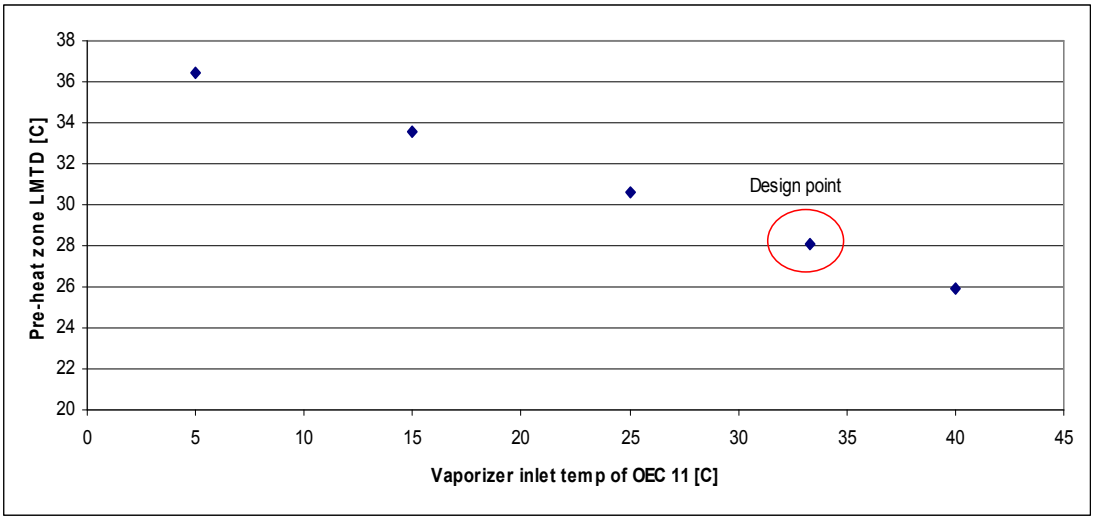

Figure 5-24: The effect of vaporizer inlet temperature change on the preheat zone LMTD

Table 5.7: Effect of vaporizer pentane inlet temperature on the global heat transfer of OEC 11

Vaporizer pentane inlet temperature [ºC]	LMTD [ºC]	Preheat zone transfer [kW]	Global heat transfer [kW]	Error introduced in global heat transfer [%]
5	36.41	11359.74	49533.74	5.55
15	33.55	10466.87	48640.87	3.65
25	30.59	9544.56	47718.56	1.68
40	25.93	8090.55	46264.55	-1.42

The brine organic Rankine cycle

The brine inlet temperature of the superheat vapour unit is unchanged at about 207.6ºC (wet steam). Figures 5-25 and 5-26 represent the vaporizer pentane outlet temperature and brine outlet temperature. For Figure 5-25 all values below 180ºC should be disregarded and for Figure 5-26 all values below 120ºC as they represent either sensor error or periods when the plant is not in operation. In Figure 5-25 the vaporizer pentane outlet temperature remains nearly unchanged. Figure 5-26 shows that the brine outlet temperature either remains at 140ºC or 120ºC. The design brine outlet temperature is 152ºC. If the plant operates at 140ºC of brine outlet temperature, then the change in LMTD is small and can be ignored.

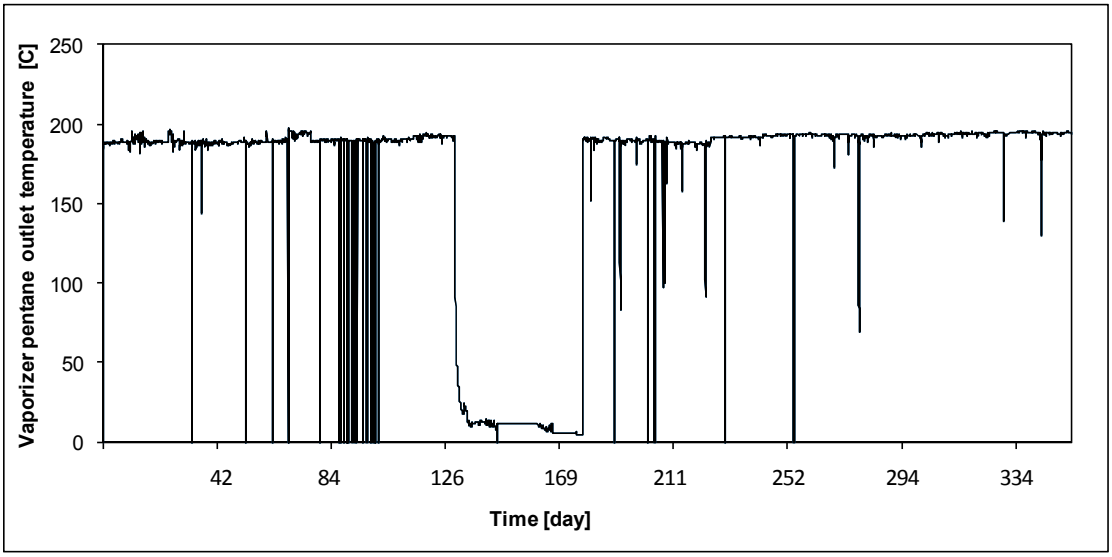

Figure 5-25: Vaporizer pentane outlet temperature of OEC 1 for the year 2007

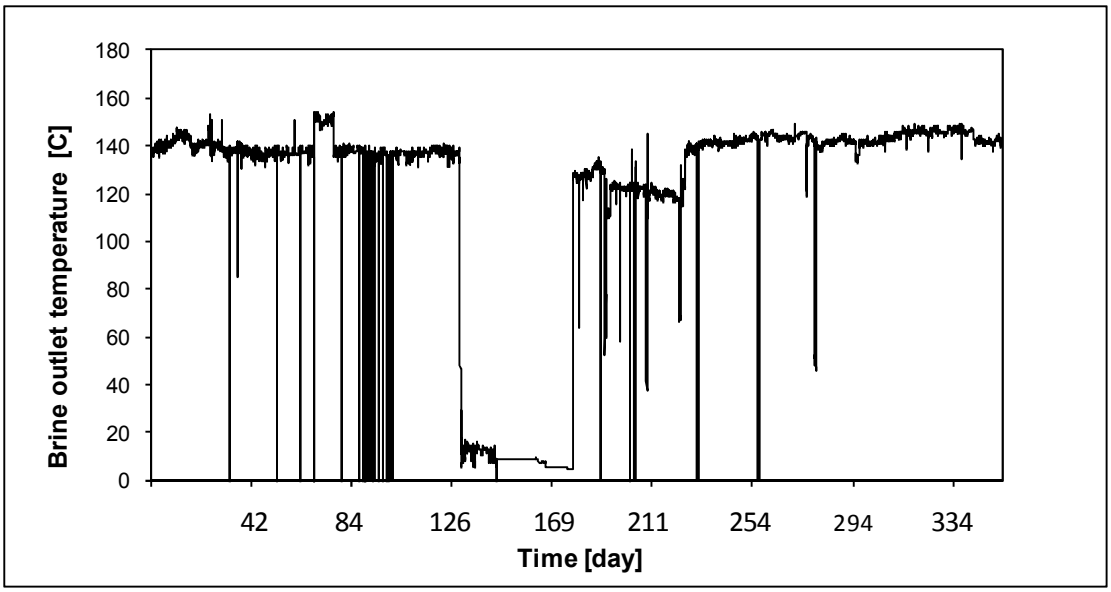

Figure 5-26: Brine outlet temperature from vaporizer of OEC 1 for the year 2007

There is a recuperator attached in the superheated vapour cycle to recover some of the heat from the turbine outlet pentane. The vaporizer inlet temperature (pentane) of OEC 1 remains nearly unchanged due to capacitance effect by the recuperator. The design heat transfer of the recuperator is 7000kW. There is no information available on the design turbine outlet temperature. However, using the information of the heat transfer in the recuperator and the condenser design operating parameters the turbine outlet temperature can be estimated. The estimated value of turbine outlet temperature is 119ºC. The physical properties are calculated based on the bulk temperature and for typical operation of the recuperator, physical properties change less significantly with the change in recuperator inlet temperature (from condenser). The mass flow rate inside the ORC cycle remains relatively unchanged over long period.

The value of UA for the recuperator can be calculated using the LMTD (28.88ºC) from the recuperator heat transfer. Assuming a constant UA, the vaporizer inlet temperature can easily be calculated. Table 5.8 summarizes the condenser outlet temperatures and the corresponding recuperator outlet temperatures. The design vaporizer inlet temperature is 85.2ºC. The vaporizer inlet temperature remains nearly unchanged for a wide range of condenser outlet temperatures. It is noteworthy here that the ambient temperature of the plant site remains within -5ºC to 30ºC for the year 2007 [72].

Table 2.8: Effect of condenser outlet temperature on vaporizer inlet temperature of OEC 1

Recuperator inlet temperature [ºC]	LMTD of recuperator [ºC]	Vaporizer inlet temperature [ºC]	Error introduced in global heat transfer [%]
5	44.64	80	-5.87
15	40.28	82.69	-2.72
25	35.62	84.86	-0.16
40	27.74	86.61	1.90

From the above discussion it is evident that both for the BOT-ORC and the BRN-ORC unit LMTD remains nearly unchanged for typical operation of the ORC units.

5.8 Summary

This chapter has presented component models for a geothermal power plant. At first simple model of a Rankine cycle is presented. Then the basics of heat exchangers are discussed. Adaptation of the simple model to a real power plant component i.e. Mokai 1 geothermal power plant is also discussed in this chapter. LMTD value is assumed constant for the heat transfer model of vaporizer for short term performance analysis (chapter 8 & 9) and justification of such assumptions is provided.

Chapter 6

System Model for Analysing Environmental Effect on Long Term Plant Performance

6.1 Introduction

Power plants have a large number of parts involving an enormous number of flow recirculations and splitting, and connections of several subsystems. The overall plant behaviour, both static and dynamic, cannot be simply inferred from that of its components, rather it is essentially determined by their interaction [84]. The main idea of this chapter is to train the component models developed in the previous chapter and connect them to create the system model of the Mokai 1 geothermal power plant which will be used for long term performance analysis presented in chapter 7.

On one hand the Mokai 1 geothermal power plant is already over a decade old, so many design changes are visible. On the other hand, in the absence of a suitable simulator, it is very difficult for the plant operators to predict its performance in advance. Modelling and simulation of this plant are not trivial jobs and specifically, in the absence of appropriate design details and performance data, one must rely on justified assumptions and engineering judgements. By the end of this chapter a simulator of Mokai 1 geothermal power plant for steady state operation will be created for long term performance modelling discussed in the next chapter.

6.2 The modelling approach

The programming is done based on modular concept to keep the component's governing equations organized. The central idea of modelling is to simultaneously

solve all governing equations. In a large process system model like the geothermal power plant, it is very difficult to keep track of all the variables necessary, modular concept minimizes the problem of keeping record of all the variables.

Modular systems use input and output ports through which all interaction with the environment occurs. They can be coupled together by connecting output ports to input ports and can have a hierarchical structure in which component systems are coupled together to form larger ones. Modules can be developed and tested as a stand-alone unit. They can also be reused in any application context in which its behaviour is appropriate and coupling to other components makes sense. Although coupling establishes output-input pathways, the systems modeller is completely free to specify how data flows along such channels. Information flow is one of many interactions that may be represented [85].

A wide rage of commercial software is available [86-90] that can be used for modelling a conventional power plant. However, it is not easy to find single software which is readily applicable for modelling geothermal power plants as geothermal power plants differ significantly from the conventional power plants (discussed in the chapter 1). The modelling presented in this chapter used the Matlab/Simulink® [88] software package interfaced with physical properties data base of common fluids, Refprop® [70]. Simulink® is based on modular system approach and provides flexibility, which is important for modelling of unconventional power plant such as the geothermal power plants.

6.3 Steady state model of the Mokai 1 geothermal power plant

In this section, a steady state model of the Mokai 1 geothermal power plant is presented based on the modular concept described in the previous section. The model is very simple and composed of generic elements including a steam turbine, pentane turbines, heat exchangers, pumps and the condensers. The system model is obtained by connecting component models presented in chapter 5 and solving simultaneously. Some engineering drawings for heat and mass balance of Mokai 1 geothermal power plant are supplied by MRP (Figure 4-3 to Figure 4-5). Many of the required values of cycle state points are not available in the Figures. Therefore, in this Chapter many of

the variable (such as the heat transfer) of Figures 4-3 to Figure 4-5 are fed as parameters to the model. For unknown values educated guess is made and then a simulation is run. From the simulation output a decision is made whether to increase or decrease the guessed values. This process is repeated unless all of the known state points converge to the known values. The guessed value(s) of a variable(s) at which the state points converge is taken as the design point of that variable. Variables like heat transfer are supplied as parameters in this chapter.

Once all unknown parameters and operating points are estimated, the heat transfer is changed from parameter to a variable and calculated using modelling approach discussed in chapter 5. Consequently, a simulator of Mokai 1 geothermal power plant for steady state operation is created. In this simulator only two input data required: geothermal fluid flow rate and steam content. As the well head condition i.e., pressure and temperature are controlled, the simulator can simulate performance using only the geothermal fluid flow rate and steam content as input data for steady state operation of Mokai 1 geothermal power plant. The steady state simulator will be used for adaptive approaches for long term performance improvement discussed in Chapter 7.

Turbine model

There are two basic types of turbines used in the Mokai 1 geothermal power plant based on working fluid: steam turbine and pentane turbine. A generic turbine model based on chapter 5 is developed then the model is customised for two different types of turbines. Figure 6-1 presents the computer program flowchart of the turbine model.

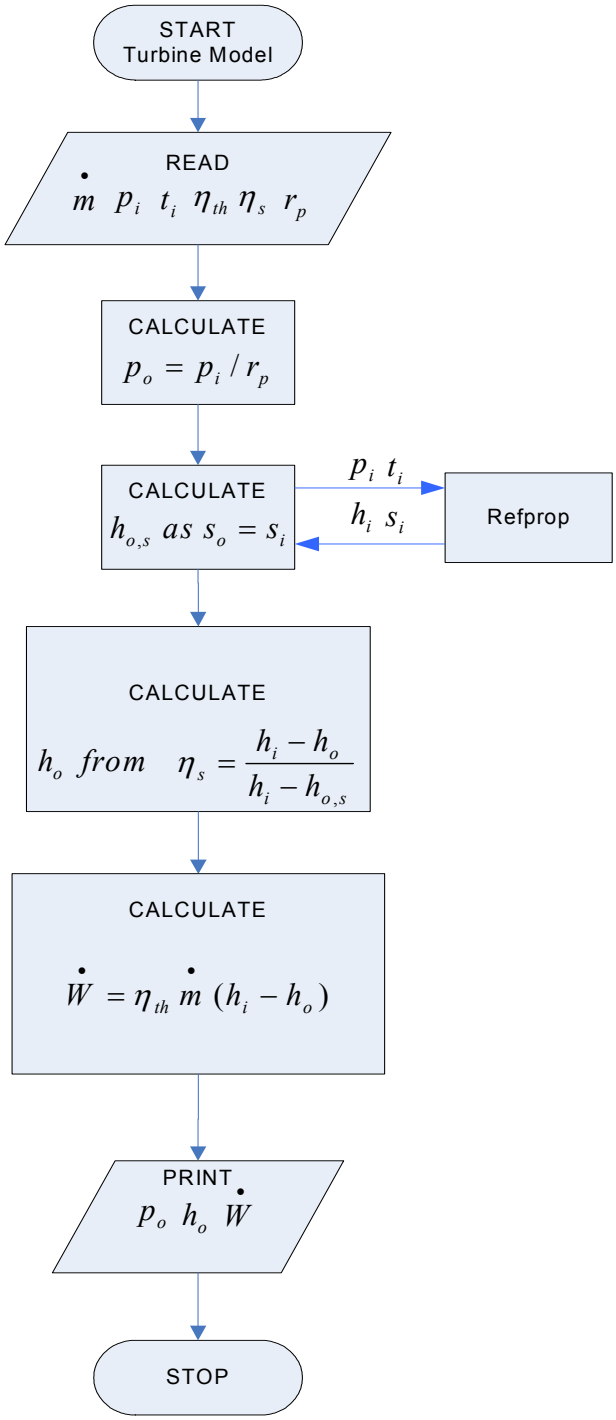

Figure 6-1: The computer program flowchart of the turbine model

Heat exchanger model

A generic heat exchanger model is developed then it was customized using the vaporizer and the condenser models. The main difference is in the heat transfer rate. The heat transfer rate is calculated separately using models presented in chapter 5 for

both the vaporizer and the condenser. It is then fed to the heat exchanger model as a parameter. If the heat transfer rate is $\dot{Q}$ [kW] then from energy balance we can write:

$$\dot{Q} = \dot{m}_{SN}(h_{o,SN} - h_{i,SN}) \tag{6.1}$$

$$-\dot{Q} = \dot{m}_{SR}(h_{o,SR} - h_{i,SR}) \tag{6.2}$$

Here, $h_{o,SN}$ and $h_{i,SN}$ are the enthalpies at the outlet and inlet of the heat exchanger cold side, respectively. $h_{o,SR}$ and $h_{i,SR}$ are the enthalpies at the outlet and inlet of the hot fluid, respectively. Heat given to a system is considered positive and heat given by a system is considered negative. As both the vaporizer and the condenser involved in phase change the value of heat transfer rate is virtually equal to the possible maximum value [73]. Figure 6-2 presents the computer program flowchart of the heat exchanger model.

The complete model

Once the modules are created and tested separately, they are integrated to model the whole plant. Figure 6-3 presents the flowchart for the whole plant. The NIST database Refprop® [70], interfaced with Matlab/Simulink® [88] was used for developing the computer model. The computer code of all the components is available in appendix 5.

6.4 Calibrating the model with existing design data from the manufacturer

Figure 6-4 shows the steady state model of Mokai 1 in Matlab/Simlink®. It can be seen from the figure that the Simulink® blocks are a very similar representation of the actual heat and mass balance diagram (Figure 4-3) of the Mokai 1 power plant which makes it easy for engineers and operators (who might use the model) to understand and operate. OEC 1 was taken to be representative of two (1 and 2) identical brine units (BRN-ORC). OEC 11 was taken to be representative of four identical (11, 12, 21 and 22) steam units (BOT-ORC).

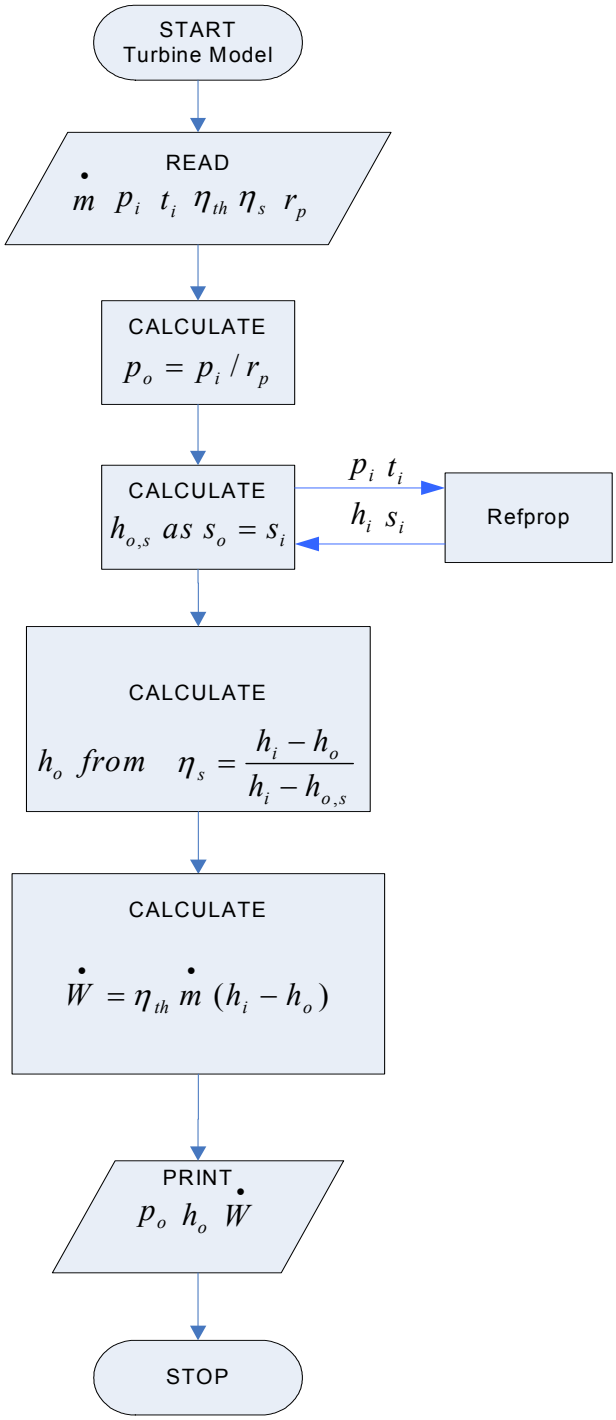

Figure 6-2: The computer program flowchart of the turbine model

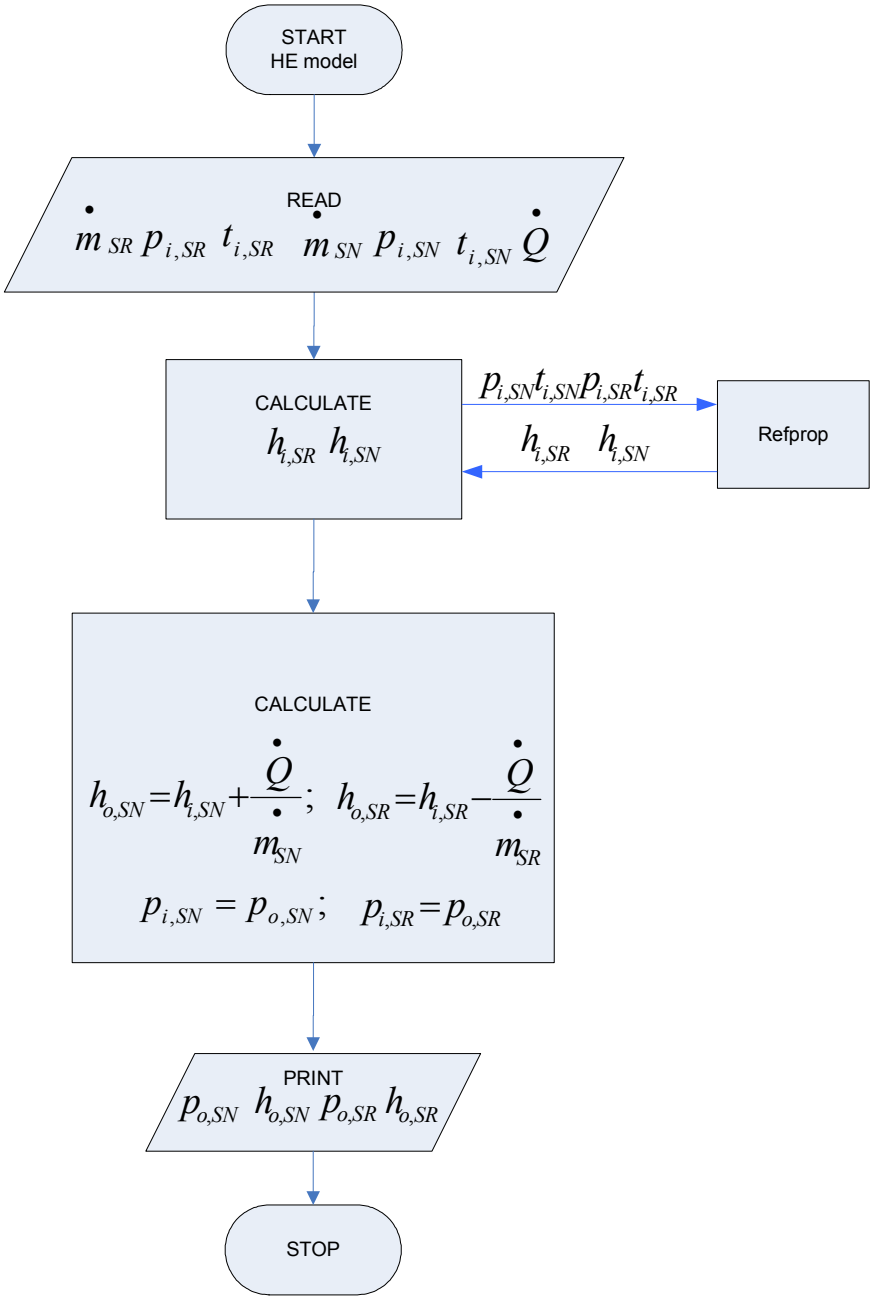

Figure 6-3: The computer program flowchart of the heat exchanger model

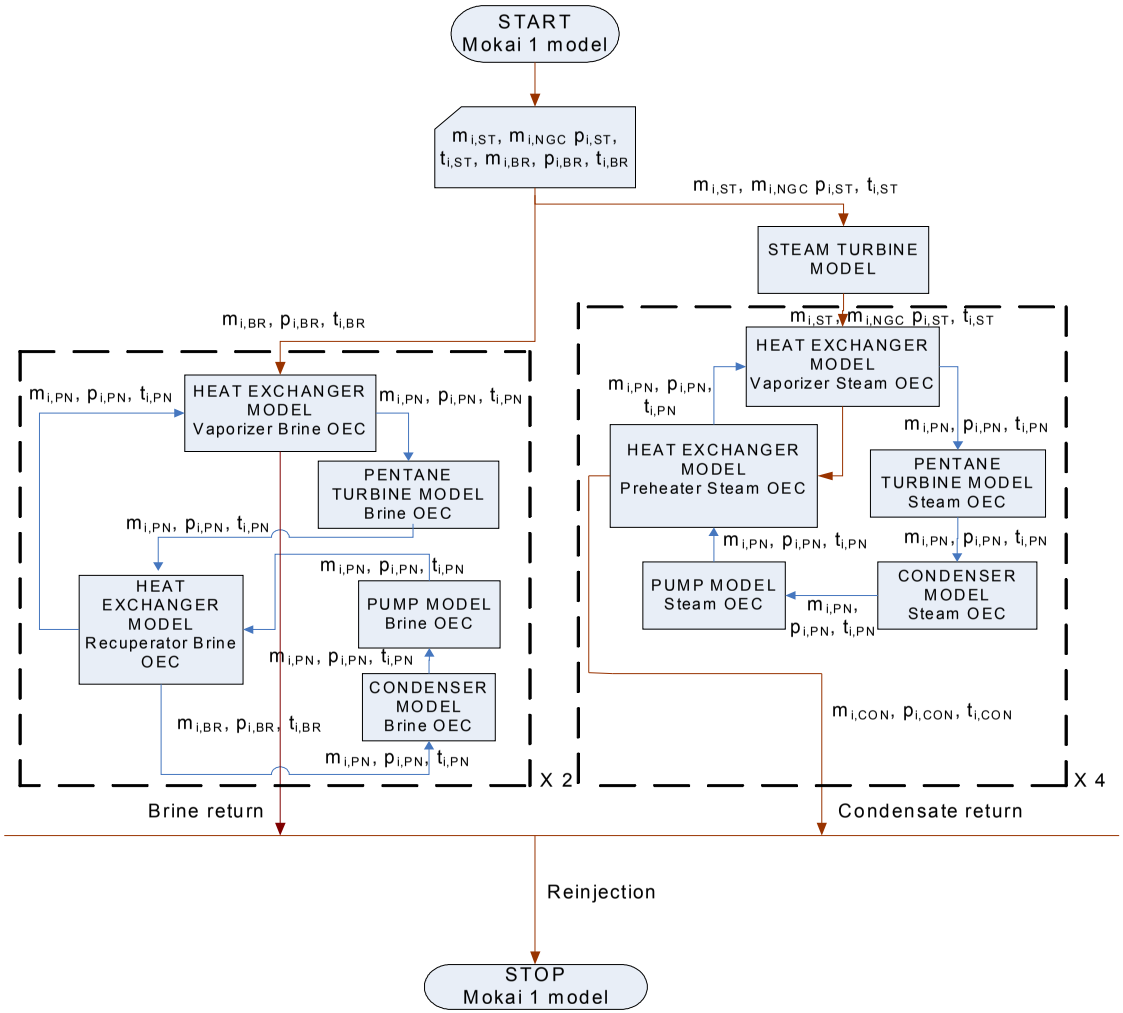

Figure 6-4: The computer program flowchart of the whole plant

Figure 6-5 presents the Simulink® graphical presentation of OEC 1 and Figure 6-6 presents the Simulink® graphical presentation of OEC 11. The resemblance to the actual process flow diagram is clear. The only difference can be seen is the block used for initialization.

Figure 6-7 presents state points of the steam turbines schematically. Table 6.1 presents simulation of the steam turbine model. Figure 6-8 shows the schematic diagram of the BOT-ORC. Table 6.2 presents results of training OEC 11, representing the bottoming ORC. In the heat and mass balance diagram of OEC 11 (Figure 4-4), the pump outlet pressure, the preheater outlet pressure and, the turbine outlet pressure and temperatures are not available. These values are determined iteratively to satisfy heat and mass balance in the cycle. Table 6.3 presents simulation of the steam inlet and outlet conditions of the bottoming cycle.

Figure 6-9 shows the schematic diagram of the BRN-ORC. Table 3.4 presents results of training of OEC 1, representing the brine ORC. In the heat and mass balance diagram of OEC 1 (Figure 4-5), the pump outlet pressure, the recuperator outlet pressure and, the turbine outlet pressure and temperatures are not available. These values are determined iteratively to satisfy heat and mass balance in the cycle. Table 6.5 presents the simulation of brine inlet and outlet conditions of the brine cycle.

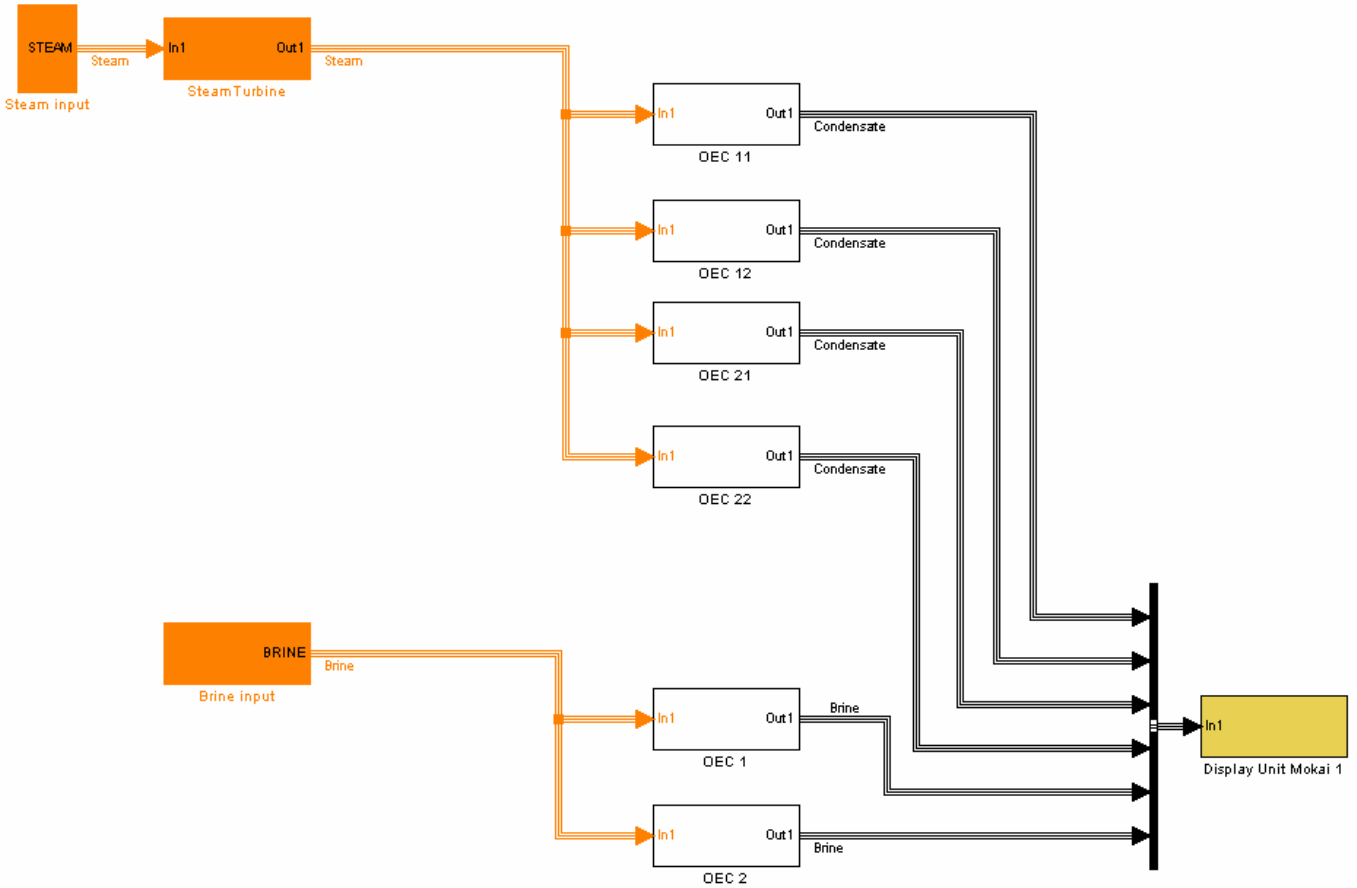

Figure 6-5: Simulink model of the Mokai 1 for steady state operation

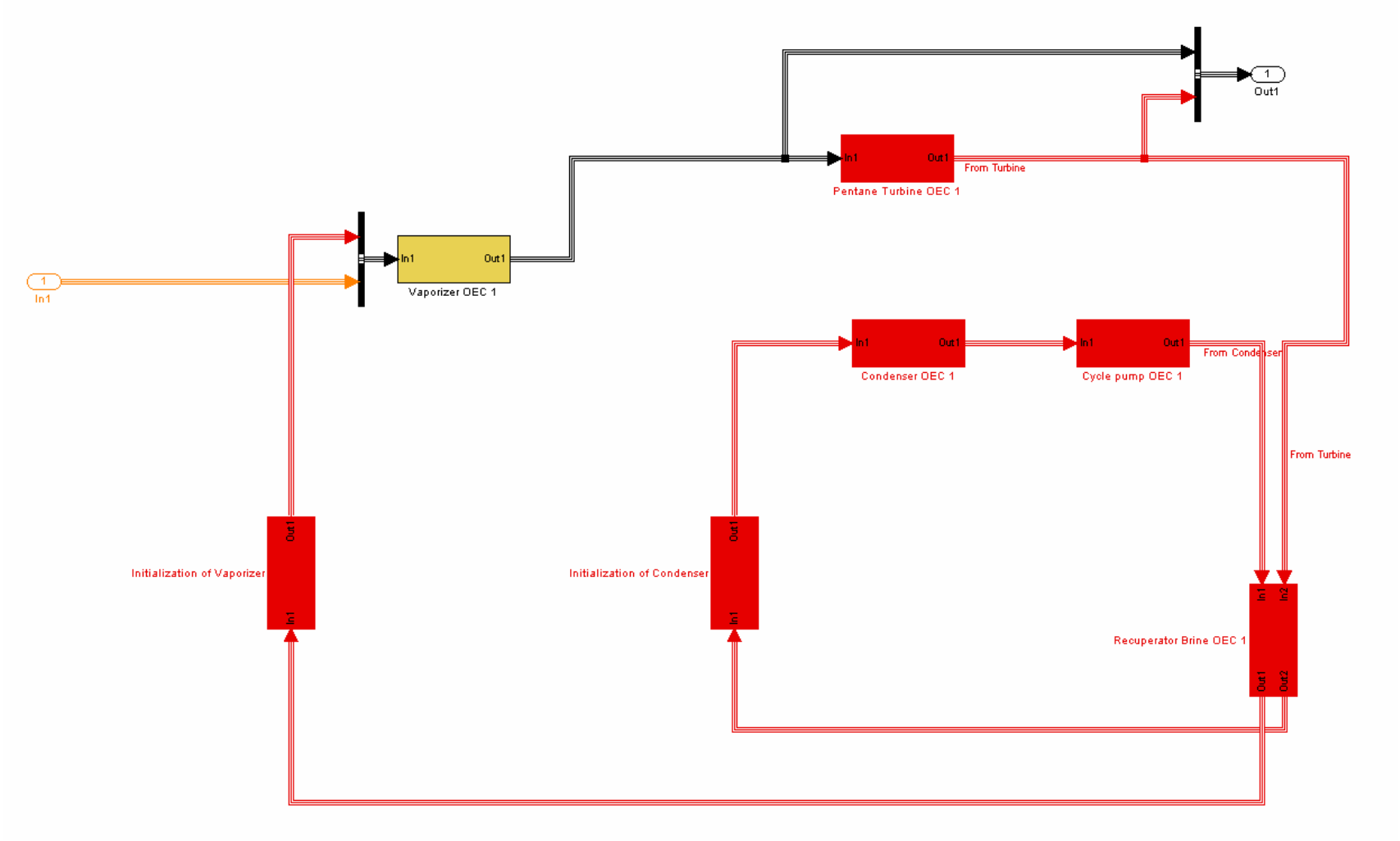

Figure 6-6: Simulink model of OEC 1 for steady state operation

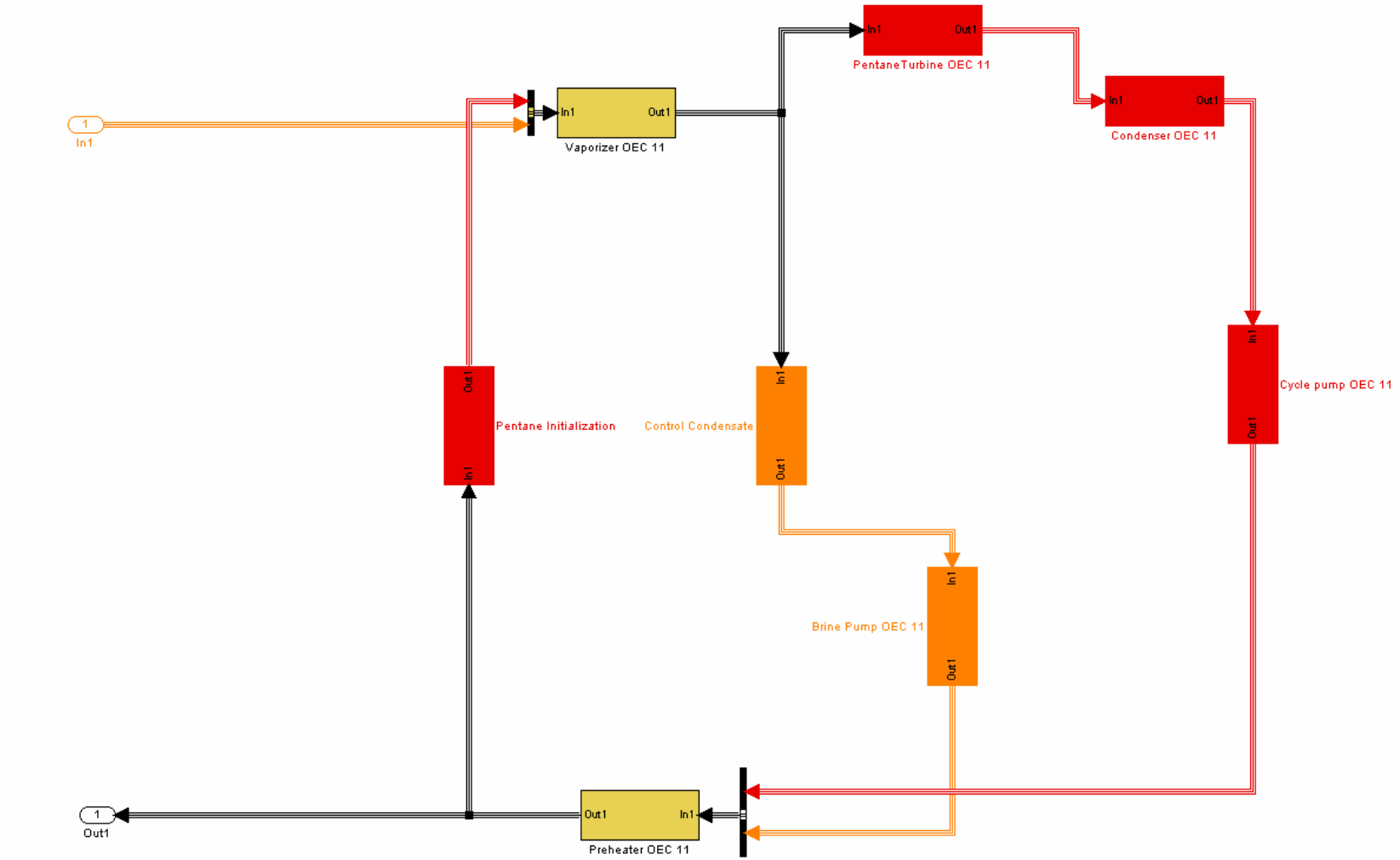

Figure 6-7: Simulink model of OEC 11 for steady state operation

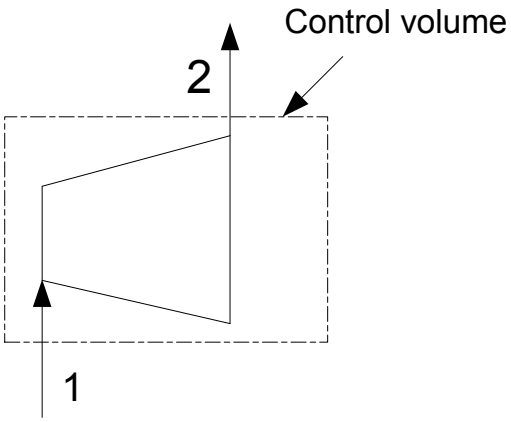

Figure 6-8: Control volume showing steam turbine states

Steam turbine parameters (Derived from Figure 4-3, supplied by MRP):
Outlet pressure: 1.34 bar
Isentropic efficiency: 0.8577 (Estimated from Figure 4-3)
Thermal efficiency: 0.964 (Estimated from Figure 4-3)

Table 6.1: Calibrating of steam turbine model

State	Properties	initial values	design	guess	estimated value
1	pressure	17.6 bar	√		17.6 bar
	temperature	205.5° C	√		205.5° C
	mass flow	85.69 kg/s	√		85.69 kg/s
2	pressure	1.34 bar	√		1.34 bar
	temperature	108° C	√		104.3° C
	quality	88.07 %	√		88.07 %
	power output 1-2	31.12 MW	√		31.12 MW

Parameters of OEC 11 (Derived from Figure 4-4, supplied by MRP):

Pump parameter:
$W_{12} = 180kW$, $p_2 = 22.3bar$
Preheater parameter:
$\dot{Q}_{78} = \dot{Q}_{2-2a} = 3.645MW$
Vaporizer parameter:
$\dot{Q}_{56} = \dot{Q}_{2a-3} = 43.38MW$
Turbine parameters:
Outlet pressure: 1.07 bar
Isentropic efficiency: 0.80 (Estimated from Figure 4-4)
Thermal efficiency: 0.94 (Estimated from Figure 4-4)
Condenser parameters:
$\dot{Q}_{41} = 42.4MW$

Table 6.2: Calibrating the bottoming ORC (OEC11) model

State	Properties	initial values	design	guess	estimated value
1	pressure	1.07 bar	√		1.07 bar
	temperature	37.07° C	√		36.05° C
	mass flow	103.50 kg/s	√		103.50 kg/s
2	pressure	5.18 bar		√	5.18 bar
	temperature	34 °C	√		36.75 °C
	mass flow	103.50 kg/s	√		103.50 kg/s
2a	pressure	5.18 bar		√	5.18 bar
	temperature	48.2°C	√		51.39°C
	mass flow	103.50 kg/s	√		103.50 kg/s
3	pressure	5.18 bar	√		5.18 bar
	temperature	93.70 °C	√		93.14 °C
	mass flow	103.50 kg/s	√		103.50 kg/s
4	pressure	1.07 bar		√	1.07 bar
	temperature	64.87° C		√	64.87° C
	mass flow	103.50 kg/s	√		103.50 kg/s
	power (3-4)	4.59 MW	√		4.59 MW

Table 6.3: Simulated steam inlet/outlet conditions

State	Properties	initial values	design	guess	estimated value
5	pressure	1.21 bar	√		1.21 bar
	temperature	104.90° C	√		104.90° C
	mass flow	21.70 kg/s	√		21.70 kg/s
6	pressure	1.09 bar	√		1.21 bar
	temperature	90° C	√		96.67° C
	mass flow	21.24 kg/s	√		21. 24 kg/s
7	pressure	19 bar		√	19 bar
	temperature	90° C	√		85.76° C
	mass flow	21.24 kg/s	√		21.24 kg/s
8	pressure	19 bar	√		19 bar
	temperature	48.9° C	√		48.9° C
	mass flow	21.24 kg/s	√		21.24 kg/s

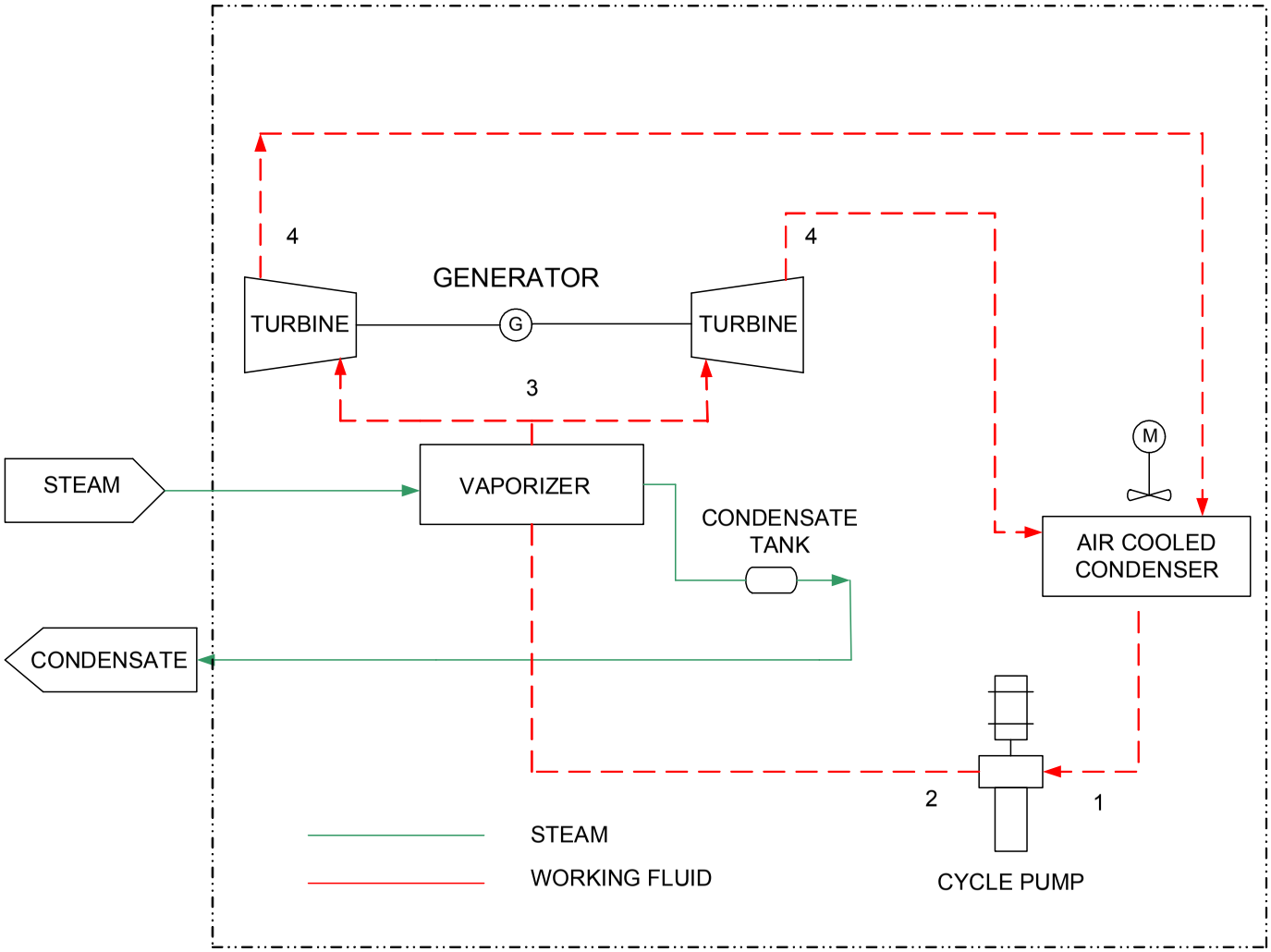

Figure 6-9: Schematic diagram showing OEC 11 states

Parameter of OEC 1 (Derived from Figure 4-5, supplied by MRP):
Pump parameter:
$W_{12} = 380kW$, $p_2 = 22.3bar$
Vaporizer parameter:
$\dot{Q}_{56} = \dot{Q}_{2a-3} = 28.88MW$
Turbine parameters:
Outlet pressure: 1.22 bar
Isentropic efficiency: 0.80 (Estimated from Figure 4-5)
Thermal efficiency: 0.935 (Estimated from Figure 4-5)
Condenser parameters:
$\dot{Q}_{4a-1} = 23.58MW$
Recuperator parameters:
$\dot{Q}_{4-4a} = \dot{Q}_{2-2a} = 7MW$

Table 6.4: Calibrating the brine ORC (OEC 11) model

State	Properties	initial values	design	guess	estimated value
1	pressure	1.15 bar	√		1.2 bar
	temperature	35.40° C	√		32.32° C
	mass flow	58.17 kg/s	√		58.17 kg/s
2	pressure	22.6 bar		√	22.6 bar
	temperature	38° C	√		38.25° C
	mass flow	58.17 kg/s	√		58.17 kg/s
2a	pressure	22.6 bar		√	22.6 bar
	temperature	85.2° C	√		83.5° C
	mass flow	58.17 kg/s	√		58.17 kg/s
3	pressure	22.3 bar	√		22.6 bar
	temperature	190.5 °C	√		189.3 °C
	mass flow	58.17 kg/s	√		58.17 kg/s
4	pressure	1.22 bar		√	1.22 bar
	temperature	119° C		√	119° C
	mass flow	58.17 kg/s	√		58.17 kg/s
	power (3-4)	5.4 MW	√		5.4 MW
4a	pressure	1.17 bar	√		1.22 bar
	temperature	62.30 °C	√		58.16°C
	mass flow	58.17 kg/s	√		58.17 kg/s

Table 6.5: Brine inlet/outlet conditions

State	Properties	initial values	design	guess	solution
5	pressure	18.6 bar	√		18.6 bar
	temperature	207.6° C	√		207.6° C
	mass flow	119.4 kg/s	√		119.4 kg/s
6	pressure	16 bar	√		16.74 bar
	temperature	152° C	√		150° C
	mass flow	119.4 kg/s	√		119.4 kg/s

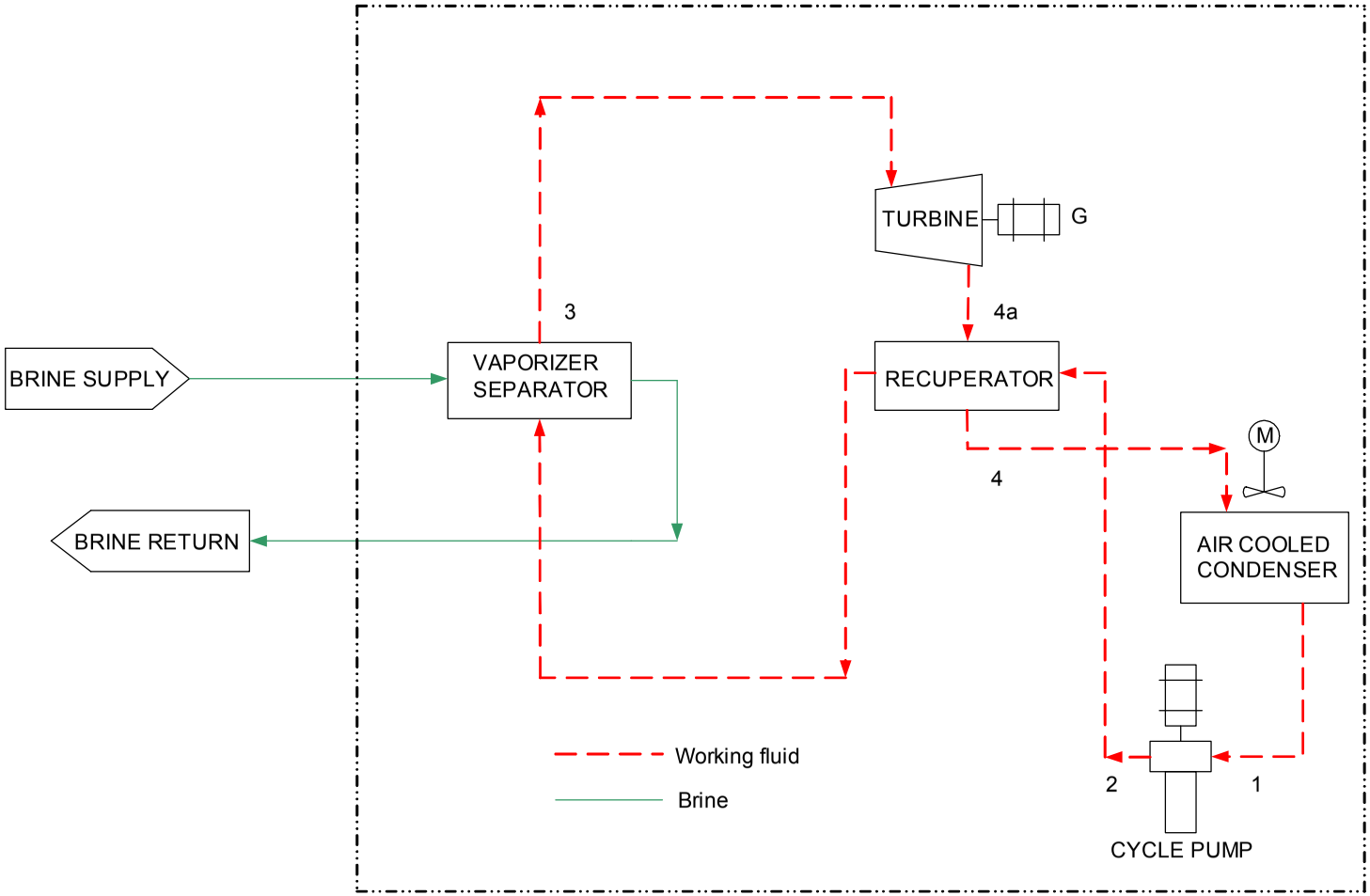

Figure 6-10: Schematic diagram showing OEC 1 states

6.5 Summary

This chapter has put together and ccalibrated models developed in Chapter 5 to existing design data from the manufacturer. This required an iterative method as the number of unknown parameters well exceeded the number of governing equations and numerous simplifying assumptions are made. The variables like heat transfer in various components are fed to the model as parameters to estimate the unknown state points in design supplied by MRP. Trial and error to estimate unknown variables is continued until all known values of the various state points converged. A simulator of Mokai 1 geothermal power plant for steady state operation is consequently created. In this simulator only two input data required: geothermal fluid flow rate and steam content. As the well head conditions (pressure and temperature) are controlled, the simulator can simulate performance using only the geothermal fluid flow rate and the steam content as input data.

Chapter 7

Adaptive Approaches for Long Term Performance Improvements

7.1 Introduction

In this chapter adaptive approach to long term performance improvements is presented. Then long term performance improvements using the adaptive approach are discussed. The steady state simulator developed in the previous chapter was used for this study. This simulator requires only two input data: geothermal fluid flow rate and steam content. The Mokai 1 geothermal power plant was chosen as the case study. The change of resource characteristics of this study is limited to enthalpy change (steam content) as it imitates the resource characteristics of Mokai 1 geothermal field. Other possible source of resource characteristics change includes: change in concentration of non-condensable gases, change in well-head pressure, change in geothermal fluid flow rate etc.

7.2 Adaptive approach for long term performance improvements

The resource characteristics of a geothermal field change significantly over time. At the time of the Mokai 1 geothermal plant commissioning, the typical enthalpy of the fields was about 1400 kJ/kg. Now typically, the fields are producing about 2000 kJ/kg and this significant increase in enthalpies has had a significant impact on plant performance. The preheaters of bottoming cycles, which were part of the original design, are no longer being used. However, the plant is producing a quantity similar to what it was designed to produce. Higher enthalpy means a higher percentage of steam and less brine in geothermal fluid. Brine OECs are suffering from a lack of brine and not being able to operate to their full potential so some of the condensate is re-

circulated to the system to increase the amount of brine. Figure 7-1 summarises resource enthalpies of year 2007 calculated using data from the plant operational log.

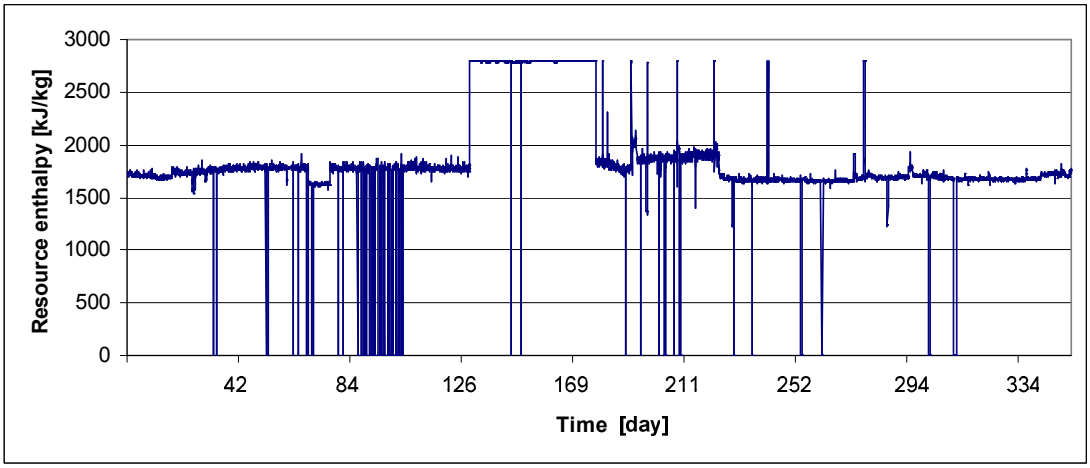

Figure 7-1: Resource enthalpy of year 2007 of Mokai 1 geothermal power plant

Geothermal power plants are very capital intensive and it is not very easy to change a plant to adapt to resource characteristics different from the original design. By appropriate reservoir modelling, it is now possible to predict future resource characteristics depending on various parameters including the rate of resource utilization, the percentage of brine reinjection etc. [57].

In an adaptive design, if provisions are allowed for a plant to adapt to resource characteristics change at the time of building, a great deal of effort and money may be saved in the long run. However, the initial investment cost might go up as a consequence of adaptive design but over the life span of the plant the total benefit may be greater. A proper economic analysis is necessary to identify cost benefit of adaptive design approach.

Applying conservation of mass at the well head,

$$\dot{m}_T = \dot{m}_b + \dot{m}_s \tag{7.1}$$

where, $\dot{m}_T$ is the total mass flow rate at the well head, $\dot{m}_b$ is the brine mass flow rate and $\dot{m}_s$ is the steam mass flow rate.

Dividing Equation (7.1) with m_T yields

$$1 = C_b + C_s \tag{7.2}$$

where, C_b is defined as brine content and C_s is defined as steam content. It is advantageous express resource characteristics as steam content (C_s).

Applying energy balance at the well head,

$$\dot{m}_T\, h_R = \dot{m}_b\, h_b + \dot{m}_s\, h_s \tag{7.3}$$

where, h_R is the resource enthalpy, h_b is the enthalpy of the brine (saturated liquid) and h_s is the enthalpy of the steam (saturated vapour).

From Equation (7.2), if the steam content of a geothermal field (C_s) increases, the brine content (C_b) must be reduced and vice versa. If we want to keep $\dot{m}_b$ and h_b unchanged as C_s increases or decreases, we must manipulate parameters of the left hand side of Equation (7.3). Since, h_R is the parameter characterised by geothermal resource, we may not be able to manipulate it. The only suitable solution would be to control the geothermal fluid flow rate ($\dot{m}_T$). When C_s increases, we can keep $\dot{m}_b$ constant by using condensate recirculation and increased geothermal fluid flow rate ($\dot{m}_T$). If we are interested only on the constant heat transfer in the vaporizer, the reinjection temperature (i.e. brine outlet temperature) can be lowered.

The following assumptions are made for the long term performance model to operate the plant within its design limits.

- To control the vaporizer steam outlet condition, excess steam is vented to the atmosphere to maintain temperature of 90˚C in the condenser.
- The off-design well-head condition is always within the wet-steam zone i.e., there is not change in temperature at the well head and the geothermal fluid is a mixture of steam and brine.

The long term performance model uses the simulator developed in chapter 6 where only two inputs: geothermal fluid mass flow rate ($\dot{m}_T$) and steam content (C_s), are needed to be supplied to the simulator to analyse performance. The following sections presents some probable situations and corresponding adaptive approach to address them.

7.3 Case study 1: designed mokai 1 geothermal power plant

Figure 4-3 in chapter 4 presented the original heat and mass balance of the Mokai 1 geothermal power plant which consists of two brine OECs and a steam turbine on top of four bottoming OECs. The designed total geothermal fluid mass flow rate is 324.58 kg/s with steam content about 35%. Normally, each turbine has an operating limit and for the steam turbine it has been fixed to 37 MW. For pentane turbine, the maximum power is fixed at 7 MW. Figure 7-2 shows the Mokai 1 plant output with increasing resource enthalpy that resembles reality i.e., increase in geothermal resource enthalpy (Figure 7-1). With increasing steam content from about 25% (1400 kJ/kg) to about 35%, the steam turbine reaches its maximum and produces the same amount thereafter. Since the steam turbine is unable to utilize the excess steam, the bottoming cycle is receiving condensate at elevated enthalpy. Therefore, the power output of the bottoming cycle is increasing and owing to a lack of brine, the brine OECs are producing much less than their capacity.

This reduced brine flow problem can be tackled in many ways. If one uses excess geothermal brine to reheat the condensate collected from the bottoming cycle, an increased mass flow of brine can be ensured for the brine OECs. Figure 7-3 presents a schematic diagram of such a design. This approach is currently used by MRP. Here, more power is being produced at the expense of more geothermal fluid, which means the resource is being utilized at a higher rate; not necessarily ensuring optimum utilization. Figure 7-4 shows a corresponding improvement in plant performance by adopting this approach. In Figure 7-4 the brine OECs produces gradually less power from 25% steam content to 35% then its power production is independent of steam content. Since, it is more efficient to directly expand steam in a turbine to produce power than in bottoming cycle, one should utilize as much as steam possible in a

steam turbine within its manufacturing limit. Therefore up to 35% steam content no need for change in original design. Figure 7-5 shows corresponding brine reinjection temperature. The reinjection temperature is calculated from the energy balance of mixing of brine and condensate before reinjecting to the geothermal field.

$$\dot{m}_T \, h_{RNG} = \dot{m}_b \, h_b + \dot{m}_c \, h_c \tag{7.4}$$

where *RNG* stands for reinjection, *b* stands for brine and *c* stands for condensate.

In Equation (7.4) h_{RNG} is unknown and the rests of the variable are known. So, h_{RNG} can be easily determined. Now, operating pressure of reinjection is known so the rest of the thermo-physical properties of reinjection including temperature can be readily calculated.

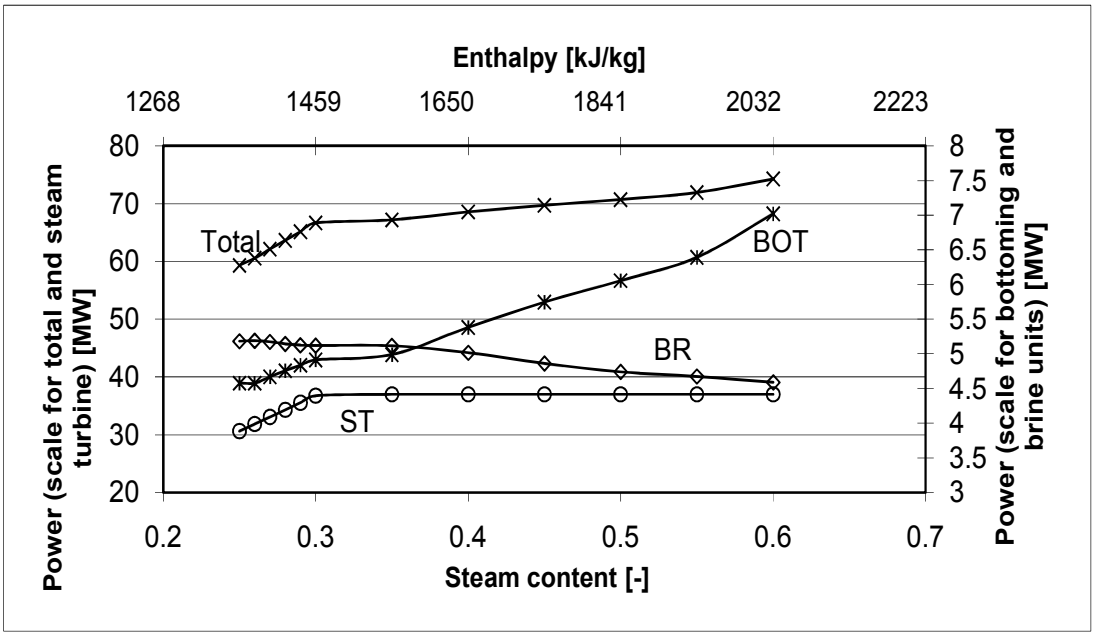

Figure 7-2: Theoretical power of the Mokai 1 power plant with increased resource enthalpy

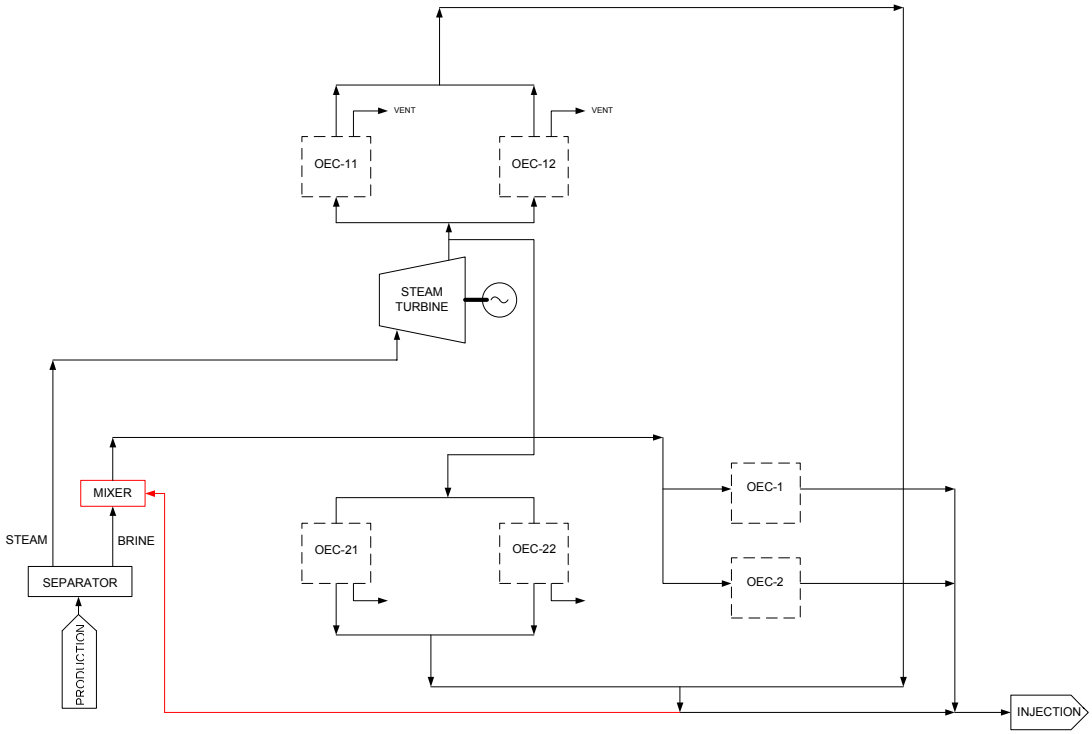

Figure 7-3: Adaptive design for an increased flow of geothermal fluid

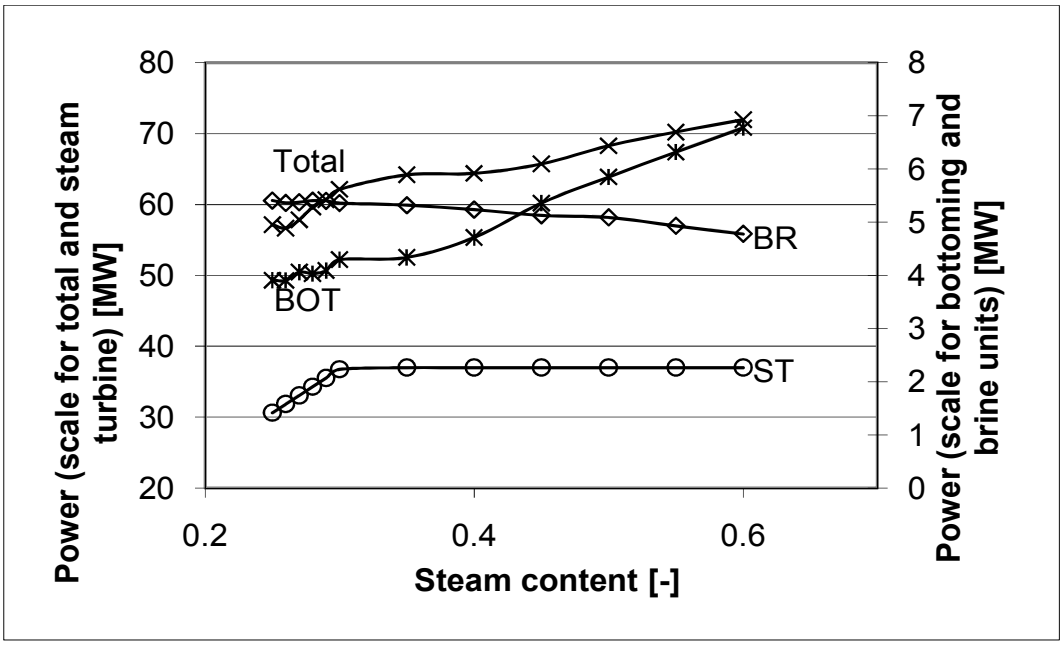

Figure 7-4: Theoretical power of the Mokai 1 power plant with increased resource enthalpy and increased mass flow of geothermal brine to keep the brine flow rate constant for the brine cycles

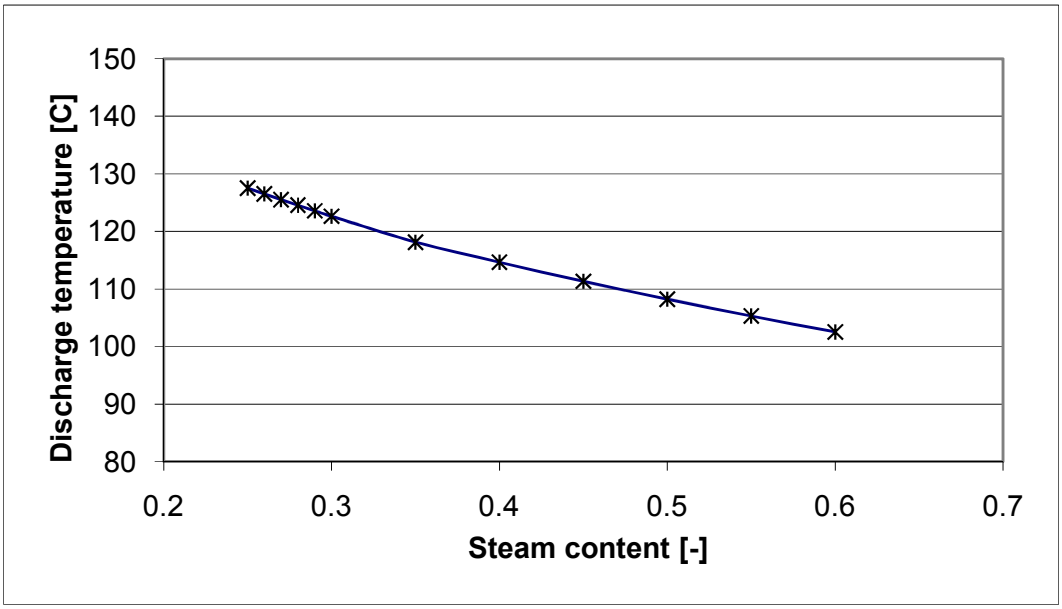

Figure 7-5: The theoretical reinjection temperature with increased resource enthalpy and increased mass flow of geothermal brine to keep the brine flow rate constant for the brine cycles

7.4 Case study 2: upgrading original steam turbine

Figure 7-6 shows the performance of Mokai 1 geothermal power plant with increasing steam content and replacing the original steam turbine with a higher capacity. The rated capacity of the new turbine is assumed 42 MW with the maximum power 47 MW. Figure 7-6 show that such an upgrade results in significant improvement in power output. However, it is associated with large capital investment. In Figure 7-6 with increasing steam content in geothermal fluid, power output of both the BOT-ORC and the steam turbine increase whereas power output of BRN-ORC decreases result in total increase in power. In 2008 MRP has upgraded the original 32 MW steam turbine with 42 MW steam turbine.

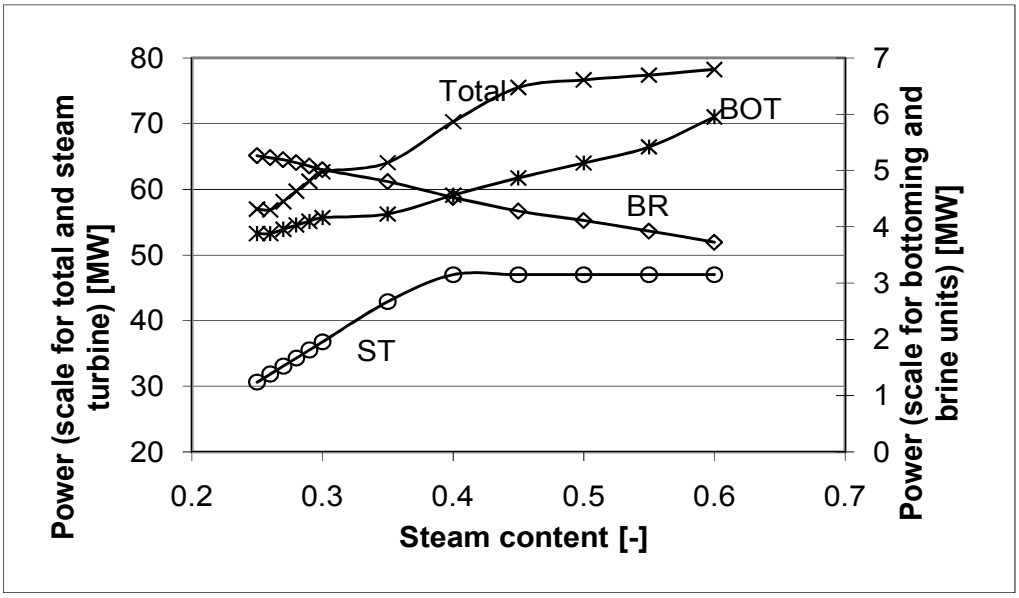

Figure 7-6: Theoretical power of the Mokai 1 power plant with increased resource enthalpy with higher capacity steam turbine

7.5 Case study 3: constant flow of geothermal fluid and lowered reinjection temperature

In Section 7.3, more geothermal fluid was used to overcome the problem of reduced brine in brine OECs that promote utilization of the resource at a higher rate. The minimum reinjection temperature for the geothermal brine of the Mokai 1 geothermal power plant is about 80°C; below which the minerals of geothermal brine lose their solubility and scaling at an unacceptable rate is the consequence. In the actual design, the reinjection temperature is about 125°C, so there is a possibility of further extracting heat from the reinjected brine. The alternative design would look same as Figure 7-3. However, the geothermal resource is utilized at constant rate i.e. mass flow of geothermal fluid to the plant is same as the design. The plant performance (power output) of Mokai 1 would look like the same as Figure 7-4 but the reinjection temperature will change. Figure 7-7 shows the corresponding reduction in reinjection temperature. The reinjection temperature is reduced using constant geothermal fluid flow rate to as low as about 95 ºC which is still higher than the lower limit of 80 ºC.

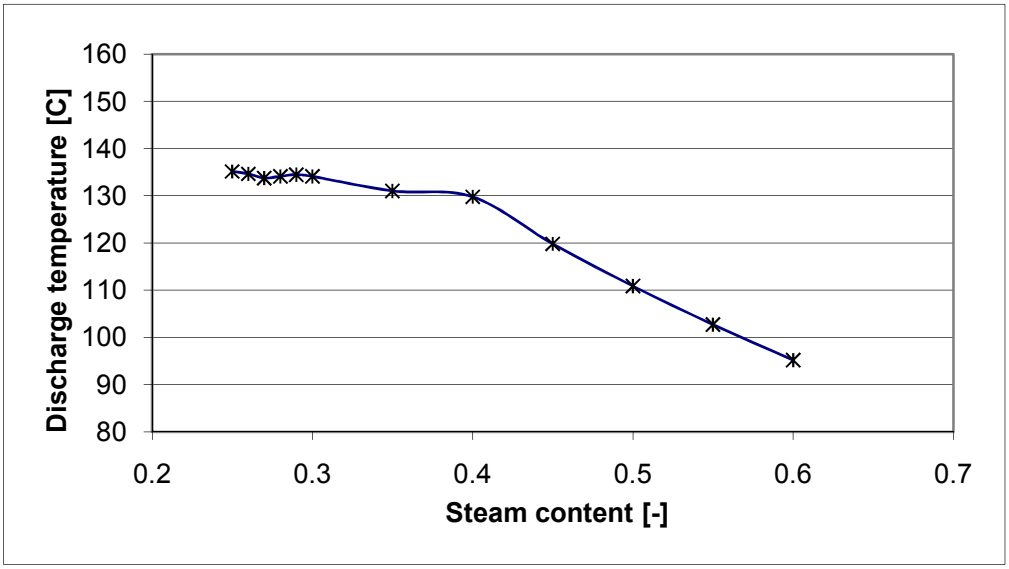

Figure 7-7: The theoretical reinjection temperature with a constant geothermal brine flow rate

7.6 Case study 4: constant flow of geothermal fluid with excess steam (50/50)

It was stated earlier that the steam turbine has a limit in producing power. Beyond this limit, the steam turbine cannot utilize the excess steam and the higher discharge enthalpy is the consequence. However, the brine OECs would suffer from lack of brine. To mitigate the problem, an alternative is possible as depicted in Figure 7-8. The excess steam can be bypassed and used to reheat condensate collected from the bottoming OECs. The results of using excess steam and condensate by mass 50/50 are presented in Figures 7-9 and 7-10. It is obvious from these two figures that on one hand the reheating of condensate by excess steam mitigates the reduced brine for brine OECs, and on the other hand the reinjection temperature is not much affected by this approach.

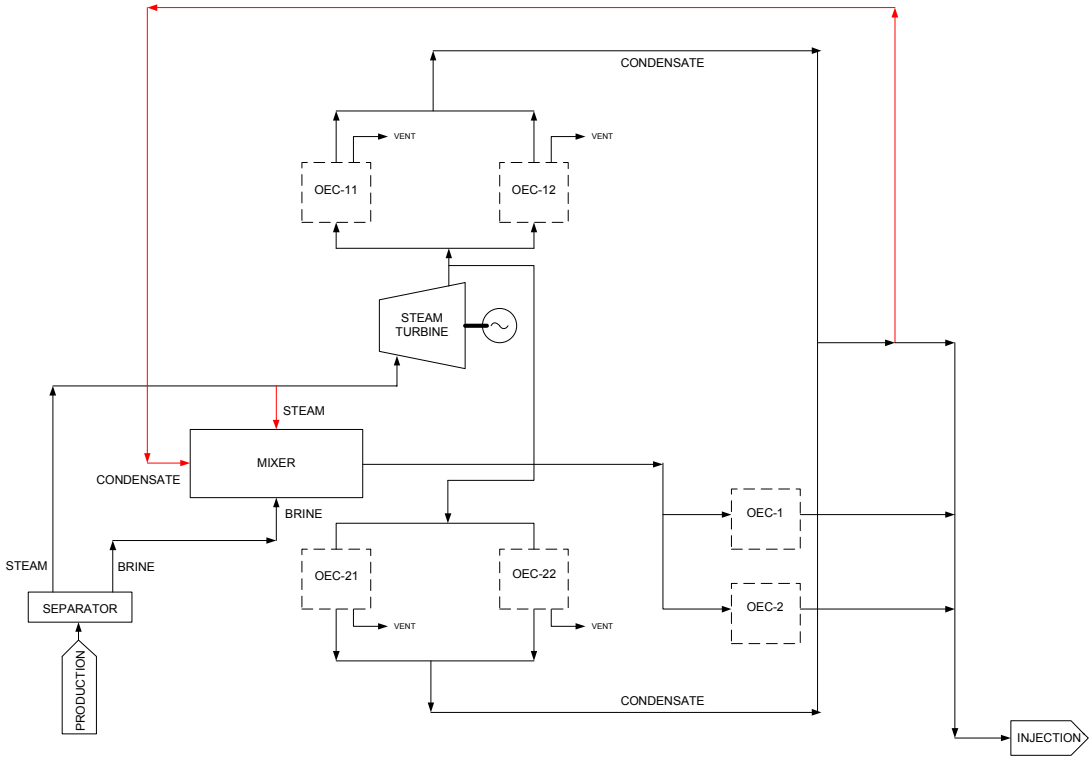

Figure 7-8: Adaptive design for a constant flow of geothermal fluid and regenerative heating

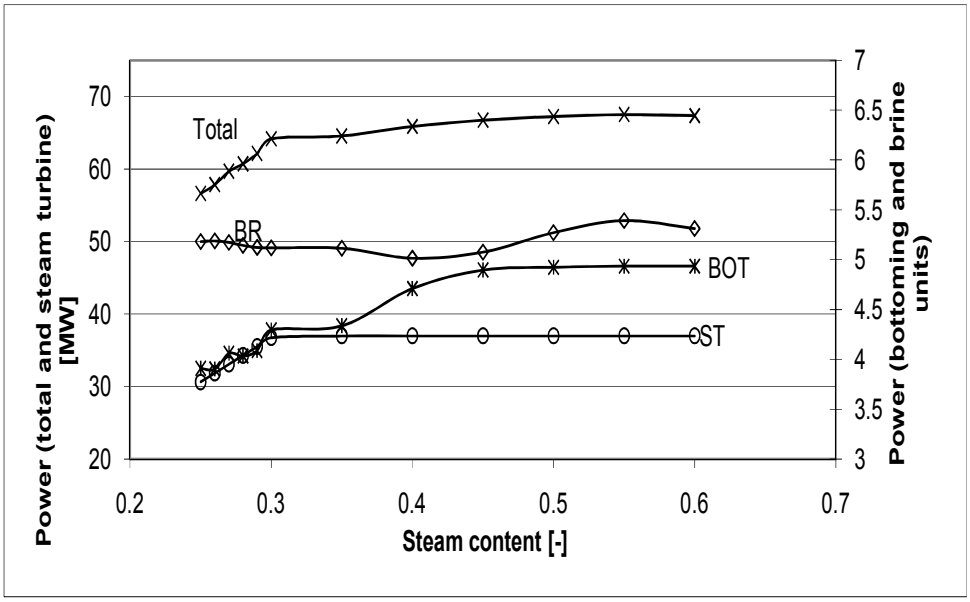

Figure 7-9: The theoretical power of the Mokai 1 power plant with increasing resource enthalpy and constant mass flow of geothermal brine with regenerative heating of the brine by excess steam

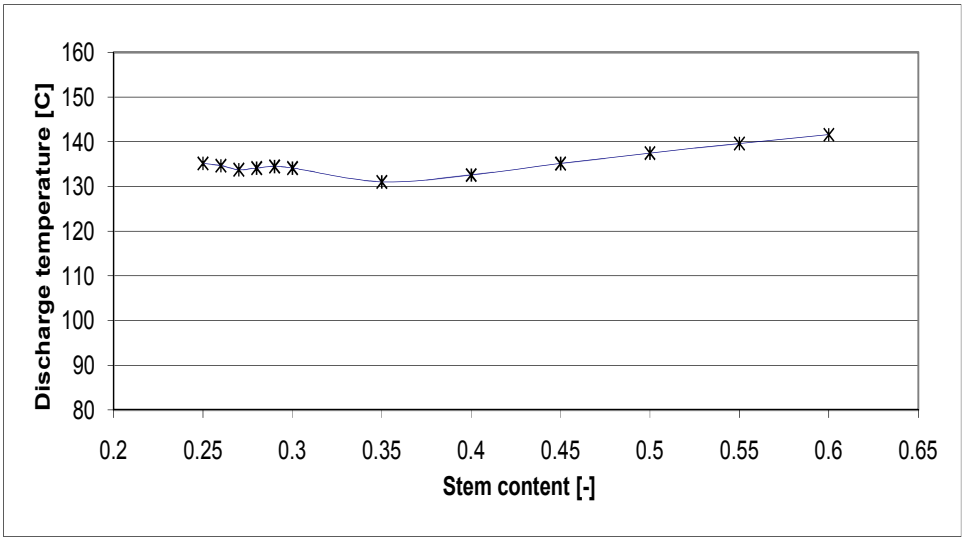

Figure 7-10: The theoretical reinjection temperature with constant geothermal brine flow rate and regenerative heating

7.7 Case study 5: decreased steam flow with constant mass flow with three bottoming and three brine cycles

Until now, we have only discussed the possible cases in which resource enthalpy (steam content) increases. However, the opposite can happen. In this section, the adaptive design to mitigate reduced enthalpy is presented. Figure 7-11 presents the alternative design for reduced geothermal enthalpy. One of the bottoming units should be designed such a way that it can be utilized as brine OEC in case the resource enthalpy reduces (more brine available). Brine OECs are more robust in design and therefore associated with high cost. However if such an adaptive option is kept at the time of building, expensive modifications to the plant can be avoided in the future.

Figures 7-11 and 7-12 present the power output and reinjection temperature of Mokai 1 geothermal power plant, respectively. The plant performance of these power producing units deteriorates as the resource enthalpy is reduced. This is obvious as the heat input to the system is reduced. However the reinjection temperatures remain within acceptable limits.

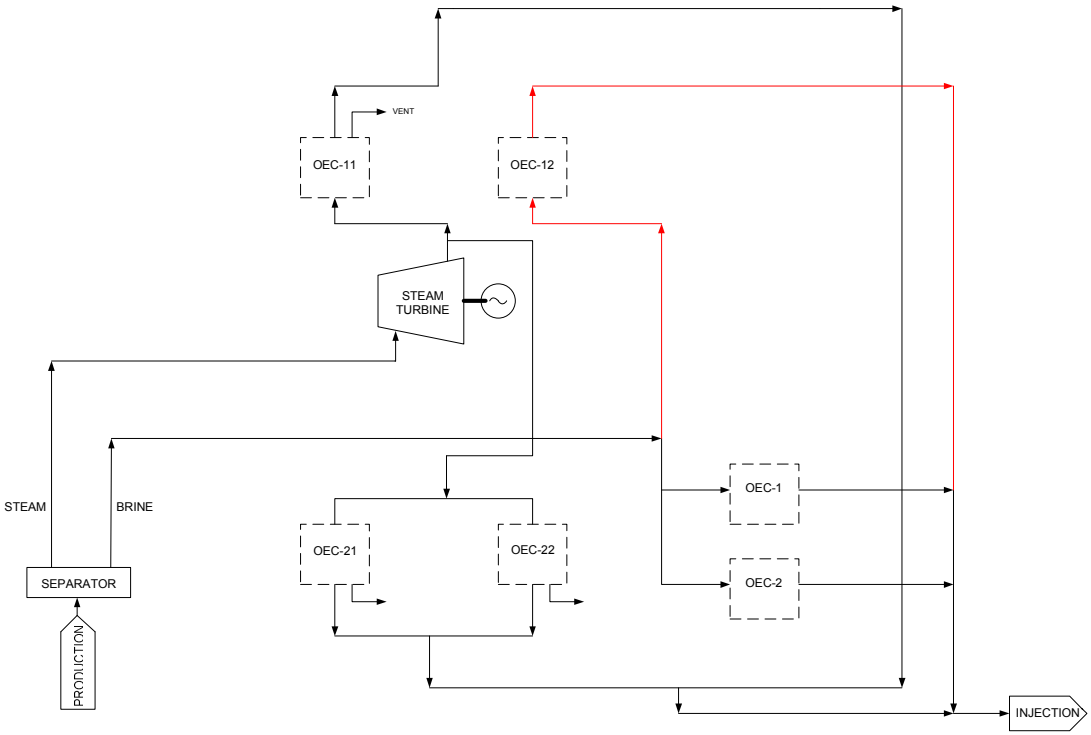

Figure 7-11: Corresponding adaptive design for a constant flow of geothermal fluid and decreased steam flow and with/without a preheater

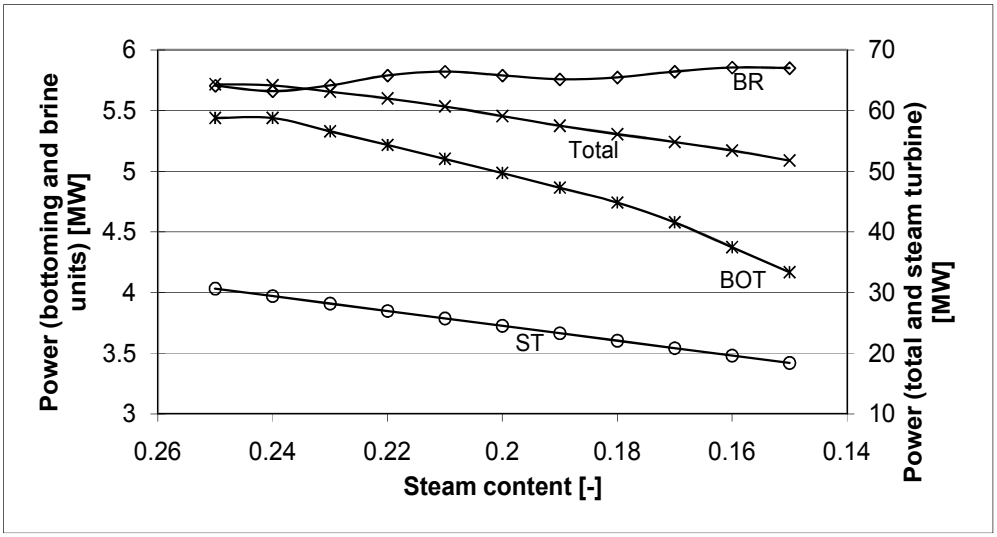

Figure 7-12: The theoretical power of the Mokai 1 power plant with decreased steam flow and constant mass flow with 3 bottoming and 3 brine cycles

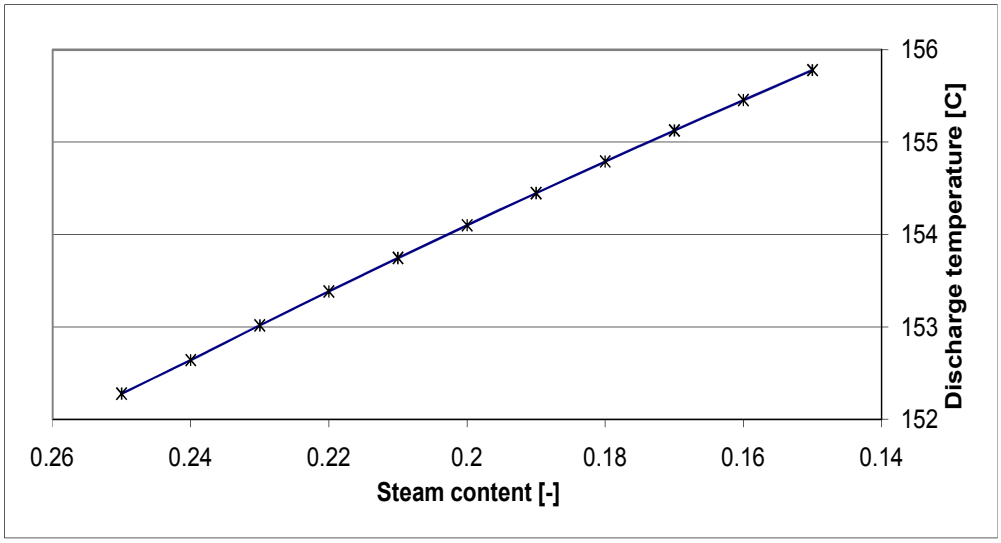

Figure 7-13: The theoretical reinjection temperature with a constant geothermal brine flow rate and decreased steam flow

7.8 Summary

This chapter has presented an adaptive design approach that takes into account the possible future resource characteristics. As geothermal power plants are very capital intensive and it is not very easy to change a plant to adapt to resource characteristics different from the original design, keeping provision for future resource characteristics can be very effective. There are five case studies presented in this chapter that analysed various possible options of the Mokai 1 power plant depending on the probable resource characteristics change. The results show provisions that could be kept in the plant for future resource characteristics. Simulations have been carried out using the simulator developed in Chapter 6 where geothermal fluid flow rate and steam content are supplied as input data to the simulator. A thorough techno-economic analysis is necessary to analyse the cost benefit of using the adaptive approach presented in this chapter.

Chapter 8

Iterative method for Analysing Environmental Effect on Short Term Plant Performance

8.1 Introduction

This chapter analyses the effect of the cooling medium temperature or the heat sink temperature on condenser and hence the performance of an organic Rankine cycle. Although, the main interest of this work is on the ORCs, the method can be applied to any closed cycle operation of a Rankine cycle. Subsequent sections discuss the development of the method, numerical aspects of the solution, the physical constraints that override the iteration termination criteria and two case studies. In the case study sections, the method is applied to a brine ORC (OEC 1) and a bottoming ORC (OEC 11). The results of simulation of the ORC models over a 48 hours period using stepwise solution are compared against the available plant performance data.

8.2 Plant dynamics

A model that predicts plant performance based on weather conditions must take into account the dynamics associated heat transfer and fluid flow. It was discussed in the literature section that one of the aims of this work is plant performance prediction. A model that can predict hourly plant performance on daily basis is good enough for this purpose. Moreover, the model should be applicable in wide range of design, optimization and engineering decision making. Models with high accuracy, such as those used for the control system synthesis are not of interest here. In an ORC power plant such as the Mokai 1 geothermal power plant, the response time of various components of the system and hence, the response time of the whole system is less than an hour. For example in the vaporizer of the ORCs in Mokai 1 geothermal power plant, it takes about 15 min to come into steady state (from experience in the plant) if

operating conditions are changed. The condenser response time subject to the operating conditions change including ambient air temperature change is about 30 min or less (from experience in the plant). The turbines and the pumps have similar order of response time and are much faster than the vaporizer and the condenser response times. The response time of the turbines can be in the order of 10-20 s [91] to 1-3 minutes (Mokai 1 geothermal power plant). This means the most important component of an ORC, specifically, Mokai 1 geothermal power plant, response time lie well below an hour. Therefore a steady state model that takes into weather effect on plant performance on hourly basis would be good enough for the current analysis. Although the model presented here is mainly meant for analysing weather effects, the model also takes into account the hourly geothermal fluid mass flow rate.

8.3 Data analysis of an ORC

In this section data of one of the BOT-ORCs, OEC 11 is analysed which provides the basis of assumptions used in developing the iterative method presented in the next section. In the plant operations log, state points 3 and 4 are recorded as p and T (Figure 8-1). State point 1 can be determined by T_4 and $Q = 0$. No information is available on state point 2. The electric power output from the unit is also recorded in the log.

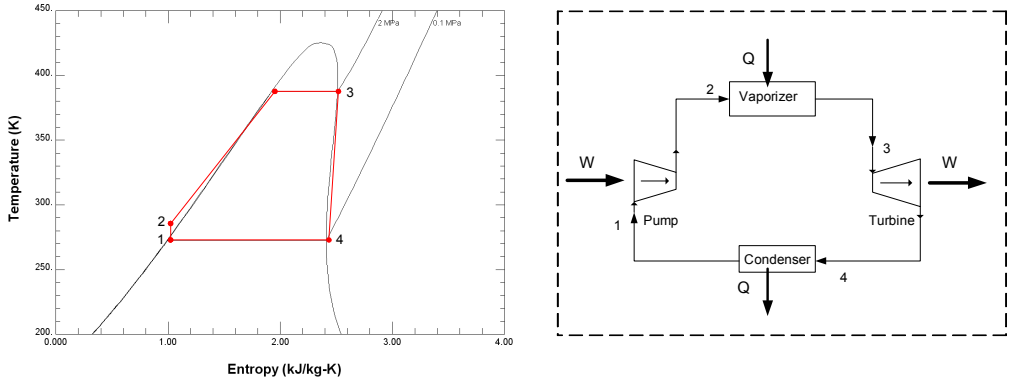

Figure 8-1: *T-s* diagram of the ORC represented in the right hand side

Using the plant performance data (p,T), the enthalpies of point 1, 3 and 4 are calculated. Now, as the pump work is much less compared to the net work done by

the system, which was discussed in chapter 5, we can assume pump work constant and assigned the design value of 180 kW. Now, using this assumption and energy balance (Equation (8.4)), we can calculate the enthalpy of the state point 2. Figure 8-2 to 8-5 presents, enthalpies vs. ambient temperature at four state points selected from the plant operations log for the year 2007 with maximum and minimum ambient temperatures -4 to 26 °C. Two of the turbines are coupled to a single generator producing power. For simplicity, these two separate cycles are assumed to have an equivalent representation of a single cycle. The pressure and temperature used for each of the data points are average of the two components. i.e. two vaporizers, two turbines and two condensers.

Figures 8-2 to 8-5, which are derived from plant data, show that ambient temperature (heat sink temperature) influences the enthalpies of four state points (1, 2, 3 and 4).

For state point 1, the effect of ambient temperature on enthalpy is the greatest. With increasing temperature from - 4 °C to 26 °C, the percentage increase of enthalpy is over 60%. As the work input in the pump is assumed constant, the effect of ambient temperature on enthalpy of state point 2 will be similar order of state point 1. The change of enthalpies at state point 3 from - 4 °C to 26 °C is the minimum of about 2.5%. The change of enthalpies at state point 4, from - 4 °C to 26 °C is about 9%. Which means that the vaporizer is affected less by the increase of ambient temperature. This is due to the fact that the level control mechanism of the vaporizer controls the pentane level by allowing some of the pentane to flow in to the condenser directly by bypass mechanism. Therefore the effect of the ambient temperature increase is less significant on the enthalpy of state point 3 (i.e., vaporizer outlet).

There is no direct measurement of mass flow rate in the cycle. However, we know the cycle electric power output and state points 3 and 4 (in the form of (p, T)) from the plant operational log. From energy balance, the cycle electric power output can be expressed as:

$$P_{el} = \eta_T \dot{m}_{cycle} (h_4 - h_3) \tag{8.1}$$

where P_{el} is cycle electric power output, η_T is the turbine-generator efficiency (which is discussed in the later sections), $\dot{m}_{cycle}$ is the cycle mass flow rate, h_3 is the enthalpy at state point 3 and h_4 is the enthalpy at state point 4.

In Equation (8.1), P_{el}, h_3 and h_4 are known from plant operational log. The value of η_T and $\dot{m}_{cycle}$ are not available. The design value of $\dot{m}_{cycle}$ is known but, we know that the Mokai 1 plant is operating at much different level than the design, so $\dot{m}_{cycle}$ should be updated.

The turbine-generator efficiency, η_T, can have real values between 0 and 1. For, η_T = 0, means there is no work done by the system and η_T = 1, means there is no loss in the system (ideal condition). From Equation (8.1), the maximum and the minimum values of $\dot{m}_{cycle}$ can be obtained depending on η_T. When, η_T = 0, $\dot{m}_{cycle}$ is the maximum (∞, unreal process) and η_T = 1, $\dot{m}_{cycle}$ is the minimum.

Figure 8-6 shows the minimum mass flow in the cycle using Equation (8.13), η_T = 1 and using corresponding values of electrical power output. The figure shows that the minimum mass flow rate in the cycle is weakly related to the ambient temperature i.e., for steady operation of the plant, mass flow rate remains unchanged for wide range of operation, this observed phenomenon is used as a postulate for developing the iterative method in the next section as there is no measurement of mass flow rate inside the cycle. Figure 8-7 shows the electric power output per unit mass flow rate (minimum). This is consistent with the Carnot efficiency, increasing the dead state temperature results in decrease in efficiency or plant performance.

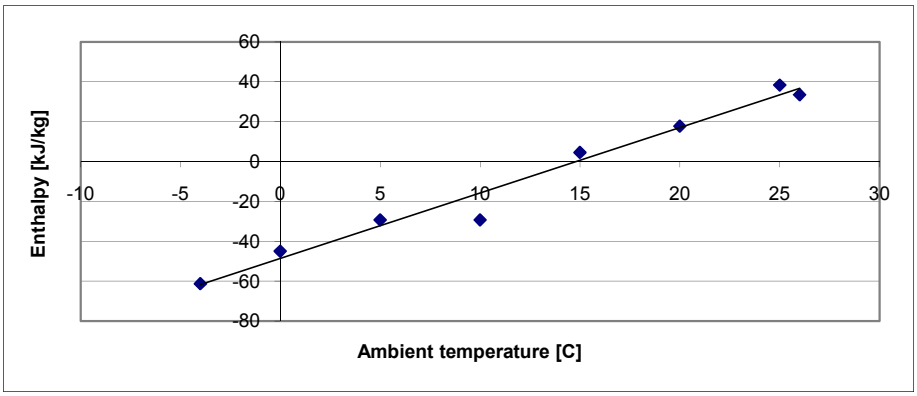

Figure 8-2: Enthalpy at state point 1 vs. ambient temperature of BOT-ORC calculated from the plant operational log data for the year 2007 and corresponding weather data of Taupo [72]

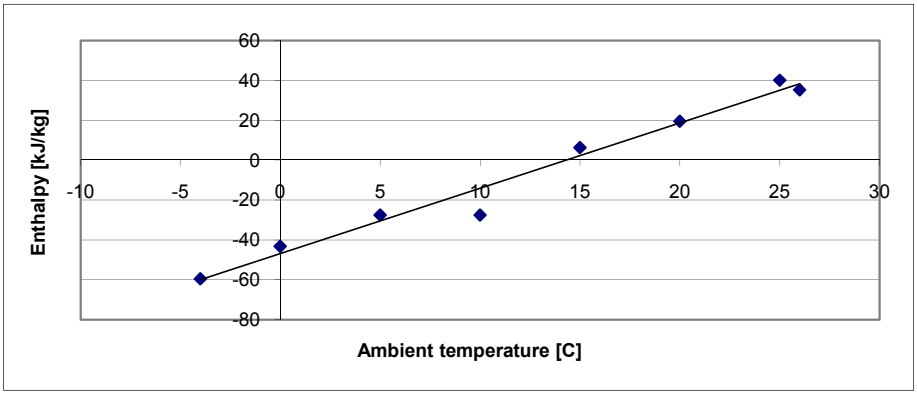

Figure 8-3: Enthalpy at state point 2 vs. ambient temperature of BOT-ORC calculated from the plant operational log data for the year 2007 and corresponding weather data of Taupo [72]

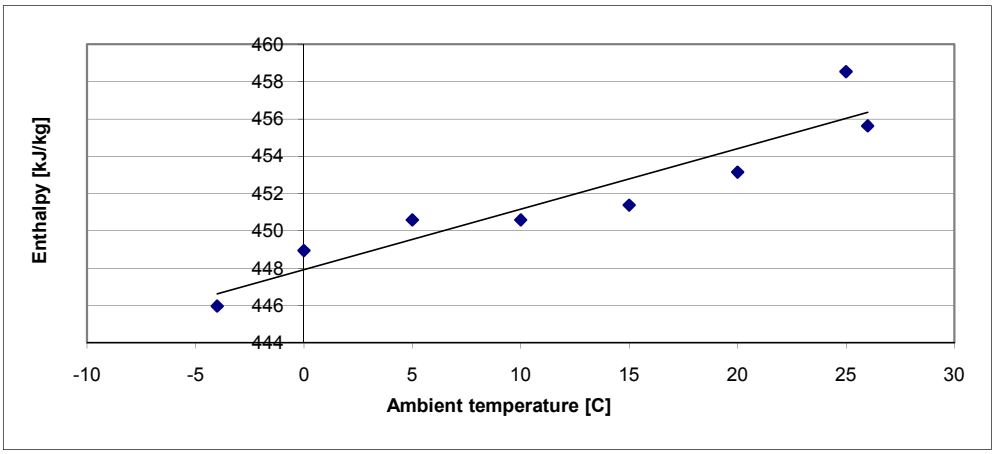

Figure 8-4: Enthalpy at state point 3 vs. ambient temperature of BOT-ORC calculated from the plant operational log data for the year 2007 and corresponding weather data of Taupo [72]

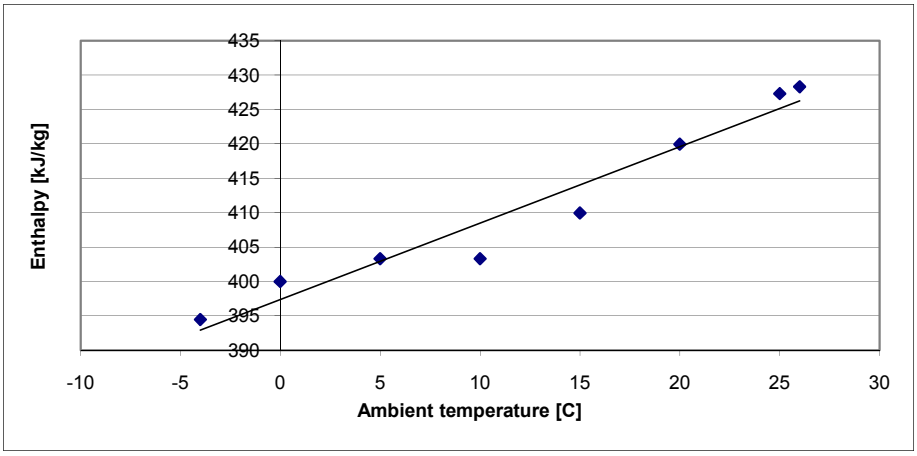

Figure 8-5: Enthalpy at state point 4 vs. ambient temperature of BOT-ORC calculated from the plant operational log data for the year 2007 and corresponding weather data of Taupo [72]

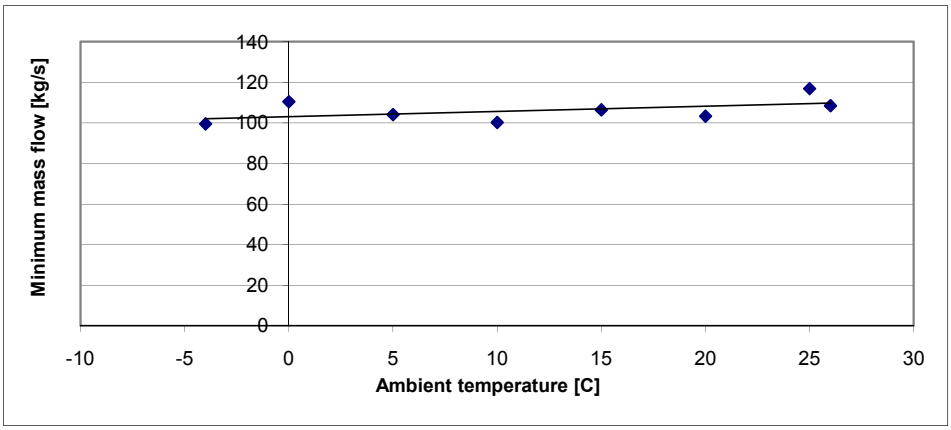

Figure 8-6: Minimum mass flow vs. ambient temperature in the cycle of BOT-ORC calculated from the plant operational log data for the year 2007 and corresponding weather data of Taupo [72]

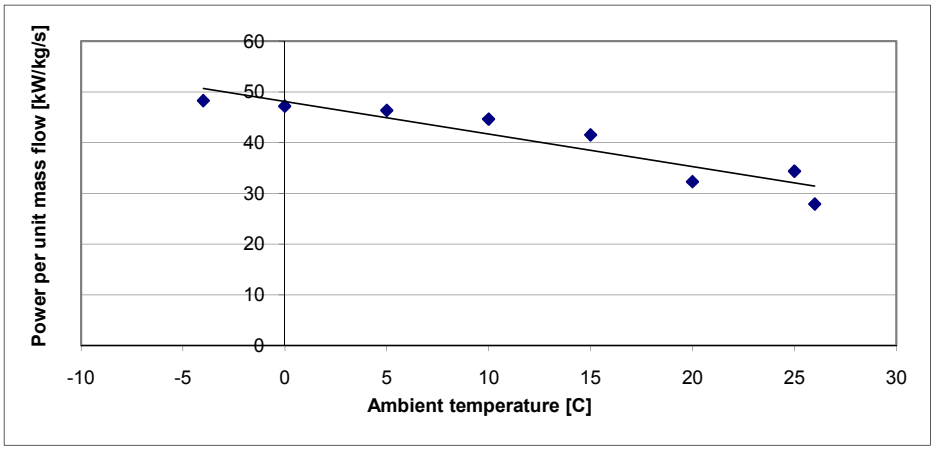

Figure 8-7: Electric power output per minimum mass flow vs. ambient temperature in the cycle of BOT-ORC calculated from the plant operational log data for the year 2007 and corresponding weather data of Taupo [72]

There is no direct measurement of mass flow rate in the physical implementation of the cycle concerned. An approximation is obtained using Equation (8.1), $\eta_T = 1$ and the generated electric power (P_{el}) as discussed earlier. The estimated mass flow rate is 106.203 kg/s, which is the average of mass flow rates of all the data points considered. This value of mass flow rate was checked against other data points giving average variation less than 5%, for the year 2007. This value of mass flow rate will be used in the simulation. It should be noted here that in all circumstances the maximum mass flow inside a cycle is constrained by energy balance in the vaporizer and the condenser.

8.4 The iterative method

This section presents an iterative method for modelling the environmental effect on short term plant performance. The weather has the most dominating effect on short term performance of an air-cooled ORC geothermal power plant as geothermal resource characteristics change less significantly in short time (hourly). Recalling Figure 8-1, process 4-1 represents constant pressure heat rejection by the condenser. Applying the first law of thermodynamics (neglecting kinetic and potential energies) for an open system, we can write:

$$\dot{m}_{cycle}(h_1 - h_4) = \dot{Q}_{41} \tag{8.2}$$

where $\dot{m}_{cycle}$ is the mass flow in the cycle, h_1 is the enthalpy at state point 1, h_4 is the enthalpy at state point 4 and $\dot{Q}_{41}$ is the condenser heat load. Since, process 4-1 is an isobaric process:

$$p_4 = p_1 \tag{8.3}$$

The condenser heat load, $\dot{Q}_{41}$, is a function of inlet condition (state point 4), outlet condition (state point 1), heat sink temperature, mass flow rate in the cycle and design of the condenser. During steady state operation of a plant, the mass flow rate in the cycle is conserved as discussed in the previous section. We assume the design of a particular condenser is fixed. Therefore, condenser inlet and outlet conditions and the heat sink temperature are the primary parameters influencing the condenser performance.

Assuming that T_{aD} is the designed heat sink temperature of the condenser, the mass flow rate, $\dot{m}_{design}$, in the cycle at sink temperature, T_{aD}, may be expressed as:

$$\dot{m}_{design} = \dot{m}_{cycle} = \frac{\dot{Q}_{41}}{(h_1 - h_4)} \tag{8.4}$$

Since the condenser heat load is directly related to the ambient temperature at constant vapour-liquid equilibrium condition, if T_{aD} increases or decreases, the condenser heat

load varies inversely. This has an adverse effect on cycle performance as power plants are generally optimized for a specific operating condition. There two ways to adapt to this condition: i) decrease cycle mass flow rate or ii) change the vapour-liquid equilibrium state in the condenser to cool the same amount of working fluid. As we discussed in the previous section, cycle mass flow rate remains unchanged for wide range of operation ORCs of Mokai 1 geothermal power plant. The only possible option is to change the vapour-liquid equilibrium state in the condenser to cool the same amount of working fluid in an ORC.

The following method is used to find the required vapour-liquid equilibrium condition in the condenser to maintain constant mass flow (Figure 8-10):

Step 1:

At first, $\dot{Q}_{41}$ is calculated based on the heat sink temperature using a condenser model (presented in chapter 2), then using Equation (8.4), the value of $\dot{m}_{cycle}$ is calculated.

Step 2:

If $\dot{m}_{cycle} = \dot{m}_{design}$, the condenser is operating at the designed vapour-liquid equilibrium condition and no further calculation is necessary.

Step 3:

If $\dot{m}_{cycle} < \dot{m}_{design}$, the equilibrium pressure, p_1, is reduced until $\dot{m}_{cycle} = \dot{m}_{design}$ and h_1 is calculated as $h_1 = f(p_1, Q = 0)$, where Q represents quality.

Step 4:

If $\dot{m}_{cycle} > \dot{m}_{design}$, the equilibrium pressure, p_1, is increased until $\dot{m}_{cycle} = \dot{m}_{design}$ and h_1 is calculated as $h_1 = f(p_1, Q = 0)$.

The back pressure of the condenser dictates the turbine outlet pressure. For positive flow to occur, the condenser pressure must be less than turbine outlet pressure ($p_1 < p_4$). In practice, the turbine outlet pressure is slightly higher than the condenser equilibrium pressure.

Recalling Figure 8-1 agian, process 1-2 represents isentropic compression of the working fluid by the cycle pump. Owing to the fact that the pump work is relatively small for an ORC, it can be assumed constant [54]. The work input to the pump may be calculated as:

$$\dot{W}_{pump} = \dot{m}_{cycle}(h_2 - h_1) \tag{8.5}$$

The enthalpy at the boiler/vaporizer outlet is described by

$$\dot{m}_{cycle}(h_{3'} - h_2) = \dot{Q}_{23} \tag{8.6}$$

where $\dot{Q}_{23}$ is the heat input to the system and we have defined a hypothetical intermediate state 3′ which is a trial solution for state 3. Knowing $h_{3'}$ and Q=1, all other thermodynamic properties related to state 3′ may be calculated (more complex problems such as superheating are discussed in the case study section).

It was discussed in the previous section that there is a control mechanism in place, if the ambient temperature increases; the vaporizer pentane liquid level is controlled by bypassing some mass to the condenser, increasing the hold up mass in the condenser. The time required for the pentane to come from the condenser via cycle pump to the vaporizer is significantly more (order of minutes) than the time required for level control mechanism to bypass some pentane directly to the condenser (order of seconds). Moreover, the mass flow rate in the cycle is unchanged i.e., the mass flow via the route condenser->pump->vaporizer->turbine->condenser does not depend on the bypass route vaporizer->condenser. So for the process 3′ to 3, the vaporizer and the condenser can be assumed decoupled via the route condenser-> cycle pump->vaporizer->turbine->condenser. The process can be presented in a simplified diagram as depicted in Figure 8-8. Initially bypass valve between the vaporizer and the condenser is closed.

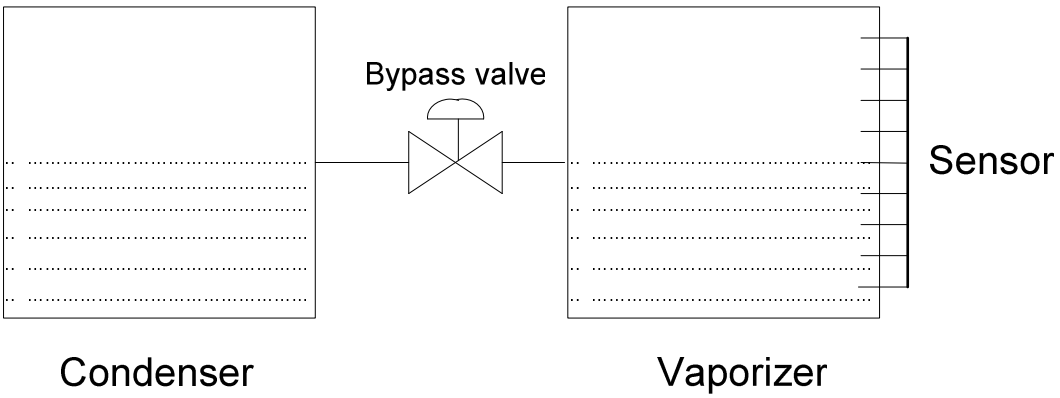

Figure 8-8: Simplified representation of the vaporizer and condenser

As the ambient temperature increases, new intermediate state 3′ is obtained in the vaporizer. Now, from the definition of enthalpy [30] for the process 3,0 to 3′ the following equation is obtained for the vaporizer:

$$du = u_{3'} - u_{3,0} = h_{3'} - h_{3,0} - (p_{3'}v_{3'} - p_{3,0}v_{3,0}) \tag{8.7}$$

where u is the internal energy and v is the specific volume (volume per unit mass). The subscript 3,0 represents the initial condition of state 3′ which is calculated from the supplied operating pressure and temperature (typical) values of the vaporizer to start the calculation.

As the ambient temperature increases, the pentane pressure-temperature equilibrium condition in the vaporizer is changed; if the pressure inside the vaporizer increases more than a set point, the bypass valve between the vessels opens to allow some mass to go into the condenser and attain a different pressure-temperature equilibrium condition in the vaporizer.

If the ambient temperature decreases, the pentane vapour production in the vaporizer decreases, which means more pentane is coming from the condenser to the vaporizer than pentane going to the condenser from the vaporizer. Equilibrium is attained within very short time. This way state point 3 is achieved from 3′.

In the intermediate process of transferring some mass from the vaporizer to the condenser (process *3′* to *3*) no work is done by the system nor does any heat transfer take place.

Let us draw a system boundary encompassing the vaporizer and the condenser for the process 3′ to 3. Applying the first law of thermodynamics on the system boundary encompassing the vaporizer and the condenser for a closed system [30]:

$$du_{3'-3} = dQ_{3'-3} - dW_{3'-3} \tag{8.8}$$

where $dQ_{3'-3}$ and $dW_{3'-3}$ are infinitesimally small, so $du_{3'-3}$ should tend to zero for the hypothetical process 3′ to 3 at equilibrium condition. The change in hold up mass in the vaporizer for the process 3′ to 3 is relatively small. If we ignore the effect of change in hold up mass in the vaporizer, the specific volume of the vaporizer remains unchanged.

Now, from Equation (8.8) and rearranging Equation (8.7) we can identify state 3 as:

$$u_{3'} - u_{3,0} = u_3 - u_{3,0} = h_3 - h_{3,0} - (p_3 - p_{3,0})v_{3,0} \tag{8.9}$$

Equation (8.9) can be solved iteratively for $Q = 1$ by altering p_3, until the left hand side of Equation (8.9) equals du of Equation (8.7). Knowing p_3 and Q =1, the rest of the thermodynamic properties associated with state 3 may be determined.

The sensitivity analysis of the ignoring the effect of change of hold up mass in the vaporizer is presented in appendix 6. The Matlab code for the iterative method is available in appendix 7 and 8.

If we assume that the work done by the turbine is isentropic then:

$$s_3 = s_4 \tag{8.10}$$

Knowing s_4 and p_4, the rest of the thermodynamic properties associated with state 4 may be determined (e.g., h_4).

Work done by the turbine is:

$$\dot{W}_T = \dot{m}_{cycle}(h_4 - h_3) \tag{8.11}$$

Equation (8.11) presents the ideal work done ($\dot{W}_T$) by the system. However, owing to irreversibilities associated with the processes (i.e. heat transfer to the surroundings,

mechanical losses, etc.) the actual electric power (P_{el}) produced by the unit is less than the ideal:

$$P_{el} = \eta_G \eta_s \dot{m}_{cycle} (h_4 - h_3) \tag{8.12}$$

where, h_4 is the ideal enthalpy, η_G is the generator efficiency, η_s is the isentropic efficiency of the turbine and calculated as:

$$\eta_s = \frac{h_{4,real} - h_3}{h_4 - h_3} \tag{8.13}$$

where, $h_{4,real}$ presents the actual enthalpy of turbine outlet. The generator efficiency η_G, is a mechanical efficiency which does not vary much for wide range of operation and often it is close to the theoretical value of 1. Defining $\eta_T = \eta_s . \eta_G$, we get:

$$P_{el} = \eta_T \dot{m}_{cycle} (h_4 - h_3) \tag{8.14}$$

Combining η_G and η_s to a single parameter η_T, reduces number of parameter to be estimated fro the available plant performance data.

The heat in to the cycle is:

$$\dot{Q}_{23} = UA\Delta T_m \tag{8.15}$$

where $\dot{Q}_{23}$ is the heat input to the cycle, U is the overall heat transfer coefficient, A is the heat transfer area and ΔT_m is the log mean temperature difference. A is constant for a heat exchanger. The overall heat transfer coefficient is calculated as a function of geothermal fluid mass flow rate using an approximate method [53, 81]:

$$U = U_r (\dot{m} / \dot{m}_r)^{0.5} \tag{8.16}$$

where U_r and $\dot{m}_r$ are the reference overall heat transfer coefficient and the reference mass flow rate. These two parameters represent the design value discussed in chapter 5.

With typical short term operation of Mokai 1 ORC heat exchanger, ΔT_m remain almost unchanged (chapter 5). Therefore, Equation (8.15) can be reduced to:

$$\dot{Q}_{23} = \dot{Q}_{23,r} (\dot{m} / \dot{m}_r)^{0.5} \tag{8.17}$$

where $\dot{Q}_{23,r}$ is the reference heat input discussed in Chapter 5.

An initial guess of the inlet state of the working fluid to the condenser is provided to the model. By working our way around the cycle, we predict a new inlet condition with an improved value. Subsequent iterations around the loop yield better results and the process converges to a unique solution within a few iterations. Figure 8-9 summaries the iterative process in *T-s* plane hypothetically. Process *1234* in black represents the initial cycle for the initial ambient temperature (in black). Once the ambient temperature increased (in red), the ORC shifts to *123′4* (red and green). As the level control mechanism takes over, the ORC reduces to *1234* in red.

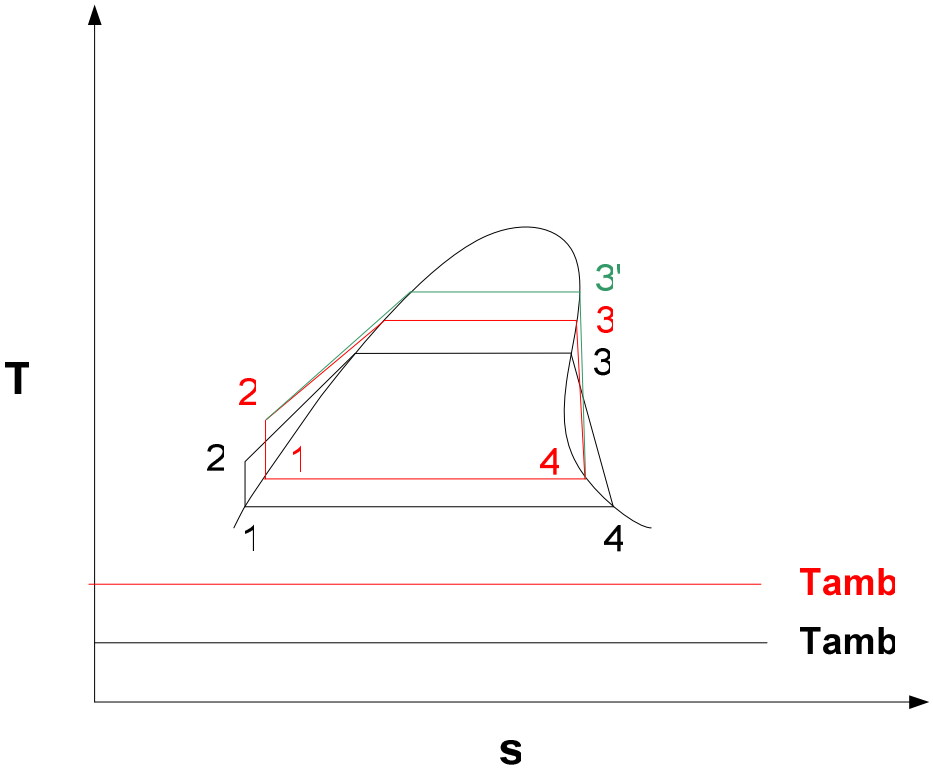

Figure 8-9: *T-s* presentation of the iterative method

Figure 8-11 shows the effect of the ambient temperature on condenser equilibrium pressure of a superheated vapour ORC unit. The condenser equilibrium pressure is very sensitive to the ambient air temperature and that explains the strong dependence of performance of an air-cooled condenser geothermal power plant on ambient air temperature. Figure 8-12 presents electric power output of a brine unit (OEC 1) as a

function of temperature at constant geothermal fluid flow rate, clearly increasing the ambient temperature results in decrease in power output. Details of the modelling involved are presented in the later sections.

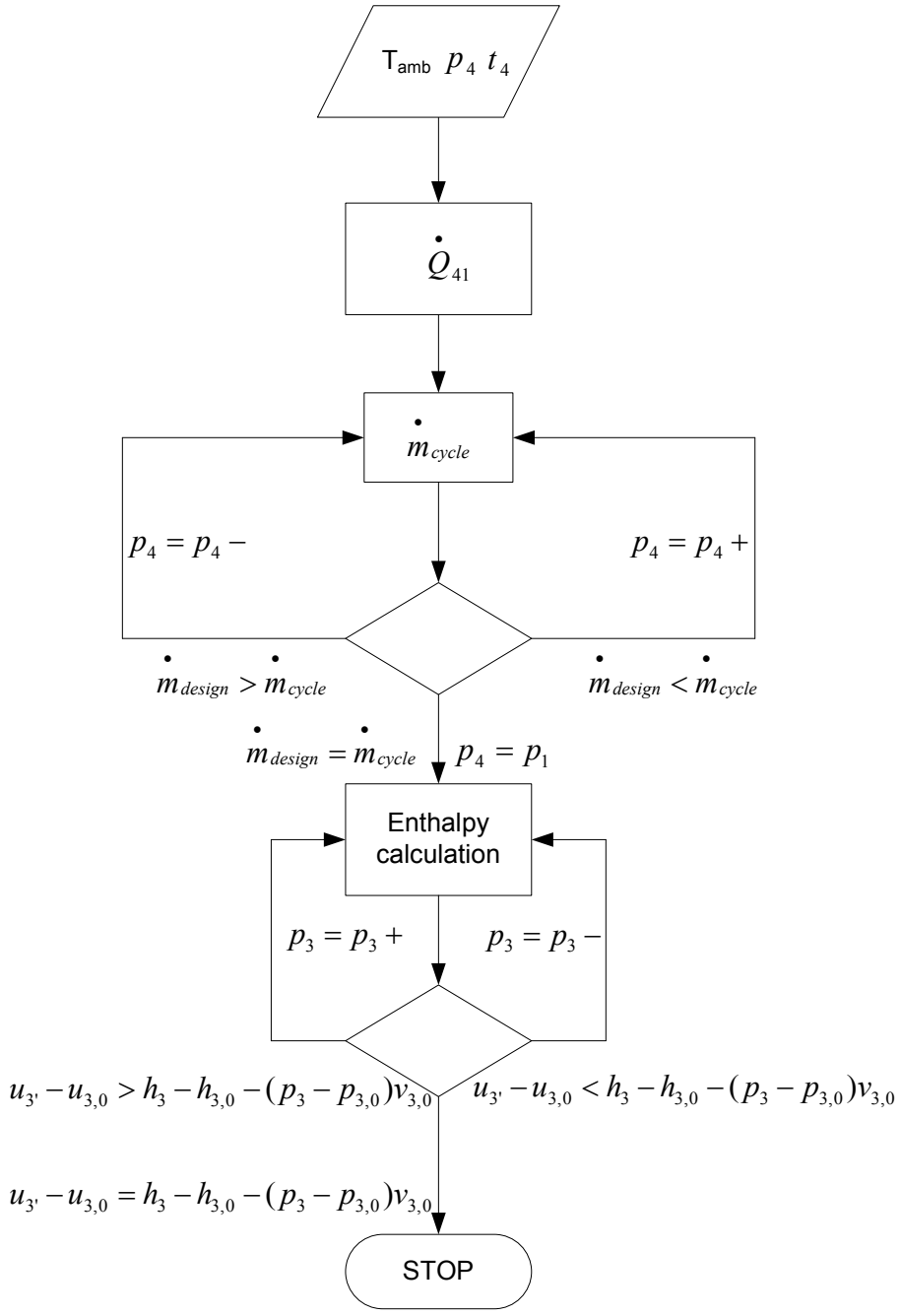

Figure 8-10: Flowchart of the iterative method

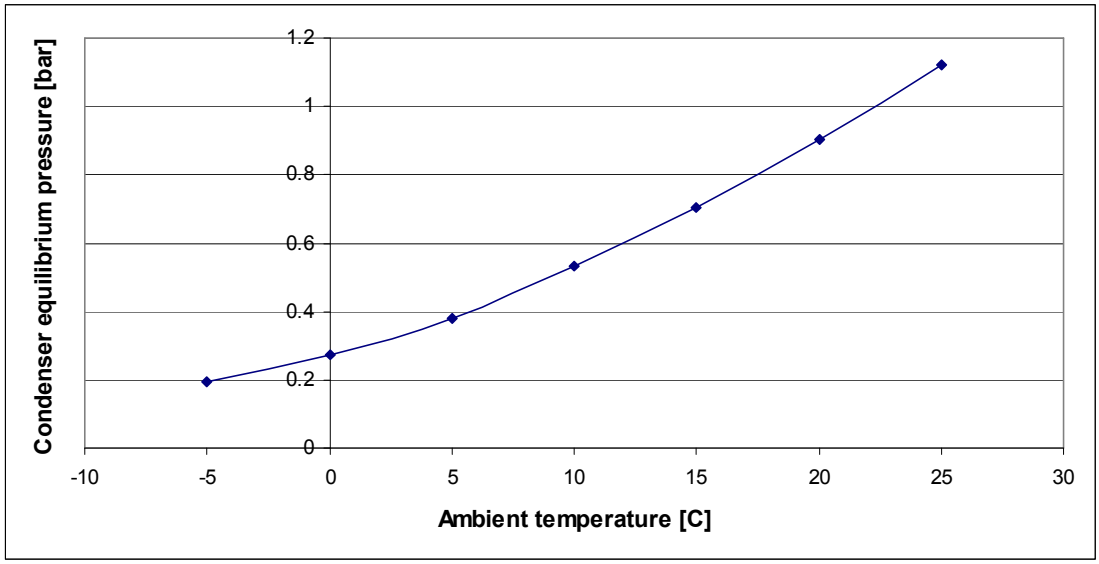

Figure 8-11: Condenser equilibrium pressure as a function of ambient temperature at constant geothermal brine flow for the temperature range of the year 2007

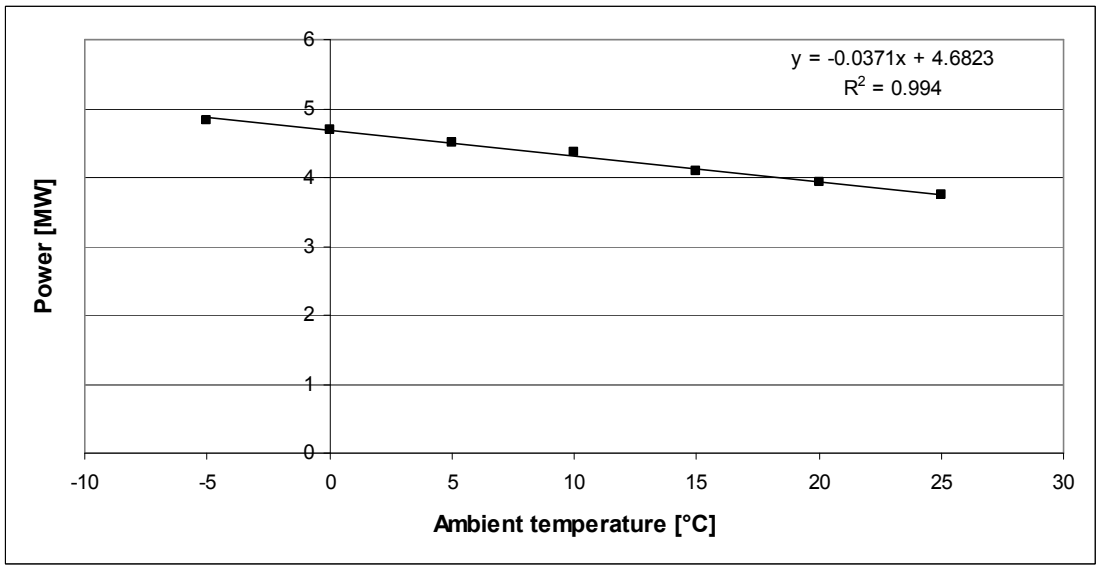

Figure 8-12: Power output of a superheated cycle unit (OEC 1) as a function of ambient temperature and constant geothermal fluid mass flow rate of 100 kg/s for the temperature range of the year 2007

8.5 Convergence, stability and uniqueness of the solution

The solution based on the developed method converges exponentially if the search parameter (equilibrium pressure) is updated each iteration proportionally to the relative error. The approach is widely used in the literature and is known as the Kalman filter [92, 93]. Figure 8-13 illustrates the typical convergence of the mass flow rate using Equation (8.4) to find the vapour-liquid equilibrium pressure for a typical air-cooled condenser. Figure 8-14 presents the convergence of *du* in Equation

(8.9) while searching for the vapour-liquid equilibrium pressure in a typical vaporizer. Here:

$$(p_1)_{n+1} = (p_1)_n \pm k_1 (e_1)_n \tag{8.18}$$

and

$$(p_3)_{n+1} = (p_3)_n \pm k_2 (e_2)_n \tag{8.19}$$

where p_3 and p_1 are the vaporizer and condenser pressures, respectively, k_1 and k_2 are tuneable parameters and *n* represents the iteration number. The use of "+" or "-" depends on whether pressure needs to be increased or reduced. For the solutions shown $k_1 = 0.2$ and $k_2 = 0.1$ were used. e_1 and e_2 are calculated according to:

$$(e_1)_n = \left| (\dot{m}_{design} - (\dot{m}_{cycle})_n) / \dot{m}_{design} \right| \tag{8.20}$$

$$(e_2)_n = \left| (du - (du_{eqbrm})_n) / du \right| \tag{8.21}$$

The stability of the solution lies in the choice of values for the two constants k_1 and k_2. Larger values of *k* improve the rate of convergence, but may introduce instabilities. Lower values of *k* improve stability at the expense of convergence. Appropriate tradeoffs may be achieved by suitable tuning.

Independent properties (i.e., *p, T, v, h* and *s)* are point functions, meaning that they are not dependent on path. Any solution obtained from the method described here must be unique. As long as the pressure values fall within the limits allowed by the thermo-physical properties of the working fluid, one should obtain the same solution regardless of the initial values of pressure used in Equations (8.18) and (8.19). Figure 8-15 shows this to be the case by demonstrating the convergence of *du* with two different initial values of equilibrium pressure. The continuous line presents the solution obtained using an initial guess of the equilibrium pressure of 10 bar. The dashed line shows the solution obtained when an initial guess of 20 bar was used. Both solutions converged to a unique operating value of 18 bar for the equilibrium.

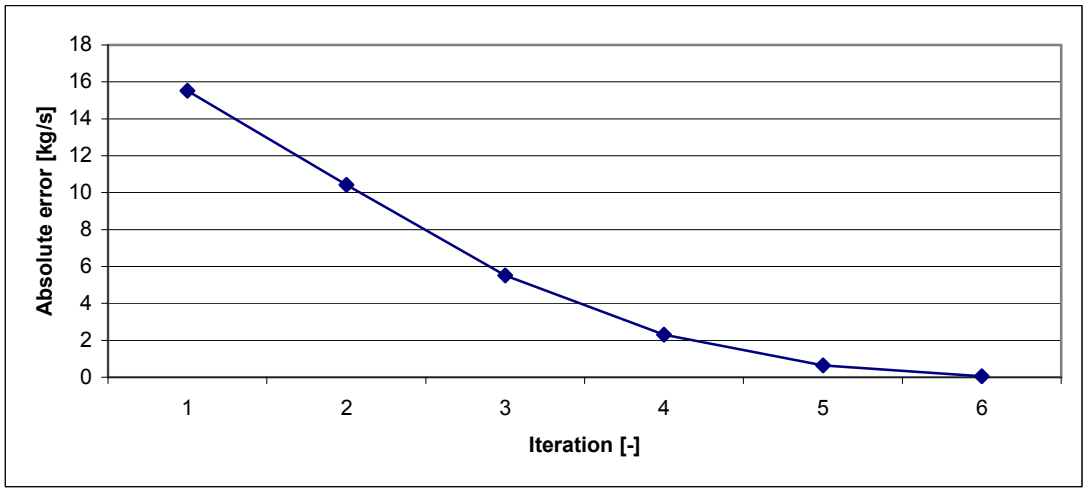

Figure 8-13: Convergence of mass flow based on Equation (8.4). Here cycle mass flow rate was kept constant and vapour-liquid equilibrium pressure was changed

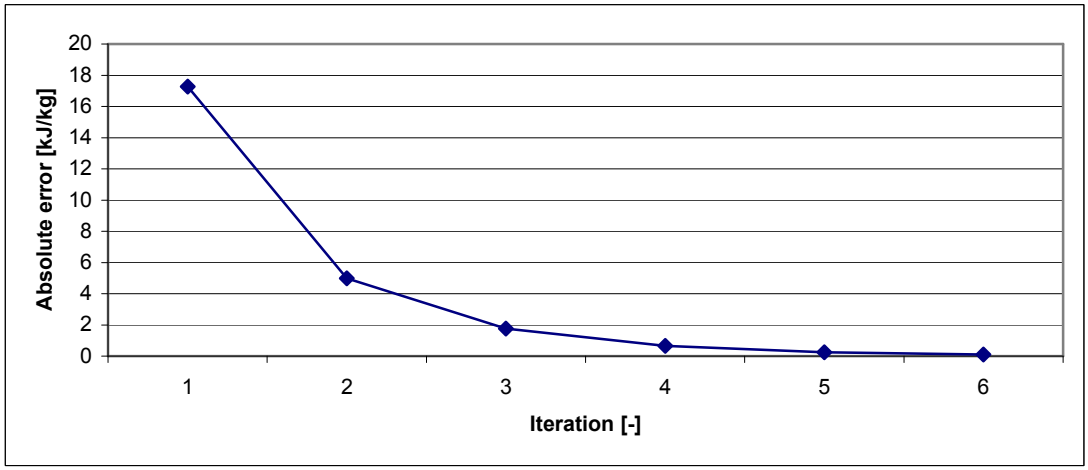

Figure 8-14: Convergence of *du* based on Equation (8.9). Here LHS is kept constant (calculated from equation (8.7)) and vapour-liquid equilibrium pressure was changed

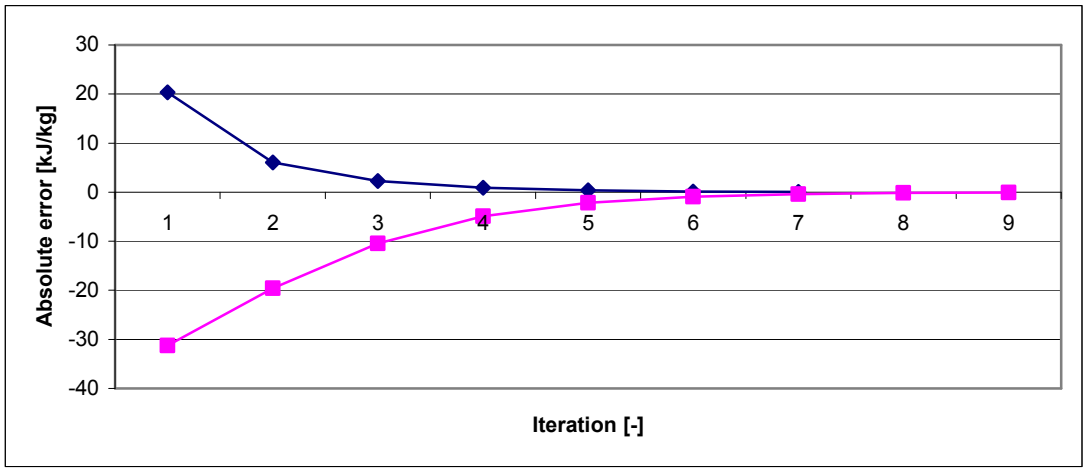

Figure 8-15: Convergence of *du* based on Equation (8.9) to calculate two different starting points. Here LHS is kept constant (calculated from Equation (8.7)) and vapour-liquid equilibrium pressure was changed

8.6 Efficiency

The cycle efficiencies are calculated as follows:

$$\eta_1 = \frac{\dot{W}_{net}}{\dot{Q}_{in}} \tag{8.22}$$

$$\eta_2 = \frac{\dot{W}_{net}}{\dot{m}\,\Delta e} \tag{8.23}$$

where η_1 and η_2 are first and second law (energetic and exergetic) efficiencies, respectively. $\dot{W}_{net}$ is the net work done by the cycle, $\dot{m}$ is the geothermal fluid flow rate and Δe is the specific exergy input to the ORC. The inlet and outlet conditions of the ORC's are controlled so Δe can be assumed constant for our case. The value of Δe can be calculated as [17]:

$$\Delta e = h_{in} - h_{out} - T_0 \Delta s \tag{8.24}$$

where h_{in} and h_{out} are the inlet and outlet enthalpies of the geothermal fluid, respectively. Δs is the difference between the inlet and outlet entropies and T_0 is the equilibrium temperature (dead state temperature). For simplicity, the equilibrium temperature is assumed to be 298.15º K.

8.7 Constrains

The performance of system components (e.g. boiler/vaporizer and condenser) is constrained by the system design. The maximum and minimum allowable pressures and temperatures of these devices are predefined. Plant performance is dependent on these limits as well as operator interaction to maintain operating conditions for maximum output. Such constraints must be applied to the equilibrium condition obtained by the iterative method. Therefore, all iterations [Equation (8.5) to (8.21)] must be terminated and assigned feasible values if extremum operating conditions are reached.

8.8 Case study 1: bottoming ORC

A bottoming ORC (OEC 11), has been chosen for this case study and uses pentane as the working fluid. The schematic of the process diagram is presented in Figure 8-16. Detailed discussion on the Mokai 1 geothermal power plant is available in Chapter 4. There are four basic processes involved:

1-2: Reversible adiabatic pumping process in the pump
2-3: Constant-pressure heat transfer in the vaporizer/preheater
3-4: Reversible adiabatic expansion in the turbine
4-1: Constant-pressure heat transfer in the condenser

Sub-processes
2-2a: Constant-pressure heat recovery in the preheater
2a-3: Constant-pressure heat transfer in the vaporizer

The sub-process 2-2a is no longer in operation and the plant is still producing a quantity of power similar to, which it was designed to produce, due to increased percentage of vapour in the geothermal fluid. Therefore, the current OEC 11 can be described as a typical ORC with four basic processes.

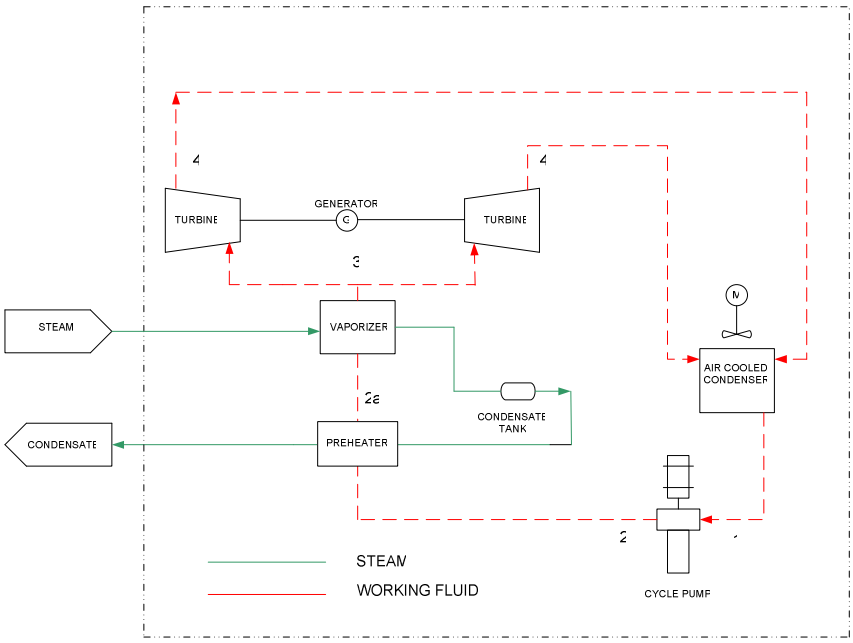

Figure 8-16: Schematic of the saturated vapour cycle

Using the iterative method, the unit is modelled for 48 hours of operation and compared against observed data. The experimental initial conditions are supplied to the model as a starting point for the simulation. The efficiency of the turbine-generator is estimated to be 0.76 from the short term data used for the simulation here. The turbine-generator efficiency combines the turbine isentropic efficiency and generator efficiency. For a different operating point the value of turbine-generator efficiency should be updated with new estimation. A constant pressure loss between the turbine outlet and condenser inlet is assumed to be the nominal observed value of 0.1 bar. Condenser heat load, $Q_{con} = f(p_4, T_4, T_{amb}, v_{air})$, is calculated from the developed condenser model discussed in chapter 5. Table 8.1 summarises the parameter values used for the simulation.

Table 8.1: Values of parameters used for the simulation of OEC 11

Parameters name	Value	Parameters name	Value
$\dot{m}_{cycle}$	106.203 [kg/s]	p_3 initial	5 [bar]
t_4 initial	61 [°C]	p_4 initial	1.2 [bar]
p_3 minimum	4.3 [bar]	p_1 initial	1.07 [bar]
p_3 maximum	5.5 [bar]	η_T	0.76 [-]

Figure 8-17 shows the total hourly steam and brine mass flow rates and corresponding ambient temperatures. Figures 8-18 through 8-20 compare the observed and simulation results associated with the BOT-ORC unit (Figure 8-16). Figure 8-18 compares observed and modelled vaporizer outlet pressure with average percentage error of 2.15%. Figure 8-19 compares observed and modelled vaporizer outlet temperatures with an average error of 1%. Figure 8-20 compares the observed and modelled electric power output of the system with the average error of 4.20%. The iteration is terminated when the tolerance limit, $|e| =< 0.1$ is reached. Figure 8-21 presents the relative error (absolute value) of modelled electric power output of the saturated vapour unit. The relative errors largely lie within 10%. Figure 8-22 presents corresponding first law and second law efficiencies. The first law efficiency varies between 7-9% and the second law efficiency varies between 37-47% depending on the ambient air temperature and geothermal fluid flow rate. The first law and the second law efficiencies are very consistent as reported by DiPippo [17].

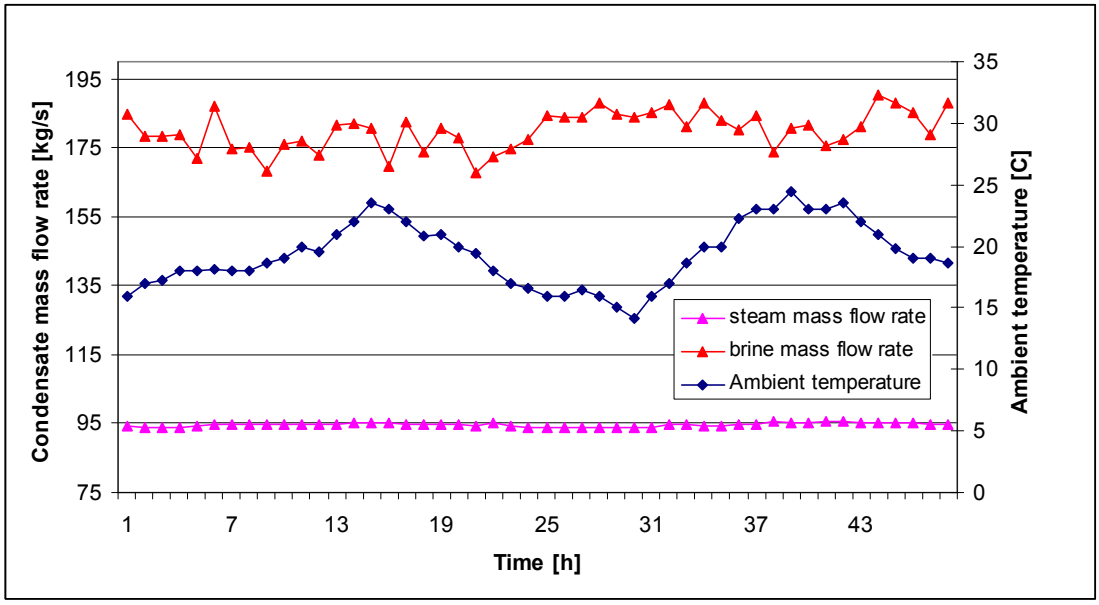

Figure 8-17: Hourly (10/01/2007-11/01/2007) total steam (BOT-ORC X 4) and brine (BRN-ORC X 2) mass flow rates and corresponding ambient temperature of Taupo [72]

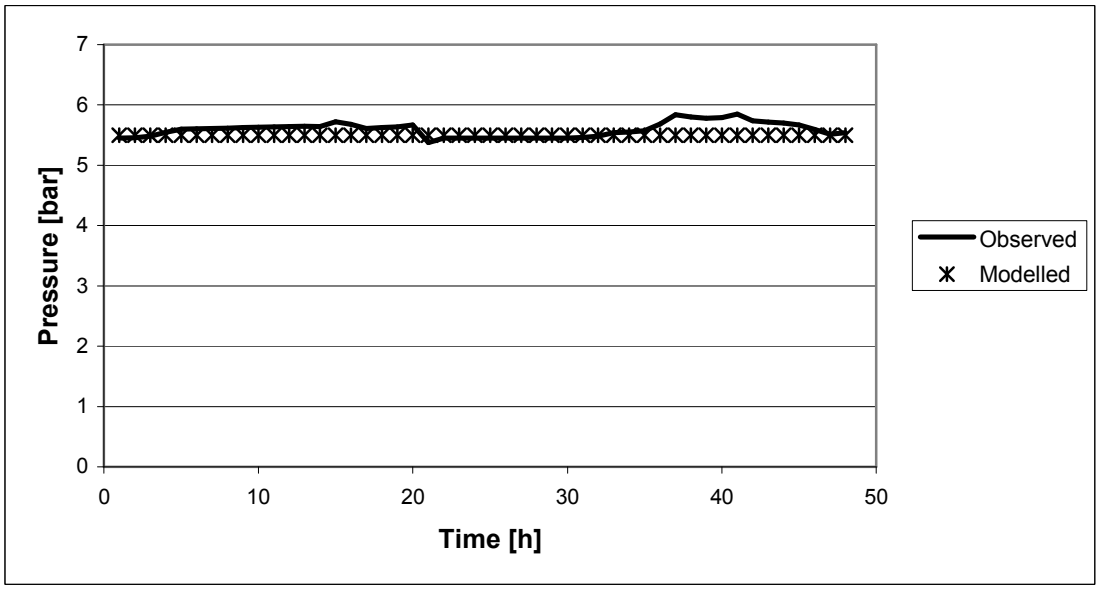

Figure 8-18: Vaporizer outlet pressures for the BOT-ORC unit over 48 hours (10/01/2007-11/01/2007) of operation with corresponding weather conditions of Taupo [72]

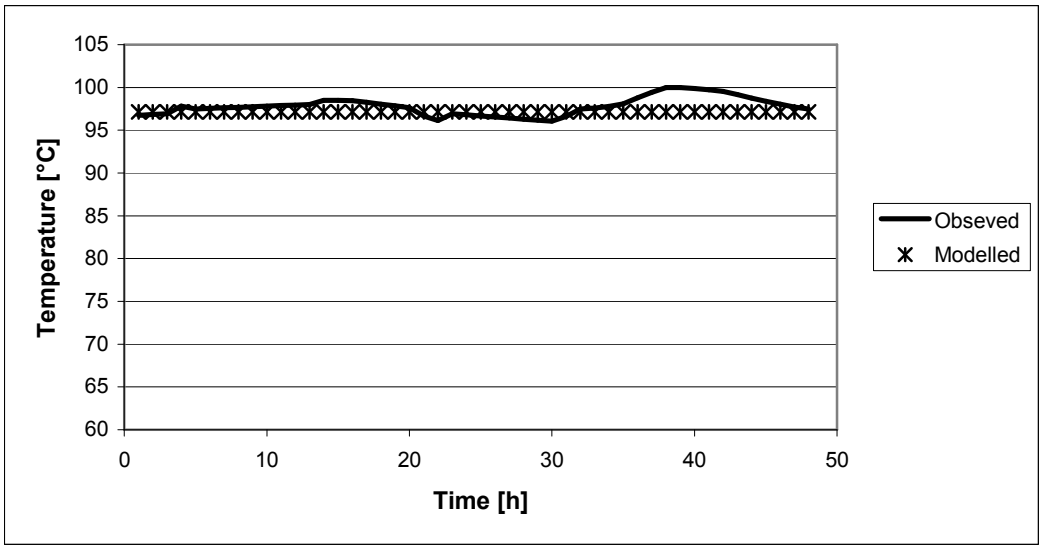

Figure 8-19: Vaporizer outlet temperatures for the BOT-ORC unit over 48 hours (10/01/2007-11/01/2007) of operation with corresponding weather conditions of Taupo [72]

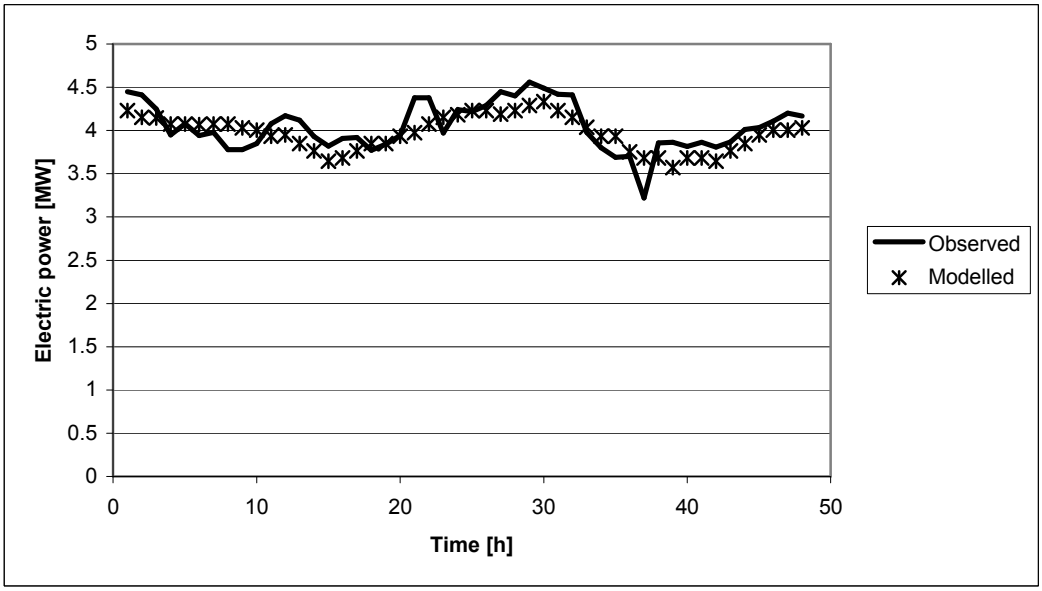

Figure 8-20: Electric power output for the BOT-ORC unit over 48 hours (10/01/2007-11/01/2007) of operation with corresponding weather conditions of Taupo [72]

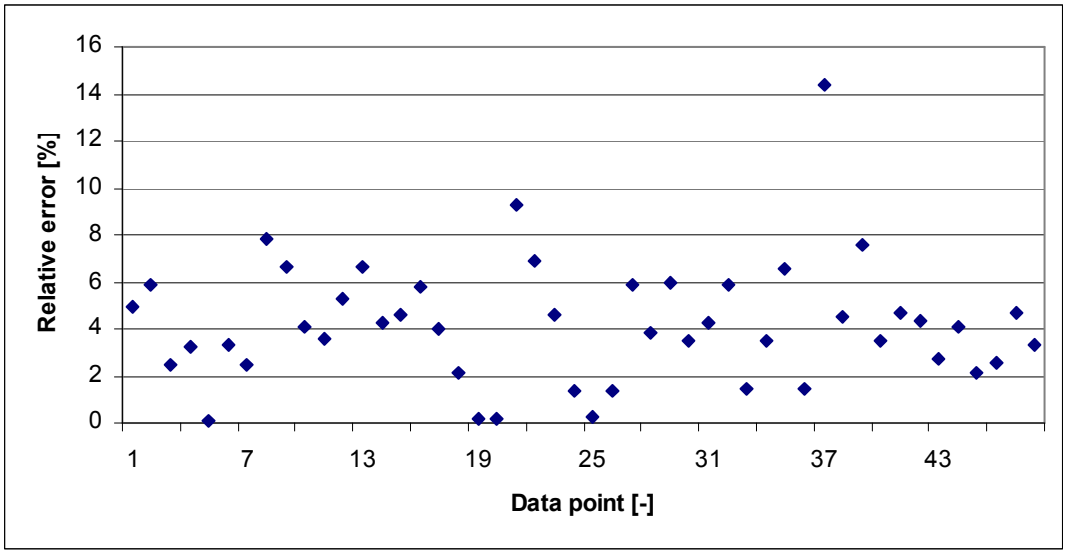

Figure 8-21: Observed relative error in modelled electric power output for the BOT-ORC unit over 48 hours (10/01/2007-11/01/2007) of operation with corresponding weather conditions of Taupo [72]

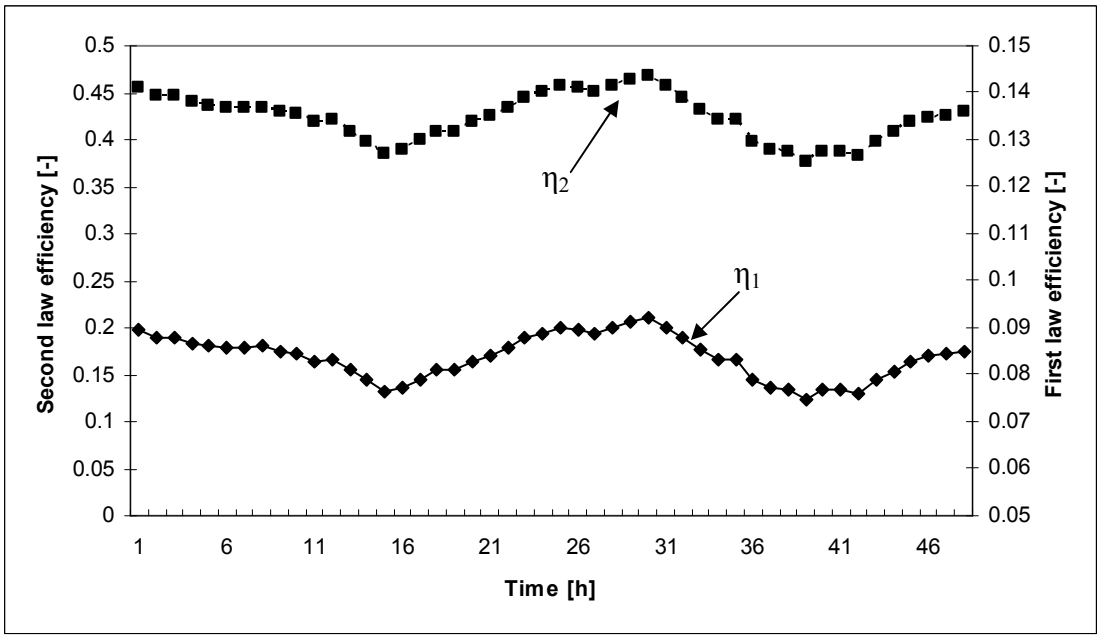

Figure 8-22: First and second law efficiencies of the saturated vapour unit over 48 (10/01/2007-11/01/2007) of operation with corresponding weather conditions of Taupo [72]

8.9 Case study 2: brine ORC

Figure 8-23 presents the schematic of the superheated vapour ORC unit used for case study 2. Superheating in the cycle adds some complexity. However, the same

iterative approach may be used to implement the system model. From a modelling perspective, there are two basic differences between the saturated and superheated vapour ORC cycles: superheating and the addition of a recuperator for heat recovery. The maximum temperature of a superheated vapour cycle is typically much higher than that of a saturated cycle. Considering the second law of thermodynamics, the effect of ambient air (heat sink) variation will be less prominent in the superheated cycle compared to a saturated cycle [56].

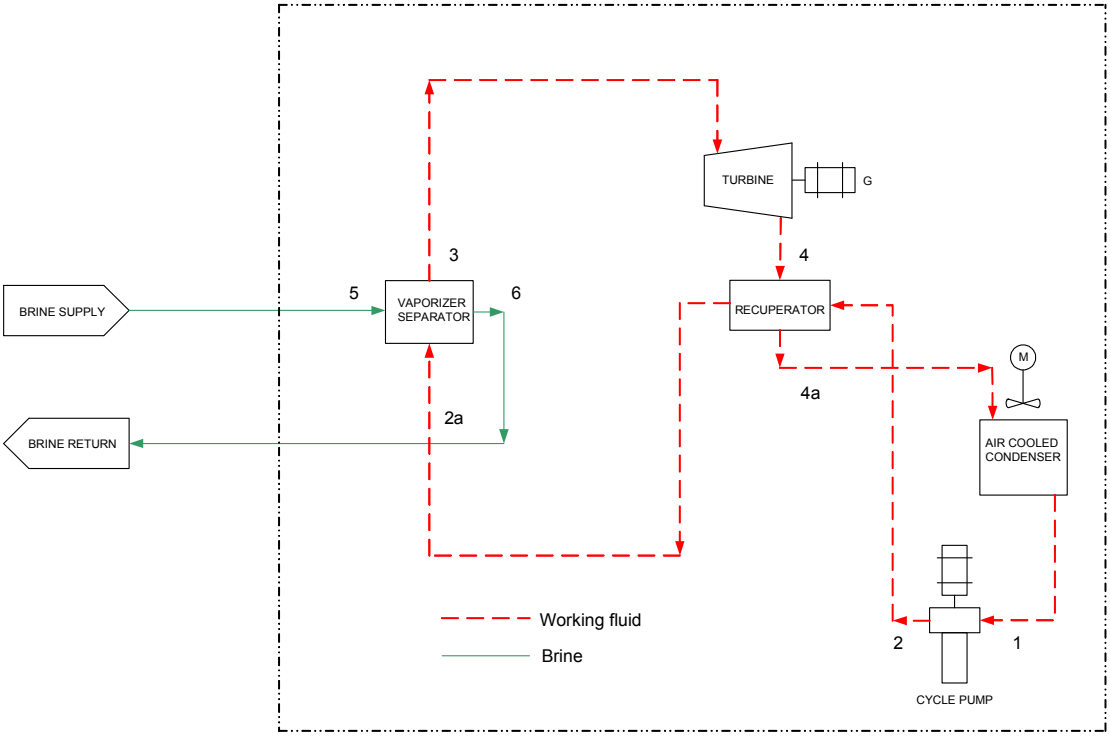

Figure 8-23: Schematic of the Superheated Vapour Cycle

The pressure loss between the vaporizer outlet and turbine inlet is assumed constant and assigned 0.5 bar which is consistent with the observed value. The pressure loss in the recuperator is assumed constant and fixed at 0.65 bar (state 4a), which is consistent with the observed value.

The condenser equilibrium condition and corresponding outlet temperature are derived in the same manner as in the case of the saturated vapour ORC. If the pump input work is assumed constant, the enthalpy of state 2 is calculated using Equation (8.5). In the superheated cycle, heat input is given as

$$\dot{Q}_{2a-3} = \dot{Q}_{vaporizer} + \dot{Q}_{separator} \tag{8.25}$$

where, Q_{2a-3} is the heat input to the system from brine. Since the design value of heat transfer of heat transfer of Q_{2a-3} and $\dot{Q}_{vaporizer}$ are known, the off design heat transfer of both Q_{2a-3} and $\dot{Q}_{vaporizer}$ can be calculated from Equation (8.17). As the design value of $\dot{Q}_{separator}$ is not readily available it is calculated from Equation (8.26).

$$\dot{Q}_{separator} = \dot{Q}_{2a-3} - \dot{Q}_{vaporizer} \tag{8.26}$$

The typical vapour-liquid equilibrium conditions to the vaporizer of the OEC 1 are supplied to the model. An improved value of the vapour-liquid equilibrium condition inside the vaporizer is calculated by the iterative method same way as for the OEC 11. The temperature at the separator outlet is calculated form the energy balance:

$$T_3 = T_{sat} + \frac{\dot{Q}_{separator}}{\dot{m}_{cycle}\, c_p} \tag{8.27}$$

where T_{sat} represents the saturated pentane temperature calculated by the iterative method, $\dot{m}_{cycle}$ is the cycle mass flow rate and c_p is the specific heat of pentane at constant pressure in the separator. It is notable that the outlet pentane vapour from the vaporizer is passed through a mechanism where any droplet which is going out, is trapped and return to the vaporizer before entering the separator. Otherwise, Equation (8.27) had to be changed to take into account the latent heat of vaporization of pentane.

The state at point 4 is determined as before, assuming isentropic expansion in the turbine. The value of electric power output is calculated using Equation (8.14) with a turbine-generator efficiency of 0.9, which was estimated from plant operational data. The turbine-generator efficiency combines the turbine isentropic efficiency and generator efficiency. Table 8.2 summarises the parameter values used for the simulation.

Table 8.2: Values of parameters used for the simulation of OEC 1

Parameters name	Value	Parameters name	Value
$\dot{m}_{cycle}$	86.37 [kg/s]	p_3 initial	18 [bar]
t_4 initial	62.3 [°C]	p_4 initial	1.17 [bar]
p_3 minimum	15 [bar]	p_1 initial	1.15 [bar]
p_3 maximum	19 [bar]	η_T	0.90 [-]

Figures 8-24 to 8-27 show the results of simulation for two days of BRN-ORC operation using the iterative modelling method. Figure 8-24 presents observed and modelled condenser outlet temperatures with an average error of 5.78%. Figure 8-25 shows observed and modelled vaporizer pressures with an average error 1.32%. Figure 8-26 presents observed and modelled vaporizer outlet temperatures with an average error of 3.4%. Figure 8-27 presents the observed and modelled electric power output of the unit with average error 2.12%. Figure 8-28 presents the relative error (absolute value) of modelled electric power of the superheated vapour which shows that the relative error remained within 6%. Lastly, Figure 8-29 presents corresponding first law and second law efficiencies. The first law efficiency varies between 15-17% and the second law efficiency varies between 38-45% which are also consistent with as reported by DiPippo [17].

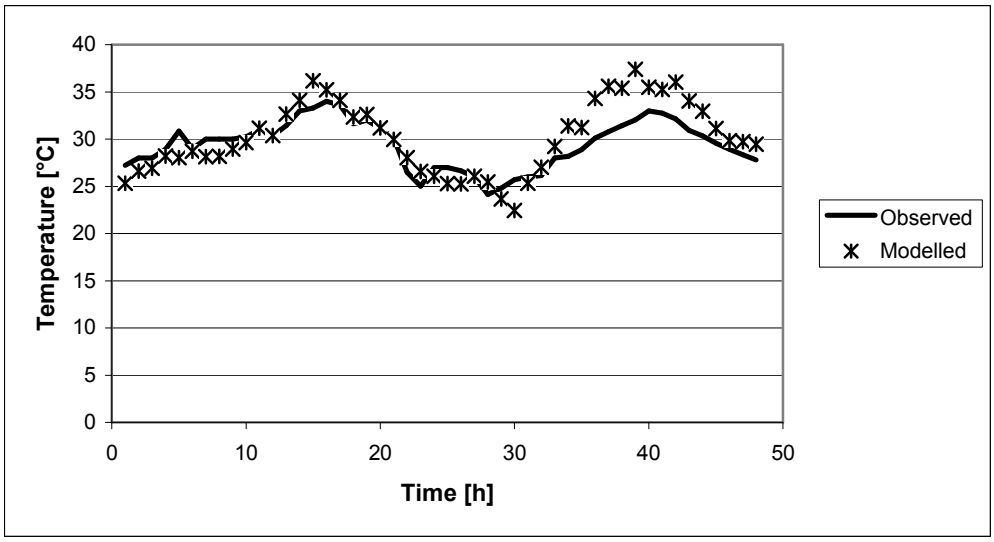

Figure 8-24: Condenser outlet temperatures for the BRN-ORC unit over 48 hours (10/01/2007-11/01/2007) of operation for corresponding weather conditions of Taupo [72]

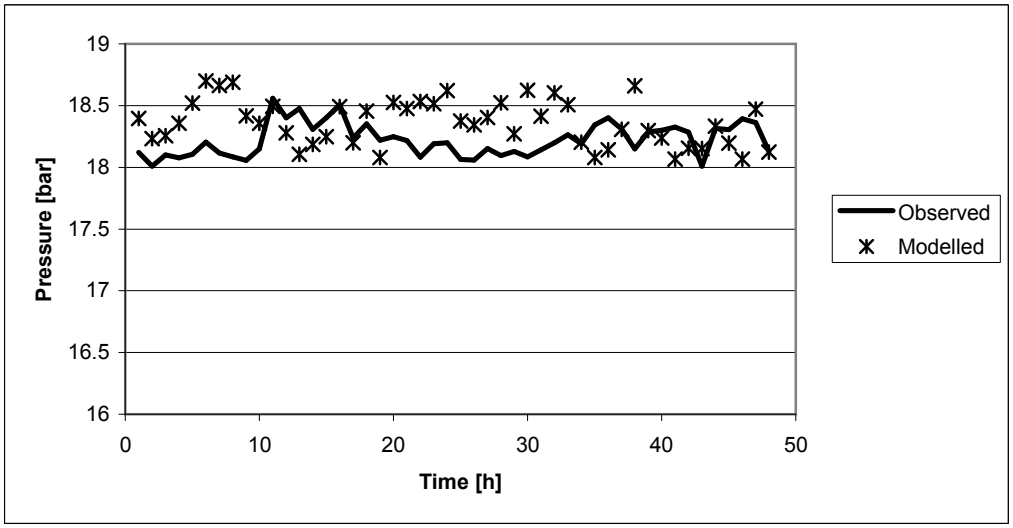

Figure 8-25: Vaporizer outlet pressures for the BRN-ORC unit over 48 hours (10/01/2007-11/01/2007) of operation for corresponding weather conditions of Taupo [72]

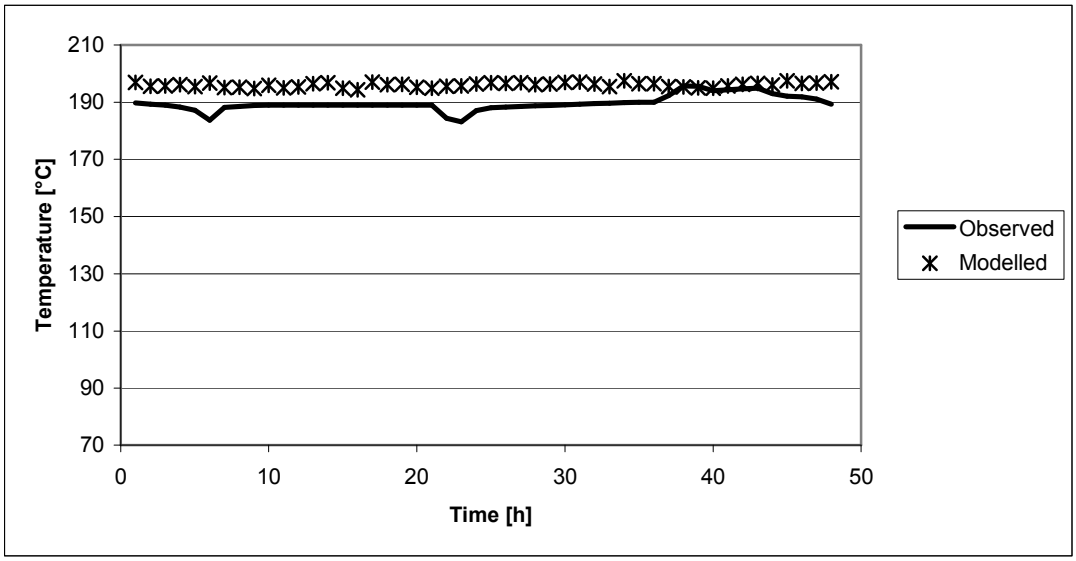

Figure 8-26: Vaporizer outlet temperatures for the BRN-ORC unit over 48 hours (10/01/2007-11/01/2007) of operation for corresponding weather conditions of Taupo [72]

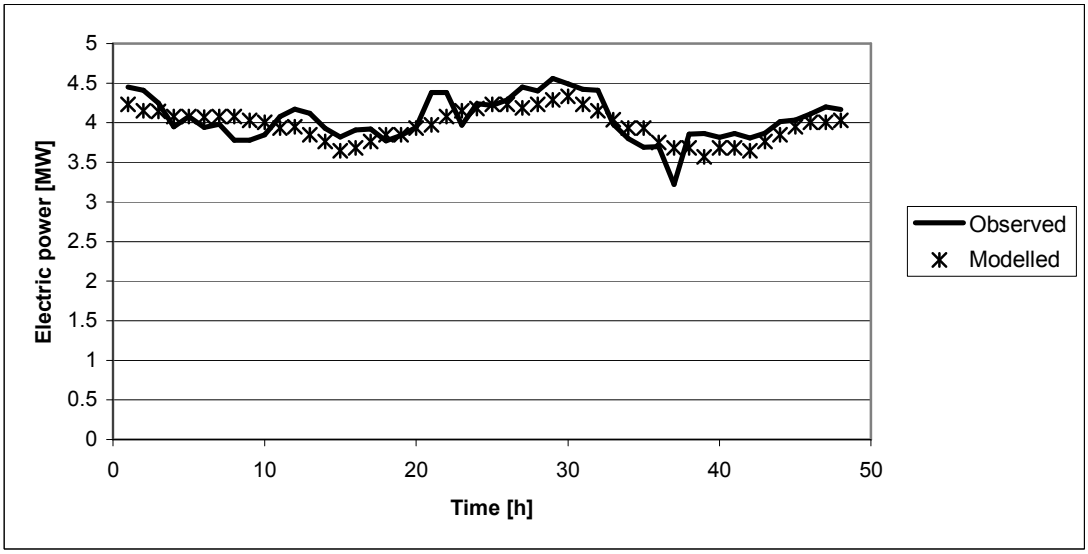

Figure 8-27: Electric power output for the BRN-ORC unit over 48 hours (10/01/2007-11/01/2007) of operation for corresponding weather conditions of Taupo [72]

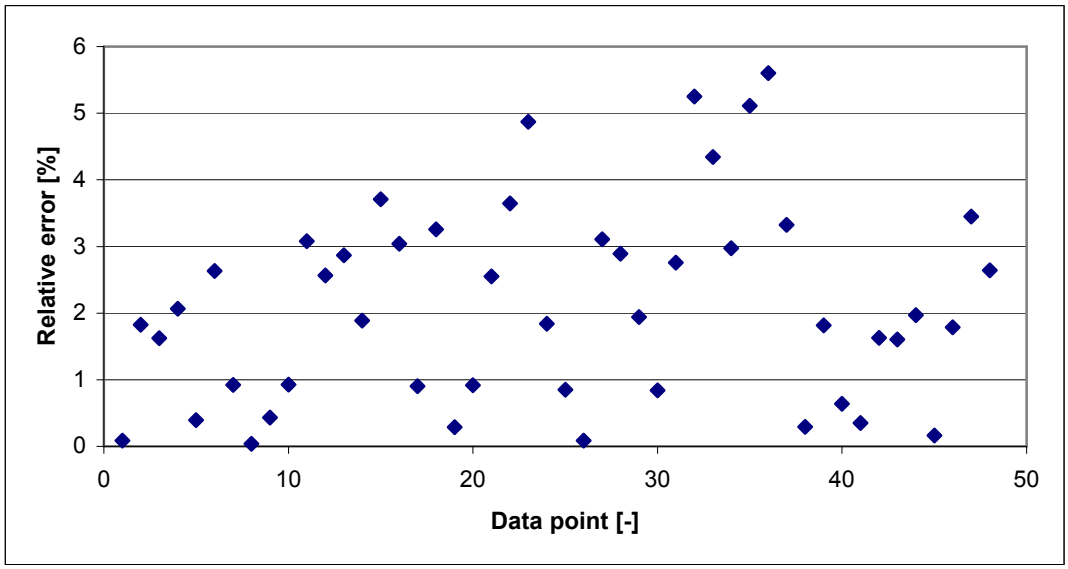

Figure 8-28: Relative error in modelled electric power output for the BRN-ORC unit over 48 (10/01/2007-11/01/2007) of operation for corresponding weather conditions of Taupo [72]

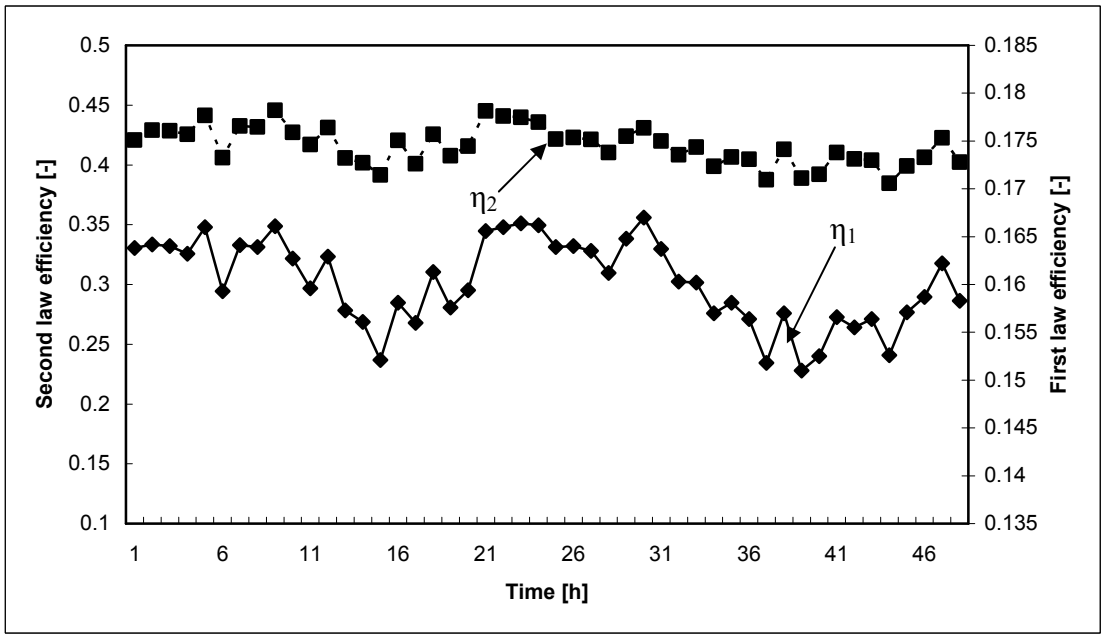

Figure 8-29: First and second law efficiencies of the BRN-ORC unit over 48 hours (10/01/2007-11/01/2007) of operation with corresponding weather conditions of Taupo [72]

8.10 Discussion on the developed iterative method

Most of the modelling works available in the literature compare their results against experimental data performed under controlled environments [19, 44]. In a real plant, uncertainty of a physical model increases over time due to degradation of the plant

[94]. In recent years application of artificial neural networks and genetic methods for modelling thermal power plant has become popular [26, 94]. These models provide a high degree of accuracy without complicated physics based models and also address the problem of increased model uncertainty with age. However, such models are very plant specific and cannot be readily used in conceptual design and developments. In contrast, the method developed here is based on fundamental thermodynamics and could be very useful in conceptual design and development.

In the saturated vapour cycle the error lies largely within 10% (Figure 8-21). Only one data point is found to lie above 14 %. However, the external parameters, i.e., ambient temperature and geothermal fluid flow rate, for this data point are very similar to the neighbouring data points. Therefore, this point can be assumed to be noise or an "outlier" [27]. Table 8.3 summarises the average and maximum relative errors of the saturated vapour cycle and the superheated vapour cycle. Wei and co-workers [44] reported a maximum relative error of 4% for their semi-empirical model. Quoilin and co-workers [19] reported the maximum error of their model to lie within 10% and commented that their error was a consequence of cumulated subcomponent models inaccuracies. Smrekar and co-workers [94] have reported a maximum relative error of 7.19% of a boiler model of a real power plant. They have used artificial neural networks for the modelling purpose. In this work, the maximum error remained at 10% and seems consistent with existing literature. Moreover, the efficiencies of both of the ORC units (energetic and exergetic) found to be very consistent with the literature [17].

The developed model is very generic and can be used for conceptual design, analysis and optimization (discussed in chapter 9). Therefore, the method presented in this paper can be considered reasonably accurate (in the context of existing methods) and very useful.

Table 8.3. Summary of results of observed and modelled electric power output.

Cycle type	Average error (|e|) [%]	Maximum error (|e|) [%]
Saturated Vapour Cycle	4.20	9.25
Superheated Vapour Cycle	2.12	5.60

8.11 Plant performance based on yearly data

In this section application of the models for high level design and analysis are discussed. Figure 8-30 shows modelled and actual electric power output for the BOT-ORC for the year 2007 where the red line represents the simulated power output and blue dots represents actual power output taken from the plant operational log. Figure 8-31 shows the modelled and actual electric power output for the BRN-ORC cycle for the year 2007 where the red line represents the simulated power output and blue dots represents actual power output taken from the plant operational log. It is clear from the two figures; the developed model can fairly follow the trend. However, a big difference exists between the actual and simulated performance. This is mainly due to fact that the geothermal fluid mass flow rates are not taken into consideration. Moreover, vapour-liquid equilibrium condition (pressure-temperature) must be supplied to the models to start simulations which should be a typical operating condition. When the average ambient temperature changes significantly, the operator intervenes and changes the vapour-liquid equilibrium conditions with the objective to increase output. Therefore, initial values given to the model should be updated for seasonal variations. However, as the main interest of this section lies on the high level design and analysis, the trends presented in the figures are fairly representative.

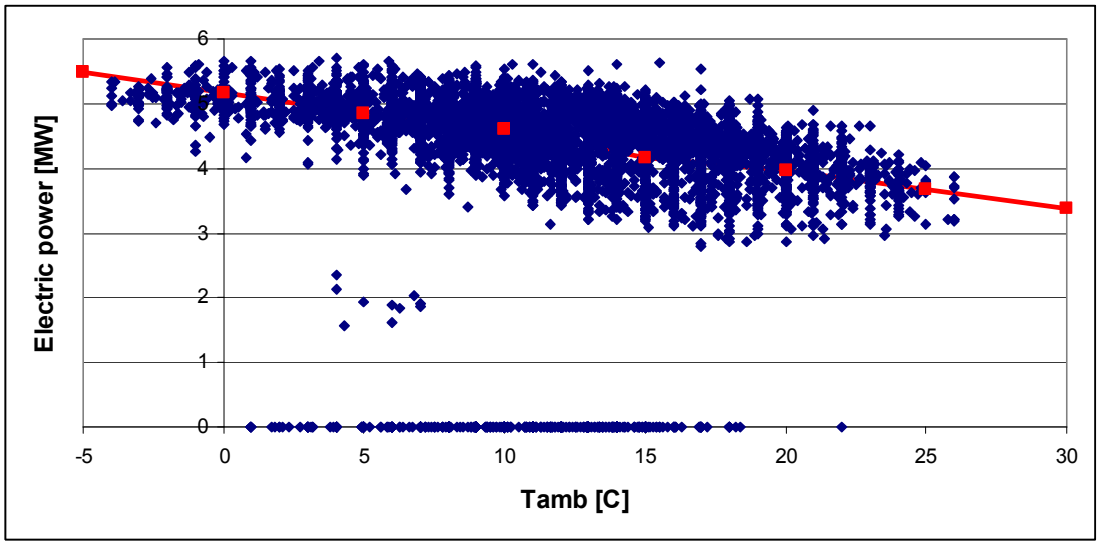

Figure 8-30: Actual and modelled (red line) electric power output for BOT-ORC for the year 2007

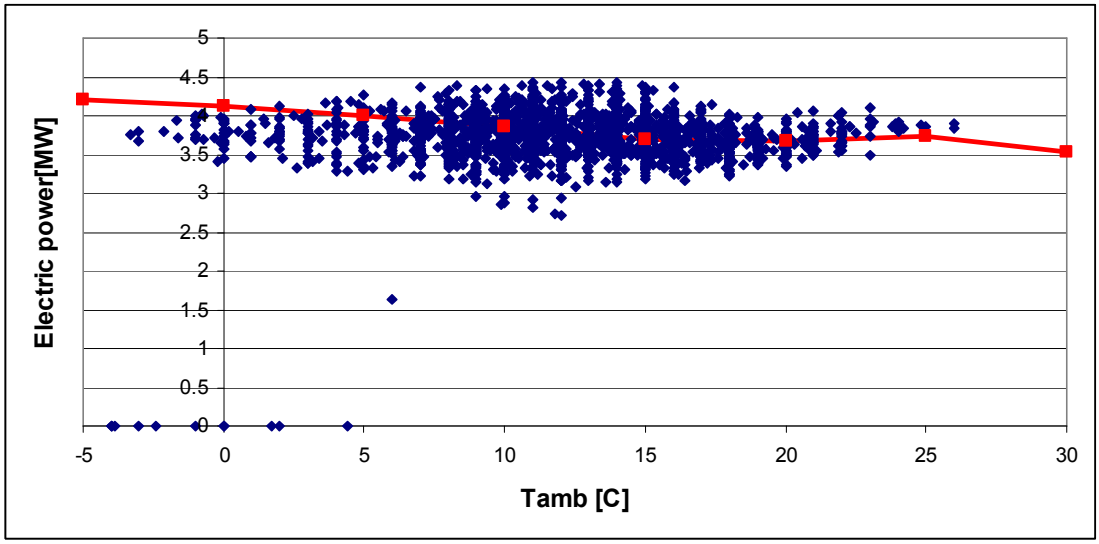

Figure 8-31: Actual and modelled (red line) electric power output for the BRN-ORC for the year 2007

Figure 8-32 shows the simulated plant performance for annual average temperature with design geothermal fluid flow rate. The average monthly temperature varies from about 7ºC to about 18ºC. Possible power outputs for the saturated vapour cycle and the superheat vapour cycle varies between 5 - 5.5 MW and between 4 - 4.8 MW, respectively. This analysis assumes constant geothermal fluid flow rate and assigned the design value.

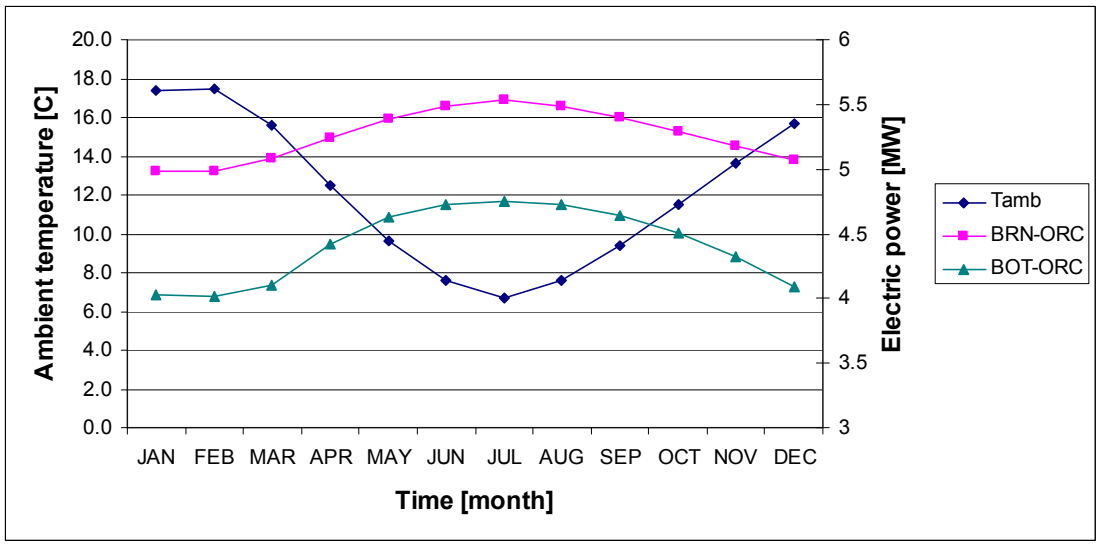

Figure 8-32: Simulated plant performance for the BOT-ORC unit and BRN-ORC unit based on monthly average monthly ambient temperature of Taupo for 1971-2000 [72]

8.12 Summary

This chapter has presented an iterative method for modelling a closed ORC. The heat sink temperature, in this case the ambient temperature, affects the modelled condenser performance. Consequently, it influences the performance of the whole cycle. This occurs in two ways: (i) changes in the equilibrium pressure inside the condenser result in a change in turbine outlet pressure and pressure ratios and (ii) changes in the condenser outlet temperature caused by the heat sink temperature also affect the pump inlet and outlet conditions as well as the vaporizer equilibrium temperature-pressure. These are competing effects. However, changes related to the turbine pressure ratio tend to dominate the power.

Calculating the vapour-liquid equilibrium condition of the condenser was performed by assuming that the mass flow rate in an ORC in steady state operation remains relatively constant. The vapour-liquid equilibrium condition of the vaporizer is found by assuming that the specific volume inside the vaporizer is unchanged for steady state operation. Termination of the iterative search for unique state solutions is achieved when reaching a slack equilibrium condition within a prescribed tolerance or by meeting a constraint. As the model essentially assumes steady state operation of the power cycle, the possible unit time where this model can be applied is bounded by the time required by a system to come into steady state.

The saturated vapour cycle yielded average error 4.20% with maximum error 9.25% and the superheated vapour cycle yielded average error 2.12% with maximum error 5.60%.

The main advantage of using the developed method lies on the fact that it requires a minimum number of inputs: condenser (p,T), vaporizer (p,T), condenser heat load, turbine efficiency (overall), pump work and the extremum conditions of all the components. These inputs should represent typical operating conditions of a plant. The model can predict the appropriate plant performance depending on the system heat input (geothermal fluid flow in this case) and the heat sink temperature. As the method is based on basic thermodynamics, rather than empirical or semi-empirical approaches, it is widely applicable. Although the main focus of this work is the ORC,

the developed method is applicable to any closed Rankine cycle. In addition, application of the developed iterative method to predict plant performance based on mean yearly weather data is also discussed in this chapter.

Chapter 9

Adaptive approaches for short term performance improvements

9.1 Introduction

In the previous chapter iterative method for modelling the short term performance of the ORCs is presented. In this chapter, two adaptive approaches to improve short term performance are discussed. Water augmented cooling system and real time (hourly) plant operating point parameters optimization have been identified as the means to improve short term performance.

9.2 Mitigation of ORC plant performance deterioration during the summer

Figure 9-1 shows the hourly temperature and relative humidity of the geothermal region near Taupo, New Zealand for a typical summer day. At midnight the temperature is low with very high relative humidity. Temperature drops further in the early morning and relative humidity increases. From midday to late afternoon, the temperature is the maximum with the lowest humidity. Dry bulb temperature is the temperature recorded by a standard thermometer. Wet bulb temperature is measured by a standard thermometer whose bulb is covered by a muslin sleeve that has been moistened by pure water. Wet bulb temperature indicates the amount of moisture contained in the air, and also the evaporation cooling temperature for water in a cooling tower.

Throughout the daytime (8 am to 8 pm; Figure 9-1) there is a large difference between the dry and wet bulb temperature as the relative humidity is low. Figure 9-2 represents dry bulb and wet bulb temperature for the year 2005 in the Taupo volcanic region. The figure shows, in the summer the difference between wet bulb and dry bulb

temperature is much higher than in the winter. This indicates an opportunity for using cooling tower system attached to air-cooled condenser to boost summer efficiency. By using evaporative cooling, the bottoming unit dead state temperature, T_L could be lowered several degrees closer to the wet bulb temperature. According to Carnot efficiency ($\eta_{Carnot} = 1 - \frac{T_L}{T_H}$), the theoretical efficiency would be increased by reducing the dead state temperature.

The direct spray method for evaporative cooling is a cheaper alternative to the cooling tower. However, the cooling performance is not as good as the cooling tower. To be on the conservative side, the effectiveness of the adiabatic evaporative cooling system (ε) was modelled as 80%. However, the effectiveness of the adiabatic evaporative cooling system very often reaches higher than 80%. Detailed discussion on evaporative cooling enhancement methods for air-cooled geothermal power plants can be found in [59].

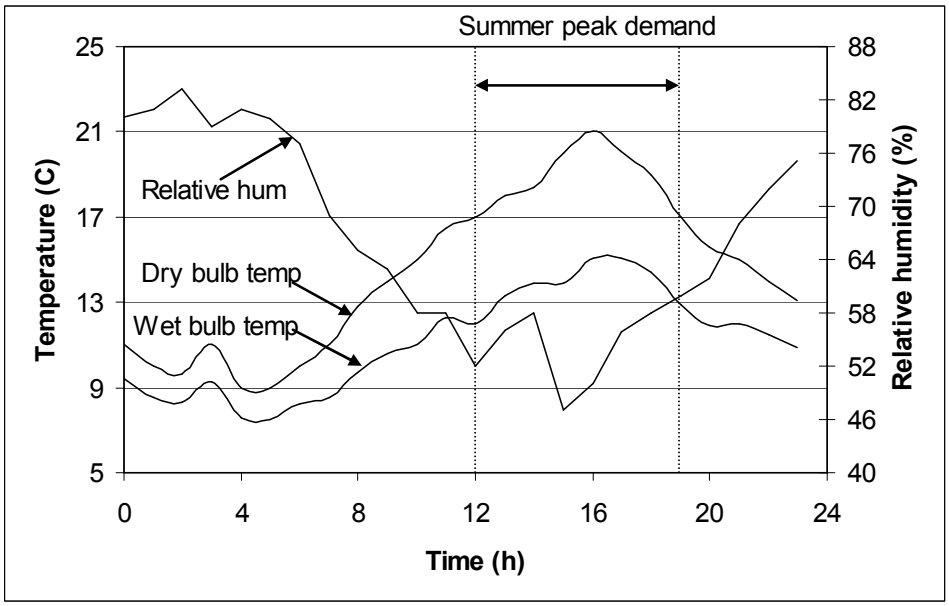

Figure 9-1: Hourly temperature and relative humidity on 01/11/2005 at Taupo volcanic zone (from [72])

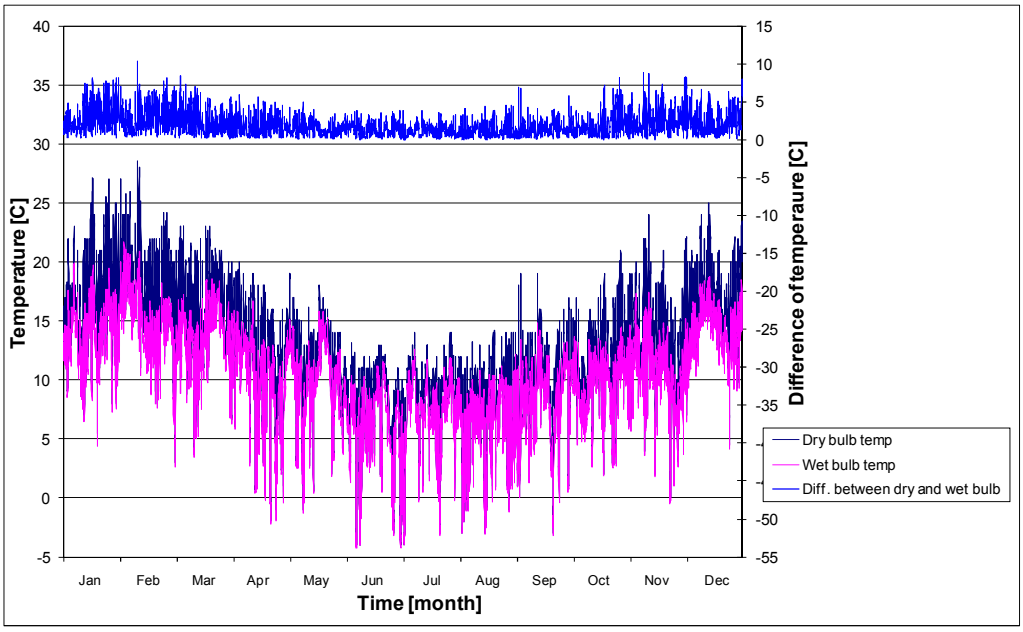

Figure 9-2: Dry bulb and wet bulb temperature of Taupo for the year (from 2005 [72])

The exit air temperature (cooled air) from a cooling system is calculated from the following equation [35]:

$$T_{a,exit} = T_{db} - \varepsilon.(T_{db} - T_{wb}) \tag{9.1}$$

where, $T_{a,exit}$ is the exit air temperature, T_{db} is the dry bulb temperature, T_{wb} is the wet bulb temperature, and $\varepsilon = 0.8$ is the effectiveness of the adiabatic evaporative cooling system. If the cooled-air from an evaporative cooling system is used to cool an existing air-cooled condenser then the cooled-air will act as the dead state temperature:

$$T_L = T_{a,exit} \tag{9.2}$$

Figure 9-3 shows the simulated gain in power output of the OEC 1 (BRN-ORC) using a water-augmented air-cooled system. Significant power gain in the summer is evident from the figure. The average gain in power in the summer (Jan, Feb, Nov and Dec) is 2.3% and the average gain for the whole year is 1.6%. Figure 9-4 shows corresponding first law efficiencies. Incorporating the water-augmented cooling to the BRN-ORC can result in about 1-2.6% gain in first law efficiency. Figure 9-5 presents second law efficiencies. If water-augmented cooling system is incorporated to BRN-ORC the second law efficiency can increase about 1-3% depending on the weather conditions.

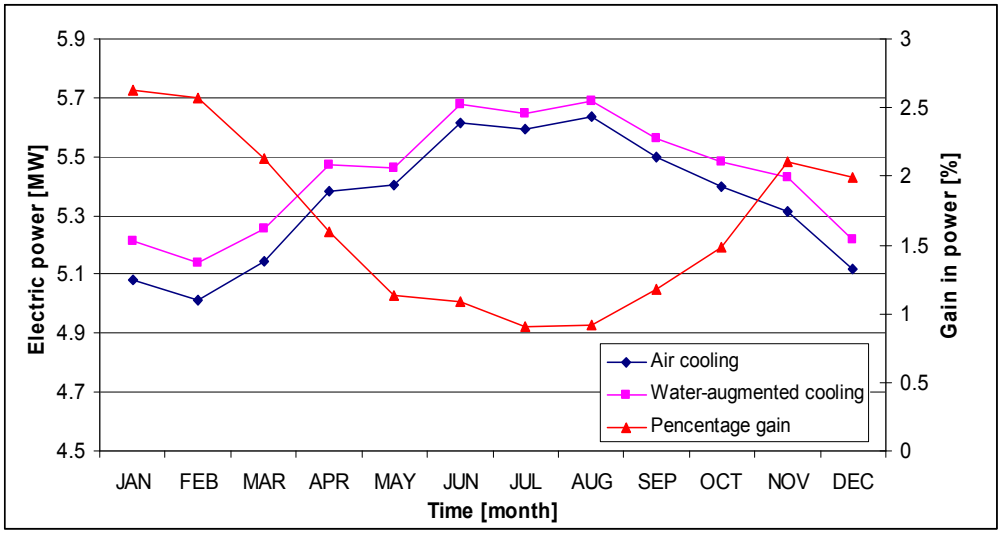

Figure 9-3: Power output of gain of BRN-ORC as a function of monthly average ambient temperature of Taupo for the year 2005 [72]

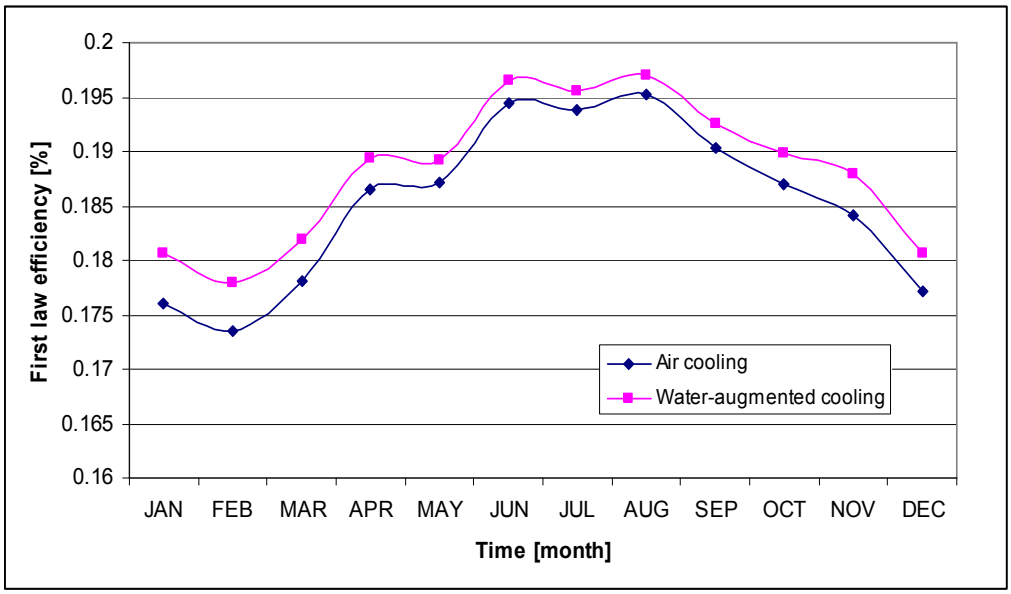

Figure 9-4: First law efficiency of BRN-ORC as a function of monthly average ambient temperature of Taupo for the year 2005 [72]

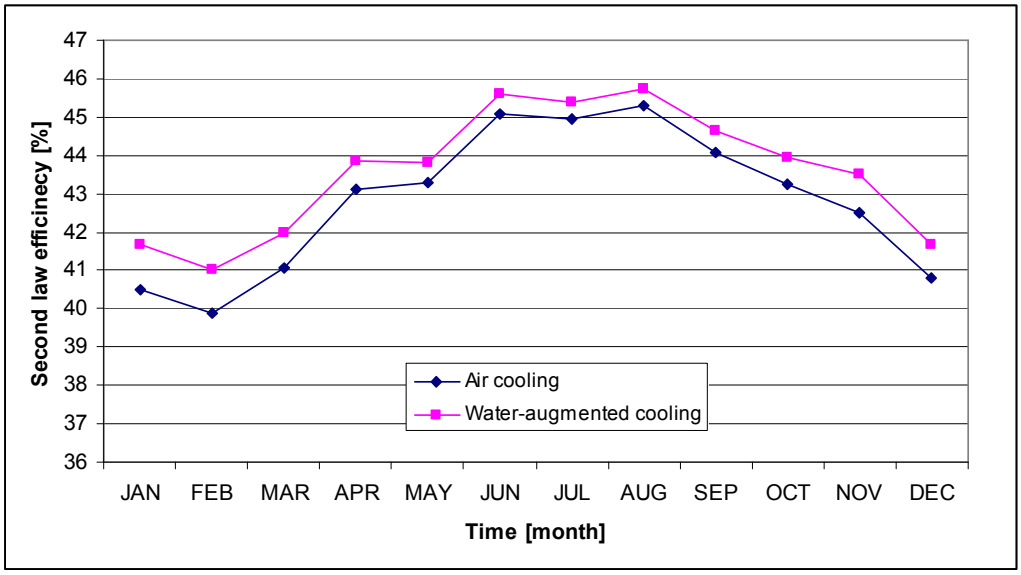

Figure 9-5: Second law efficiency of BRN-ORC as a function of monthly average ambient temperature of Taupo for the year 2005 [72]

9.3 Discussion on water augmented cooling

9.3.1 Cost and benefits

As the simulation results show, incorporating a water-augmented cooling to the air-cooled system of BRN-ORC can translate to 1.6% gain in power output throughout the year in conservative calculations. The gain reaches 2.3% in summer peak, which is the time when power is needed most and power companies enjoy higher profit margins as the unit price of electricity is higher. In the simulation we have used a representative of the BRN-ORCs.

The BRN-ORCs operate at a higher temperature than the BOT-ORCs. DiPippo [56] showed that the binary cycles operating at a higher temperature are less susceptible to the ambient air temperature compared to the binary cycles that operate at a lower temperature. Therefore, the BOT-ORCs are more susceptible to the ambient temperature; i.e., the BOT-ORCs have higher potential to gain from water-augmented cooling. If we assume that the BOT-ORC and the BRN-ORC have the same gain using water-augmented cooling, our cost benefit analysis will be on the conservative side. Here, cost benefit analysis is carried out assuming BOT-ORCs to have same gain as the BRN-ORCs using water-augmented cooling.

Power plants are capital intensive, so small gain in performance can translate in to large revenue. The Mokai 1 plant has 2 brine ORCs and 4 bottoming ORCs with total design capacity of 28.8 MW from these binary units. A 1.6% gain in power would generate an extra 460 kW for Mokai 1 binary cycle units. Assuming 90% service factor, the increased generation is equivalent to 3626 MWh per year or USD $363,000, assuming an average consumer price of 10.4 cents/kWh [95]. However, the actual price may be higher as the price of electricity increases during periods of high demand.

Environmental considerations make the figures even more attractive. Typical geothermal power plants in New Zealand are considered to have 75% lower CO_2 emissions than a standard combined cycle power plant and 90% lower emissions than pulverized coal fired power plant [96]. A standard gas fired combined cycle power plant is reported to have a total global warming potential (GWP) of 474 g-CO_2 equivalent/kWh [97]. That means simply improving the plant performance by incorporating the evaporative cooling system for the Mokai 1 binary units could eliminate 1302 tonnes of CO_2 emissions from gas fired combined cycle or 3906 tonnes of CO_2 from coal fired steam turbine power plant over a year.

The cost of evaporative cooling could be rather high if a modern cooling tower was installed with a cooling water circuit to a heat exchanger substituted for the air-cooled condensers. However, the cost could be quite low if a simple design deploying water misters at the inlet of the existing air-cooled condenser was used. This kind of a system could be turned on or off according to the weather forecast. Of course, the cooling achieved would be a lower percentage of the wet bulb temperature with such a simple system.

9.3.2 Comparison to other renewable energy investments

In the Mokai 1 binary units, the air cooled condenser systems use induced draft heat exchangers, in which the working fluid (pentane) is condensed while flowing in the tubes as the air flows outside of the finned tubes in a cross flow pattern (discussed in chapter 5). If a simple water spray system was added at the air inlet of the condenser,

evaporative cooling effect could be achieved at low cost. However, constant moisture on the condenser fins would contribute to corrosion.

With a simple modification, fibreglass cooling towers could be installed under the existing condensers. Here, the purpose of the cooling tower would not be to cool water but to cool the incoming air by evaporative cooling and prevent water from coming in direct contact with the existing condenser. A schematic of the proposed modification is illustrated in Figure 9-6. A typical fibreglass tower would cost about USD $1800 [98] each for a small tower of 1.3 m x 1 m (height x diameter). There are total 180 fans attached to the condensers. Therefore, the total cost for the summer evaporative improvement would be approximately USD $0.4 million, assuming 50% shipping and installation cost, the total cost will be USD $0.6 million. This investment would provide summer peak generation capacity of around 590 kW, USD $1017/kW. This cost is much less than the usual USD $2000/kW to USD $3000/kW [96] needed to build a new geothermal power plant. The investment cost calculated based on the average annual gain is USD $1305/kW, still lower than the typical installation cost of a new plant.

Solar photo-voltaic cells, installed in the North Island on the site of high summer air conditioning use would be effective at meeting peak demand. Some solar PV technologies are reported to have efficiency as high as 27% [99], However, commercially available PV cells normally have efficiency of 8-10%. If we assume 10% efficiency and assume New Zealand average annual solar radiation of 1566 kWh/m^2, the gain achieved from incorporating water augmented cooling to the Mokai 1 binary cycle units is equivalent to 23147 m^2 of PV collector area. PV cells cost roughly USD $5000 to $10,000 /kW [99]. If we assume USD $5,000/kW and 25% service factor for PV, the equivalent service from incorporating water augmented cooling to the Mokai 1 binary cycle units would cost approximately USD 9.2 million.

In New Zealand, many power companies offer a night control for hot water heating at a lower rate. Thus, the demand for electric water heating is highest in the off-peak times. However, it is illustrative to compare the return on investment between installation of residential solar hot water systems and water cooling towers at a geothermal power plant. An experimental investigation by Western and Benseman

[100] shows that a typical household solar thermal system saves 37.5 kWh per 25 kWh/m^2 of solar radiation over a theoretical six day period with annual mean solar radiation of 1566 kWh/m^2 in a particular location in New Zealand. Introducing an evaporative cooling system to the Mokai 1 binary cycle units would roughly serve as equivalent to 1549 m^2 collector area of solar thermal systems annually.

Western and Benseman [100] found that a typical household with three family members consumes 3985 kWh in water heating in New Zealand. With the estimated improvement in the Mokai 1 plant, 910 households can meet their hot water demand from the increased geothermal generation annually. Of course from the exergy conservation point of view, it is not advisable to heat water with electricity, although in New Zealand, most of the household use electricity for their hot water need. Low population density might have contributed to this trend.

Wind energy is of high interest in New Zealand at the present time. The government has provided carbon credit subsidies for the current wind farm developments. Wind is not considered to be a peak-demand power source, as the scheduled delivery is problematic. There is no way to accurately estimate how often high wind conditions would coincide with summer peak loads. Over the course of a year, assuming a typical wind utilisation factor of 20%, the cooling installation would produce the same amount of power as a 2.4 MW wind turbine. The typical wind turbines are quoted between USD $1000-2000/kW. The cost of water augmented cooling of USD $1305/kW based on annual average improvement is at the lower end of wind turbine cost. In New Zealand there also trends to be local resistance to the landscape changes that accompany wind farm developments.

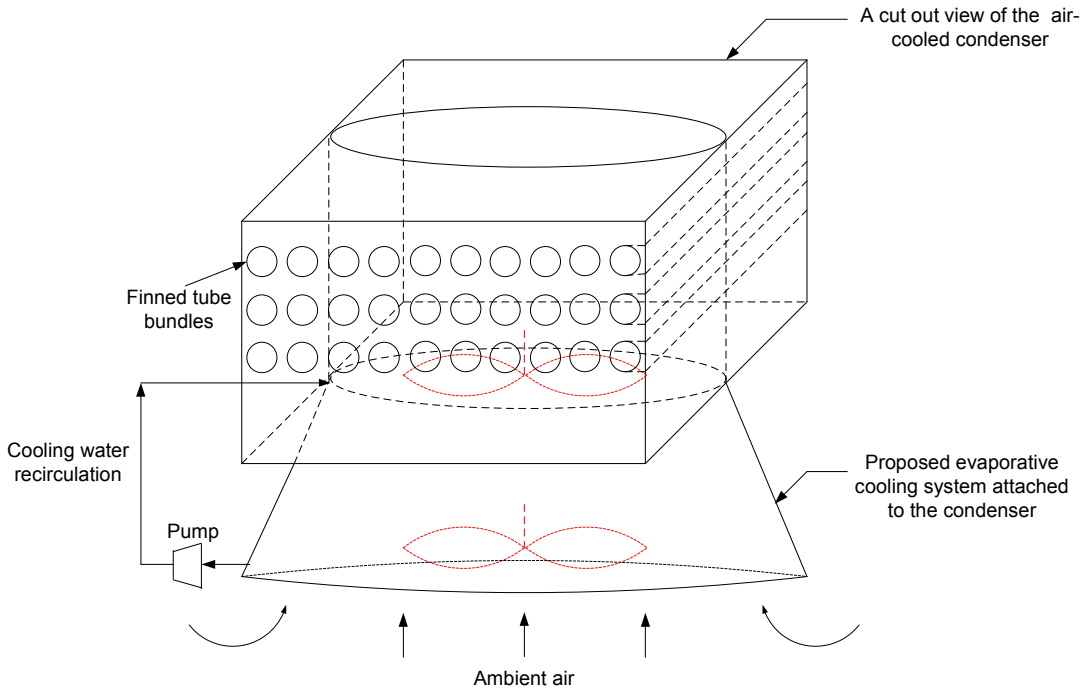

Figure 9-6: Schematic of proposed water-augmented air-cooled system for the Mokai 1 geothermal ORC

9.4 Optimization of plant performance

One of the major purposes of the modelling of binary cycles is the optimization. Optimization can be achieved in the context of efficiency, cost, maximum output and so on. From a mathematical point of view, optimization is the minimization or maximization of a function subject to a set of constraints on its variables [61]. The mathematical formulation of an optimization problem generally has the following form:

Minimization of an objective function $f(x)$

$$\text{subject to, } h(x) = 0$$

$$g(x) \leq 0$$

where, x is the vector of a set of continuous real variables; $h(x) = 0$ and $g(x) \leq 0$ are sets of equality and inequality constraints, respectively.

If an optimization problem is to maximize rather than minimize f, then we can easily accommodate this change by minimizing $-f$ in the formulation.

As a binary cycle geothermal power plant uses low enthalpy sources, a large heat transfer area is required. Moreover, binary cycles very often use air-cooled condensers. Therefore, the prime cost associated with such plants is the cost of heat transfer devices [50, 101]. The objective function associated with it for minimization is:

$$f(x) = \frac{A}{W_{OUT}} \tag{9.3}$$

where, A is the total heat transfer area used in the geothermal power plant.

A geothermal plant can produce the most power but may not run at the highest efficiency and vice versa. Since, geothermal energy is renewable, it is therefore, less important to run a plant at the highest thermal efficiency but it is very important to utilize the geothermal resources in sustainable way. The specific power output of a plant with respect to the geothermal fluid flow rate is of more interest [60]. The objective function for maximization is:

$$f(x) = \frac{W_{OUT}}{\dot{m}} \tag{9.4}$$

where, W_{OUT} is the power output of the plant and $\dot{m}$ is the geothermal fluid flow rate. The constraints of this objective function can be the pinch point, the limit on the maximum geothermal fluid flow rate, specified cooling water temperature etc.

Equation (9.4) necessarily represents a resource optimization. However, ORC geothermal power plants are characterised by its environment, resource and weather conditions. Therefore, an optimization effort must incorporate weather effect in the analysis. Recalling the energy balance around turbine-generator

$$\eta_T \dot{m}_{cycle}(h_3 - h_4) = P_{el} \tag{9.5}$$

The objective function is to maximize P_{el}.

For a given period of time η_T varies less significantly, therefore, it can be assumed constant. This leaves P_{el} as a function of $\dot{m}_{cycle}$ and $(h_3 - h_4)$ only. $\dot{m}_{cycle}$ is dependent on geothermal fluid flow rate and imposed constrains such the condenser

heat load. $(h_3 - h_4)$ is dependent on vaporizer and condenser conditions which are dependent on both geothermal fluid flow rate and ambient air temperature. Therefore optimization of the air-cooled ORC geothermal power plant performance for maximum power output is complex.

Figure 9-7 represents simulated electric power output of OEC 11 as a function of steam flow rate at different vaporizer working pressures. The ambient temperature is kept constant at 15°C and working fluid mass flow rate is kept constant at 100 kg/s. Figure 9-8 represents electric power output of OEC 11 as a function of working fluid flow rate at different ambient temperatures under constant geothermal fluid mass flow rate of 25 kg/s and vaporizer working pressure of 5.5 bar. Curves in Figure 9-7 and under red line of Figure 9-8 (power output constrained by turbine operating limit) represent influence of different parameters on plant performance. The cycle mass flow rate is a strong function of the geothermal fluid mass flow rate. The condenser operating pressure is a strong function of the ambient temperature. Therefore, combination of these two sets of curves (Figure 9-7 and under red line of Figure 9-8) i.e. simultaneous change in geothermal fluid flow rate and change in ambient temperature might have an optimum operating point or a range of optimum operating points. Due to the two independent parameters, ambient air temperature and geothermal fluid flow rate, and various constrains imposed to the system, the optimization problem may become highly nonlinear and may involve in discontinuities.

Algorithms for function optimization are generally limited to convex regular functions. However, many functions are multi-modal, discontinuous, and nondifferentiable. Traditional search techniques (such the simplex method [102]) use characteristics of the problem to determine the next sampling point (e.g., gradients, Hessians, linearity, and continuity) limiting their applications. Stochastic search techniques such as the Genetic Algorithm (GA) make no such assumptions. Instead, the next sampled point(s) is (are) determined based on stochastic sampling/decision rules. Therefore GA is suitable for difficult problems with the objective functions that do not possess “nice” properties such as continuity, differentiability, satisfaction of the Lipschitz Condition [103-105].

Genetic algorithms search the solution space of a function through the use of simulated evolution, i.e., the survival of the fittest strategy. In general, the fittest individuals of any population tend to reproduce and survive to the next generation, thus improving successive generations. However, inferior individuals can, by chance, survive and also reproduce. Genetic algorithms have been shown to solve linear and non linear problems by exploring all regions of the state space and exponentially exploiting promising areas through mutation, crossover, and selection operations applied to individuals in the population [105]. Owing to the powerful capabilities discussed above, GA has been used as the optimization tool for this analysis. The freeware Matlab [88] interface "Genetic Algorithm Optimization Toolbox (GAOT)" written by Houck et al. [103] has been used and it is available at [106].

For demonstration of optimization, OEC 11 model presented in chapter 8 has been used as it is the simpler among the two types of ORCs used in Mokai 1 geothermal power plant. There are two assumptions made in chapter 8: mass flow rate of working fluid in the cycle and vaporizer specific volume are constant. However, these assumptions have been omitted here as the central idea of optimization is to maximize power output. Changing cycle mass flow rate may result in improved performance. Controlling the vaporizer pentane level i.e. the vaporizer specific volume results in loss in potential work, the vaporizer is assumed to have only the physical constrains. Therefore, the Equation (8.5) reduces to

$$\dot{m}_{cycle}(h_3 - h_2) = \dot{Q}_{23} \tag{9.6}$$

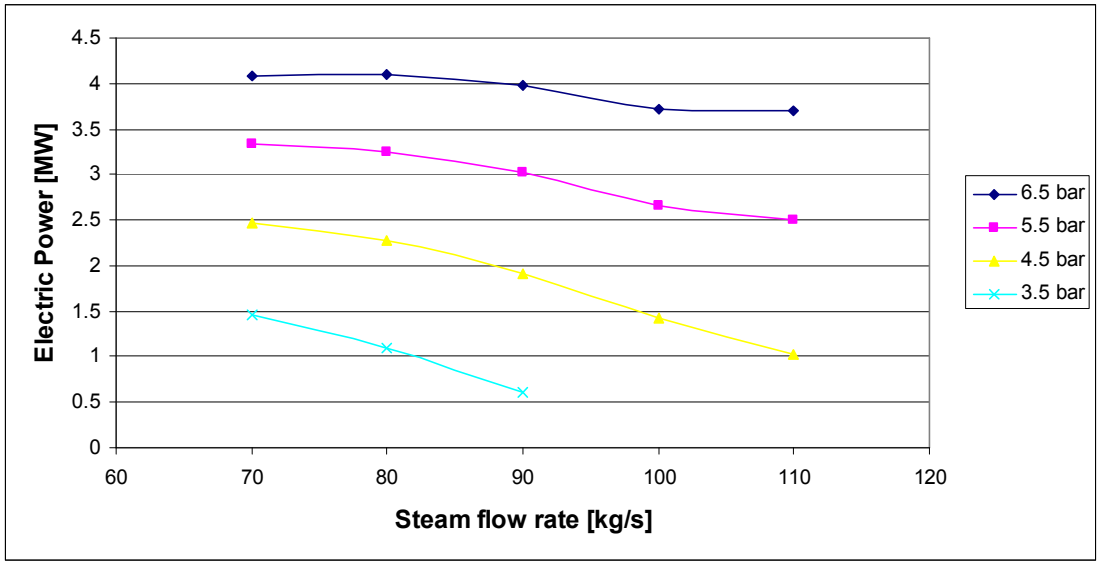

Figure 9-7: Electric power output of OEC 11 as a function of steam flow rate vaporizer working pressure under constant temperature of 15°C working fluid mass flow rate of 100 kg/s.

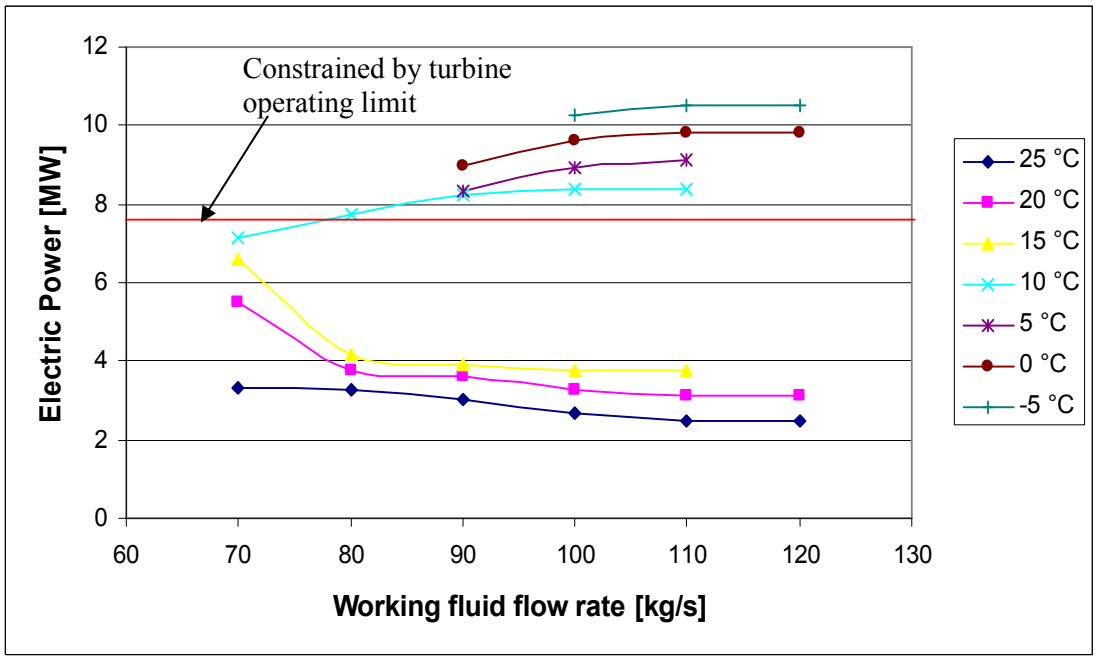

Figure 9-8: Electric power output of OEC 11 as a function of working fluid flow rate ambient temperature under constant geothermal fluid mass flow rate of 25 kg/s and vaporizer working pressure of 5.5 bar

For OEC 11, the pressure loss in the condenser assumed to be constant and assigned to the value of original design of 0.1 bar i.e.

$$p_4 = p_1 + 0.1 \tag{9.7}$$

The condenser equilibrium condition is determined using the iterative method presented in chapter 8. Equations (9.5)-(9.7) are solved for OEC 11 with an objective to maximize "P_{el}" under the following constrains:

$$\dot{m}_{cycle} <= \frac{\dot{Q}_{41}}{(h_1 - h_4)} \tag{9.8}$$

$$4bar <= p_3 <= 6bar \tag{9.9}$$

$$60\ kg/s <= \dot{m}_{cycle} <= 120\ kg/s \tag{9.10}$$

The Matlab code for operating point parameters optimization is available in appendix 9.

9.5 Results and discussion on plant performance optimization

For each set of ambient temperature and geothermal fluid flow rate, a set of optimized vaporizer pressure, cycle mass flow rate and power output is obtained. To demonstrate accuracy of the results, the optimized values of vaporizer pressure and cycle mass flow rate are taken as the guessed values of simplex method and an optimization was carried out. Matlab [88] function "fminsearch" was used for the demonstration of optimization using simplex method [102]. Table 9.1 shows the results. It is evident that GA optimized the plant performance with equivalent results that could be obtained from simplex method if an appropriate initial conditions were provided (here the optimized values of GA are used as the initial guessed values for simplex method). In few cases the simplex method failed to converge, even using outputs of GA. From this discussion it is evident that the GA can be used to optimize the plant performance that would provide results equivalent to the traditional methods if solution is obtainable by a traditional method.

Figure 9-9 shows the results of optimization of OEC 11 unit for a day operation. In Figure 9-9, power output increased for the same resource and ambient temperature by manipulating the vaporizer working pressure and working fluid flow rate, as high as, 50% improvement in power is possible to achieve by the optimization. Therefore, real time (hourly) optimization requires further investigations.

Using the same optimization technique two figures are created. Figure 9-10 and 9-11 present optimum working fluid flow rate and optimum vaporizer working pressure

under different geothermal fluid flow rates and ambient temperatures. A high degree of nonlinearity is observed from the optimized solutions. These two figures can be used in practical operation of the power plant. In OEC 11 however, there is no provision for controlling mass flow rate. The vaporizer working pressure can be manipulated and the working fluid mass flow rate can only be increased or decreased using vaporizer inlet valve and turbine bypass valve but no provision is available to measure the actual mass flow rate. If a new system is design that allows controlling working fluid flow rate, the discussed optimization technique can be used with vary simple adaptation. Figure 9-12 schematically presents proposed control system of operating point optimization of an ORC.

Table 9.1: Results of optimization of model of the OEC 11 under 21.7 kg/s steam flow rate

T_{amb}	Genetic Algorithm			Simplex method		
	$\dot{m}_{cycle}$	p_4	P_{el}	$\dot{m}_{cycle}$	p_4	P_{el}
[°C]	[kg/s]	[bar]	[MW]	[kg/s]	[bar]	[MW]
-5	96.168	5.588	7.5	96.168	5.588	7.5
0	96.785	5.360	7.5	96.785	5.360	7.5
5	91.702	5.337	7.5	91.702	5.337	7.5
10	95.995	5.654	7.5	91.702	5.337	7.5
15	84.365	5.884	6.847	Does not converge		
20	70.231	5.343	5.115	Does not converge		
25	76.331	5.973	3.537	Does not converge		

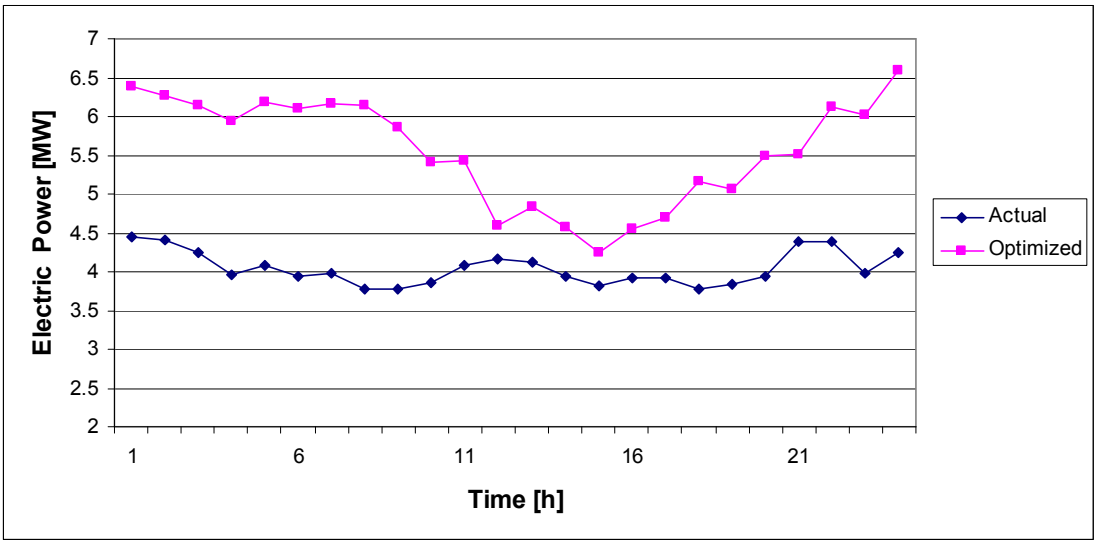

Figure 9-9: Optimized vs actual power output of a day of OEC 11

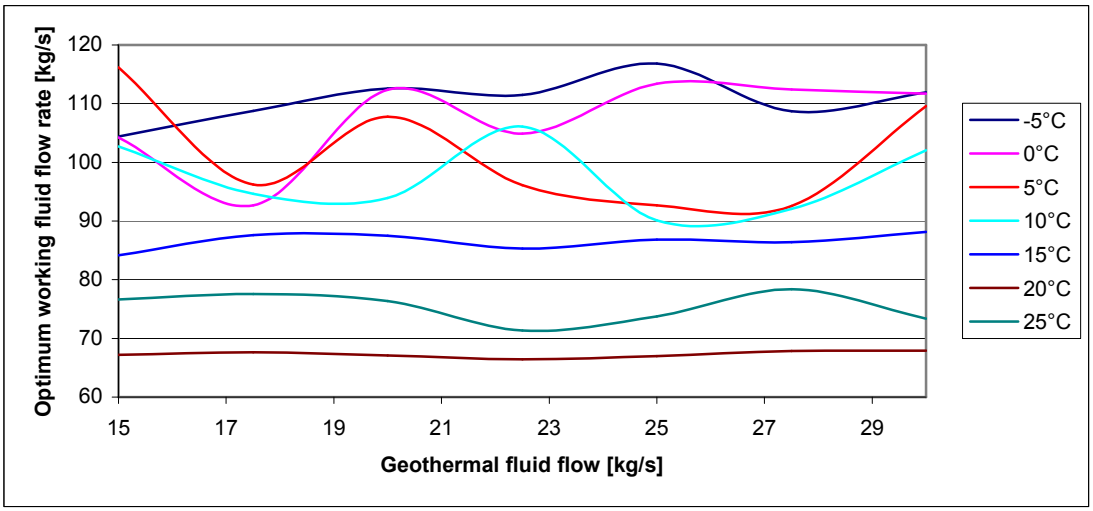

Figure 9-10: Optimized working fluid flow rate under each set of geothermal fluid flow rate and ambient temperature of OEC 11

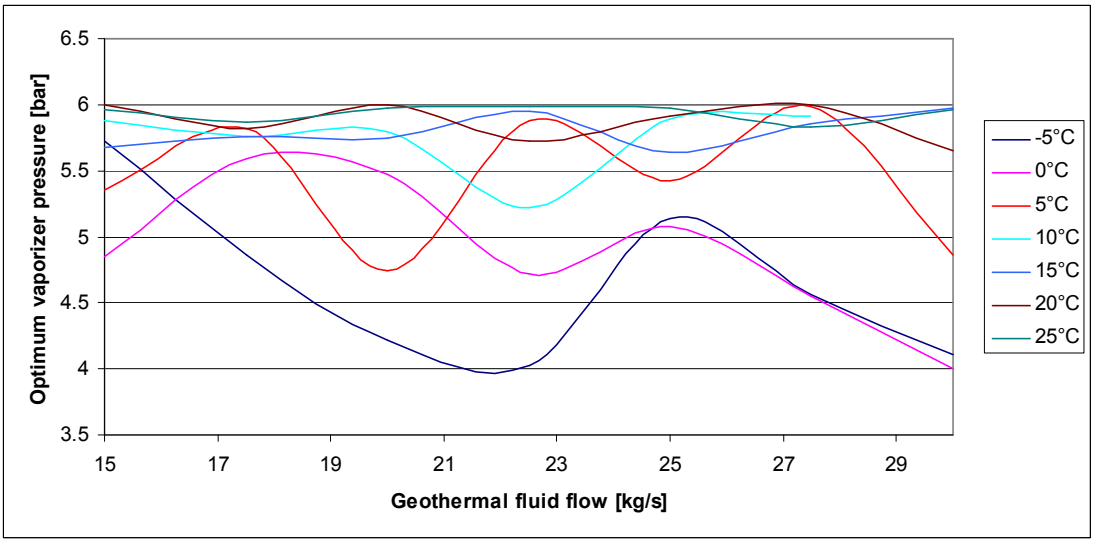

Figure 9-11: Optimized vaporizer working pressure under each set of geothermal fluid flow rate and ambient temperature OEC 11

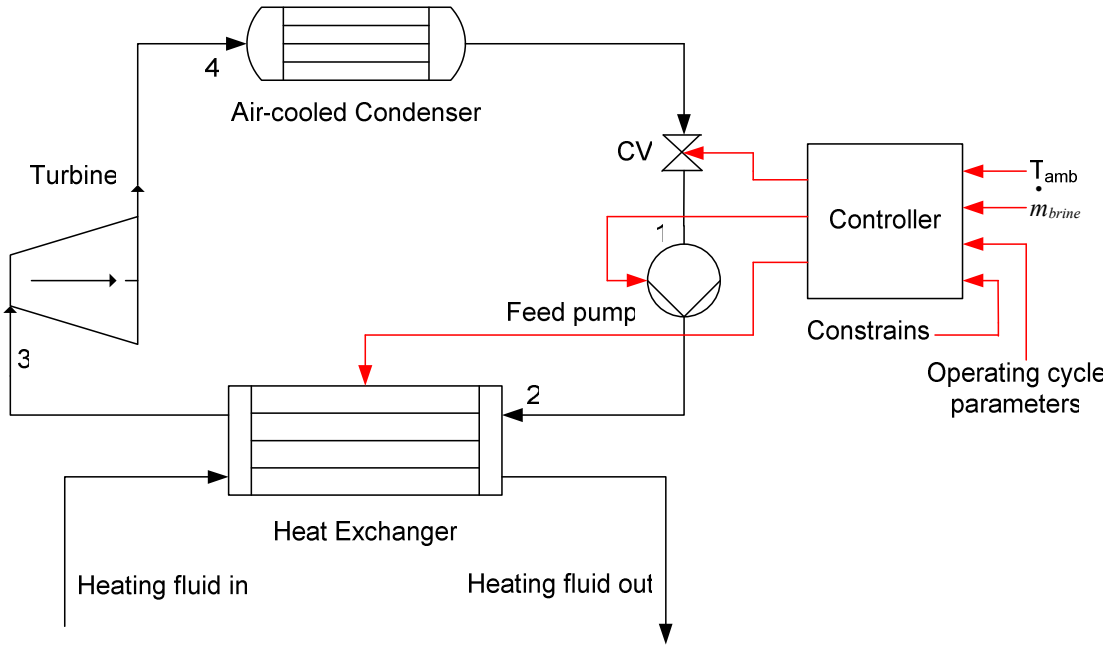

Figure 9-12: Schematic of the proposed control system for short term performance improvement by operating point optimization

9.6 Summary

Water-augmented cooling system is proposed as an option to mitigate the reduced power output during the summer. The simulated average gain in power of an ORC during the summer (Jan, Feb, Nov and Dec) by incorporating a water-augmented cooling system is found 2.3% and the average gain for the whole year is found 1.6% based on the weather data of Taupo for the year 2005. A cost benefit analysis showed that water-augmented cooling system is more economical compared to other alternative renewable energies considered to meet summer peak demand. From the green house gas emissions perspective, water-augmented cooling is better option than the gas fired peaking plants.

This chapter has also presented plant performance optimization of ORC geothermal power plant that takes into account both ambient temperature and geothermal fluid flow rate. Traditional optimization techniques are found to be not very suitable for the optimization problem presented in this chapter. Genetic Algorithm (GA) is used as the optimization tool. GA is a stochastic search technique that uses simulated evolution, i.e., the survival of the fittest strategy. In general, the fittest individuals of any population tend to reproduce and survive to the next generation, thus improving

successive generations. However, inferior individuals can, by chance, survive and also reproduce.

One of the ORC units of Mokai 1 geothermal power plant has been used as a case study. The results of optimization show that the power output can be increased using such optimization techniques by manipulating working fluid flow rate and vaporizer equilibrium pressure, as high as, 50% improvement in power is possible to achieve by the optimization. It was found that only 1-2% improvement by water-augmented cooling translates in to large benefit, a huge potential improvement (50%) by operating point parameters optimization therefore requires further investigations.

Chapter 10

Conclusion and Future Work

This dissertation has presented the basics of geothermal power generation, the current research and the relevance for this work. Often, the geothermal resources deviate from the time of commissioning of a plant. Therefore, a plant should adapt its design to continue its operation. This thesis proposed a methodology to address the problem of resource characteristics change.

The low temperature geothermal source for power generation was the focus of this investigation. The binary cycle power plant is used to generate electricity from the low temperature geothermal sources. Typically, these plants use air-cooled condensers and their performance deteriorates in the summer. This work analyses the effect of environment on binary cycle geothermal power plant. A decade old geothermal power plant, Mokai 1 in Taupo, New Zealand, was taken as a case study.

The following conclusions and recommendations for future work can be drawn from this study:

Conclusions

- A steady state model for the Mokai 1 geothermal power plant has been developed and compared with the design data. In the absence of information about some parameters, the iterative method has been used. It was found that the steady state model is competent and generates data that are within 5% of the design.
- Geothermal power plants are very site specific and the resource characteristics of a field tend to change significantly over time. An adaptive approach has evolved during the course of the investigation, which may save money and effort in the future by having provision to adapt to changes in resource characteristics based on geothermal reservoir modelling. This investigation was carried out using the developed steady state model.

- This work has presented a new method for modelling the environmental effect on closed organic Rankine cycle. This is the major contribution of this work. The ambient temperature affects the condenser performance. Hence, it influences the performance of the whole cycle in two ways. Firstly, by changing the equilibrium pressure inside the condenser which results in change in turbine outlet pressure that leads to change in turbine pressure ratio. The turbine pressure ratio is a major parameter determining power generated by a turbine; therefore, the plant output is affected. Secondly, by changing the condenser outlet temperature with the ambient temperature, the pump inlet and outlet conditions are changed and consequently vaporizer equilibrium temperature and pressure are influenced. However, these two effects are in opposite direction with first one being the prominent in the overall plant performance.
- The developed method is found to be very robust and converge exponentially.
- The model showed effectiveness in both cycles: saturated vapour (OEC 11) and superheated vapour (OEC 1).
- The model is effective even for modelling hourly operation of the units with appropriate initial conditions and constraints.
- The main interest of this research is on ORC but the developed method can be applied to any Rankine cycle of closed type.
- Water-augmented cooling system is proposed as an option to mitigate the reduced power output during the summer. The simulated average gain in power of an ORC during the summer by incorporating a water-augmented cooling system is found 2.3% and the average gain for the whole year is found 1.6% based on the weather data of Taupo for the year 2005.
- A cost benefit analysis showed that water-augmented cooling system is more economical compared to other alternative renewable energies considered to meet summer peak demand. From the green house gas emissions perspective, water-augmented cooling is better option than the gas fired peaking plants.
- An optimization was carried out that takes into account environmental effect (both local weather condition and geothermal resource characteristics). The analysis showed that manipulating operating parameters (i.e. pressure,

temperature, mass flow rate), the plant performance can be optimized under different weather conditions and resource characteristics.

- This work has developed a base for further developments in plant design and operation. As the models developed here are very generic, they can be used easily in new plant design through simple adaptation.
- Plant operators can use the developed iterative method to predict the plant performance of a binary cycle, which will ensure more accurate dispatch.

Future work

- A thorough cost benefit analysis is necessary to find out the effectiveness of the adaptive design approach for long term performance improvements.
- Further study is necessary to find out the effect of scale deposition on the vaporizer in the long term.
- Further study of hourly operating point parameters optimization including experimental study has been identified as an important area of investigation.

Nomenclature

A	area (m^2)
cp	specific heat at constant pressure (kJ K^{-1} kg^{-1})
d	diameter (m)
e	relative error (-)
e	specific exergy (kJ kg^{-1})
h	specific enthalpy (kJ kg^{-1})
h	convective heat transfer coefficient (kW $m^{-2}K^{-1}$)
k_1	proportionality constant (-)
k_2	proportionality constant (-)
k	conductivity (kW $m^{-1}K^{-1}$)
$\dot{m}$	mass flow rate (kg s^{-1})
p	pressure (bar)
P_{el}	electric power (MW)
Q	heat transfer (MJ)
$\dot{Q}$	heat transfer rate (MW)
s	specific entropy (kJ K^{-1} kg^{-1})
T	temperature (ºC)
u	specific internal energy (kJ kg^{-1})
u	velocity (m s^{-1})
U	overall heat transfer coefficient (kW m^{-2} K^{-1})
v	specific volume (m^3 kg^{-1})
v_{air}	velocity of air (m s^{-1})
$\dot{V}$	volumetic flow rate (m^3 s^{-1})

W	work done (MJ)
$\dot{W}$	work rate or power (MW)
x	quality (-)

Subscript

amb	ambient
BR	brine
BRN	brine
BOT	bottoming
con	condenser
geo	geothermal
H	high
L	low
in	input
i	inside
o	outside
PN	pentane
r	reference
s	isentropic
ST	steam
SN	sink
SR	source
T	turbine
1-4	states

Greek letters

η	efficiency (-)
ε	heat exchanger effectiveness (-)
ρ	density (kg m^{-3})
μ	viscosity (Pa s)

References

1 **Dantas, A., Krumdieck, S. and Page, S.** Energy Risk to Activity Systems as a Function of Urban Form. In NZ, L.T., ed (Land Transport New Zealand, PO Box 2840, Waterloo Quay, Wellington, New Zealand, 2007).

2 **Campbell, C.J.** *The Dawn of the Second Half of the Age of oil, Kinsale 2021, An Energy Descent Action Plan – Version.1*. 2005).

3 **D. Meadows, J.R., D. Meadows** *Limits to Growth, The 30-Years Update*. 2004).

4 **UN**. United Nations, Our Common Future, report from the world Commission on Environment and Development. (Oxford: Oxford University Press, 1987).

5 **UNFCCC**. The United Nations Framework Convention on Climate Change. Available at: http://unfccc.int/essential_background/items/2877.php. 1994.

6 **UNFCCC**. The United Nations Framework Convention on Climate Change. Available at: http://unfccc.int/resource/docs/convkp/kpeng.html. 2005.

7 **Barbier, E.** Geothermal energy technology and current status: an overview. *Renewable and Sustainable Energy Reviews*, 2002, **6**(1-2), 3-65.

8 **EECA**. The Energy Efficiency and Conservation Authority, New Zealand: Renewable Energy -Industry Status Report 2006.

9 **NZGA**. http://www.nzgeothermal.org.nz/geothermal_energy/geothermal_benefits.asp. 2008.

10 **MED**. Ministry of Economic Development, New Zealand: Energy Data File. 2009.

11 **Kutscher, C.F.** The Status and Future of Geothermal Electric Power. *American Solar Energy Society, Madison, Wisconsin*, 2000.

12 **DiPippo, R.** *Gothermal Power Plants: Principles, Applications and Case Studies*. (Elsevier Ltd., 2005).

13 **Berkeley, U.** http://www.ucmp.berkeley.edu/history/wegener.html. 2008.

14 **MIT**. The future of geothermal energy- Impact of Enhanced Geothermal Systems (EGS) on the United States in the 21st century. (Massachusetts Institute of Technology, 2006).

15 **Etemoglu, A.B. and Can, M.** Classification of geothermal resources in Turkey by exergy analysis. *Renewable and Sustainable Energy Reviews*, 2007, **11**(7), 1596-1606.

16 **IEA**. *World Energy Outlook*. (International Energy Agency, 2008).

17 **DiPippo, R.** Second Law assessment of binary plants generating power from low-temperature geothermal fluids. *Geothermics*, 2004, **33**(5), 565-586.

18 **Weng, C.-K., Ray, A. and Xiaowen, D.** Modelling of power plant dynamics and uncertainties for robust control synthesis. *Applied Mathematical Modelling*, 1996, **20**(7), 501-512.

19 **Quoilin, S., Lemort, V. and Lebrun, J.** Experimental study and modeling of an Organic Rankine Cycle using scroll expander. *Applied Energy*, 2009, **xxx**, xxx-xxx.

20 **Weng, C.K., Edwards, R.M. and Ray, A.** ROBUST WIDE-RANGE CONTROL OF NUCLEAR-REACTORS BY USING THE FEEDFORWARD-FEEDBACK CONCEPT. *Nuclear Science and Engineering*, 1994, **117**(3), 177-185.

21 **Pampin, R., Karditsas, P.J., Loughlin, M.J. and Taylor, N.P.** PPCS thermal analysis of bounding accident scenarios using improved computational modelling. *Fusion Engineering and Design*, 2006, **81**(18), 2127-2142.

22 Wang, J.-R., Lin, H.-T., Cheng, Y.-H. and Shih, C. TRACE modeling and its verification using Maanshan PWR start-up tests. *Annals of Nuclear Energy*, 2009(36), 527–536.
23 Kaliatka, A., Uspuras, E. and Vaisnoras, M. Analysis of BDBA in RBMK-1500 reactor with long-term loss of heat removal from the core. *Annals of Nuclear Energy*, 2008, **35**(12), 2219-2233.
24 Gay, R.R., Palmer, C.A. and Erbes, M.R. *Power plant performance monitoring*. (R-Squared Publishing, 2004).
25 Li, K.W. and Priddy, A.P. *Power plant system design*. (John Wiley & Sons. Inc., 1985).
26 Ghaffari, A., Chaibakhsh, A. and Lucas, C. Soft computing approach for modeling power plant with a once-through boiler. *Engineering Applications of Artificial Intelligence*, 2007, **20**(6), 809-819.
27 Smrekar, J., M.Assadi, M.Fast, I.Kusˇtrin and S.De. Development of artificial neural network model for a coal-fired boiler using real plant data *Energy*, 2009, **34**, 144-152.
28 Korakianitis, T., Grantstrom, J., Wassingbo, P. and Massardo, A.F. Parametric performance of combined-cogeneration power plants with various power and efficiency enhancements. *Journal of Engineering for Gas Turbines and Power*, 2005, **127**(1), 65-72.
29 Szargut, J., Morris, D.R. and Steward, F.R. *Exergy analysis of thermal, chemical, and metallurgical processes*. (Hemisphere publishing corporation, 1988).
30 Bejan, A. *Advanced Engineering Thermodynamics*. (John Wiley & Sons, Inc., 1997).
31 Bejan, A., Tsatsaronis, G. and Moran, M. *Thermal Design & Optimization*. (John Wiley & Sons, Inc., 1996).
32 El-Masri, M.A. Exergy Analysis of Combined Cycles: Part 1—Air Cooled Brayton Cycle Gas Turbines. *Transactions of the ASME*, 1987, **109**, 228–235.
33 Chin, W.W. and El-Masri, M.A. Exergy Analysis of Combined Cycles: Part 2—Analysis and Optimization of Two-Pressure Steam Bottoming Cycles. *Journal of Engineering for Gas Turbines and Power*, 1987, **109**, 237–243.
34 Erdem, H.H. and Sevilgen, S.H. Case study: Effect of ambient temperature on the electricity production and fuel consumption of a simple cycle gas turbine in Turkey. *Applied Thermal Engineering*, 2006, **26**(2-3), 320-326.
35 Dawoud, B., Zurigat, Y.H. and Bortmany, J. Thermodynamic assessment of power requirements and impact of different gas-turbine inlet air cooling techniques at two different locations in Oman. *Applied Thermal Engineering*, 2005, **25**(11-12), 1579-1598.
36 Chuang, C.-C. and Sue, D.-C. Performance effects of combined cycle power plant with variable condenser pressure and loading. *Energy*, 2005, **30**(10), 1793-1801.
37 Durmayaz, A. and Sogut, O.S. Influence of cooling water temperature on the efficiency of a pressurized-water reactor nuclear-power plant. *International Journal of Energy Research*, 2006, **30**(10), 799-810.
38 Liu, P., Duan, H. and Zhao, W. Numerical investigation of hot air recirculation of air-cooled condensers at a large power plant. *Applied Thermal Engineering*, 2009(29), 1927–1934.
39 Casella, F. Modeling, Simulation, Control, and Optimization of a Geothermal Power Plant. *IEEE Transactions on Energy Conversion*, 2004, **19**, 170-178.
40 Ogriseck, S. Integration of Kalina cycle in a combined heat and power plant, a case study. *Applied Thermal Engineering*, 2009, **29**(14-15), 2843-2848.

41 **Lolos, P.A. and Rogdakis, E.D.** A Kalina power cycle driven by renewable energy sources. *Energy*, 2009, **34**(4), 457-464.
42 **Zamfirescu, C. and Dincer, I.** Thermodynamic analysis of a novel ammonia-water trilateral Rankine cycle. *Thermochimica Acta*, 2008, **477**(1-2), 7-15.
43 **Schuster, A., Karellas, S., Kakaras, E. and Spliethoff, H.** Energetic and economic investigation of Organic Rankine Cycle applications. *Applied Thermal Engineering*, 2009, **29**(8-9), 1809-1817.
44 **Wei, D., Lu, X., Lu, Z. and Gu, J.** Dynamic modeling and simulation of an Organic Rankine Cycle (ORC) system for waste heat recovery. *Applied Thermal Engineering*, 2008, **28**(10), 1216-1224.
45 **Bruno, J.C., Lopez-Villada, J., Letelier, E., Romera, S. and Coronas, A.** Modelling and optimisation of solar organic rankine cycle engines for reverse osmosis desalination. *Applied Thermal Engineering*, 2008, **28**(17-18), 2212-2226.
46 **Sohel, M.I., Sellier, M., Brackney, L.J. and Krumdieck, S.** Efficiency improvement for geothermal power generation to meet summer peak demand. *Energy Policy*, 2009, **37**(9), 3370-3376.
47 **Bombarda, P., Invernizzi, C.M. and Pietra, C.** Heat recovery from Diesel engines: A thermodynamic comparison between Kalina and ORC cycles. *Applied Thermal Engineering*, 2010, **30**(2-3), 212-219.
48 **Mlcak, H.A.** An introduction to the Kalina Cycle. *Joint Power Generation Conference* 1996, **30**, 765-776.
49 **Bombarda, P. and Gaia, M.** Geothermal Binary Plants Utilising an Innovative Non-Flammable Azeotropic Mixture as Working Fluid. *Proceedings 28th NZ Geothermal Workshop*, 2006, 6.
50 **Madhawa Hettiarachchi, H.D., Golubovic, M., Worek, W.M. and Ikegami, Y.** Optimum design criteria for an Organic Rankine cycle using low-temperature geothermal heat sources. *Energy*, 2007, **32**(9), 1698-1706.
51 **DiPippo, R.** Ideal thermal efficiency for geothermal binary plants. *Geothermics*, 2007, **36**(3), 276-285.
52 **Sohel, M.I., Sellier, M., Brackney, L.J. and Krumdieck, S.** An iterative method for modelling the air-cooled Organic Rankine Cycle geothermal power plant. *International Journal of Energy Research*, 2010.
53 **Bai, O., Nakamura, M., Ikegami, Y. and Uehara, H.** A Simulation Model for Hot Spring Thermal Energy Conversion Plant With Working Fluid of Binary Mixtures. *Journal of Engineering for Gas Turbines and Power*, 2004, **126**(3), 445-454.
54 **Wei, D., Lu, X., Lu, Z. and Gu, J.** Performance analysis and optimization of organic Rankine cycle (ORC) for waste heat recovery. *Energy Conversion and Management*, 2007, **48**, 1113–1119.
55 **DiPippo, R.** *Geothermal Power Plants: Principles, Applications and Case Studies*. (Elsevier Ltd., 2005).
56 **DiPippo, R.** The Effect of Ambient Temperature on Geothermal Binary-Plant Performance. *Geothermal hot line*, 1989, **19**, 68-70.
57 **RJVL**. ROTOKAWA GEOTHERMAL DEVELOPMENT Resource Consent Applications and Assessment of Environmental Effects. (Rotokawa Joint Venture Limited, C/- Mighty River Power Limited, 160 Peachgrove Road, PO Box 445, HAMILTON, New Zealand, 2007).
58 **Pritchard, G.** The must-run dispatch auction in an electricity market. *Energy Economics*, 2002, **24**(3), 199-216.

59 **Kutscher, C. and Costenaro, D.** Assessment of Evaporative Cooling Enhancement Methods for Air-Cooled Geothermal Power Plants. *Geothermal Resources Council (GRC) Annual Meeting September 22−25, 2002.*Reno, Nevada, 2002).
60 **Desideri, U. and Bidini, G.** Study of possible optimisation criteria for geothermal power plants. *Energy Conversion and Management*, 1997, **38**(15-17), 1681-1691.
61 **Lu, S. and Goswami, D.Y.** Optimization of a novel combined power/refrigeration thermodynamic cycle. *Journal of Solar Energy Engineering, Transactions of the ASME*, 2003, **125**(2), 212-217.
62 **Dai, Y., Wang, J. and Gao, L.** Parametric optimization and comparative study of organic Rankine cycle (ORC) for low grade waste heat recovery. *Energy Conversion and Management*, 2009, **50**, 576–582.
63 **Santamouris, M.J. and Lefas, C.C.** Design and control of hybrid solar houses using microcomputers. *Energy*, 1986, **11**(7), 709-716.
64 **Bakos, G.C.** Improved energy management method for auxiliary electrical energy saving in a passive-solar-heated residence. *Energy and Buildings*, 2002, **34**(7), 699-703.
65 **Ekren, O. and Kucuka, S.** Energy saving potential of chiller system with fuzzy logic control. *International Journal of Energy Research*, 2010, **34**, 897–906.
66 **Van Wylen, G., Sonntag, R. and Borgnakke, C.** *Fundamentals of Classical Thermodynamics*. (John Wiley & Sons, Inc., 1994).
67 **Eastop, T.D. and McConkey, A.** *Applied Thermodynamics for Enginnering Technologists*. (Longman Group UK Limited, 1993).
68 **Gu, Z. and Sato, H.** Optimization of cyclic parameters of a supercritical cycle for geothermal power generation. *Energy Conversion and Management*, 2001, **42**(12), 1409-1416.
69 **Gu, Z. and Sato, H.** Performance of supercritical cycles for geothermal binary design. *Energy Conversion and Management*, 2002, **43**(7), 961-971.
70 **REFPROP**. National Institute of Standards and Technology (NIST), http://www.nist.gov/. 2007).
71 **Google**. http://maps.google.co.nz/. 2009.
72 **NIWA**. http://cliflo.niwa.co.nz/. (National Institute of Weather and Atmospheric Research (NIWA), 2008).
73 **Holman, J.P.** *Heat Transfer*. (McGraw-Hill, 1992).
74 **Zukauskas, A.** Heat transfer from tubes in cross flow. *Adv. Heat Transfer*, 1972, **8**, 93-160.
75 **Mueller, A.C.** *Hand Book of Heat Exchanger Design*. (Begell House, Inc., 1992).
76 **Shaobo, H., Zhang, Z., Huang, Z. and Xie, A.** Performance optimization of solar multi-stage flash desalination process using Pinch technology. *Desalination*, 2008, **220**(1-3), 524-530.
77 **Jawahar, C.P., Raja, B. and Saravanan, R.** Thermodynamic Studies on NH3 - H2O Absorption Cooling System using Pinch Point Approach. *International Journal of Refrigeration*, 2010, **In Press, Accepted Manuscript**.
78 **Piccolo, C. and Bezzo, F.** A techno-economic comparison between two technologies for bioethanol production from lignocellulose. *Biomass and Bioenergy*, 2009, **33**(3), 478-491.
79 **Gnielinski, V.** New equations for heat and mass transfer in trubulent pipe channel flow. *Int. Chem. Eng.*, 1976, **16**, 359-368.

80 **Sohel, M.I., Sellier, M., Brackney, L.J. and Krumdieck, S.** Dynamic Modelling and Simulation of an Organic Rankine Cycle Unit of a Geothermal Power Plant. *Proceedings World Geothermal Congress 2010 Bali, Indonesia, 25-29 April 2010*, 2010.
81 **Nakaoka, T. and Uehara, H.** Performance test of a shell-and-plate type evaporator for OTEC. *Exper Therm Fluid Sci*, 1988, **1**(3), 283-291.
82 **Yildirim, G.G.a.N.** Effect of Non-Condensable Gases on geothermal power plant performance. Case study: Kizildere Geothermal Power Plant-Turkey. *Int. J. Exergy*, 2008, **5**(5/6), 684-695.
83 **Gokcen, E.D.Y.a.G.** Exergy analysis and performance evaluation of Kizildere Geothermal Power Plant, Turkey. *Int. J. Exergy*, 2004, **1**(3), 316-333.
84 **Casella, F.** PhD Thesis: Modelling, Simulation, and Control of a Geothermal Power Plant. *Dipartimento di Elettronica e Informazione* (POLITECNICO DI MILANO, MILANO, 1999).
85 **Zeigler, B.P., Praehofer, H. and Kim, T.G.** *Theory of Modeling and Simulation Interated Discrete Event and Continuous Complex Dynamic Systems*. (Academic Press, 2000).
86 **Ordys, A., Pike, A., Johnson, M., Katebi, R. and Grimble, M.** *Modelling and simulation of power generation plants*. (Springer-Verlg, 1994).
87 **PSE**. Process Systems Enterprise Ltd. http://www.psenterprise.com/. 2008.
88 **MathWorks**. www.mathworks.com. 2008.
89 **Automation, A.** http://www.andritzautomation.com. IDEAS.
90 **Thermoflow**. http://www.thermoflow.com.
91 **Jurado, F., Cano, A. and Carpio, J.** Enhancing the Distribution System Stability Using Micro-Turbines and Fuel Cells. *Proceedings of the IEEE Power Engineering Society Transmission and Distribution Conference*, pp. 717-7222003).
92 **Maybeck, P.S.** *Stochastic models, estimations, and control Volume 1*. (Academic press, 1979).
93 **KALMAN, R.E.** A New Approach to Linear Filtering and Prediction Problems. *Transactions of the ASME–Journal of Basic Engineering*, 1960, **82**, 35-45.
94 **Smrekar, J., Assadi, M., Fast, M., Kusˇtrin, I. and De, S.** Development of artificial neural network model for a coal-fired boiler using real plant data *Energy*, 2009, **34**, 144-152.
95 **MED**. Energy Data File. (Ministry of Economic Development (MED), New Zeland, http://www.med.govt.nz/energy/info/, 2007 a).
96 **EECA**. Renewable Energy -Industry Status Report (year ending March 2006). In The Energy Efficiency and Conservation Authority (ECCA), N.Z.G., http://www.eeca.govt.nz/ ed2006).
97 **Kannan, R., Leong, K.C., Osman, R., Ho, H.K. and Tso, C.P.** Gas fired combined cycle plant in Singapore: energy use, GWP and cost--a life cycle approach. *Energy Conversion and Management*, 2005, **46**(13-14), 2145-2157.
98 **LCS**. http://www.legacychillers.com/. (Lagacy Chillers Systems 2008).
99 **Solardyne**. http://www.solardyne.com/solarpvpanels.html. 2008.
100 **Western, B.E. and Benseman, R.F.** Testing domestic solar water heaters--The New Zealand experience. *Solar Energy*, 1985, **35**(6), 471-476.
101 **Uehara, H. and Ikegami, Y.** Optimization of a Closed-Cycle OTEC System. *Journal of Solar Energy Engineering*, 1990, **112**.
102 **LAGARIAS, J.C., REEDS, J.A., WRIGHT, M.H. and WRIGHT, P.E.** Convergence properties of the Nelder-Mead simplex method in low dimensions. *SIAM J. OPTIM.*, 1998, **9**(1), 112-147.

103 Houck, C.R., Jonies, J.A. and Kay, M.G. A genetic algorithm for function optimization: A Matlab implementation. *ACM Transactions on Mathematical Software*, 1996.
104 Goldberg, D.E. *Genetic Alogrithms in search, optimization and Machine Learning*. (Addision-Wesley Longman, Inc., 1989).
105 Michalewicz, Z. *Genetic Algorithms + Data Structures = Evolution Programs*. (Springer-Verlang, New York, 1994).
106 Houck, C.R., Jonies, J.A. and Kay, M.G.
http://www.ise.ncsu.edu/mirage/GAToolBox/gaot/. 2009.

Appendices

Appendix 1: Some pictures of the Mokai 1 geothermal power plant with the major components

Figure 1: The Mokai 1 geothermal power plant (air-cooled condenser bank)

Figure 2: A production well
of geothermal fields in Mokai

Figure 3: Steam separator and condensate
collector (partial at right)

Figure 4: Condensate collector and separator (right partial and full in Figure above)

Figure 5: Steam turbine

Figure 6: Main heat exchanger (vaporizer and separator) of a brine OEC

Figure 7: Turbines of bottoming OEC are connected to a common generator

Figure 8: Condenser at Mokai from the side

Appendix 2: Holman, J.P. *Heat Transfer*. (McGraw-Hill, 1992)

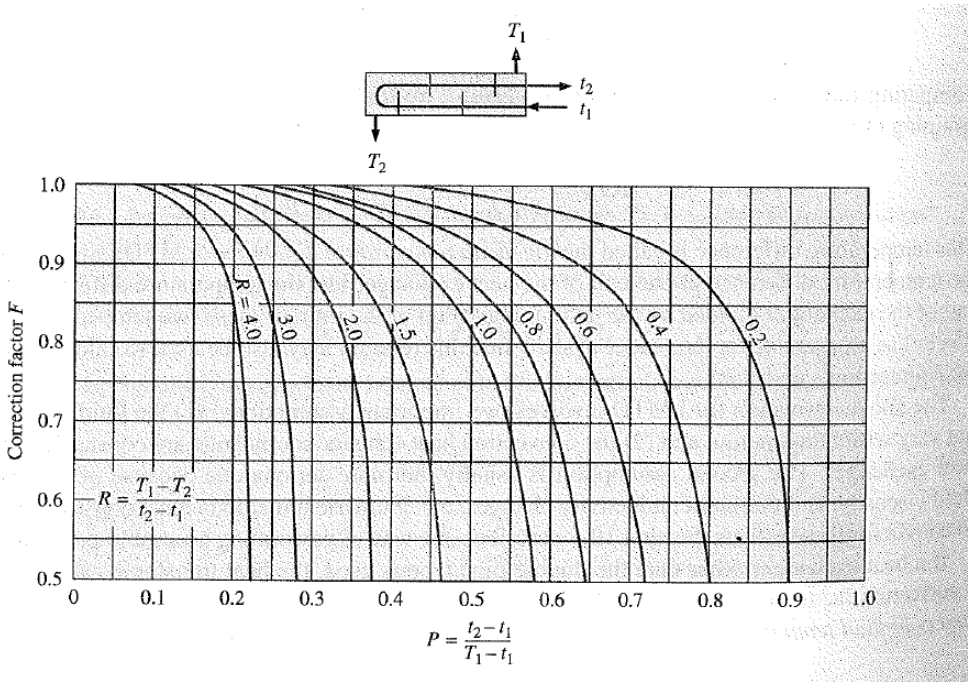

Appendix 3: Holman, J.P. Heat Transfer. (McGraw-Hill, 1992)

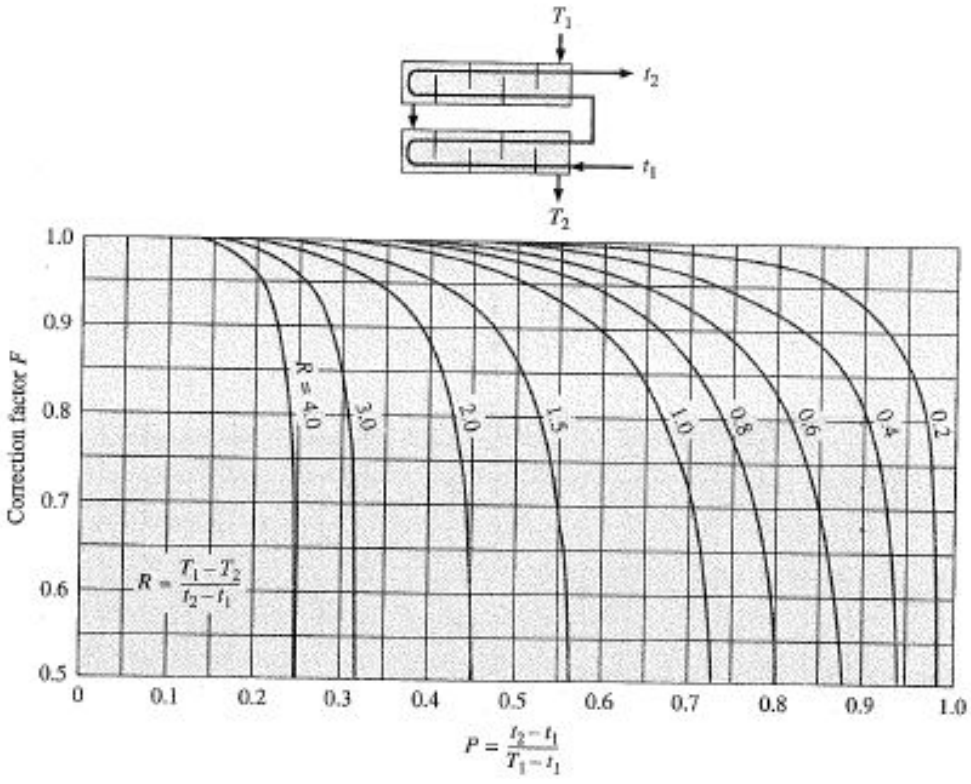

Appendix 4: In the limiting case where geothermal fluid mass flow rate changes less significantly, LMTD can be assumed unchanged with reasonable accuracy

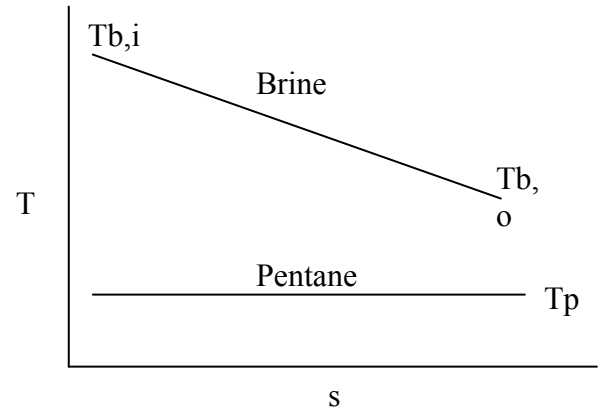

The Figure presented above shows hypothetical heat transfer process between geothermal fluid and working fluid (pentane). Design LMTD can be calculated from the following Equation:

$$\Delta T_m = \frac{T_{b,i} - T_{b,o}}{\ln \dfrac{T_{b,i} - T_p}{T_{b,o} - T_p}} \tag{1}$$

Now, design point heat transfer can written as:

$$\dot{Q}_r = \dot{m}_r \, c_P (T_{b,i} - T_{b,o}) \tag{2}$$

where, $\dot{Q}_r$ is the design heat transfer and $\dot{m}_r$ is the design geothermal fluid flow rate. The brine inlet temperature is controlled so $T_{b,i}$ can be assumed constant in Equation (2). The value of c_P does not change much also. Now, heat transfer for off design can be calculated from the following Equation:

$$\dot{Q} = \dot{m} c_P (T_{b,i} - T) \tag{3}$$

where, $\dot{Q}$ is the off design heat transfer, $\dot{m}$ is the off design geothermal fluid flow rate and T is the off design geothermal fluid outlet temperature. Here, $\dot{m}$ is an independent veriable.

From the empirical relation discussed in chapter 5 (Equation (5.51)):

$$\dot{Q} = \dot{Q}_r \cdot \sqrt{\frac{\dot{m}}{\dot{m}_r}} \tag{4}$$

Let's assume, $\frac{\dot{m}}{\dot{m}_r} = y$, so Equation (4) becomes:

$$\dot{Q} = \dot{Q}_r \cdot \sqrt{y} \tag{5}$$

From Equation (2), (3) and (5),

$$\dot{Q} = \dot{Q}_r \cdot \sqrt{y} = \dot{m}_r \, c_P (T_{b,i} - T_{b,o}) \cdot \sqrt{y} \tag{6}$$

$$\Rightarrow \dot{m} \, c_P (T_{b,i} - T) = \dot{m}_r \, c_P (T_{b,i} - T_{b,o}) \cdot \sqrt{y} \tag{7}$$

$$\Rightarrow \frac{\dot{m}}{\dot{m}_r} (T_{b,i} - T) = (T_{b,i} - T_{b,o}) \cdot \sqrt{y} \tag{8}$$

$$\Rightarrow y \cdot (T_{b,i} - T) = (T_{b,i} - T_{b,o}) \cdot \sqrt{y} \tag{9}$$

$$\Rightarrow T = T_{b,i} - \frac{T_{b,i} - T_{b,o}}{\sqrt{y}} \tag{10}$$

We know that in Mokai 1 geothermal power plant, the resource mass flow rate changes less significantly on yearly basis (Figure 5-19). Therefore, $y \to 1$. Let us say, $y = 1 + x$, where $|x| << 1$. Now, putting the value of y in Equation (10) we get:

$$T = T_{b,i} - \frac{T_{b,i} - T_{b,o}}{\sqrt{1+x}} \tag{11}$$

Now, we know that $(1+x)^n = 1 + \frac{nx}{1!} + \frac{n(n-1)x^2}{2!} + \cdots$

So, we can write neglecting the higher order terms,

$$T = T_{b,i} - \frac{T_{b,i} - T_{b,o}}{1 + \frac{1}{2}x} = f(x) \tag{12}$$

Now, taking lim both side of the above equation:

$$\lim_{x \to 0} f(x) = \lim_{x \to 0} T_{b,i} - \frac{T_{b,i} - T_{b,o}}{1 + \frac{1}{2}x} \tag{13}$$

$$\lim_{x \to 0} f(x) = T_{b,o} \tag{14}$$

which means in limiting case when, x is relatively small, brine outlet temperature varies less significantly. This leads to

$$\Delta T_m = \frac{T_{b,i} - T_{b,o}}{\ln \dfrac{T_{b,i} - T_p}{T_{b,o} - T_p}} \approx const. \qquad \text{when } |x| << 1 \qquad (15)$$

So, from the above analytical treatment we can conclude that for short period of operation of the ORCs of Mokai 1 geothermal power plant, where geothermal fluid flow rate changes less significantly, the LMTD value can be assumed constant.

Appendix 5: The Matlab functions code for the steady state model of the Mokai 1 geothermal power plant

GPentaneEnthalpy.m

```
function h   =property(pin,tin)
               tin=273.15+tin;%convert from c to k
               pin=101*pin;%convert from bar to kpa
               h=refpropm('H','T',tin,'P',pin,'pentane')/1000; %
entalpy

end
```

GPentaneTemperature.m

```
function T   =property(pin,hin)
               hin=hin*1000;%convert from c to k
               pin=101*pin;%convert from bar to kpa
               T=refpropm('T','P',pin,'H',hin,'pentane')-273.15; %
entalpy

end
```

GPentaneTurbineHV2.m

```
function hout =property(pin,tin,select,out_parameter_val,eta_s)
               tin=273.15+tin;%convert from c to k
               pin=101*pin;%convert from bar to kpa

              if (select == 1.0)
                   %disp(parameter);% display the control parameter
                   out_parameter_val=out_parameter_val*101;%convert
from bar to kpa
                   sin=refpropm('S','T',tin,'P',pin,'pentane'); %
entropy of inlet
                   hin=refpropm('H','T',tin,'P',pin,'pentane'); %
enthalpy of inlet

                   sout_s=sin; % if Isentropic efficiency 100%

hout_s=refpropm('H','P',out_parameter_val,'S',sin,'pentane'); %
entalpy for 100% isentropic efficiency
                   hout=(hin-eta_s*(hin-hout_s))/1000; %entalpy of
outlet
                   pout=out_parameter_val/101; % outlet pressure

tout=refpropm('T','P',1.17*101,'H',hout*1000,'pentane')-
273.15;%outlet temperature
               elseif (select == 2.0)
                  % disp(parameter);% display the control parameter

out_parameter_val=out_parameter_val+273.15;%convert from c to k
                   sin=refpropm('S','T',tin,'P',pin,'pentane'); %
entropy of inlet
                   hin=refpropm('H','T',tin,'P',pin,'pentane'); %
enthalpy of inlet
                   h_temp=refpropm('H','P',pin,'Q',1,'pentane'); %
entalpy
```

```
                    s_temp=refpropm('S','P',pin,'Q',1,'pentane'); %
entropy
                    if (h_temp>hin) % chek for the state
                    hin=h_temp;
                    sin=s_temp;
                    end
                    sout_s=sin; % if Isentropic efficiency 100%

hout_s=refpropm('H','T',out_parameter_val,'S',sin,'pentane'); %
entalpy for 100% isentropic efficiency
                    hout=(hin-eta_s*(hin-hout_s))/1000; %entalpy of
outlet

pout=refpropm('P','T',out_parameter_val,'H',hout*1000,'pentane')/101;
% outlet pressure
                    tout=out_parameter_val-273.15;

               end

end
```

GPentaneTurbinePV2.m

```
function pout =property(pin,tin,select,out_parameter_val,eta_s)
                tin=273.15+tin;%convert from c to k
                pin=101*pin;%convert from bar to kpa

               if (select == 1.0)
                    %disp(parameter);% display the control parameter
                    out_parameter_val=out_parameter_val*101;%convert
from bar to kpa
                    sin=refpropm('S','T',tin,'P',pin,'pentane'); %
entropy of inlet
                    hin=refpropm('H','T',tin,'P',pin,'pentane'); %
enthalpy of inlet

                    sout_s=sin; % if Isentropic efficiency 100%

hout_s=refpropm('H','P',out_parameter_val,'S',sin,'pentane'); %
entalpy for 100% isentropic efficiency
                    hout=(hin-eta_s*(hin-hout_s))/1000; %entalpy of
outlet
                    pout=out_parameter_val/101; % outlet pressure

tout=refpropm('T','P',1.17*101,'H',hout*1000,'pentane')-
273.15;%outlet temperature
                elseif (select == 2.0)
                   % disp(parameter);% display the control parameter

out_parameter_val=out_parameter_val+273.15;%convert from c to k
                    sin=refpropm('S','T',tin,'P',pin,'pentane'); %
entropy of inlet
                    hin=refpropm('H','T',tin,'P',pin,'pentane'); %
enthalpy of inlet
                    h_temp=refpropm('H','P',pin,'Q',1,'pentane'); %
entalpy
                    s_temp=refpropm('S','P',pin,'Q',1,'pentane'); %
entropy
                    if (h_temp>hin) % chek for the state
                    hin=h_temp;
                    sin=s_temp;
```

```
                    end
                    sout_s=sin; % if Isentropic efficiency 100%

hout_s=refpropm('H','T',out_parameter_val,'S',sin,'pentane'); %
entalpy for 100% isentropic efficiency
                    hout=(hin-eta_s*(hin-hout_s))/1000; %entalpy of
outlet

pout=refpropm('P','T',out_parameter_val,'H',hout*1000,'pentane')/101;
% outlet pressure
                    tout=out_parameter_val-273.15;

                end

end
```

GPentaneTurbineTV2.m

```
function tout =property(pin,tin,select,out_parameter_val,eta_s)
                tin=273.15+tin;%convert from c to k
                pin=101*pin;%covert from bar to kpa

                if (select == 1.0)
                    %disp(parameter);% display the control parameter
                    out_parameter_val=out_parameter_val*101;%convert
from bar to kpa
                    sin=refpropm('S','T',tin,'P',pin,'pentane'); %
entropy of inlet
                    hin=refpropm('H','T',tin,'P',pin,'pentane'); %
enthalpy of inlet
                    sout_s=sin; % if Isentropic efficiency 100%

hout_s=refpropm('H','P',out_parameter_val,'S',sin,'pentane'); %
entalpy for 100% isentropic efficiency
                    hout=(hin-eta_s*(hin-hout_s))/1000; %entalpy of
outlet
                    pout=out_parameter_val/101; % outlet pressure

tout=refpropm('T','P',out_parameter_val,'H',hout*1000,'pentane')-
273.15;%outlet temperature
                elseif (select == 2.0)
                   % disp(parameter);% display the control parameter

out_parameter_val=out_parameter_val+273.15;%convert from c to k
                    sin=refpropm('S','T',tin,'P',pin,'pentane'); %
entropy of inlet
                    hin=refpropm('H','T',tin,'P',pin,'pentane'); %
enthalpy of inlet
                    h_temp=refpropm('H','P',pin,'Q',1,'pentane'); %
entalpy
                    s_temp=refpropm('S','P',pin,'Q',1,'pentane'); %
entropy
                    if (h_temp>hin) % chek for the state
                    hin=h_temp;
                    sin=s_temp;
                    end
                    sout_s=sin; % if Isentropic efficiency 100%
```

```
hout_s=refpropm('H','T',out_parameter_val,'S',sin,'pentane'); %
entalpy for 100% isentropic efficiency
                    hout=(hin-eta_s*(hin-hout_s))/1000; %entalpy of
outlet

pout=refpropm('P','T',out_parameter_val,'H',hout*1000,'pentane')/101;
% outlet pressure
                    tout=out_parameter_val-273.15;

               end

end
```

GSteamTurbineHV2.m

```
function hout =property(pin,tin,select,out_parameter_val,eta_s)
                tin=273.15+tin;%convert from c to k
                pin=101*pin;%convert from bar to kpa

               if (select == 1.0)
                    %disp(parameter);% display the control parameter
                    out_parameter_val=out_parameter_val*101;%convert
from bar to kpa
                    h_p_t=refpropm('H','T',tin,'P',pin,'water'); %
enthalpy of inlet
                    h_p_x=refpropm('H','P',pin,'Q',1,'water'); %
enthalpy of inlet of saturated steam
                    if (h_p_x>=h_p_t)
                    hin=h_p_x;
                    sin=refpropm('S','P',pin,'Q',1,'water'); %
entropy of inlet of saturated steam
                    else
                    hin=h_p_t;
                    sin=refpropm('S','T',tin,'P',pin,'water'); %
entropy of inlet
                    end
                    sout_s=sin; % if Isentropic efficiency 100%

hout_s=refpropm('H','P',out_parameter_val,'S',sin,'water'); % entalpy
for 100% isentropic efficiency
                    hout=(hin-eta_s*(hin-hout_s))/1000; %entalpy of
outlet
                    pout=out_parameter_val/101; % outlet pressure

tout=refpropm('T','P',1.17*101,'H',hout*1000,'water')-273.15;%outlet
temperature
                elseif (select == 2.0)
                   % disp(parameter);% display the control parameter

out_parameter_val=out_parameter_val+273.15;%convert from c to k
                    h_p_t=refpropm('H','T',tin,'P',pin,'water'); %
enthalpy of inlet
                    h_p_x=refpropm('H','P',pin,'Q',1,'water'); %
enthalpy of inlet of saturated steam
                    if (h_p_x>=h_p_t)
                    hin=h_p_x;
                    sin=refpropm('S','P',pin,'Q',1,'water'); %
entropy of inlet of saturated steam
```

```
                    else
                    hin=h_p_t;
                    sin=refpropm('S','T',tin,'P',pin,'water'); %
entropy of inlet
                    end
                    sout_s=sin; % if Isentropic efficiency 100%

hout_s=refpropm('H','T',out_parameter_val,'S',sin,'water'); % entalpy
for 100% isentropic efficiency
                    hout=(hin-eta_s*(hin-hout_s))/1000; %entalpy of
outlet

pout=refpropm('P','T',out_parameter_val,'H',hout*1000,'water')/101; %
outlet pressure
                    tout=out_parameter_val-273.15;
               elseif(select == 3.0)
                    if (out_parameter_val>1)|| (out_parameter_val<0)
                    disp('Error 0<x<=1 ');
                    return;
                    end

                    h_p_t=refpropm('H','T',tin,'P',pin,'water'); %
enthalpy of inlet
                    h_p_x=refpropm('H','P',pin,'Q',1,'water'); %
enthalpy of inlet of saturated steam
                    if (h_p_x>=h_p_t)
                    hin=h_p_x;
                    sin=refpropm('S','P',pin,'Q',1,'water'); %
entropy of inlet of saturated steam
                    else
                    hin=h_p_t;
                    sin=refpropm('S','T',tin,'P',pin,'water'); %
entropy of inlet
                    end
                    sout_s=sin; % if Isentropic efficiency 100%
                    x=out_parameter_val*100;% convert in percentage
                    tin_temp=tin; % keep tin unchanged
                    for i=1:1:1000000000
                    tnew= tin_temp-0.1; % calculate temperature
iteratively

xnew=refpropm('Q','T',tnew,'S',sout_s,'water')*100; % new quality
                    if abs(x-xnew)<= 0.1
                    hout_s=refpropm('H','T',tnew,'Q',x/100,'water');%
enthalpy
                    break
                    end
                    tin_temp=tnew;
                    end

                    hout=(hin-eta_s*(hin-hout_s))/1000; %entalpy of
outlet
                    hout_tem=hout*1000;
                    for i=1:1:1000000000
                    tnew= tin-0.1; % calculate temperature
iteratively

xnew=refpropm('Q','T',tnew,'H',hout_tem,'water')*100; % new quality
                    if abs(x-xnew)<= 0.1
                    tout=tnew-273.15;
```

```
pout=refpropm('P','T',tnew,'Q',x/100,'water')/101;
                    break
                    end
                    tin=tnew;
                    end



                end

end
```

GSteamTurbinePV2.m

```
function pout =property(pin,tin,select,out_parameter_val,eta_s)
                tin=273.15+tin;%convert from c to k
                pin=101*pin;%convert from bar to kpa

                if (select == 1.0)
                    %disp(parameter);% display the control parameter
                    out_parameter_val=out_parameter_val*101;%convert
from bar to kpa
                    h_p_t=refpropm('H','T',tin,'P',pin,'water'); %
enthalpy of inlet
                    h_p_x=refpropm('H','P',pin,'Q',1,'water'); %
enthalpy of inlet of saturated steam
                    if (h_p_x>=h_p_t)
                    hin=h_p_x;
                    sin=refpropm('S','P',pin,'Q',1,'water'); %
entropy of inlet of saturated steam
                    else
                    hin=h_p_t;
                    sin=refpropm('S','T',tin,'P',pin,'water'); %
entropy of inlet
                    end
                    sout_s=sin; % if Isentropic efficiency 100%

hout_s=refpropm('H','P',out_parameter_val,'S',sin,'water'); % entalpy
for 100% isentropic efficiency
                    hout=(hin-eta_s*(hin-hout_s))/1000; %entalpy of
outlet
                    pout=out_parameter_val/101; % outlet pressure

tout=refpropm('T','P',1.17*101,'H',hout*1000,'water')-273.15;%outlet
temperature
                elseif (select == 2.0)
                   % disp(parameter);% display the control parameter

out_parameter_val=out_parameter_val+273.15;%convert from c to k
                    h_p_t=refpropm('H','T',tin,'P',pin,'water'); %
enthalpy of inlet
                    h_p_x=refpropm('H','P',pin,'Q',1,'water'); %
enthalpy of inlet of saturated steam
                    if (h_p_x>=h_p_t)
                    hin=h_p_x;
                    sin=refpropm('S','P',pin,'Q',1,'water'); %
entropy of inlet of saturated steam
```

```
                    else
                    hin=h_p_t;
                    sin=refpropm('S','T',tin,'P',pin,'water'); %
entropy of inlet
                    end
                    sout_s=sin; % if Isentropic efficiency 100%

hout_s=refpropm('H','T',out_parameter_val,'S',sin,'water'); % entalpy
for 100% isentropic efficiency
                    hout=(hin-eta_s*(hin-hout_s))/1000; %entalpy of
outlet

pout=refpropm('P','T',out_parameter_val,'H',hout*1000,'water')/101; %
outlet pressure
                    tout=out_parameter_val-273.15;
               elseif(select == 3.0)
                    if (out_parameter_val>1)|| (out_parameter_val<0)
                    disp('Error 0<x<=1 ');
                    return;
                    end

                    h_p_t=refpropm('H','T',tin,'P',pin,'water'); %
enthalpy of inlet
                    h_p_x=refpropm('H','P',pin,'Q',1,'water'); %
enthalpy of inlet of saturated steam
                    if (h_p_x>=h_p_t)
                    hin=h_p_x;
                    sin=refpropm('S','P',pin,'Q',1,'water'); %
entropy of inlet of saturated steam
                    else
                    hin=h_p_t;
                    sin=refpropm('S','T',tin,'P',pin,'water'); %
entropy of inlet
                    end
                    sout_s=sin; % if Isentropic efficiency 100%
                    x=out_parameter_val*100;% convert in percentage
                    tin_temp=tin; % keep tin unchanged
                    for i=1:1:1000000000
                    tnew= tin_temp-0.1; % calculate temperature
iteratively

xnew=refpropm('Q','T',tnew,'S',sout_s,'water')*100; % new quality
                    if abs(x-xnew)<= 0.1
                    hout_s=refpropm('H','T',tnew,'Q',x/100,'water');%
enthalpy
                    break
                    end
                    tin_temp=tnew;
                    end

                    hout=(hin-eta_s*(hin-hout_s))/1000; %entalpy of
outlet
                    hout_tem=hout*1000;
                    for i=1:1:1000000000
                    tnew= tin-0.1; % calculate temperature
iteratively

xnew=refpropm('Q','T',tnew,'H',hout_tem,'water')*100; % new quality
                    if abs(x-xnew)<= 0.1
                    tout=tnew-273.15;
```

```
pout=refpropm('P','T',tnew,'Q',x/100,'water')/101;
                    break
                    end
                    tin=tnew;
                    end



                end

end
```

GSteamTurbineTV2.m

```
function tout =property(pin,tin,select,out_parameter_val,eta_s)
                tin=273.15+tin;%convert from c to k
                pin=101*pin;%convert from bar to kpa

                if (select == 1.0)
                    %disp(parameter);% display the control parameter
                    out_parameter_val=out_parameter_val*101;%convert
from bar to kpa
                    h_p_t=refpropm('H','T',tin,'P',pin,'water'); %
enthalpy of inlet
                    h_p_x=refpropm('H','P',pin,'Q',1,'water'); %
enthalpy of inlet of saturated steam
                    if (h_p_x>=h_p_t)
                    hin=h_p_x;
                    sin=refpropm('S','P',pin,'Q',1,'water'); %
entropy of inlet of saturated steam
                    else
                    hin=h_p_t;
                    sin=refpropm('S','T',tin,'P',pin,'water'); %
entropy of inlet
                    end
                    sout_s=sin; % if Isentropic efficiency 100%

hout_s=refpropm('H','P',out_parameter_val,'S',sin,'water'); % entalpy
for 100% isentropic efficiency
                    hout=(hin-eta_s*(hin-hout_s))/1000; %entalpy of
outlet
                    pout=out_parameter_val/101; % outlet pressure

tout=refpropm('T','P',1.17*101,'H',hout*1000,'water')-273.15;%outlet
temperature
                elseif (select == 2.0)
                   % disp(parameter);% display the control parameter

out_parameter_val=out_parameter_val+273.15;%convert from c to k
                    h_p_t=refpropm('H','T',tin,'P',pin,'water'); %
enthalpy of inlet
                    h_p_x=refpropm('H','P',pin,'Q',1,'water'); %
enthalpy of inlet of saturated steam
                    if (h_p_x>=h_p_t)
                    hin=h_p_x;
```

```
                    sin=refpropm('S','P',pin,'Q',1,'water'); %
entropy of inlet of saturated steam
                    else
                    hin=h_p_t;
                    sin=refpropm('S','T',tin,'P',pin,'water'); %
entropy of inlet
                    end
                    sout_s=sin; % if Isentropic efficiency 100%

hout_s=refpropm('H','T',out_parameter_val,'S',sin,'water'); % entalpy
for 100% isentropic efficiency
                    hout=(hin-eta_s*(hin-hout_s))/1000; %entalpy of
outlet

pout=refpropm('P','T',out_parameter_val,'H',hout*1000,'water')/101; %
outlet pressure
                    tout=out_parameter_val-273.15;
               elseif(select == 3.0)
                    if (out_parameter_val>1)|| (out_parameter_val<0)
                    disp('Error 0<x<=1 ');
                    return;
                    end

                    h_p_t=refpropm('H','T',tin,'P',pin,'water'); %
enthalpy of inlet
                    h_p_x=refpropm('H','P',pin,'Q',1,'water'); %
enthalpy of inlet of saturated steam
                    if (h_p_x>=h_p_t)
                    hin=h_p_x;
                    sin=refpropm('S','P',pin,'Q',1,'water'); %
entropy of inlet of saturated steam
                    else
                    hin=h_p_t;
                    sin=refpropm('S','T',tin,'P',pin,'water'); %
entropy of inlet
                    end
                    sout_s=sin; % if Isentropic efficiency 100%
                    x=out_parameter_val*100;% convert in percentage
                    tin_temp=tin; % keep tin unchanged
                    for i=1:1:1000000000
                    tnew= tin_temp-0.1; % calculate temperature
iteratively

xnew=refpropm('Q','T',tnew,'S',sout_s,'water')*100; % new quality
                    if abs(x-xnew)<= 0.1
                    hout_s=refpropm('H','T',tnew,'Q',x/100,'water');%
enthalpy
                    break
                    end
                    tin_temp=tnew;
                    end

                    hout=(hin-eta_s*(hin-hout_s))/1000; %entalpy of
outlet
                    hout_tem=hout*1000;
                    for i=1:1:1000000000
                    tnew= tin-0.1; % calculate temperature
iteratively

xnew=refpropm('Q','T',tnew,'H',hout_tem,'water')*100; % new quality
                    if abs(x-xnew)<= 0.1
```

```
                    tout=tnew-273.15;

pout=refpropm('P','T',tnew,'Q',x/100,'water')/101;
                    break
                    end
                    tin=tnew;
                    end



                end

end
```

GWaterEnthalpy.m

```
function h    =property(pin,tin,dome,x)


                tin=273.15+tin;%convert from c to k
                pin=101*pin;%convert from bar to kpa
                if (dome==1)
                h=refpropm('H','T',tin,'P',pin,'water')/1000; %
entalpy
                elseif (dome==2)
                h=refpropm('H','P',pin,'Q',x,'water')/1000; % entalpy
                end


end
```

GWaterEnthalpyTurbineInlet.m

```
function hin    =property(pin,tin)

                    pin=pin*101;% conversion from bar to kPa
                    tin=tin+273.15;% conversion from C to K
                    h_p_t=refpropm('H','T',tin,'P',pin,'water'); %
enthalpy of inlet
                    h_p_x=refpropm('H','P',pin,'Q',1,'water'); %
enthalpy of inlet of saturated steam
                    if (h_p_x>=h_p_t)
                    hin=h_p_x/1000; % inlet enthalpy
                    else
                    hin=h_p_t/1000;% inlet enthalpy
                    end


end
```

GWaterTemperature.m

```
function T    =property(pin,hin)
                hin=hin*1000;%convert from J/kg to kJ/kg
                pin=101*pin;%convert from bar to kpa
                T=refpropm('T','P',pin,'H',hin,'WATER')-273.15; %
temperature

end
```

GQCondenser.m

```
function Q=properties(p_Pentane,t_Pentane,tamb,air_velocity)
p_Pentane=p_Pentane*101;
t_Pentane=t_Pentane+273.15;
tamb=tamb+273.15;


tsat=refpropm('T','P',p_Pentane,'Q',0,'Pentane'); %w/mK

if abs(t_Pentane-tsat)<=0.0001
   t_Pentane=t_Pentane+1.0;
end

tw=tsat-1;

Q=GQCondenserIteration(p_Pentane,t_Pentane,tamb,air_velocity,tw);
for c=1:100
Q_new=GQCondenserIteration(p_Pentane,t_Pentane,tamb,air_velocity,tw);
    if abs(Q-Q_new)<=0.1 Q=Q_new; end
    tw=tw-0.1;
end


end
```

GQCondenserIteration.m

```
function Q=properties(p_Pentane,t_Pentane,tamb,air_velocity,tw)
p_Pentane=p_Pentane*101;
t_Pentane=t_Pentane+273.15;
tamb=tamb+273.15;

% calculating alfa_i
k_Pentane=refpropm('L','T',(t_Pentane),'Q',0,'Pentane'); %w/mK
roh_Pentane_l=refpropm('D','T',(t_Pentane),'Q',0,'Pentane'); %kg/m^3
roh_Pentane_g=refpropm('D','T',(t_Pentane),'Q',1,'Pentane'); %kg/m^3
meu_Pentane_l=refpropm('V','T',(t_Pentane),'Q',0,'Pentane');%Pa.s
d_i=23.41/1000;%m
g=9.81; %m/s^2
tsat=refpropm('T','P',p_Pentane,'Q',0,'Pentane'); %w/mK

if abs(t_Pentane-tsat)<=0.0001
   t_Pentane=t_Pentane+1.0;
end


hl=refpropm('H','T',(t_Pentane),'Q',0,'Pentane');% enthalpy of
saturated liquid
hg=refpropm('H','T',(t_Pentane),'Q',1,'Pentane');% enthalpy of
saturated vapor
h=refpropm('H','T',t_Pentane,'P',p_Pentane,'Pentane');% enthalpy of
the incoming fluid
```

```
delta_h=hg-hl;% difference between enthalpies hv
x=refpropm('Q','T',t_Pentane,'P',p_Pentane,'Pentane');% quality
if x<=0.01
   x=0.01;
end

omega=0.728*(1+((1-x)/x)*(roh_Pentane_g/roh_Pentane_l)^0.667)^(-
0.75);%
one=k_Pentane^3;
two=roh_Pentane_l;
three=(roh_Pentane_l-roh_Pentane_g);
four=g*delta_h;
five=(meu_Pentane_l*d_i*(tsat-tw));
alfa_i=omega*(one*two*three*four/five)^0.25; % heat transfer
coefficient inside the tube



% calculating alfa_0

t_bulk=(tamb+tw)/2;
w_air=2*air_velocity;% maximum velocity
k_air=7E-05*(t_bulk -273.15)+ 0.0241;%w/mK
roh_air=-0.0033*(t_bulk -273.15)+ 1.249; %kg/m^3
meu_air=(4E-05*(t_bulk -273.15)+ 0.0167)/1000; %Pa.s
Pr_air=0.706; % taken as constant
d_o=25.41/1000; % external diameter
Re_air=(roh_air*air_velocity*d_o)/meu_air; %renolds number
a=2.24;
b=4.09;
s=2.54/1000;
h=15.80/1000;
nf=0.75;
A_t=29.61 ;
A_f=28.44 ;
A_r=1.17;
A_i=1.35;
A_nb=1.46;
n_f=0.75;
bw=1/1000;
N=1584; % total no. of tube
k_stl=(55+52)/2; %w/mk
cp_air=1.01; %kW/kgK
A_air_flow=575; % m^2
Air_density=1.21; %kg/m^3
alfa=(k_air/d_o)*0.19*(a/b)^0.2*(s/d_o)^0.18*(h/d_o)^-
0.14*Re_air^0.65*Pr_air^0.33;
alfa_0=1/A_t*(alfa*(A_f*n_f+A_r)); % heat transfer coefficient
outside the tube

alfa_wall=1/(bw/(k_stl*(A_nb/A_t)));

Rfi=0;
Rfo=0;

U=1/(Rfi*(A_t/A_i)+1/(alfa_i*(A_i/A_t))+bw/(k_stl*(A_nb/A_t))+1/alfa_
0+Rfo); % w/m^2K
U=U/1000; % kw/m^2K
```

```
%Calculation of heat transfer
tout=tw-exp(-
(U*A_t)/(A_air_flow*air_velocity*Air_density*cp_air))*(tw-tamb);


LMTD=(tout-tamb)/(log(((tw-tamb)/(tw-tout))));
Q=U*A_t*N*LMTD;

end
```

Appendix 6: Sensitivity analysis of the assumption that the change in hold up mass in the ORC vaporizer, due to the change in ambient air temperature is negligible

The detailed information of the vaporizer pressure-temperature control mechanism is not available. However it is known (Figure 8-6) the cycle mass flow rate remains nearly unchanged for wide range of operation. The vaporizer level control valve is not effective in controlling the vaporizer pentane level due to change in the ambient temperature, as the pressure and temperature are coupled in the wet vapour zone (phase change). Figure 1 shows the opening of the level control valve for the year 2007 of OEC 1. Figure 2 shows the opening of the level control valve for the first day of year 2007, there is no instantaneous change in the level control valve is observed. This implies vaporizer pressure-temperature condition is controlled by the bypass valve when ambient temperature changes, not by the vaporizer level control valve. The level control valve in both the figures reduces over time to adjust to the pentane mass loss occurs during the normal operation of the plant.

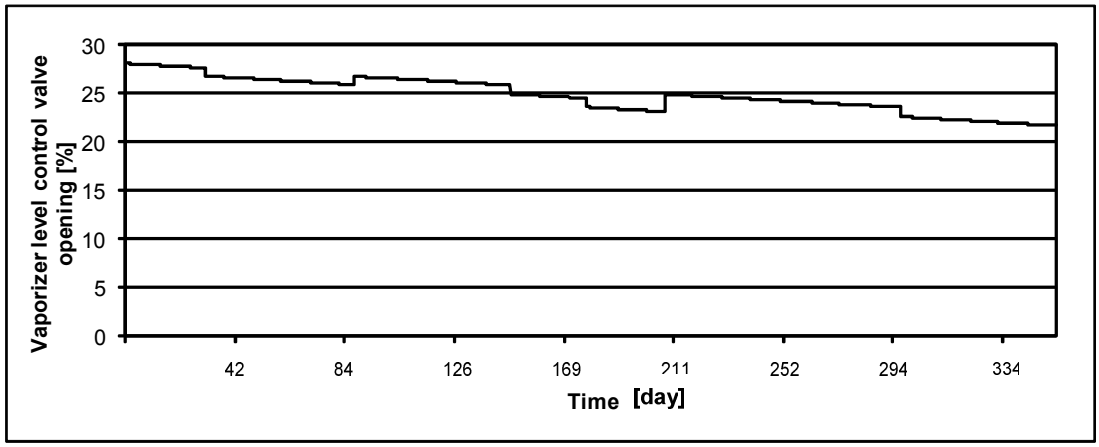

Figure 1: Level control valve opening for the year 2007 of OEC 1 taken from plant operational log

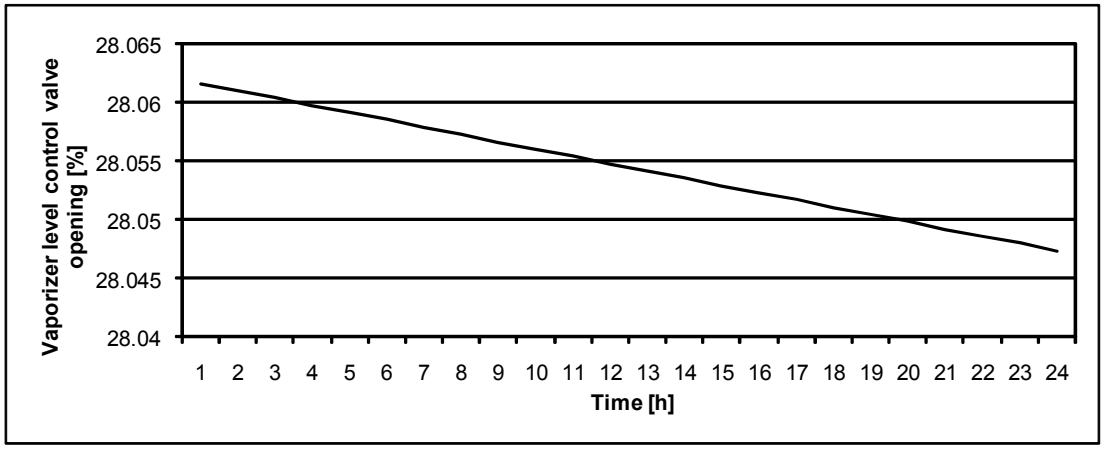

Figure 2: Level control valve opening on 01/01/2007 of OEC 1 taken from plant operational log

Figure 3 presents the simplified cross sectional view of the vaporizers used in the ORCs. The volume occupied by liquid pentane can be calculated by the following Equations:

$$V_l = (V_{Shell} - V_{tube}) - (\frac{1}{2} r_{shell}^2 (2\cos^{-1}((h_l - r_{shell}) / r_{shell})) - (h_l - r_{shell})\sqrt{(2h_l r_{shell} - h_l^2)})\, L_V \quad (1)$$

for pentane level higher than or equal to the top of the tube channel.

And,

$$V_l = (V_{Shell} - V_{tube}) - (\frac{1}{2} r_{shell}^2 (2\cos^{-1}((h_l - r_{shell}) / r_{shell})) - (h_l - r_{shell})\sqrt{(2h_l r_{shell} - h_l^2)})\, L_V + (\frac{1}{2} r_{tube}^2 (2\cos^{-1}((h_l - r_{tube}) / r_{tube})) - (h_l - r_{tube})\sqrt{(2h_l r_{tube} - h_l^2)})\, L_V \quad (2)$$

for a pentane level lower than or equal to the top of the tube channel.

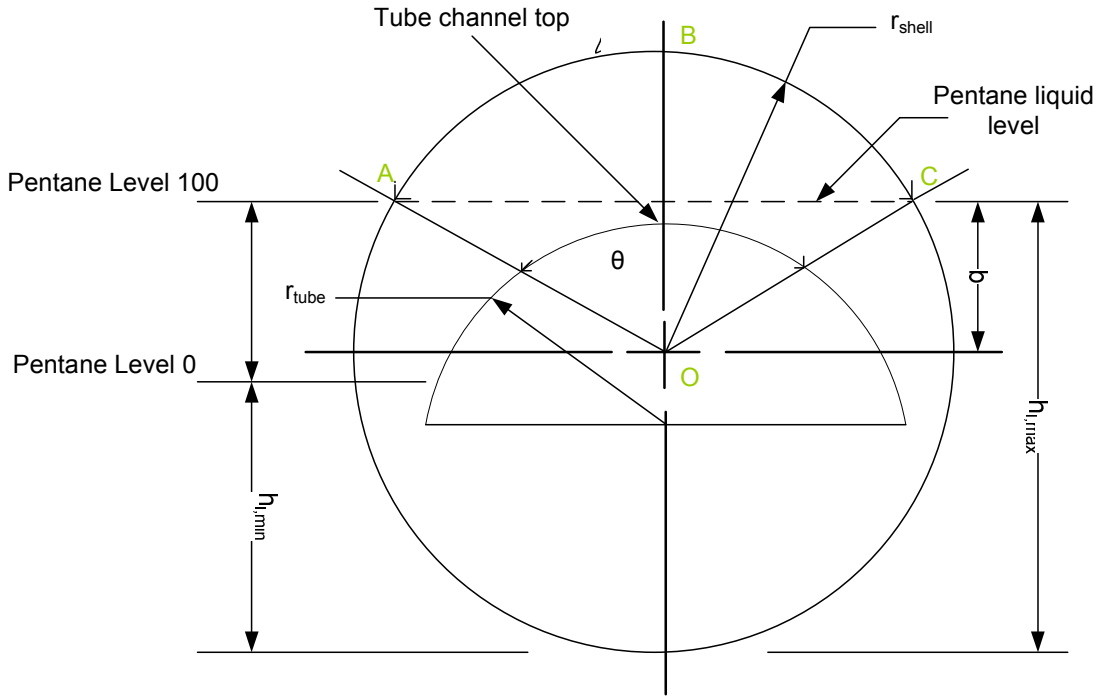

Figure 3: Simplified cross sectional view of the vaporizers

Here, V_{tube} is the volume (external) of the tube side channel, V_{Shell} is the volume of the space inside the shell, V_l is the volume occupied by the pentane liquid, V_{vapour} is the vapour occupied by pentane vapour, h_l is the height of the pentane liquid level from the bottom of the vaporizer, r_{shell} is the internal radius of the shell, r_{tube} is the outer radius of the tube and L_V is the length of the vaporizer. $(V_{Shell} - V_{tube})$ represents the empty volume (occupied by both pentane vapour and liquid) of the vaporizer.

When h_l is the maximum, the volume occupied by the pentane liquid is the maximum and when h_l is the minimum the volume occupied by the pentane liquid is the minimum.

The BRN-ORC

When the vaporizer pentane level is maximum (h_l = maximum) then the top of the tube surface is fully submerged in the pentane level. In this case, Equation (1) is used to calculate the volume occupied by pentane level. When the vaporizer pentane level is minimum (h_l = minimum) then the top of the tube surface is exposed to pentane vapour. In this case Equation (2) is used to calculate the volume occupied by pentane

liquid level. The required parameters are given below (taken from the design data supplied by MRP):

$h_{l,minimum}$ = 0.676 m; $h_{l,maximum}$ = 1.286 m; $(V_{Shell} - V_{tube})$ = 14.112 m^3; L_V = 11.58 m; r_{shell} = 0.816 m; and r_{tube} = 0.604 m.

The calculated volumes are:

$V_{l,\max imum}$ = 10.364 m^3 ; $V_{l,\min imum}$ = 5 m^3

The BOT-ORC

When the vaporizer pentane level is maximum (h_l = maximum) then the top of the tube surface is at the same level of the pentane level. When the vaporizer pentane level is minimum (h_l = minimum) then the top of the tube surface is exposed to pentane vapour. In both cases Equation (2) is used to calculate the volume occupied by pentane level. The required parameters are given below (taken from the design data supplied by MRP):

$h_{l,minimum}$ = 0.416 m; $h_{l,maximum}$ = 0.914 m; $(V_{Shell} - V_{tube})$ = 11.3 m^3; L_V = 15.61 m; r_{shell} = 0.886 m; and r_{tube} = 0.780 m.

The calculated volumes are:

$V_{l,\max imum}$ = 4.5 m^3 ; $V_{l,\min imum}$ = 3.138 m^3

Heat and mass balance of the vaporizer

Figure 4 shows the heat and mass balance of a heat exchanger (vaporizer). According to the conservation of the mass of working fluid:

$$\frac{d}{dt}(M_b) = \dot{m}_{b,i} - \dot{m}_{b,o} \tag{3}$$

If we ignore the effect of heat loss to the ambient, we can write the heat balance as:

$$\frac{d}{dt}(M_b h_b) = \dot{m}_{b,i}\, h_{b,i} - \dot{m}_{b,o}\, h_{b,o} + \dot{Q} \tag{4}$$

Here, M_b is the hold up mass, $\dot{m}_{b,i}$ is the inlet mass flow rate, $\dot{m}_{b,o}$ is outlet mass flow rate, $h_{b,i}$ is the inlet enthalpy, $h_{b,o}$ is outlet enthalpy of pentane and $\dot{Q}$ is the supplied heat to the system.

Here, a simple assumption was made that for a small time interval, the pressure and temperature changes are negligible; therefore, we can use enthalpy instead of the internal energy of the system.

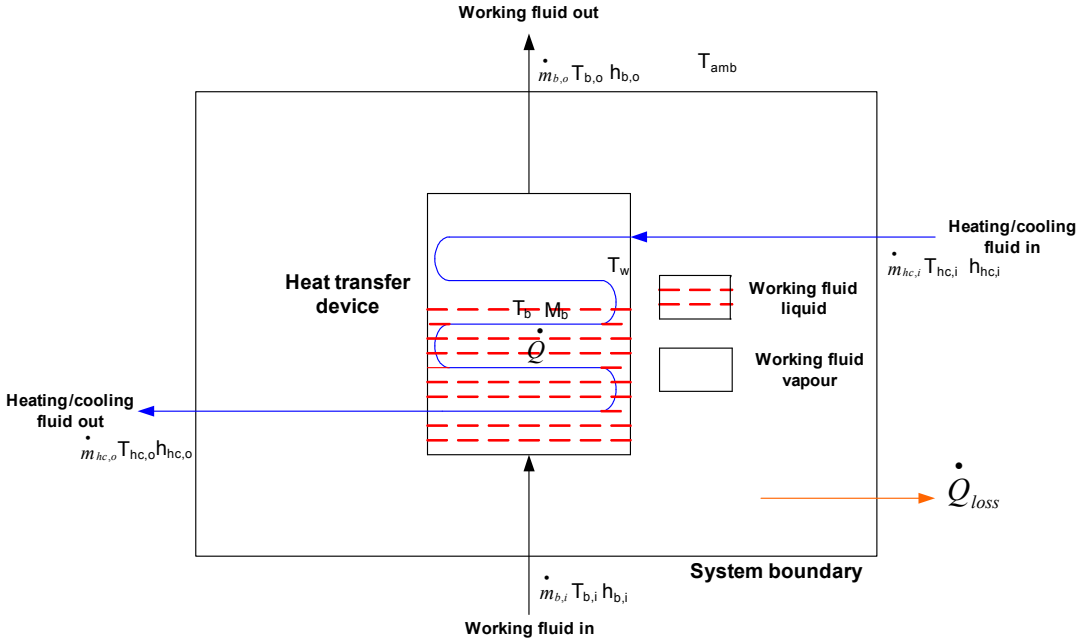

Figure 4: Schematic diagram of heat and mass balance of a heat-exchanging device

The hourly operation of the plant is considered steady state. Therefore left hand side of Equations (3) and (4) becomes zero. In the ORCs the vaporizer pentane outlet condition is controlled ($h_{b,o}$), therefore the vaporizer pentane outlet condition can vary little. The vaporizer pentane inlet condition is affected by ambient temperature. The maximum and minimum ambient temperature of Taupo was found to remain within -5 to 35 ºC i.e., the maximum possible change in temperature is 23 ºC. The

mass flow rate required to be bypassed if the temperature increases 23ºC, can be calculated from Equation (4).

Table 1 presents the change in hold up mass or specific volume (mass per unit volume) of both the BRN-ORC and the BOT-ORC. The results show that the hold up mass or the specific volume (as volume is constant change in hold up mass is same as change in specific volume) remained below 1% for the maximum possible ambient temperature change. Therefore, the assumption of the effect of change of hold up mass is negligible is a good approximation.

Table 1: change in hold up mass with the maximum temperature change

	Designed value	Maximum deviated $h_{b,i}$ based on maximum deviated temperature [kJ/kg]	Change in hold up mass or specific volume	
			$M_{b,\max}$	$M_{b,\min}$
BRN-ORC	$\dot{m}_{b,i}$ = 58.16 [kg/s] ρ_l = 413.6 [kg/m^3] $\dot{Q}$ = 28880 [kW] $h_{b,i}$ = 123 [kJ/kg] $h_{b,o}$ = 557.1 [kJ/kg] $M_{b,\max}$ = 4286.3 [kg] $M_{b,\min}$ = 2068.0 [kg]	$h_{b,i}$ = 135.79	0.242 [%]	0.502 [%]
BOT-ORC	$\dot{m}_{b,i}$ = 103.43 [kg/s] ρ_l = 545.4 [kg/m^3] $\dot{Q}$ = 43375 [kW] $h_{b,i}$ = 29.13 [kJ/kg] $h_{b,o}$ = 449.31 [kJ/kg] $M_{b,\max}$ = 2454.3 [kg] $M_{b,\min}$ = 1711.73 [kg]	$h_{b,i}$ = 50.75	0.583 [%]	0.837 [%]

Appendix 7: Code for short term performance of OEC 1

Model_OEC1.m

```
function pout=calculate_OEC1(tamb,mb)

p_initial_input=1.17;
t_initial_input=62.3;
p_initial=1.15;

termination_array_1=[0 0 0 0 0 0 0 0 0 0];
termination_array_2=[0 0 0 0 0 0 0 0 0 0];

termination_array_1(1)=0;
termination_array_2(1)=0;

termination_array_1(2)=p_initial_input;
termination_array_2(2)=t_initial_input;



mdot_cycle=43.1873;
mb=mb/2;% data is for two brine units


for c=1:10
%calculatio of heat transfer
Q_r=28880;
mb_dot_s=119.44;
Qin_OEC1=Q_r*(mb/mb_dot_s)^0.5;
Qin_OEC1_super_heat=7126.2*(mb/mb_dot_s)^0.5;
Qin_OEC1_vaporizer=23317*(mb/mb_dot_s)^0.5;
%Qin=46249.076*1;
%-----------------------------------

t_vaporizer=157.7612;% at min equlibrium (12C tamb)
p_vaporizer=18;% at min equlibrium (12C tamb)
p_vaporizer_max=19;
p_vaporizer_min=15.0;
Q_cond=GQCondenser_Quasi_SS(p_initial_input,t_initial_input,tamb,3.65
);
hl=refpropm('H','P',(p_initial*101),'Q',0,'Pentane');
hg=refpropm('H','T',(t_initial_input+273.15),'P',(p_initial_input*101
),'Pentane');
mdot_max=Q_cond/((hg-hl)/1000);

%Condenser calculation for higher than design amb temp
if mdot_cycle>=mdot_max
    while  mdot_cycle>=mdot_max
        % p_initial_input=p_initial_input+0.05;

Q_cond=GQCondenser_Quasi_SS(p_initial_input,t_initial_input,tamb,3.65
);
         hl=refpropm('H','P',(p_initial_input*101),'Q',0,'Pentane');
```

```
hg=refpropm('H','T',(t_initial_input+273.15),'P',(p_initial_input*101
),'Pentane');
          err=abs(mdot_max-mdot_cycle)/mdot_cycle;
          p_initial_input=p_initial_input+0.2*err;
          mdot_max=Q_cond/((hg-hl)/1000);
          if abs(mdot_cycle-mdot_max)<=0.01
              break;
          end

    end
else
    %Condenser calculation for higher than design amb temp
     while  mdot_cycle<mdot_max
        % p_initial_input=p_initial_input-0.05;

Q_cond=GQCondenser_Quasi_SS(p_initial_input,t_initial_input,tamb,3.65
);
          hl=refpropm('H','P',(p_initial_input*101),'Q',0,'Pentane');

hg=refpropm('H','T',(t_initial_input+273.15),'P',(p_initial_input*101
),'Pentane');
          err=abs(mdot_max-mdot_cycle)/mdot_cycle;
          p_initial_input=p_initial_input-0.2*err;
          mdot_max=Q_cond/((hg-hl)/1000);
          if abs(mdot_cycle-mdot_max)<=0.01
              break;
          end
     end
end

    p4_das=p_initial_input;
    p1=p4_das-0.5;
    t1=refpropm('T','P',(p1*101),'Q',0,'Pentane')-273.15;
    h1=refpropm('H','P',(p1*101),'Q',0,'Pentane')/1000;
    h2=h1+380/(mdot_cycle);
    %h3_new=(Qin_OEC1+7000)/(mdot_cycle)+h2;
    h3_a_new=(Qin_OEC1_vaporizer+6031.67)/(mdot_cycle)+h2;
    h3_a_new_temp= 505.6925;% start at eq at 130 C
    p3_a_new_temp=10.9260;


   %calculation of eqlibrium condtion for new h3
    while abs(h3_a_new-h3_a_new_temp)>=0.1
     %p3_a_new_temp= p3_a_new_temp+0.01;

h3_a_new_temp=refpropm('H','P',(p3_a_new_temp*101),'Q',1,'Pentane')/1
000;
     err=h3_a_new-h3_a_new_temp;
     p3_a_new_temp= p3_a_new_temp+0.01*err;
     if p3_a_new_temp>=p_vaporizer_max
         break;
     else
     p3_a_new= p3_a_new_temp;
     t3_a_new= refpropm('T','P',(p3_a_new_temp*101),'Q',1,'Pentane')-
273.15;

v3_a_new=1/refpropm('D','P',(p3_a_new_temp*101),'Q',1,'Pentane');
     end
```

```
    end


h3_a_old=refpropm('H','T',(t_vaporizer+273.15),'Q',1,'Pentane')/1000;

u3_a_old=refpropm('U','T',(t_vaporizer+273.15),'Q',1,'Pentane')/1000;

v3_a_old=1/refpropm('D','T',(t_vaporizer+273.15),'Q',1,'Pentane');

    % calculation of u3
    %p3_a_new
    u3_a=u3_a_old+h3_a_new-h3_a_old-(p3_a_new*v3_a_new-
p_vaporizer*v3_a_old);
    delu3=u3_a-u3_a_old;
    LHS=delu3;

    p3_a_temp=17; %bar
    RHS=refpropm('H','P',(p3_a_temp*101),'Q',1,'Pentane')/1000-
h3_a_old-(p3_a_temp*v3_a_old-p_vaporizer*v3_a_old);
    %err=0;

    while abs(LHS-RHS)>=0.1

     RHS=refpropm('H','P',(p3_a_temp*101),'Q',1,'Pentane')/1000-
h3_a_old-(p3_a_temp*v3_a_old-p_vaporizer*v3_a_old);
     err=LHS-RHS;

    % else

h3_a_temp=refpropm('H','P',(p3_a_temp*101),'Q',1,'Pentane')/1000;

u3_a_temp=refpropm('U','P',(p3_a_temp*101),'Q',1,'Pentane')/1000;

s3_a_temp=refpropm('S','P',(p3_a_temp*101),'Q',1,'Pentane')/1000;
     t3_a_temp= refpropm('T','P',(p3_a_temp*101),'Q',1,'Pentane')-
273.15;
     p3_a_temp_new = p3_a_temp+0.01*err;
     if p3_a_temp_new>=p_vaporizer_max
        break;
     else
         p3_a_temp=p3_a_temp_new;
     end

     if abs(LHS-RHS)<=0.1
         break;
     end

      end

      if p3_a_temp<=p_vaporizer_min
         p3_a_temp=p_vaporizer_min;

h3_a_temp=refpropm('H','P',(p3_a_temp*101),'Q',1,'Pentane')/1000;

u3_a_temp=refpropm('U','P',(p3_a_temp*101),'Q',1,'Pentane')/1000;

s3_a_temp=refpropm('S','P',(p3_a_temp*101),'Q',1,'Pentane')/1000;
```

```
        t3_a_temp=
refpropm('T','P',(p3_a_temp*101),'Q',1,'Pentane')-273.15;
     end
    p3=p3_a_temp-0.3;
    t3=t3_a_temp+Qin_OEC1_super_heat/(mdot_cycle*2.7332); %cp =2.7332
at 18 bar and 189 C temp;
    h3=refpropm('H','T',(t3+273.15),'P',(p3*101),'Pentane')/1000;
    s3=refpropm('S','T',(t3+273.15),'P',(p3*101),'Pentane')/1000;
    s4=s3;
    p4=p4_das+0.5;
    t4=refpropm('T','P',(p4*101),'S',s4*1000,'Pentane')-273.15;
    h4=refpropm('H','P',(p4*101),'S',s4*1000,'Pentane')/1000;
    t4_das=t4-6031.67*0.8/(mdot_cycle*1.73); %cp =1.73

    termination_array_1(c+2)=p1;
    termination_array_2(c+2)=t4_das;


    if abs(termination_array_1(c)-termination_array_1(c+1))<=0.1 &&
abs(termination_array_2(c)-termination_array_2(c+1))<=0.1
        break;
    end

    p_initial_input=p1;
    t_initial_input=t4_das;

end

    %k=1.1173;
   pout=mdot_cycle*0.9*(h3-h4)/1000;
   % pout_cp=2.1406*101*(t3-t4)
    %pout_fit=(-303.62*rp^2 + 3189.8*rp - 3247.9)/1000

    x(1)=p1;
    x(2)=t1;
    x(3)=p3;
    x(4)=t3;
    x(5)=p4;
    x(6)=t4;
    x(7)=pout;


end
```

Appendix 8: Code for short term performance of OEC 11

Model_OEC11.m

```
function [x]=calculate_OEC1(tamb,mb)
p_initial_input=1.17;
t_initial_input=62.3;
p_initial=1.15;

termination_array_1=[0 0 0 0 0 0 0 0 0 0];
termination_array_2=[0 0 0 0 0 0 0 0 0 0];

termination_array_1(1)=0;
termination_array_2(1)=0;

termination_array_1(2)=p_initial_input;
termination_array_2(2)=t_initial_input;



mdot_cycle=43.1873;
mb=mb/2;% data is for two brine units


for c=1:10
%calculatio of heat transfer
Q_r=28880;
mb_dot_s=119.44;
Qin_OEC1=Q_r*(mb/mb_dot_s)^0.5;
%Qin_OEC1_super_heat=7126.2*(mb/mb_dot_s)^0.5;
Qin_OEC1_vaporizer=23317*(mb/mb_dot_s)^0.5;
Qin_OEC1_super_heat=Qin_OEC1-Qin_OEC1_vaporizer;
%Qin=46249.076*1;
%-----------------------------------

t_vaporizer=157.7612;% at min equlibrium (12C tamb)
p_vaporizer=18;% at min equlibrium (12C tamb)
p_vaporizer_max=19;
p_vaporizer_min=15.0;
Q_cond=GQCondenser_Quasi_SS(p_initial_input,t_initial_input,tamb,3.58
);
hl=refpropm('H','P',(p_initial*101),'Q',0,'Pentane');
hg=refpropm('H','T',(t_initial_input+273.15),'P',(p_initial_input*101
),'Pentane');
mdot_max=Q_cond/((hg-hl)/1000);

%Condenser calculation for higher than design amb temp
if mdot_cycle>=mdot_max
    while  mdot_cycle>=mdot_max
        % p_initial_input=p_initial_input+0.05;

Q_cond=GQCondenser_Quasi_SS(p_initial_input,t_initial_input,tamb,3.58
);
         hl=refpropm('H','P',(p_initial_input*101),'Q',0,'Pentane');

hg=refpropm('H','T',(t_initial_input+273.15),'P',(p_initial_input*101
),'Pentane');
```

```
        err=abs(mdot_max-mdot_cycle)/mdot_cycle;
        p_initial_input=p_initial_input+0.2*err;
        mdot_max=Q_cond/((hg-hl)/1000);
        if abs(mdot_cycle-mdot_max)<=0.01
            break;
        end

    end
else
    %Condenser calculation for higher than design amb temp
     while  mdot_cycle<mdot_max
        % p_initial_input=p_initial_input-0.05;

Q_cond=GQCondenser_Quasi_SS(p_initial_input,t_initial_input,tamb,3.58
);
        hl=refpropm('H','P',(p_initial_input*101),'Q',0,'Pentane');

hg=refpropm('H','T',(t_initial_input+273.15),'P',(p_initial_input*101
),'Pentane');
        err=abs(mdot_max-mdot_cycle)/mdot_cycle;
        p_initial_input=p_initial_input-0.2*err;
        mdot_max=Q_cond/((hg-hl)/1000);
        if abs(mdot_cycle-mdot_max)<=0.01
            break;
        end
     end
end

    p4_das=p_initial_input;
    p1=p4_das-0.65;
    t1=refpropm('T','P',(p1*101),'Q',0,'Pentane')-273.15;
    h1=refpropm('H','P',(p1*101),'Q',0,'Pentane')/1000;
    h2=h1+380/(mdot_cycle);
    %h3_new=(Qin_OEC1+7000)/(mdot_cycle)+h2;
    h3_a_new=(Qin_OEC1_vaporizer+6031.67)/(mdot_cycle)+h2;
    h3_a_new_temp= 505.6925;% start at eq at 130 C
    p3_a_new_temp=10.9260;


   %calculation of eqlibrium condtion for new h3
    while abs(h3_a_new-h3_a_new_temp)>=0.1
     %p3_a_new_temp= p3_a_new_temp+0.01;

h3_a_new_temp=refpropm('H','P',(p3_a_new_temp*101),'Q',1,'Pentane')/1
000;
     err=h3_a_new-h3_a_new_temp;
     p3_a_new_temp= p3_a_new_temp+0.01*err;
     if p3_a_new_temp>=p_vaporizer_max
         break;
     else
     p3_a_new= p3_a_new_temp;
     t3_a_new= refpropm('T','P',(p3_a_new_temp*101),'Q',1,'Pentane')-
273.15;

v3_a_new=1/refpropm('D','P',(p3_a_new_temp*101),'Q',1,'Pentane');
     end

    end
```

```
h3_a_old=refpropm('H','T',(t_vaporizer+273.15),'Q',1,'Pentane')/1000;

u3_a_old=refpropm('U','T',(t_vaporizer+273.15),'Q',1,'Pentane')/1000;

v3_a_old=1/refpropm('D','T',(t_vaporizer+273.15),'Q',1,'Pentane');

    % calculation of u3
    %p3_a_new
    u3_a=u3_a_old+h3_a_new-h3_a_old-(p3_a_new*v3_a_new-
p_vaporizer*v3_a_old);
    delu3=u3_a-u3_a_old;
    LHS=delu3;

    p3_a_temp=17; %bar
    RHS=refpropm('H','P',(p3_a_temp*101),'Q',1,'Pentane')/1000-
h3_a_old-(p3_a_temp*v3_a_old-p_vaporizer*v3_a_old);
    %err=0;

    while abs(LHS-RHS)>=0.1

     RHS=refpropm('H','P',(p3_a_temp*101),'Q',1,'Pentane')/1000-
h3_a_old-(p3_a_temp*v3_a_old-p_vaporizer*v3_a_old);
     err=LHS-RHS;

    % else

h3_a_temp=refpropm('H','P',(p3_a_temp*101),'Q',1,'Pentane')/1000;

u3_a_temp=refpropm('U','P',(p3_a_temp*101),'Q',1,'Pentane')/1000;

s3_a_temp=refpropm('S','P',(p3_a_temp*101),'Q',1,'Pentane')/1000;
     t3_a_temp= refpropm('T','P',(p3_a_temp*101),'Q',1,'Pentane')-
273.15;
     p3_a_temp_new = p3_a_temp+0.01*err;
     if p3_a_temp_new>=p_vaporizer_max
        break;
     else
         p3_a_temp=p3_a_temp_new;
     end

     if abs(LHS-RHS)<=0.1
         break;
     end

      end

      if p3_a_temp<=p_vaporizer_min
         p3_a_temp=p_vaporizer_min;

h3_a_temp=refpropm('H','P',(p3_a_temp*101),'Q',1,'Pentane')/1000;

u3_a_temp=refpropm('U','P',(p3_a_temp*101),'Q',1,'Pentane')/1000;

s3_a_temp=refpropm('S','P',(p3_a_temp*101),'Q',1,'Pentane')/1000;
         t3_a_temp=
refpropm('T','P',(p3_a_temp*101),'Q',1,'Pentane')-273.15;
     end
    p3=p3_a_temp-0.3;
    t3=t3_a_temp+Qin_OEC1_super_heat/(mdot_cycle*3.1245); %cp =3.1245
```

```
    h3=refpropm('H','T',(t3+273.15),'P',(p3*101),'Pentane')/1000;
    s3=refpropm('S','T',(t3+273.15),'P',(p3*101),'Pentane')/1000;
    s4=s3;
    p4=p4_das+0.5;
    t4=refpropm('T','P',(p4*101),'S',s4*1000,'Pentane')-273.15;
    h4=refpropm('H','P',(p4*101),'S',s4*1000,'Pentane')/1000;
    t4_das=t4-6031.67*0.8/(mdot_cycle*1.73); %cp =1.73

    termination_array_1(c+2)=p1;
    termination_array_2(c+2)=t4_das;


    if abs(termination_array_1(c)-termination_array_1(c+1))<=0.1 &&
abs(termination_array_2(c)-termination_array_2(c+1))<=0.1
        break;
    end

    p_initial_input=p1;
    t_initial_input=t4_das;

end

    %k=1.1173;
   pout=mdot_cycle*0.9*(h3-h4)/1000;
   % pout_cp=2.1406*101*(t3-t4)
    %pout_fit=(-303.62*rp^2 + 3189.8*rp - 3247.9)/1000
    n2=(pout*1000-380)/(97.174*mb);

    x(1)=p1;
    x(2)=t1;
    x(3)=p3;
    x(4)=t3;
    x(5)=p4;
    x(6)=t4;
    x(7)=pout;

end
```

Appendix 9: Code for optimization function of OEC 11

optimize_OEC11_tamb_ms.m

```
function [sol,pout]=optimize_OEC11_tamb_ms(sol,options)
mdot_cycle=sol(1);
p3=sol(2);
        mdot_cycle=mdot_cycle/2;
ms= 120;% data is for four bot units
tamb=   25;% ambient temp

%calculatio of heat transfer
ms_dot_s=21.70;
Qin=(43375*(ms/ms_dot_s)^0.5)/2;

%-----------------------------------

p1=1.07;% initialization
p2=p3;
t1=refpropm('T','P',(p1*101),'Q',1,'Pentane')-273.15;

Q_cond=GQCondenser_Quasi_SS(p1,t1+1,tamb,3.58);

h1=refpropm('H','P',(p1*101),'Q',0,'Pentane')/1000;
h2=refpropm('H','T',(t1+273.15),'P',(p2*101),'Pentane')/1000;
h3=refpropm('H','P',(p3*101),'Q',1,'Pentane')/1000;
h4=refpropm('H','P',(p1*101),'Q',1,'Pentane')/1000;
mdot_max=Q_cond/((h4-h1));

mdot_cycle_calculated=Qin/(h3-h2);
if mdot_cycle>=mdot_cycle_calculated
    mdot_cycle=mdot_cycle_calculated;
end




if mdot_cycle>=mdot_max
    while  mdot_cycle>=mdot_max

          Q_cond=GQCondenser_Quasi_SS(p1,t1+1,tamb,3.58);
          h1=refpropm('H','P',(p1*101),'Q',0,'Pentane');
          h4=refpropm('H','P',(p1*101),'Q',1,'Pentane');
          err=abs(mdot_max-mdot_cycle)/mdot_cycle;
          p1=p1+0.2*err;
          mdot_max=Q_cond/((h4-h1)/1000);
          if abs(mdot_cycle-mdot_max)<=0.1


         h1=refpropm('H','P',(p1*101),'Q',0,'Pentane')/1000;
         p4=p1+0.1;
         h4=refpropm('H','P',(p4*101),'Q',1,'Pentane')/1000;
         t1=refpropm('T','P',(p1*101),'Q',0,'Pentane')/1000;

         break;
          end
```

```
    end
else

    %Condenser calculation for higher than design amb temp
     while  mdot_cycle<mdot_max

         Q_cond=GQCondenser_Quasi_SS(p1,t1,tamb,3.58);
         h1=refpropm('H','P',(p1*101),'Q',0,'Pentane');
         h4=refpropm('H','P',(p1*101),'Q',1,'Pentane');
         err=abs(mdot_max-mdot_cycle)/mdot_cycle;
         p1=p1-0.2*err;
         mdot_max=Q_cond/((h4-h1)/1000);
         if abs(mdot_cycle-mdot_max)<=0.1

        h1=refpropm('H','P',(p1*101),'Q',0,'Pentane')/1000;
       p4=p1+0.1;
        h4=refpropm('H','P',(p4*101),'Q',1,'Pentane')/1000;
        t1=refpropm('T','P',(p1*101),'Q',0,'Pentane')/1000;

         break;
         end
     end
end
h2=refpropm('H','T',(t1+273.15),'P',(p3*101),'Pentane')/1000;


wp=180;
wt=0.9*mdot_cycle*(h3-h4);

pout=2*(wt-180)/1000;

if pout>=7.5
    pout=7.5;
end
sol(3)=pout;
sol(1)=mdot_cycle*2;

end
```

Appendix 10: Publication 1
Sohel, M.I., Sellier, M., Brackney, L.J. and Krumdieck, S. Efficiency improvement for geothermal power generation to meet summer peak demand. Energy
Policy, 2009, 37(9), 3370-3376.

Energy Policy
Volume 37, Issue 9, September 2009, Pages 3370-3376
New Zealand Energy Strategy

doi:10.1016/j.enpol.2008.12.036 | How to Cite or Link Using DOI

Efficiency improvement for geothermal power generation to meet summer peak demand

M. Imroz Sohel[a], **Mathieu Sellier**[a], **Larry J. Brackney**[b] **and Susan Krumdieck**[a],

[a]Department of Mechanical Engineering, University of Canterbury, Private bag 4800, Christchurch 8140, New Zealand

[b]Department of Electrical and Computer Engineering, University of Canterbury, Private bag 4800, Christchurch, New Zealand

Received 26 June 2008;
accepted 15 December 2008.
Available online 20 February 2009.

Abstract

Geothermal power is an important part of New Zealand's renewable electricity supply due to its attractive cost and reliability. Modular type binary cycle plants have been imported and installed in various geothermal fields in New Zealand, with plans for further expansion. Power output of these plants deteriorates in the summer because plant efficiency depends directly on the geothermal resource and the ambient temperature. As these plants normally use air-cooled condensers, incorporating a water-augmented air-cooled system could improve the power output in summer thereby matching the peak air-conditioning demand. In this work, power generation for the Rotokawa plant was characterized using a similar plant performance and local weather. The improved performance was modelled for retrofit with a wet-cooling system. Maximum generation increase on the hottest day could be 6.8%. The average gain in power over the summer, November–February, was 1.5%, and the average gain for the whole year was 1%. With current binary unit generation capacity at the Rotokawa plant of 35 MW, investment in a water-augmented air-cooled system could provide 2 MW of peak generation on the hottest days. This investment in efficiency is found to compare favourably to other supply options such as solar PV, wind or gas.

Keywords: Geothermal power generation; Thermal plant efficiency; Peak power generation

Appendix 11: Publication 2

Sohel, M.I., Sellier, M., Brackney, L.J. and Krumdieck, S. Dynamic Modelling and Simulation of an Organic Rankine Cycle Unit of a Geothermal Power Plant. *Proceedings World Geothermal Congress 2010 Bali, Indonesia, 25-29 April*, 2010.

Proceedings World Geothermal Congress 2010
Bali, Indonesia, 25-29 April 2010

Dynamic Modelling and Simulation of an Organic Rankine Cycle Unit of a Geothermal Power Plant

M. Imroz Sohel[1*], Susan Krumdieck[1], Mathieu Sellier[1], Larry J. Brackney[2]

[1] Department of Mechanical Engineering, University of Canterbury, Christchurch, New Zealand.

[2] Department of Electrical and Computer Engineering, University of Canterbury, Christchurch, New Zealand.

* Corresponding author. Email: mso32@student.canterbury.ac.nz; mohammed.imroz.sohel@gmail.com

Tel: +64 3 3642987 ext 7243; Fax: +64 3 3642078;

Keywords: Geothermal power, dynamic modelling, binary cycle, ORC.

ABSTRACT

This article presents a dynamic model of a 5.4 MW binary cycle unit of a geothermal power plant. The plant is an Organic Rankine Cycle (ORC) where pentane is used as the motive fluid and it is powered by the separated brine from the geothermal fluid. It is found that the inlet brine properties including brine mass flow rate, and the ambient air temperature are the two most important parameters influencing the plant performance. Specifically, the plant performance is highly dependent on the ambient air temperature as the ORC uses air-cooled condenser. Moreover, the inlet brine property changes less significantly with respect to time compared to the ambient air temperature. Simulation has been carried out where, brine inlet properties and ambient air temperature are fed as inputs to the computer model. The simulated plant performance has been compared with the actual plant performance data. It has been found that the developed model is very competent in predicting plant performance. The average percentage error of the theoretical and the observed power outputs remain within 5%.

1. INTRODUCTION

Geothermal plants have a large number of parts involving an enormous number of flow recirculations and splitting, and connections of several subsystems. The overall plant behaviour, both static and dynamic, cannot be simply inferred from that of its components, rather it is essentially determined by their interaction (Casella 1999). Although a wide range of literature is available on the steady state operation of a geothermal power plant, dynamic models are not very common. Dynamic models are very useful in two areas, firstly, in controlling and monitoring the system for transient conditions, particularly when the load demand or the quality or flow of geothermal fluid suddenly changes (Wei et al. 2008). It is necessary to keep the proportion of liquid and vapour phases in the condenser and evaporator within acceptable ranges to avoid stalling or temperature shocks. Secondly, it is very convenient for the plant operators to know what the power output could be under given ambient conditions, plant parameters and geothermal fluid flow rate. The plant operators need to inform the dispatcher beforehand how much power they can produce as the price of the electricity depends on it. Normally, there is a huge penalty for the plant owners, if they produce more than promised to avoid grid overload (Pritchard 2002). A dynamic model can ease this problem by predicting power output in advance with high accuracy.

This paper presents a dynamic model of a 5.4 MW binary cycle unit of a geothermal power plant. The brine inlet properties and the ambient air temperature are used as the inputs to the model. The developed dynamic model meant for predicting the plant performance depending on weather condition and brine inlet properties. Therefore, transient phenomenons i.e. starting up or shutting down processes are not discussed here. These are done manually in the plant. The following section introduces the plant. Modelling of each of the component then follows. Results and discussions are presented in the last section of the paper.

2. THE ORC UNIT

Figure 1 shows the process flow diagram of the ORC unit. It is powered by brine from the geothermal fluid. The brine, which is at about 205°C, passes through the vaporizer-separator providing heat for the ORC unit. Pentane taking heat from the brine changes its phase from liquid to vapor in the vaporizer then superheated in the separator. It is then passes through the turbine producing work. Then it passes through a recuperator before being cooled by an air-cooled condenser. The recuperator recovers some of the heat from the pentane vapor coming from the turbine reducing the heat load in the condenser. The pentane liquid after the cycle-pump passes through the recuperator, where it is heated to an elevated temperature. Then the pentane liquid enters the vaporizer completing the cycle. Figure 2 presents the *T-s* plane presentation of the cycle.

2.1 Modeling of the Components

Following sections present modeling of each of the components. The components are modeled separately and then they are connected to form the model of the geothermal power unit. The model developed for this study were solved using commercial software packages Matlab/Simulink® and gPROMS® (MathWorks 2008; PSE 2008).

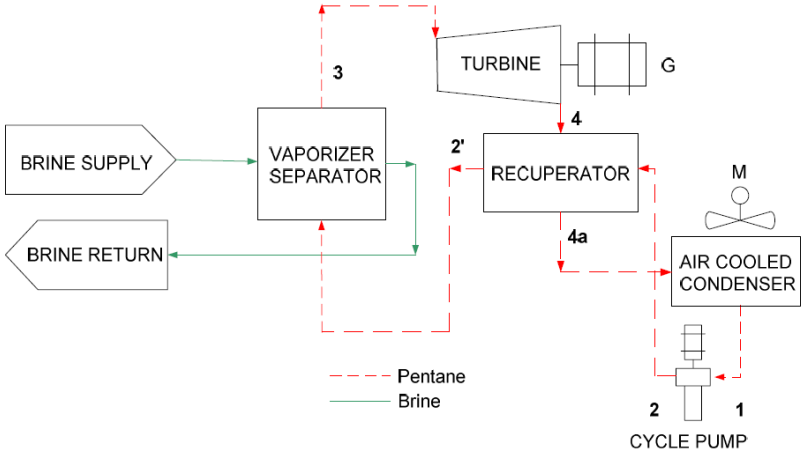

Figure 1: Process diagram of the ORC unit

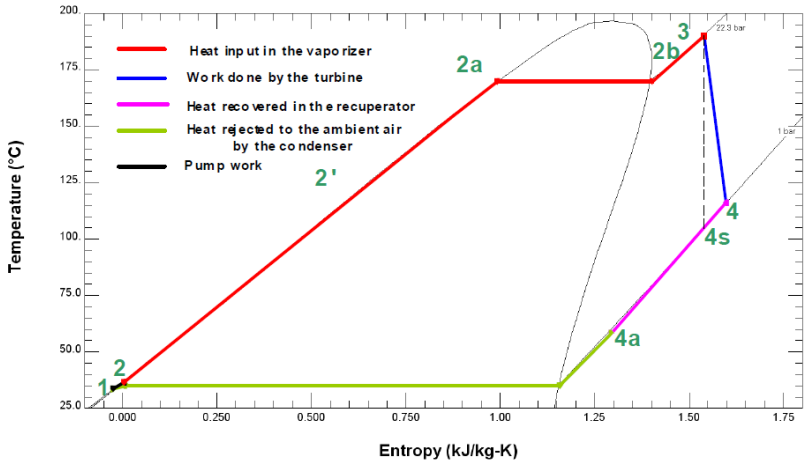

Figure 2: *T,s*-diagram of the ORC

2.2 The vaporizer-separator model

Some of the authors in the literature i.e. (Wei et al. 2008) have used discretization techniques to dynamically model vaporizers and condensers which take into account temperature gradient along the geometry of a heat exchanging device. However, models based on lumped parameters by some other authors i.e. (Bai et al. 2004) have yielded reasonably high accuracy with appropriate assumptions. It also avoids complicated calculations. If Biot number is less than 0.1 then the lumped capacitance method can be applied with reasonably accuracy(Holman 1992).

Figure 3 shows a schematic diagram of the vaporizer-separator. A simplified view of the vaporizer and a simplified view of the separator are presented in Figure 4 and Figure 5, respectively.

Both the vaporizer and the separator are shell and tube type heat exchangers with brine on the tube side and working fluid (pentane) on the shell side. The vaporizer is fitted with a level control arrangement. There are two sensors fixed to two different elevations of the vaporizer. The bottom one is assigned to 0 and top one is 100. The pentane level is kept within this operating range, and if the pentane level goes below 0 or above 100, a shut down sequence is initiated. The vaporizer level indicates quantity (mass) pentane inside the vaporizer/separator know as hold up mass.

The following assumptions were made for the vaporizer model:

1. The temperature and pressure are assumed to be the same for the vaporizer and the lower half of

the separator. Therefore, the holdup mass of pentane vapor in the lower part of separator is added to the total holdup mass of pentane in the vaporizer.

2. There is a temperature gradient in the separator along the diameter towards the vertical direction. To approximate it, the upper half of the separator is assumed responsible for the superheating.
3. The holdup mass of pentane in the upper half of the separator is negligible.
4. Heat capacity of the material of the vaporizer/separator is negligible. The Biot number of combined vaporizer and separator is 0.00433 (<0.1) which justifies such assumption (Holman 1992).
5. Heat loss to the environment is negligible.

Using the above assumptions, the heat balance equation of the vaporizer in lumped parameter form is given as follows:

$$\frac{d}{dt}(M_l h_{2a} + M_v h_{2b}) = \dot{m}_2 h_2 + Q^V - \dot{m}_{2b} h_{2b} \quad (1)$$

Here, M_l is the holdup mass of liquid; h_{2a} is the enthalpy of the holdup liquid; M_v is the holdup mass of vapour; h_{2b} is the enthalpy of the holdup vapour; $\dot{m}_2$ is the mass flow of inlet liquid; h_2 is the enthalpy of inlet liquid; Q^V is the heat input in the vaporizer and lower half of theseparator; and $\dot{m}_{2b}$ is the mass flow of outlet vapour.

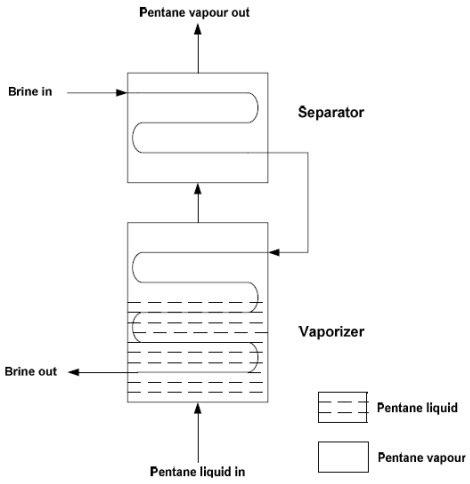

Figure 3: Schematic diagram of the vaporizer and separator

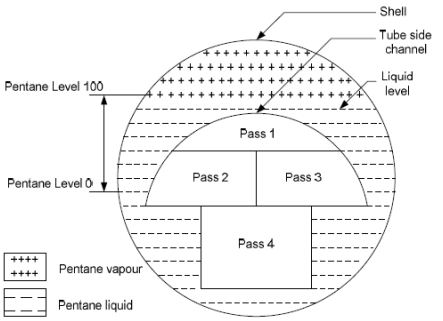

Figure 4: Simplified cross-sectional view of the vaporizer

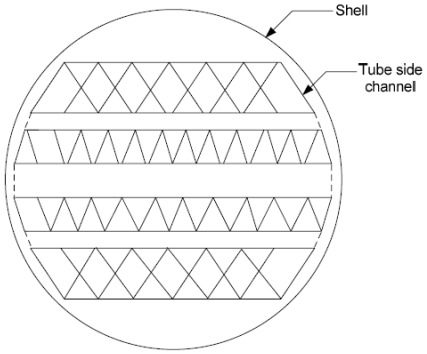

Figure 5: Simplified cross sectional view of the separator

The heat transfer from the brine to the working fluid is calculated from the following equation.

$$Q^T = U^T A^T \Delta t_m^T \quad (2)$$

Where, U^T is the overall heat transfer coefficient, A^T is the total effective heat transfer area of the vaporizer and the separator and Δt_m^T is the combined log mean temperature deference (LMTD) and calculated as:

$$\Delta t_m^T = \frac{(T_{i,B} - T_3) - (T_{o,B} - T_{2a})}{\ln \frac{(T_{i,B} - T_3)}{(T_{o,B} - T_{2a})}} \quad (3)$$

Unfortunately, it is not possible to calculate the LMTD for the vaporizer and the separator separately. In the ORC cycle, the outlet temperature of the brine from the separator before entering the vaporizer is not known. Therefore, the LMTD for the combined vaporizer and separator was used.

The value of the overall heat transfer coefficient for the combined vaporizer and separator is calculated using the following approximated equation as presented by Bai et al. (Bai et al. 2004) taken from experimental results presented by Nakaoka and Uehara (Nakaoka and Uehara 1988).

$$U^T = U_S^T (\dot{m}_B^T / \dot{m}_{S,B}^T)^{0.5} \quad (4)$$

Here, $\dot{m}_B^T$ is the brine mass flow, U_S^T is the standard heat transfer coefficient and $\dot{m}_{S,B}^T$ is the standard brine mass flow.

At first, the total heat transfer is calculated, then it is divided between the separator and the vaporizer in the same ratio as observed, Q^V=87.2% and Q^S=12.8% of Q^T.

Equation 4 is an approximated relationship devised from experimental data from a shell and plate heat exchanger. However, in the ORC unit, the vaporizer and separator are shell and tube type. Therefore, to increase the accuracy of the calculation, iteration was carried out.

At first using equation (4), U^T was calculated. Using equation (2), Q^T was calculated. Now, brine side heat transfer,

$$Q^T = \dot{m}_B c_p (T_{i,B} - T_{o,B}) \quad (5)$$

From the above equation, keeping $T_{i,B}$ constant, the value of $T_{o,B}$ can be calculated. Using the new value of $T_{o,B}$, the value of Δt_m^T, can be calculated and so forth.

From conservation of mass in the vaporizer we get,

$$\frac{d}{dt}(M_l + M_v) = \dot{m}_2 - \dot{m}_{2b} \quad (6)$$

Where, M_l and M_v are holdup masses of pentane liquid and vapor in the vaporizer and lower half of the separator, respectively. $\dot{m}_2$ is the pentane liquid mass flow to the vaporizer and $\dot{m}_{2b}$ is the pentane vapor flow from the vaporizer.

The combined space inside the vaporizer and the separator is constant. As the holdup mass of the upper half is ignored, the following relationships can be expressed for the vaporizer:

$$V_T = V_V + 0.5V_S \quad (7)$$

$$V_T = V_v + V_l \quad (8)$$

$$V_l = M_l / \rho_l \quad (9)$$

$$V_v = M_v / \rho_v \quad (10)$$

Here, V_T is the total volume of the space inside the vaporizer and the lower half of the separator, V_V is the volume of the space inside the vaporizer and V_S is the volume of the space inside the separator. V_l is the volume of the liquid pentane inside the vaporizer and V_v is the volume of the vapor on top of the pentane liquid level and the space of the lower half of the separator. ρ_l and ρ_v are the density of saturated liquid and saturated vapor.

The mass flow of pentane vapor depends on the amount of heat given to the fluid from the brine. From energy balance, the following equation can be derived:

$$\dot{m}_{2b} = \frac{Q^V - \dot{m}_2 (h_{2a} - h_2)}{L_v} \quad (11)$$

Where, L_v is the latent heat of vaporization. The outlet temperature from the separator is calculated depending on the state of the pentane vapor. If $h_{2b} = h_{sat}$ then:

$$T_3 = T_{sat} + \frac{Q^S}{cp\,\dot{m}_{2b}} \quad (12)$$

If $h_{2b} < h_{sat}$ then

$$T_3 = T_{sat} + \frac{Q^S - m_{2b}(h_{sat} - h_{2b})}{cp\,\dot{m}_{2b}} \quad (13)$$

If $h_{2b} > h_{sat}$ then

$$T_3 = T_{sat} + \frac{Q^S + m_{2b}(h_{2b} - h_{sat})}{cp\,\dot{m}_{2b}} \quad (14)$$

Here, the suffix *sat* stands for saturation. All the physical properties needed for equations 9 - 14 are taken from (REFPROP 2007).

$$h_3 = h_{2b} + \frac{Q^S}{\dot{m}_{2b}} \quad (15)$$

Figure 6 represents a simplified view of Figure 4 with an explanation of various parameters. The line *AC* represents the level of pentane in the vaporizer. The volume of vapor above this line can be calculated by multiplying area bounded by *ABC* with the length of the vaporizer. This area is equal to the area bounded by *ABCO* minus the area of the triangle *ACO*.

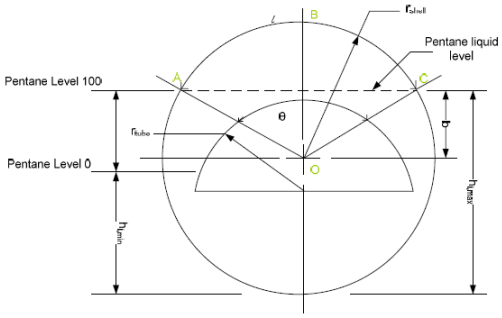

Figure 6: Simplified cross sectional view of the vaporizer

It can be easily shown that for a pentane level higher than or equal to the top of the tube channel, the height of the pentane level from the bottom of the shell, h_l can be calculated from the following equation:

$$V_l = (V^S - V_{tube}) - (\frac{1}{2} r_{shell}^2 (2\cos^{-1}((h_l - r_{shell})/r_{shell})) - (h_l - r_{shell})\sqrt{(2h_l r_{shell} - h_l^2)})\, l_V \quad (16)$$

If the liquid pentane level is lower than the top of the tube channel, h_l can be calculated iteratively from the following equation:

$$V_l = (V^S - V_{tube}) - (\frac{1}{2} r_{shell}^2 (2\cos^{-1}((h_l - r_{shell})/r_{shell})) - (h_l - r_{shell})\sqrt{(2h_l r_{shell} - h_l^2)})\, l_V + (\frac{1}{2} r_{tube}^2 (2\cos^{-1}((h_l - r_{tube})/r_{tube})) - (h_l - r_{tube})\sqrt{(2h_l r_{tube} - h_l^2)})\, l_V \quad (17)$$

Where, h_l is the height of the pentane liquid level from the bottom of the vaporizer, r_{shell} is the internal radius of the shell, r_{tube} is the outer radius of the tube, V_{tube} is the volume (external) of the tube side channel and l_v is the length of the vaporizer.

The liquid level, h_l is explained in Figure 6:

$$h_l = r_{shell} + b \quad (18)$$

The percentage of liquid level is calculated from the following equation,

$$l_{\%} = \frac{(h_l - h_{l,\min})}{(h_{l,\max} - h_{l,\min})} \times 100 \quad (19)$$

Equations 7 - 10 and 16-17 are pure algebraic equations and are a part of a system of differential equations forming a typical higher index problem. An index greater than 1 implies that there are algebraic relations between dynamic variables. A higher index problem can be solved by reducing its index to 1 using dummy derivatives (Mattsson and Siiderlind 1993). gPROMS can solve a high *index* automatically. However, one must provide consistent initial conditions to start simulation. The gPROMS model was exported to Simulink via gO:Simulink interface.

2.3 The turbine model

The response time of a turbine can be in the order of 10-20 s (Jurado et al. 2003) to 1-3 minutes. The available data of the plant operation is for one-hour interval so we are interested in plant performance where unit time is 60 min or an hour. Therefore, the turbines can be assumed to have static behaviour with respect to the unit time of our interest. Ou Bai et al. and Wei et al. (Bai et al. 2004; Wei et al. 2008) have used such static representation of turbine models used for dynamic modelling of binary cycles.

Figure 1 presents *T-s* presentation of a Rankine cycle with the process 3-4_s as an ideal turbine. The work done by an ideal turbine can be calculated knowing the state points 3 and 4_s and calculated as:

$$W_T = \dot{m}(h_3 - h_{4s}) \quad (20)$$

Where, W_T is work done by the turbine, $\dot{m}$ is the mass flow rate of the working fluid through the turbine, h_3 is the enthalpy of the working fluid at point 3 and h_{4s} is the enthalpy of the working fluid at the outlet of the turbine at isentropic condition.

For a reversible adiabatic (isentropic) process, the entropy at the inlet of the turbine must be equal to the entropy at the outlet:

$$s_3 = s_{4s} \quad (21)$$

The losses in the turbine are primarily those related to the flow of the working fluid through the turbine. Heat transfer to the surroundings also represents a loss, but this is of usually of secondary importance. The governing procedures may also cause a loss in the turbine, particularly if a throttling process is used to govern the turbine. The losses associated with irreversibilities cause the turbine efficiency to deteriorate from the ideal.

The efficiency of a turbine (isentropic efficiency) is defied as:

$$\eta_s = \frac{h_3 - h_4}{h_3 - h_{4,s}} \quad (22)$$

The work done by a real turbine is calculated as:

$$W_T = \dot{m}(h_3 - h_4) \quad (23)$$

Heat transferred to the surrounding is not incorporated in the equation 23, as it is the less significant part. In case the heat transfer becomes significant, following equation should be used to calculated actual work done:

$$W_a = W_T - Q_L \quad (24)$$

Where, W_a presents the actual work done by the turbine and Q_L is the heat transfer to the surroundings.

The value of isentropic efficiency is calculated from a developed turbine map. It is reported by many authors i.e. (Erdem and Sevilgen 2006) that ambient temperature has a prominent effect on turbine performance. Therefore, the ambient temperature has been taken into account to develop the maps for this work:

$$\eta_s = \frac{a}{T_{amb}} + b.r_p + c \quad (25)$$

Where, T_{amb} is the ambient air temperature in *K*, r_p is the turbine pressure ratio (inlet to utlet), η_s is the isentropic efficiency and *a, b, c* are constants. Values of the constants are optimized using available plant operation data.

2.4 The recuperator model

The residence time of pentane in the recuperator is in the order of few minutes. Therefore, it can be assumed to have static characteristics. The heat transfer from the turbine outlet fluid to condenser outlet fluid is calculated from the following equation:

$$Q^{Rec} = U^{Rec} A^{Rec} \Delta t_m^{Rec} \quad (26)$$

Where, U^{Rec} is the overall heat transfer coefficient, A^{Rec} is the effective heat transfer area of the recuperator and Δt_m^{Rec} is the log mean temperature deference and calculated as:

$$\Delta t_m^{Rec} = \frac{(T_4 - T_2) - (T_{4a} - T_{2'})}{\ln \frac{(T_4 - T_2)}{(T_{4a} - T_{2'})}} \quad (27)$$

The value of the heat transfer coefficient is calculated using the following approximated equation:

$$U^{Rec} = U_S^{Rec} (\dot{m}_{2b} / \dot{m}_{2b,s})^{0.5} \quad (28)$$

Here, $\dot{m}_{2b}$ is the turbine outlet mass flow, U_S^{Rec} is the standard heat transfer coefficient and $\dot{m}_{2b,s}$ is the standard turbine outlet mass flow.

2.5 The condenser model

The ORC unit uses an air-cooled condenser. The following equation is used to calculate the outlet enthalpy:

$$h_1 = h_4 - \frac{Q_{con}}{\dot{m}_{2b}} \quad (29)$$

Modelling assumptions for the condenser are listed below:

- The mass flow rate is conserved.
- The minimum temperature of the condenser is 7°C more than the saturated temperature of the pentane at the prevailing pressure in the condenser.
- There is a minimum temperature difference of 8°C between the ambient temperature and the condenser outlet temperature to provide heat transfer from the pentane to the ambient air.
- Lumped heat capacity method was used for the calculation. The calculated Biot number of the fins is 8.4 X 10^{-6} . It is much less than 0.1, the criterion for such analysis (Holman 1992).

2.5.1 Calculation of heat transfer coefficient of horizontal inside tubes

The equations used to model heat transfer coefficients are taken from (Mueller 1992). The equation for heat transfer coefficient is calculated from the following equation of horizontal tubes assuming a stratified layer:

$$\alpha_i = \Omega \left[\frac{k_l^3 \rho_l (\rho_l - \rho_g) g \Delta h_v}{\eta_l d_i (T_{sat} - T_w)} \right]^{1/4} \quad (30)$$

Where, ρ_l is the density of fluid at a liquid state, ρ_g is the density of fluid at a vapour state, η_l is the dynamic viscosity, T_{sat} is the saturation temperature, T_w is the wall temperature and Δh_v is the change in enthalpy.

$$\Omega = 0.728 \left[1 + \left(\frac{1 - x_g}{x_g} \right) \left(\frac{\rho_g}{\rho l} \right)^{\frac{2}{3}} \right]^{-3/4} \quad (31)$$

2.5.2 Calculation of heat transfer coefficient of horizontal outside tubes

The condenser tubes have circular fins attached to them. While calculating the total heat transfer from a finned tube, one must take into account the heat transfer through the fins as well. The weighted heat transfer coefficient for the finned tube is:

$$\alpha_o A_t = \alpha (A_f \eta_f + A_r) \quad (32)$$

Where, A_r is the surface of the tube that is not covered by fins, A_f is the surface of the fin and A_t is the total surface area, $A_t = A_f + A_r$. The fin efficiency, η_f for the condenser tube is taken as 75%, which is a typical value.

The average Nusselt number for a finned tube in a bank with a staggered tube arrangement with the number of rows less than 4 can be calculated using following equation

$$Nu = 0.19 \left(\frac{a}{b}\right)^{0.2} \left(\frac{s}{d}\right)^{0.18} \left(\frac{h}{d}\right)^{-0.14} \mathrm{Re}^{0.65} \mathrm{Pr}^{0.33} \quad (33)$$

Where, $a = s_1 / d$, $b = s_2 / d$, s_1, s_2 are transverse and longitudinal bank pitch, and s is fin spacing. This equation is valid in the range $10^2 <$ Re < 2 X 10^4.

$$Nu = \frac{\alpha d}{k} \quad (34)$$

and

$$\mathrm{Re} = \frac{\rho w d}{\eta} \quad (35)$$

Where d is the tube diameter at the fin base and w is the maximum velocity of the fluid, which occurs at the minimum free cross section of the finned-tube bank (Figure 7).

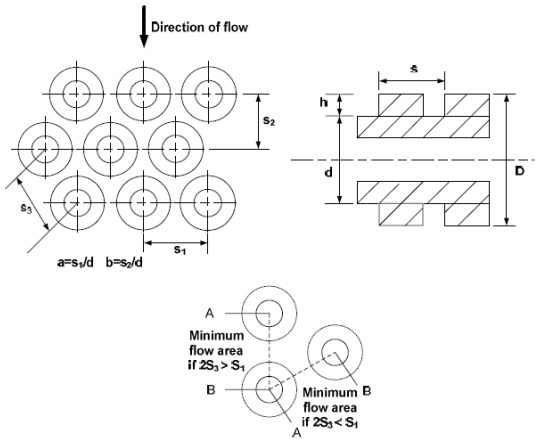

Figure 7: Definitions of quantities for flow in finned-tube banks.

The overall heat transfer from a finned-tube heat surface can be obtained using the following equation:

$$\frac{1}{U^C} = R_{fi}\left(\frac{A_t}{A_i}\right) + \frac{1}{\alpha_i (A_i / A_t)} + \frac{b_w}{k_w (A_{nb} / A_t)} + \frac{1}{\alpha_0} + R_{fo} \quad (36)$$

Where, R_{fi} = fouling resistance on the inside surface; A_i = inside surface area; A_{nb} = means the bare surface area; b_w = tube wall thickness; R_{fo}= fouling resistance on the outside surface.

The total amount of heat rejected from the condenser is calculated using the following equation:

$$\dot{Q}^C = U^C A_t^C \Delta t_m^C \quad (37)$$

Logarithmic mean temperature difference (LMTD) needed in the above equation is calculated as:

$$\Delta t_m^C = \frac{T_o - T_{amb}}{\ln\left[(T_w - T_{amb})/(T_w - T_o)\right]} \quad (38)$$

Where, T_o and T_{amb} are outlet and inlet temperatures of cooling air, respectively. T_w is the wall temperature and it is approximated with reasonably good accuracy as:

$$T_w = (9.T_{sat} + T_{amb})/10 \quad (39)$$

The fluid properties are evaluated at an average (bulk) temperature:

$$T_b = \frac{T_1 + T_{4a}}{2} \quad (40)$$

In equation 38, the outlet temperature of air, T_o is not known and is calculated iteratively. As an initial guess, T_o is taken to be the same as T_w. From the air side energy balance the heat transfer rate can be calculated:

$$\dot{Q}^C = U^C A_t^C \Delta t_m^C = \dot{m}\, Cp(T_o - T_i) \quad (41)$$

The initial LMTD can be calculated using the above mentioned equation. From this value of LMTD a refined value of T_o can be calculated iteratively, using equation 38. Finally, using the obtained T_o, a better approximation of LMTD is obtained.

Free convection occurs at the headers (where condenser tubes are connected in bundles at the inlet and outlet) of the condenser and pipeline from the condenser to the recuperator. However, it was found that the quantity of heat transfer is very low (approximately 0.05%) compared to that of the condenser itself. Therefore, the effect of heat transfer through headers and pipeline are not taken into consideration. The simplified equation for free convection from a horizontal cylinder surface to air at atmospheric pressure under laminar flow condition was used for the analysis (Holman 1992).

The outlet temperature of the header depends on the holdup mass in the header and is calculated from the following equation:

$$M^c \frac{T_1}{dt} = \dot{m}_P (T_1' - T_1) \quad (42)$$

Here, c_p is assumed to be constant, therefore is cancelled out from both sides of the equation. M^c represents the holdup mass in the condenser header and T_1' presents pentane inlet temperature to the condenser header and calculated using h_1 and saturation pressure.

2.5 The cycle pump

It was found for the designed values, the ratio between the total enthalpy of pentane at the cycle pump outlet and the combined heat input at the recuperator and the vaporizer is about 1.03%, which implies that the effect change of pump output pressure (enthalpy) is insignificant compared to the total heat input. Therefore, the pump work can be assumed constant (Wei et al. 2007). The pump outlet pressure has been fixed at 23 bar for the simulation carried for this work. Moreover, the pump is also assumed to have static characteristics same as the turbine because of its fast response.

2.6 The pressure drops in pipes and valves

The pressure drops in various valves are assumed negligible. The valves operating in the pentane cycle include the vaporizer pentane-level control valve, situated between the cycle pump and the vaporizer, and the flow control valve situated just after the vaporizer and the turbine inlet. In a typical operation of the plant, the flow control valve is set to its maximum and therefore its effect can be ignored.

There are a few other valves attached to the unit, which are not used in normal operation of the plant. Such valves include the bypass valve from the vaporizer to the condenser and the valve for the purge system. The bypass valve is a safety system and only operates in emergencies. The purge systems are actuated when backpressure builds up in the condenser. Although there is an automated purge system working in the unit, its response is very slow and most of the time it is done manually. Therefore, it is beyond the scope of this work.

For flow through pipes, there exist major and minor losses (Potter and Wiggert 2002). For simplicity of the model, only major losses are considered:

$$h_{loss} = f\frac{l}{d}\frac{v^2}{2g} \quad (43)$$

However, an easy to use model for pressure drop (Wei et al. 2008) has been adopted for the modelling:

$$\frac{\dot{m}}{\dot{m}_s} = \sqrt{\frac{\Delta p}{\Delta p_s}\cdot\frac{\rho}{\rho_s}} \quad (44)$$

Here, suffix s stand for standard or observed value.

2.7 The turbine-generator coupling

A generator is coupled to the turbines and has heavy rotating parts. However, in normal operations, the generator is maintained at a constant speed so the effect of the inertia of angular velocity does not affect the electrical power output. With a change in thermal power output, the speed of the generator changes and there is a control arrangement to adjust its speed. The target speed for this generator is 1500 rpm. The change in electrical power output is the sum of

change of thermal power output and change of angular momentum of the generator shaft:

$$\frac{dP_{el}}{dt} = \frac{d}{d\tau}(\eta_{el}.P_{th}) + \frac{d}{d\tau}(\frac{1}{2}I\omega^2) \quad (45)$$

Where, P_{el} is the electrical power output, P_{th} is the thermal power output, η_{el} is the electrical energy conversion efficiency and assumed to be constant, I is the mass moment of inertia and ω is the angular velocity. It is easy to show from the above equation that:

$$P_{el} = \eta_{el}.P_{th} + \frac{1}{2}I(\omega^2 - \omega_0^2) \quad (46)$$

Where, ω_0 is the angular velocity at time, $t = 0$. Now, it is known that electric power produced in a generator is proportional to its angular velocity:

$P_{el} \propto \omega$, or,

$P_{el} = k\omega$,

or $\omega = \frac{P_{el}}{k}$ (47)

Putting this value in equation 46 one gets:

$$P_{el} = \eta_{el}.P_{th} + \frac{1}{2}I(\frac{P_{el}^2}{k^2} - \omega_0^2) \quad (48)$$

2.8 Results and discussion

The simulation was carried out for 1000 hours of operation of the power generating unit. The ambient temperature and the brine mass flow rate were supplied to the model and it predicted the performance of ORC unit accordingly. Figure 8 summarises the ambient temperature for the 1000 hours of operation. The ambient temperature has both daily change and seasonal change. The seasonal change in temperature is easily understood from the Figure 8. To show how ambient temperature changes over a typical day, a magnified view of the marked area is presented in Figure 9. The condenser performance is directly related to the ambient temperature and consequently the electrical power output. Further discussion is presented later in this section. Figure 10 summarises the brine mass flow rate used for the simulation. Both the ambient temperature and the brine flow rate are actual values of an hour interval for 1000 hours of operation of the plant.

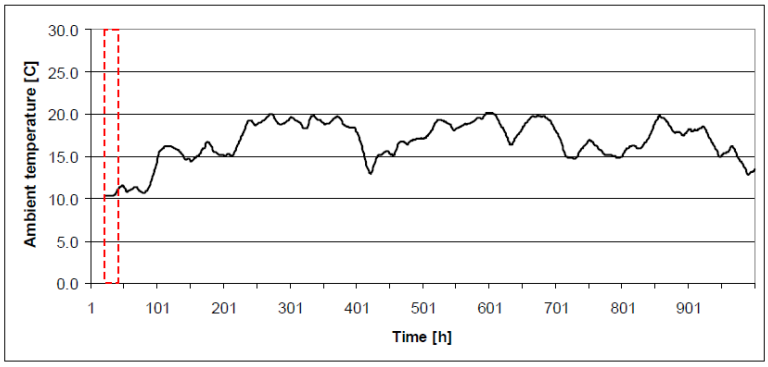

Figure 8: Ambient temperature of the plant vicinity for 1000 hours of operation of the ORC unit (averaged 24 hours).

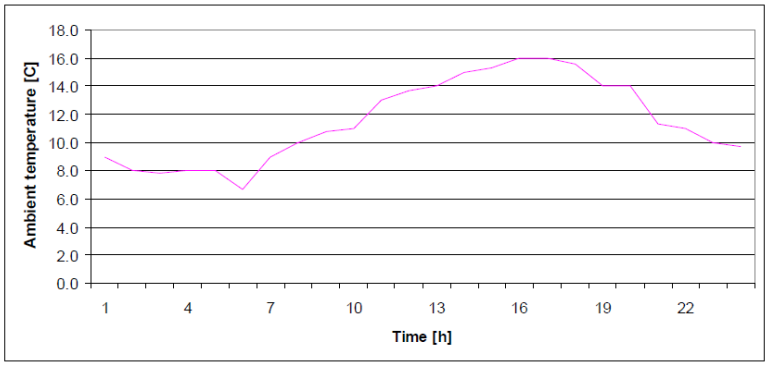

Figure 9: Ambient temperature of the plant vicinity for a day operation of the ORC unit.

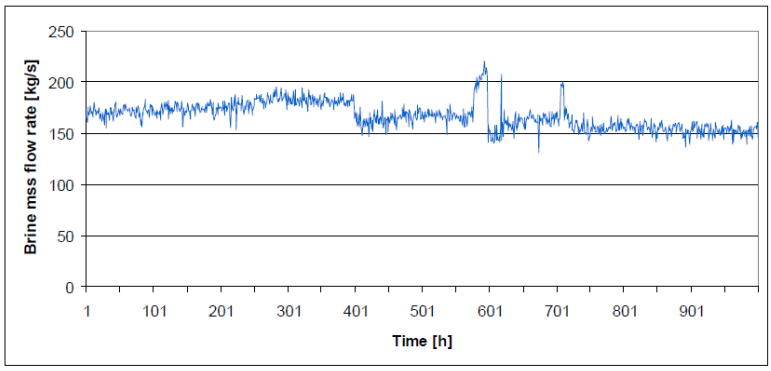

Figure 10: Brine mass flow rate for 1000 hours of operation of the ORC unit.

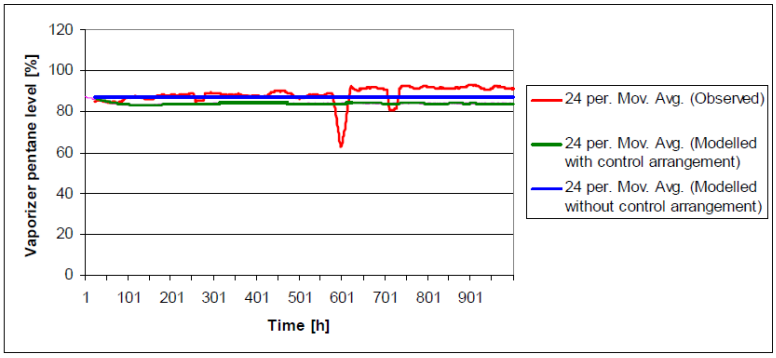

Figure 11: Vaporizer pentane level for 1000 hours of operation of the ORC unit

2.8.1 The vaporizer pentane level

The pentane level in the vaporizer plays a very significant role in the system dynamics. There is a feedback control mechanism to control the pentane level. An operator gives a set point (reference value) from the key board as judged appropriate depending on their experience. Once a set point is provided, it takes about 10-15 minutes for the controller to change the pentane level from its original to the new set point. After the controller takes over, the pentane level does not change significantly. The controller does not take into account the flow rate of the pentane outlet of the vaporizer directly but measures the pentane level. The pentane mass flow is a direct consequence of the of the heat transfer from the brine to the pentane in the vaporizer and the quantity of heat transfer is dependent mainly on the brine flow rate as the brine is fed at a constant temperature. The brine flow rate has changed significantly over time from the designed value or even from the state when the plant was first built. In case of abrupt change in the brine mass flow, the operators change the pentane level's set point and there is also a control mechanism which bypasses the pentane vapour in case of a sudden increase in pentane vapour generation. A PID Simulink block has been used (P=0.8; I= 0.01; D= 0.01) as the controller.

If the level control mechanism works properly, other than from the effect of sudden change in brine mass flow, the pentane level in the vaporizer can be assumed to have an insignificant effect. Figure 11 compares the actual pentane level, the pentane level with the feedback control having its level set point at 84% and the pentane level without feedback control. It can be seen from Figure 11 that, at about 75 hours of operation of the unit, the model with feedback control gives a better match with the actual value. However, over time, it changes and the model without the feedback controller gives a close match. By choosing an appropriate value of the set point of the pentane level, the feedback control will eventually give a better result than the model without feedback control. However, a feedback loop is associated with a long simulation time and clumsy calculations. As can be seen from the Figure, the difference in result between the model without feedback control and the actual is not very significant and it can be assumed that the control mechanism is in use and it makes the pentane level follow a set point. This will save a lot of calculations and consequently computation time at the expense of accuracy. Nonetheless, the model without feedback control produces reasonably accurate results. All the results of simulation presented in this section use no feedback control for the vaporizer pentane level.

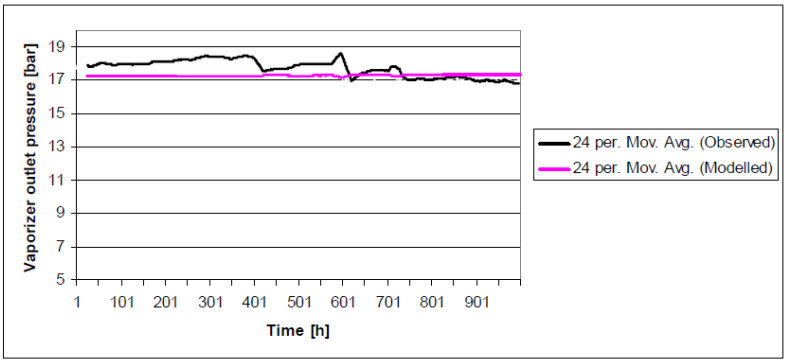

Figure 12: Vaporizer outlet pressure for 1000 hours of operation

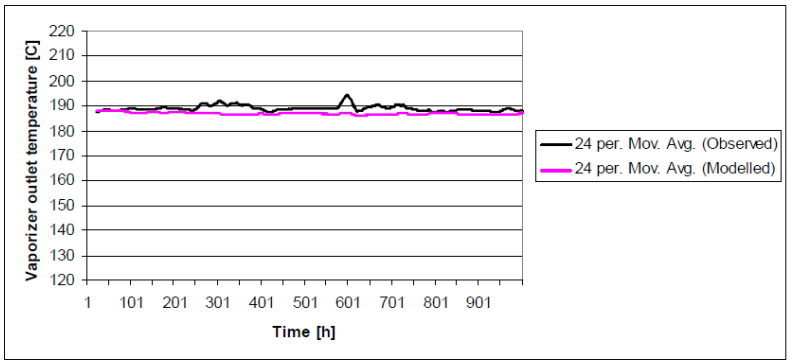

Figure 13: Vaporizer outlet temperature for 1000 hours operation

2.8.2 The vaporizer outlet pressure

Figure 12 presents the observed and modelled vaporizer outlet pressure for 1000 hours of operation of the vaporizer. A reasonably close match is easily perceived and the average percentage error is found to be 3.5%. The maximum value of percentage error is quite high (9.27%), and this occurred due to abrupt change in the mass flow of brine. This error occurred at 579 hours of operation which is the peak of a sudden change of mass flow (Figure 10). There were two big peaks of sudden mass flow change at around 580 hours and 700 hours that stayed for a while. These two peaks had a significant effect on the simulation results whereas they do not have the same significant effect on actual operations as these peaks are normally tackled by operators by changing the pentane level, bypassing excess pentane to the condenser, operating the purge system of the condenser manually, and the speed control system of the turbines etc. Therefore, the inability to control these peaks can be considered as a limitation of the developed model. Further models can be developed with capabilities to manage the effect of sudden change; however, the main idea of modelling the power plant is to predict future plant performance depending on geothermal resources and weather. With sudden changes in resource characteristics and weather, plant operators can take over the control from the automatic control. The legitimacy of not developing a model with ability to tackle sudden changes relies on it.

2.8.3 The vaporizer outlet temperature

Figure 13 shows the observed and the modelled pentane temperatures at the vaporizer outlet. The average percentage error is found to be 1.1% and the percentage error has a maximum value of 5.14%. A good match between the actual and the modelled vaporizer temperatures is very important. The state of the pentane vapour (p, T, h) at the vaporizer outlet dictates how much energy is available to produce power as the turbine outlet pressure is given to the model externally. In actual plant operation, the turbine outlet pressure does not change much and it is related to the condenser pressure.

2.8.4 The electric power output

Figure 14 presents the comparison of the actual and modelled electric power output from the ORC unit. It is evident from the figures (14-15) that the developed model is capable of predicting both daily and seasonal load changes. The average percentage error is 4.8%. All error is calculated as absolute value and the maximum value of percentage error is very high (31.46%). This error occurred at 619 hours of operation for the same reason as discussed in previous paragraphs. There are two peaks of brine mass flow at about 579 and 720 which are taken care of by operators and the control mechanism in place in actual plant operations. The error in vaporizer outlet temperature however, was not much affected by this sudden change in brine mass flow; the main reason behind it is that the dynamics of temperature change

are associated with very large mass (pentane mass itself, vaporizer mass, separator mass, pipes mass, condenser mass etc.) and it is much slower than the dynamic of the turbine. Nonetheless, the model is very competent in predicting performance in normal operations of the plant and if a saturation block is used which limits mass flow rate to imitate the bypass mechanism, the performance of the model can be improved (Figure 16). The average percentage error is 4.5% and the maximum value is 27.18%.

2.8.5 The condenser outlet temperature

Figure 17 presents the condenser outlet temperature of the unit for 1000 hours of operation. It is very clear from the Figure that the modeled condenser outlet temperature follows the observed values very competently. However, the temperatures are measured in °C and are low. Therefore, the relative errors are high. The average of percentage error is 10%, but if we use temperature in absolute scale, the average percentage error would be very low 0.89%, with the maximum values of percentage error is 4.03%.

2.8.6 The brine outlet temperature

Figure 18 shows the observed vs. modelled brine outlet temperature and a close match between the two values is clear. The average percentage error is 1.43% and the maximum value is 6.90%. All error is calculated as absolute value and it can be seen from the Figure that the typical value of the brine outlet temperature is about 140°C.

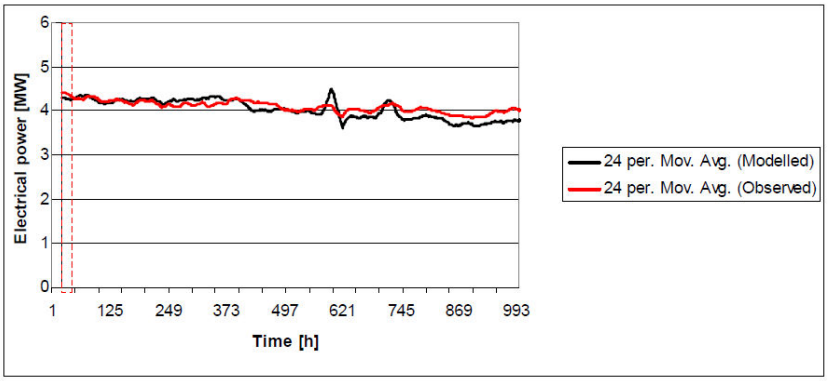

Figure 14: Electrical power output for 1000 hours of operation

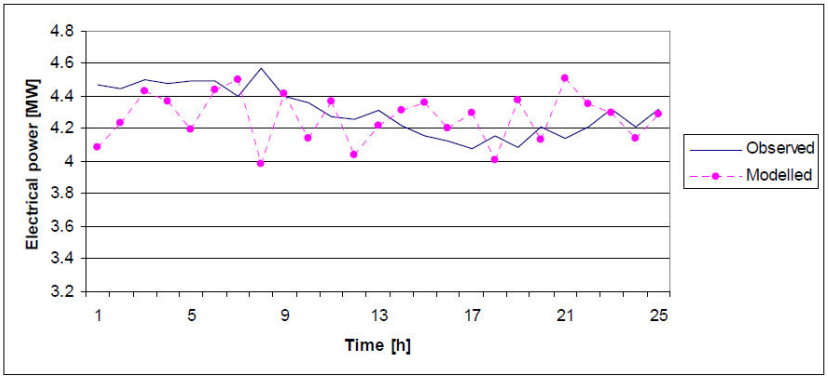

Figure 15: Electrical power output for a day's operation

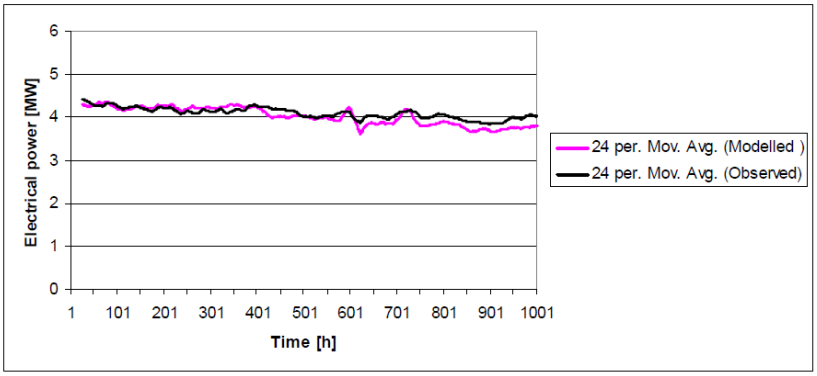

Figure 16: Electrical power output for 1000 hours of operation with a maximum pentane mass flow of 48.5 kg/s

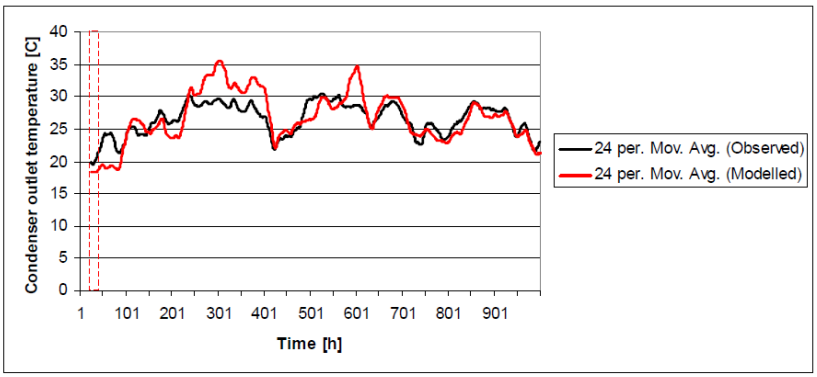

Figure 17: Condenser outlet temperature for 1000 hours

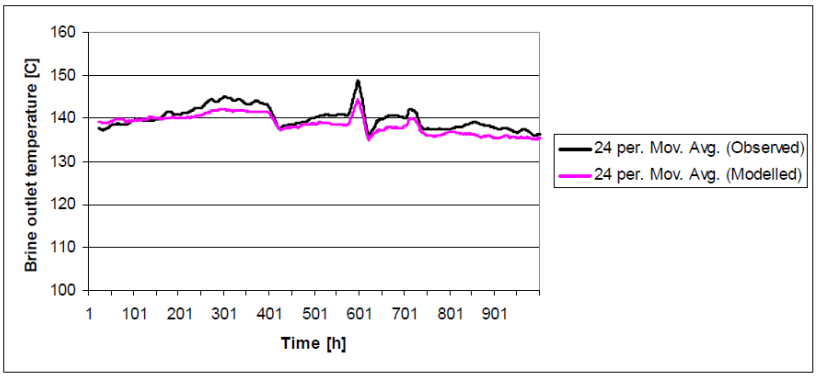

Figure 18: Brine outlet temperature for 1000 hours operation

2.9 Conclusions

Steady state model of geothermal power plants are commonly available in the literature. However, dynamic models are not very common. In this paper a dynamic model of an ORC unit of a geothermal power plant is presented. The model takes into account effect of internal and external parameters, which are necessary to simulate the plant performance with reasonable accuracy. The results of simulation are also presented and compared against the plant performance data. It was found that the developed model is competent to predict the plant performance with reasonably high accuracy. The average percentage error of electric power output remains within 5%.

REFERENCES

Bai, O., Nakamura, M., Ikegami, Y., and Uehara, H. (2004). "A Simulation Model for Hot Spring Thermal Energy Conversion Plant With Working Fluid of Binary Mixtures." *Journal of Engineering for Gas Turbines and Power*, 126(3), 445-454.

Casella, F. (1999). "PhD Thesis: Modelling, Simulation, and Control of a Geothermal Power Plant," PhD, POLITECNICO DI MILANO, MILANO.

Erdem, H. H., and Sevilgen, S. H. (2006). "Case study: Effect of ambient temperature on the electricity production and fuel consumption of a simple cycle gas turbine in Turkey." *Applied Thermal Engineering*, 26(2-3), 320-326.

Holman, J. P. (1992). *Heat Transfer*, 7 Ed., McGraw-Hill.

Jurado, F., Cano, A., and Carpio, J. (Year). "Enhancing the Distribution System Stability Using Micro-Turbines and Fuel Cells." *Proceedings of the IEEE Power Engineering Society Transmission and Distribution Conference*, 717-722.

MathWorks. (2008). "www.mathworks.com."

Mattsson, S. E., and Siiderlind, G. (1993). "A New Technique for Solving High-Index Differential-Algebraic Equations Using Dummy Derivatives." *SIAM journal on scientific computing* 14(3), 677-692

Mueller, A. C. (1992). *Hand Book of Heat Exchanger Design*, Begell House, Inc.

Nakaoka, T., and Uehara, H. (1988). "PERFORMANCE TEST OF A SHELL-AND-PLATE TYPE EVAPORATOR FOR OTEC." *Exper Therm Fluid Sci*, 1(3), 283-291.

Potter, M. C., and Wiggert, D. C. (2002). *Mechanics of Fluids*, 3rd Ed., Bill Stenquist.

Pritchard, G. (2002). "The must-run dispatch auction in an electricity market." *Energy Economics*, 24(3), 199-216.

PSE. (2008). "Process Systems Enterprise Ltd. http://www.psenterprise.com/."

REFPROP. (2007). "National Institute of Standards and Technology (NIST), http://www.nist.gov/." <http://www.nist.gov/>.

Wei, D., Lu, X., Lu, Z., and Gu, J. (2007). "Performance analysis and optimization of organic Rankine cycle (ORC) for waste heat recovery." *Energy Conversion and Management*, 48, 1113–1119.

Wei, D., Lu, X., Lu, Z., and Gu, J. (2008). "Dynamic modeling and simulation of an Organic Rankine Cycle (ORC) system for waste heat recovery." *Applied Thermal Engineering*, 28(10), 1216-1224.

Appendix 12: Publication 3
Sohel, M.I., Sellier, M., Brackney, L.J. and Krumdieck, S. An iterative method for modelling the air-cooled organic Rankine cycle geothermal power plant. Int. J. Energy Res. (2010), DOI: 10.1002/er.1706.

An iterative method for modelling the air-cooled organic Rankine cycle geothermal power plant

1. M. Imroz Sohel[1,*],
2. Mathieu Sellier[2],
3. Larry J. Brackney[3],
4. Susan Krumdieck[2]

Article first published online: 29 APR 2010

DOI: 10.1002/er.1706

Issue

International Journal of Energy Research

Volume 35, Issue 5, pages 436–448, April 2011

Keywords:

- geothermal power plant;
- air-cooling;
- organic Rankine cycle;
- performance analysis

Abstract

This work presents an iterative method for modelling the effect of ambient air temperature on the air-cooled organic Rankine cycle. The ambient temperature affects the condenser performance, and hence the performance of the whole cycle, in two ways. First, changing the equilibrium pressure inside the condenser, the turbine outlet pressure and the turbine pressure ratio vary. Since the turbine pressure ratio is a major parameter in determining the power generated by a turbine, the plant output is directly affected. Second, changing the condenser outlet

temperature with ambient temperature, the pump inlet and outlet conditions are changed. Thus, the vapourizer equilibrium temperature and pressure are influenced. The developed method iteratively seeks the equilibrium conditions for both the condenser and vapourizer. Two case studies based on a real plant performance have been carried out to demonstrate the validity of the method. The developed method demonstrates robustness and converges regardless of the initial conditions allowed by the physical properties of the working fluid. This method is effective for cycles that use saturated vapour as well as superheated vapour under static or dynamic conditions with appropriate initial conditions and constraints. The developed method may be applied to any Rankine cycle with closed cycle operation.

Appendix 13: Publication 4

M. Imroz Sohel, Susan Krumdieck and Mathieu Sellier, Adaptive design approach for geothermal plant with changing resource characteristics, *World Renewable Energy Congress 8-11 May 2011, Linköping, Sweden* (Accepted).

An adaptive design approach for a geothermal plant with changing resource characteristics

M. Imroz Sohel[1,*], Mathieu Sellier[2], Susan Krumdieck[2]

[1] *Scion, Te Papa Tipu Innovation Park, 49 Sala Street, Rotorua, New Zealand*
[2] *Department of Mechanical Engineering, University of Canterbury, Private bag 4800, Christchurch, New Zealand*
* *Corresponding author. Tel: +64 7 3435730; fax: +64 7 3435375; E-mail address: mohammed.sohel@scionresearch.com*

Abstract: Geothermal power plants are designed for optimal utilization of geothermal resource. However, geothermal fields typically undergo significant changes in resource characteristics such as pressure, temperature and steam quality over their life span. With appropriate reservoir modelling it is possible to predict the future resource characteristics of a geothermal field to a reasonable degree of accuracy. We propose a new adaptive design approach that would allow geothermal power plants to take into account the change of resource characteristics that occur over a 30-40 years time horizon based on the results of reservoir modelling. Currently, it is difficult and expensive to modify or renovate an existing plant due to space constraints, piping arrangements, transportation of machinery etc. The adaptive design approach would allow cost effective modifications in operation and equipment to adjust to changes in resource characteristics in the future. A simple model for a typical combined cycle geothermal power plant is considered as a test case for the adaptive design approach. Simulation is carried out using changes in both wellhead specific enthalpy and mass flow rate. There are four case studies presented in this paper that analysed various possible options of the hypothetical power plant depending on the changes in resource characteristics. Taking into account the results of the simulation, alternative plant designs are presented and improvements in performance are discussed. Although, the initial investment cost might go up as a consequence of adaptive design, over the life span of the plant the total benefit may be greater.

Keywords: *Geothermal power, resource characteristics change, adaptive design, low temperature power source.*

1. Introduction

We are at a point of time when on one hand, the negative effects of anthropogenic atmospheric alteration are more evident than ever, and on the other, the demand for energy is ever increasing. Although it claimed that there exists a vast reserve of fossil fuel, field by field petroleum production is decreasing [1]. The huge challenge of emission reduction, growing energy demand and peak oil can be approached in two ways. Firstly, by improving energy conversion efficiency of traditional energy sources and secondly, switching to more and more renewable energy sources. Unfortunately, most renewable energy sources are dependent on climatic variation and are not suitable for base load operations. Geothermal energy, on the contrary, provides a clean, reliable source of renewable energy. Energy concentration in geothermal sources is much higher than in many other renewable sources. Moreover, geothermal power plants are considered to have significant lower CO_2 emissions than a standard combined cycle power plant or a pulverized coal fired power plant [2].

Current research and development trends towards geothermal power generation, specifically, low temperature power cycles are noticeable [3-12]. Geothermal power plants are generally designed based on constant resource characteristics. However, it has been observed in many plants that the resource characteristics change significantly throughout the lifetime of the plant [13]. Consequently, deterioration of plant performance and unplanned design changes

occur. However, geothermal power plants are very capital intensive and it is not very easy to change a plant to adapt to resource characteristics different from the original design.

By appropriate reservoir modelling, it is possible to predict future resource characteristics depending on various parameters including the rate of resource utilization, the percentage of brine reinjection etc [14]. In this paper we propose an adaptive design approach where provisions are kept for a plant to adapt to resource characteristics changes at the time of building which may save a great deal of effort and money in the long run. We have presented several case studies to demonstrate the benefit of the adaptive design approach.

2. Methodology

We have taken a hypothetical combined cycle geothermal power plant for our study. The geothermal fluid is a mixture of steam and brine. Steam is separated from the brine in a suitable separator then used to power a steam turbine. The exhaust steam from the steam turbine is used to power bottoming organic Rankine cycle units (BOT-ORC). The separated brine is also used in other organic Rankine cycle units (BRN-ORC). After the heat recovery, both condensed steam and geothermal brine are mixed together and reinjected to the reservoir. Pentane is used as the working fluid in the binary cycles. Fig. 1 shows a schematic of the hypothetical power plant. The base case considered here has four BOT-ORCs and two BRN-ORCs as presented in Fig. 1.

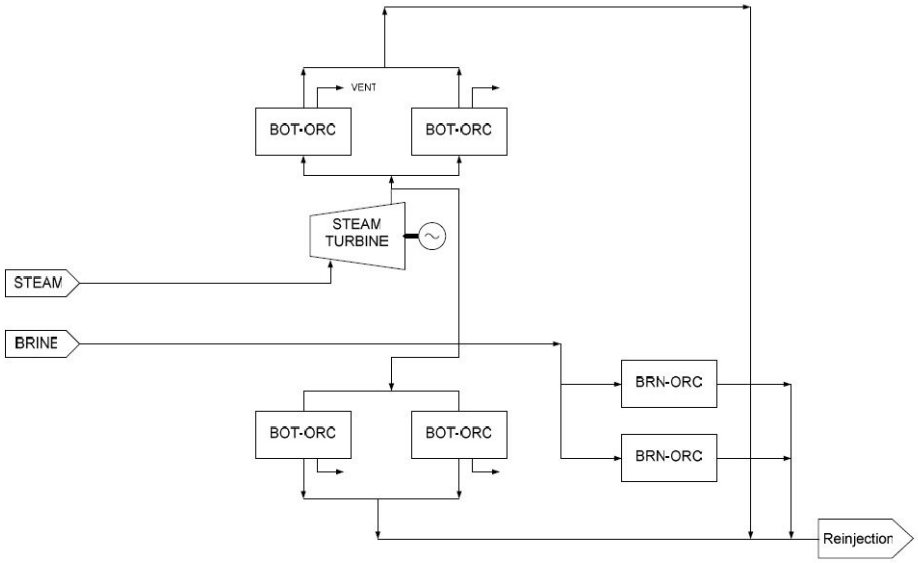

Fig. 1. Schematic diagram of the combined cycle geothermal power plant.

2.1. The component model

Simple models have been used for the analysis presented here. Independent component modules are developed in Matlab/Simulink [15] which can be connected later to develop a system model. The thermo-physical properties are calculated using the REFPROP [16] database. The working fluid flow round the cycle and each process may be analysed using the energy conservation, mass conservation and entropy generation applied to a system boundary around each system component. Changes in kinetic energy and potential energy may be

neglected and equilibrium conditions can be assumed at the cross-sections of both inlet and outlet. Detailed discussion on the modelling of these ORCs is available in our previous work [9].

2.2. The Resource Affected Performance Model

A geothermal field passes through four different phases or periods [13]: (1) development, (2) sustainment, (3) decline and (4) renewable. During the last phase, a geothermal resource approaches the ideal of a sustainable and renewable resource. To attain this pahse requires prudent management of the resource. In a Resource Affected Performance Model (RAPM) we change the geothermal resource characteristics and observe the effect on plant performance. We assume that the reservoir modelling predicts that the geothermal resource enthalpy will increase from about 1400 kJ/kg to 2000 kJ/kg over the life time of the power plant. An adaptive design approach is discussed here which keeps provision for this change in resource characteristics.

Applying conservation of mass at the well head

$$\dot{m}_T = \dot{m}_b + \dot{m}_s \tag{1}$$

where, $\dot{m}_T$ is the total mass flow rate at the well head, $\dot{m}_b$ is the brine mass flow rate and $\dot{m}_s$ is the steam mass flow rate. Dividing Eq. (1) with $\dot{m}_T$ yields

$$1 = C_b + C_s \tag{2}$$

where, C_b is defined as brine content and C_s is defined as steam content. It is advantageous to express resource characteristics as steam content (C_s). Applying energy balance at the well head

$$\dot{m}_T h_R = \dot{m} h_b + \dot{m} h_s \tag{3}$$

where, h_R is the resource enthalpy, h_b is the enthalpy of the brine (saturated liquid) and h_s is the enthalpy of the steam (saturated vapour). The reinjection temperature is calculated from the energy balance of mixing of brine and condensate before reinjecting to the geothermal field.

$$\dot{m}_T h_{RNG} = \dot{m}_b h_b + \dot{m}_c h_c \tag{4}$$

where *RNG* stands for reinjection, *b* stands for brine and *c* stands for condensate.

From Eq. (2), if the steam content of a geothermal field (C_s) increases, the brine content (C_b) must be reduced and vice versa. If we want to keep $\dot{m}_b$ and h_b unchanged as C_s increases or decreases, we must manipulate parameters of the left hand side of Eq. (3). Since, h_R is the parameter characterised by geothermal resource, we may not want to manipulate it. The only suitable solution would be to control the geothermal fluid flow rate ($\dot{m}_T$). When C_s increases, we can keep $\dot{m}_b$ constant by using condensate recirculation and increased geothermal fluid

flow rate ($\dot{m}_T$). If we are interested only on the constant heat transfer in the vaporizer, the reinjection temperature (i.e. brine outlet temperature) can be lowered. The following assumptions are made for the RAPM.

1. Operating state points of the geothermal power plant remain unchanged i.e., the change in mass flow rate in steam and brine are only responsible for the change in overall heat transfer coefficient.
2. To control the vaporizer steam outlet condition, excess steam is vented to the atmosphere.
3. The off-design well-head condition is always within the wet-steam zone i.e., there is no change in temperature at the well head and the geothermal fluid is a mixture of steam and brine.

3. Results

There are four case studies presented which analyze adaptive design approach to address the change in geothermal resource characteristics. These case studies present four possible solutions for the assumed future resource characteristics.

3.1. The base case

Normally, each turbine has an operating limit and for the steam turbine it has been fixed to 37 MW. For the pentane turbine the maximum power is fixed at 7 MW. Fig. 2 shows the plant output in the base case as the resource enthalpy increases. With increasing steam content from about 25% (1400 kJ/kg) to about 35%, the steam turbine reaches its maximum and produces the same power thereafter. Since the steam turbine is unable to utilize the excess steam, the bottoming cycle is receiving condensate at an elevated mass flow rate. Therefore, the power output of the BOT-ORC increases and owing to a lack of brine, the BRN-ORCs are producing much less than their capacity.

3.2. Case study 1: increased geothermal fluid flow rate

The reduced brine flow problem can be tackled in many ways. If one uses excess geothermal brine to reheat the condensate collected from the BOT-ORC, an increased mass flow of brine can be ensured for the BRN-ORC. Fig. 3 presents a schematic diagram of such a design. Here, more power is being produced at the expense of more geothermal fluid, which means the resource is being utilized at a higher rate; not necessarily ensuring optimum utilization. Fig. 4 shows a corresponding improvement in plant performance by adopting this approach. It is noticeable from Fig. 4 that the BRN-ORC produces gradually less power from 25% steam content to 35% then its power production is independent of steam content. Since, it is more efficient to directly expand steam in a turbine to produce power than in bottoming cycle, one should utilize as much steam as possible in the steam turbine within its manufacturing limit. By increasing the geothermal fluid flow rate, the brine reinjection temperature does not change much.

3.3. Case study 2: upgrading the steam turbine

Fig. 5 shows the performance of the geothermal power plant with increasing steam content when the original steam turbine is replaced with a higher capacity. The rated capacity of the new turbine is assumed 42 MW with the maximum power 47 MW. It is evident from the figure that such an upgrade results in significant improvement in power output. However, it is associated with large capital investment.

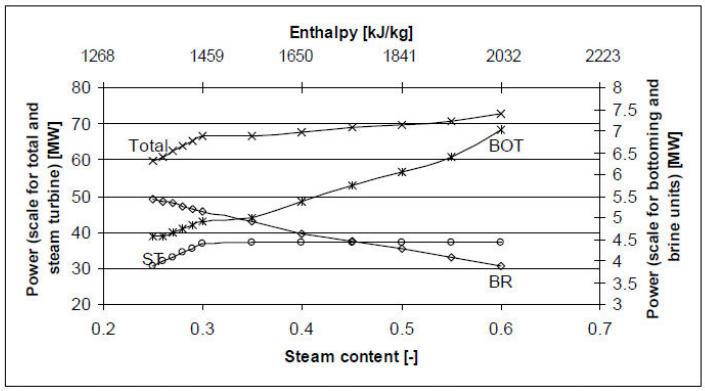

Fig. 2. Theoretical power for the base case as a function of resource enthalpy

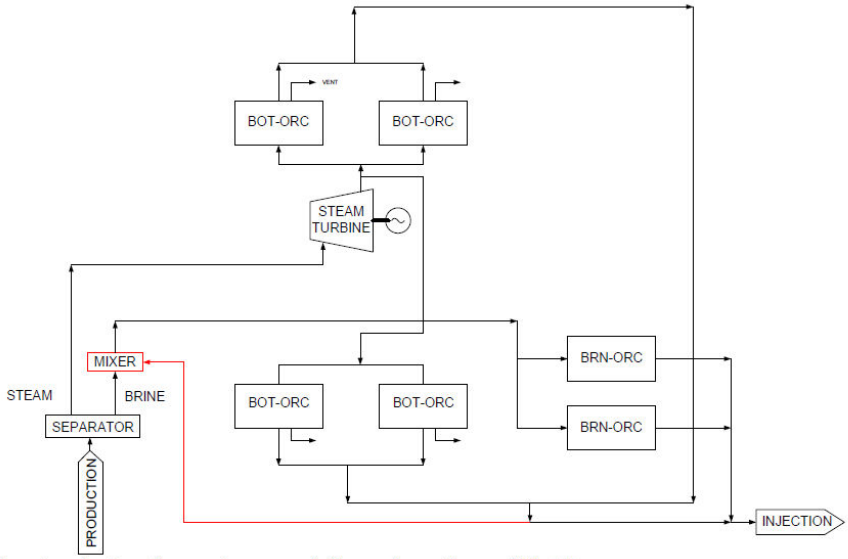

Fig. 3. Adaptive design for an increased flow of geothermal fluid

3.4. Case Study 3: constant flow of geothermal fluid and lowered reinjection temperature

In case 1, more geothermal fluid was used to overcome the problem of reduced brine in BRN-ORCs which results in utilization of the resource at a higher rate. The reinjection temperature of the geothermal brine is not affected much. In the base case, the reinjection temperature is about 125°C. The minimum recommended reinjection temperature of the site is about 80 ºC to prevent silica formation. So there is a possibility of further extracting heat from the reinjected brine.

The alternative design would look the same as Fig. 3. However, the geothermal resource is utilized at constant rate i.e. mass flow of geothermal fluid to the plant is the same as the base case. The plant performance would look like the same as Fig. 4 but the reinjection temperature will change. Fig.6 shows the corresponding reduction in reinjection temperature. It is clear from Fig. 6 that it is possible to stabilize the brine flow rate of the BRN-ORCs and consequently power output by keeping the reinjection temperature within an acceptable limit (80 ºC).

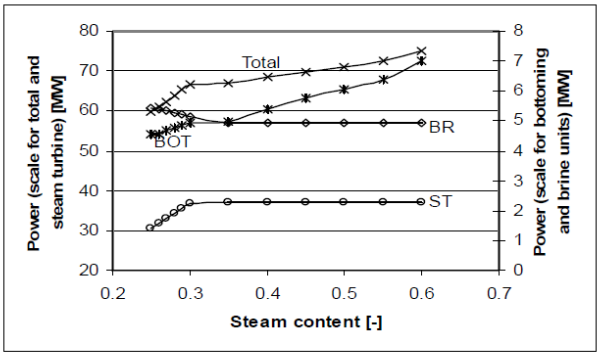

Fig. 4. Theoretical power for base case with increased mass flow of geothermal brine to keep the brine flow rate constant for the BRN-ORC as function of resource enthalpy

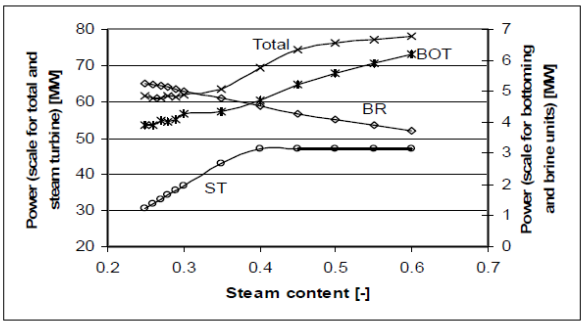

Fig. 5. Theoretical power of the geothermal power plant with a higher capacity steam turbine

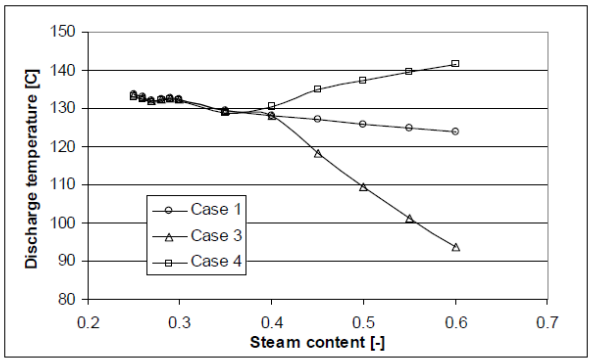

Fig. 6. Theoretical reinjection temperatures for case 1, case 3 and case 4

3.5. Case study 4: constant flow of geothermal fluid with excess steam (50/50)

It was stated earlier that the steam turbine has a power producing limit. Beyond this limit, the steam turbine cannot utilize the excess steam and the consequence is a higher discharge

enthalpy. Another possible alternative is depicted in Fig. 7. The excess steam can be bypassed and used to reheat the condensate collected from the BOT-ORCs. The results of mixing excess steam (50%) and condensate (50%) are presented in Fig. 8. It is clear from Fig. 8 that the reheating of the condensate by excess steam mitigates the reduced brine for the BRN-ORCs. The reinjection temperature is not reduced by this approach (Fig. 6).

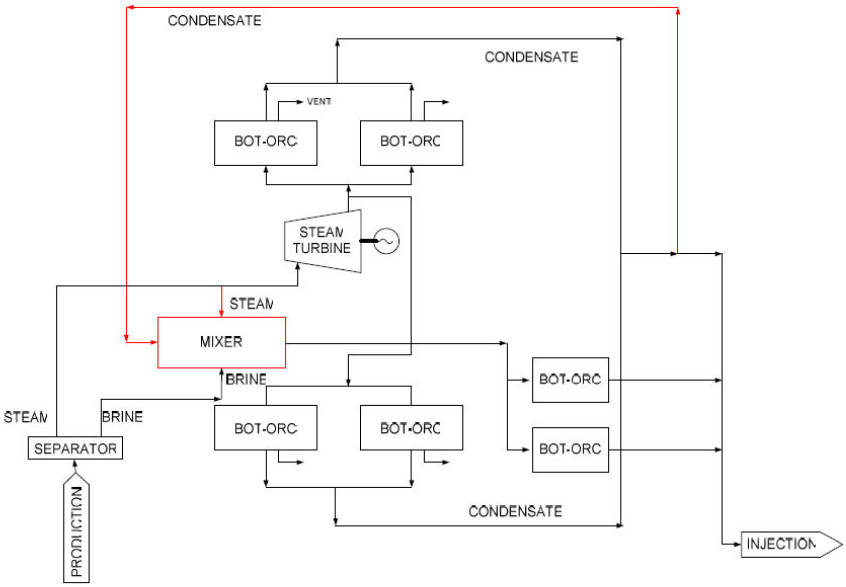

Fig.7. Adaptive design for a constant flow of geothermal fluid and regenerative heating

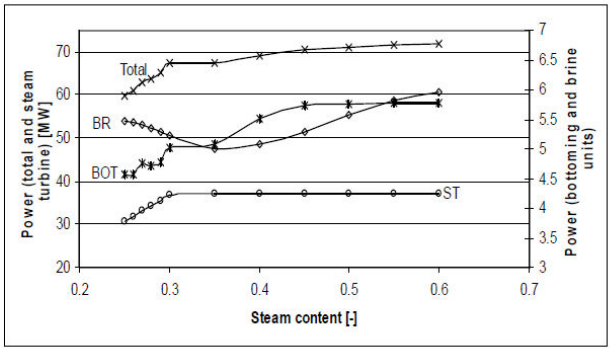

Fig. 8. Theoretical power of the geothermal power plant and constant mass flow of geothermal brine with regenerative heating of the brine by excess steam

4. Discussion and conclusion

This paper has introduced an alternative design approach that takes into account possible changes in future resource characteristics. As geothermal power plants are very capital intensive and it is not very easy to change a plant to adapt to resource characteristics different from the original design, keeping provision for future resource characteristics can be very effective. Although, the initial investment cost might go up as a consequence of adaptive design, over the life span of the plant the total benefit may be greater. A proper cost benefit

analysis is necessary to identify the economic benefit. There are four case studies presented in this paper that analysed various possible options of the hypothetical power plant depending on the hypothetical changes in resource characteristics. The results show provisions that could be kept in the plant for future resource characteristics. The next phase is to do a cost benefit analysis of these options and select the optimum option. In this paper we have only discussed adaptive design approach for increasing resource enthalpy. Similarly, adaptive design for a decreasing resource enthalpy can also be carried out which will provide different provision for the geothermal power plant. One such provision is that one or more of the BOT-ORCs can be designed in such a way that they can be used as BRN-ORCs when geothermal resource enthalpy reduces to utilize the increased brine available.

References

[1] IEA, *World Energy Outlook*. 2008: International Energy Agency.
[2] Barbier, E., *Geothermal energy technology and current status: an overview.* Renewable and Sustainable Energy Reviews, 2002. **6**(1-2): p. 3-65.
[3] DiPippo, R., *Second Law assessment of binary plants generating power from low-temperature geothermal fluids.* Geothermics, 2004. **33**(5): p. 565-586.
[4] Chen, H., D.Y. Goswami, and E.K. Stefanakos, *A review of thermodynamic cycles and working fluids for the conversion of low-grade heat.* Renewable and Sustainable Energy Reviews, 2010. DOI:10.1016/j.rser.2010.07.006
[5] Bombarda, P. and M. Gaia. *Geothermal Binary Plants Utilising an Innovative Non-Flammable Azeotropic Mixture as Working Fluid.* in *Proceedings 28th NZ Geothermal Workshop*. 2006.
[6] Madhawa Hettiarachchi, H.D., et al., *Optimum design criteria for an Organic Rankine cycle using low-temperature geothermal heat sources.* Energy, 2007. **32**(9): p. 1698-1706.
[7] DiPippo, R., *Ideal thermal efficiency for geothermal binary plants.* Geothermics, 2007. **36**(3): p. 276-285.
[8] Sohel, M.I. and M. Jack, *Efficiency improvements by geothermal heat integration in a lignocellulosic biorefinery.* Bioresource Technology, 2010. **101** p. 9342-9347.
[9] Sohel, M.I., et al., *An iterative method for modelling the air-cooled organic Rankine cycle geothermal power plant.* International Journal of Energy Research, 2010. DOI: 10.1002/er.1706
[10] Sohel, M.I., et al., *Dynamic Modelling and Simulation of an Organic Rankine Cycle Unit of a Geothermal Power Plant.* Proceedings World Geothermal Congress 2010 Bali, Indonesia, 25-29 April 2010.
[11] Atrens, A.D., H. Gurgenci, and V. Rudolph, *Electricity generation using a carbon-dioxide thermosiphon.* Geothermics, 2010. **39**(2): p. 161-169.
[12] Atrens, A.D., H. Gurgenci, and V. Rudolph, *CO2 Thermosiphon for Competitive Geothermal Power Generation.* Energy & Fuels, 2008. **23**(1): p. 553-557.
[13] DiPippo, R., *Geothermal Power Plants: Principles, Applications and Case Studies*. 2005: Elsevier Ltd.
[14] RJVL, *ROTOKAWA GEOTHERMAL DEVELOPMENT Resource Consent Applications and Assessment of Environmental Effects*. 2007, Rotokawa Joint Venture Limited, C/- Mighty River Power Limited, 160 Peachgrove Road, PO Box 445, HAMILTON, New Zealand.
[15] MathWorks, *www.mathworks.com*. 2008.
[16] REFPROP. *National Institute of Standards and Technology (NIST),* 2007. Available from: http://www.nist.gov/.